DOCTOR OF PHILOSOPHY

Biohydrogen as a Fuel

Understanding and Engineering Hydrogenase Enzymes for Biotechnological Applications

Lamont, Ciaran Mitchell

Award date:
2016

Biohydrogen as a Fuel: Understanding and Engineering Hydrogenase Enzymes for Biotechnological Applications

Ciaran Mitchell Lamont

September, 2016

Thesis submitted to the University of Dundee in partial fulfilment of the requirements for the degree of Doctor of Philosophy.

Table of Contents

Table of Figures ix

Table of Tables xii

Acknowledgements xiii

Declaration xiv

Abstract xv

Publications xvii

Conferences xvii

Internship xvii

Common Abbreviations xviii

Amino-acid Abbreviations xxi

1. Introduction 1

1.1 The need for alternative fuels 2

1.2 Biofuels 3

1.3 Hydrogen: the ideal fuel? 5

1.4 Biohydrogen 10

1.5 Hydrogenase enzymes 15

1.5.1 [Fe]-hydrogenases 16

1.5.2 [FeFe]-hydrogenases 18

1.5.3 [NiFe]-hydrogenases 20

1.5.4 Group 1: Uptake [NiFe]-hydrogenases 23

1.5.5 Group 2: Cyanobacterial uptake [NiFe]-hydrogenases and H_2 Sensors 24

1.5.6 Group 3: Bidirectional heteromultimeric cytoplasmic [NiFe]-hydrogenases 24

1.5.7 Group 4: Membrane-associated, energy-conserving and H_2-producing [NiFe]-hydrogenases 25

1.5.8 Group 5: Actinobacterial, high-affinity H_2-oxidising [NiFe]-hydrogenases 25

1.6 Hydrogenase inhibitors, and adaptations to counter these 27

1.6.1 O_2 tolerance in hydrogenases 27

1.6.2 Unusual redox potentials and enzyme kinetics 28

1.6.3 Modifications to gas channels 30

1.6.4 Additional maturation proteins 31

1.7 The hydrogenases of *E. coli* 33

1.7.1 Hyd-1 33

1.7.2 Hyd-2 37

1.7.3 Hyd-3 39

1.7.4 Hyd-4 44

1.8 [NiFe] active site formation 46

1.9 [Fe-S] biosynthesis 50

1.10 The hydrogenases of *C. necator* 52

1.11 Hydrogenases: beyond biofuels 55

1.12 Synthetic biology 57

1.13 Aims 59

2. Heterologous production of an NADH-linked [NiFe]-hydrogenase in *Escherichia coli* 60

2.1 Introduction 61

2.1.1 Heterologous hydrogenase production could augment H_2 yield 61

2.1.2 Linking NADH to H_2: The Soluble Hydrogenase from *Cupriavidus necator* 61

2.2 Aims 63

2.3 Results 64

2.3.1 The design and expression of synthetic operons encoding the *C. necator* soluble hydrogenase and its maturases 64

2.3.2 The synthetic maturase operons are functional and can activate endogenous *E. coli* [NiFe]-hydrogenases 69

2.3.3 Attempts to purify the SH complex 71

2.3.4 Production of an active SH in *E. coli* 72

2.4 Discussion 80

2.4.1 Complementation by the *C. necator* maturases 80

2.4.2 Comprehensive design of operons for expression and characterisation of the SH 84

2.4.3 Possible routes to improve SH functionality 86

2.4.4 Was SH codon optimisation required? 89

2.4.5 SH activity cannot rescue fermentative growth of an Δ*adhE* mutant. 90

3. Towards the construction of intracellular hydrogen biosensors in *Escherichia coli*. 94

3.1 Introduction 95

3.1.1 The need for a genetic screen for increased hydrogen production 95

3.1.2 The Regulatory Hydrogenase (RH) of *C. necator* 95

3.2 Aims 101

3.3 Results 102

3.3.1 Initial attempts at RH heterologous production 102

3.3.2 Design and optimisation of a synthetic *hoxABCJ** operon 104

3.3.3 Initial attempts to assess biosensor functionality 107

3.3.4 Constructing an RH-dependent live/die screen 111

3.3.5 Amplification of the biosensor signal 115

3.3.6 Attempts to adapt Hyd-2 as a biosensor 118

3.4 Discussion 130

3.4.1 Possible problems with the upstream promoter regions 130

3.4.2 Possible problems with the synthetic RH operon 132

3.4.3 Towards improving the Biosensor systems 138

3.4.4 Other potential hydrogenase candidates to use 140

4. Characterisation of a chimeric metalloenzyme for H_2 production from pyruvate 142

4.1 Introduction 143

4.1.1 Natural modes of H_2 production in *E. coli* metabolism 143

4.1.2 Pyruvate::ferredoxin oxidoreductase 143

4.1.3 Linking PFOR activity to the hydrogen-evolving Hyd-3 144

4.2 Aims 146

4.3 Results 147

4.3.1 Synthesis of the ferredoxin::Hyd-3 fusion 147
4.3.2 Assessing the functionality of the Fd-Hyd-3 fusion enzyme 148
4.3.3 Effect of Fd-Hyd-3 fusion and PFOR on the cell metabolome 149
4.4 Discussion 155
4.4.1 A novel enzyme system is functional in *E. coli* 155
4.4.2 Reconciliation of GC and HPLC data 158
4.4.3 Strategies to further improve enzymatic activity 161
5. Further characterisation of a chimeric metalloenzyme for H_2 production 163
5.1 Introduction 164
5.1.1 Glycerol is a desirable substrate for industrial H_2 production 164
5.1.2 Glycerol metabolism in *E. coli* 164
5.1.3 Thiosulfate reductase in *Salmonella enterica* 168
5.1.4 A Hyd-2/thiosulfate reductase chimera exhibits activity *in vitro* 170
5.1.5 Proteorhodopsin 172
5.2 Aims 174
5.3 Results 175
5.3.1 Predictive modelling of chimeric constructs 175
5.3.2 Assessment of the Phs-Hyd-2 chimeras *in vivo* activity by gas chromatography 178
5.3.3 New construct design in an attempt to further improve H_2 yield 182
5.4 Discussion 185
5.4.1 Further characterisation of a novel metalloenzyme in *E. coli* 185
5.4.2 Insights into HybO-PhsB fusion peptides *via* predictive modelling 186
5.4.3 GC data suggests PR does not aid chimera functionality 187
5.4.4 Possible strategies to further improve enzyme activity 189
5.4.5 Further work to confirm the route to quinol pool reduction 191
5.4.6 Glycerol fermentation in *E. coli* 192
6. Future perspectives 194
6.1 Introduction 195

6.2 The alteration native *E. coli* metabolism 196

6.3 Heterologous expression of foreign genes in a host cell 198

6.4 Engineering of fusion peptides to construct artificial chimeric enzymes 200

6.5 Compartmentalisation of metabolic pathways 201

6.5.1 Co-encapsulation of SH and GAPDH within a BMC 203

6.5.2 Heterologous production of the Pdu BMC in *E. coli* 207

6.6 Protein engineering 209

6.7 The future state of industrial biohydrogen production 212

6.8 Concluding remarks 214

7. Materials and methods 216

7.1 Bacterial strains 217

7.2 Cell culturing 219

7.3 Media and additives 220

7.4 Buffers and solutions 221

7.5 Molecular biology techniques 223

7.5.1 Plasmid DNA preparation 223

7.5.2 Tables of plasmids 224

7.5.3 Preparation of competent cells and transformation with plasmid DNA 229

7.5.4 Polymerase chain reaction (PCR) 230

7.5.5 Table of primers 232

7.5.6 QuickChange site directed mutagenesis 238

7.5.7 Agarose gel electrophoresis 238

7.5.8 DNA gel extraction and purification 239

7.5.9 DNA digestion by restriction endonucleases for cloning 239

7.5.10 DNA ligation 239

7.5.11 Suicide ligations 240

7.5.12 Fusion PCR 241

7.5.13 Insertion of His-tags 244

7.5.14 pMAK705 homologous recombination for chromosomal gene deletion and insertion 246

7.5.15 DNA sequencing 247

7.5.16 Synthetic operon synthesis 247

7.6 Protein methods 248

7.6.1 SDS-PAGE 248

7.6.2 Semi-dry Western immunoblotting 249

7.6.3 Determining protein concentrations 250

7.6.4 ^{35}S-Methionine radiolabelling 250

7.6.5 Purification of His-tagged proteins by nickel affinity chromatography 250

7.7 Hydrogenase *in vitro* activity assays 252

7.7.1 Redox dye-linked hydrogenase assay 252

7.8 Gas chromatography (GC) 254

7.9 *In vivo* biosensor activity assays 255

7.9.1 Blue plate test 255

7.9.2 β-gal assay 255

7.9.3 Live/die screen plate assay 256

7.10 High-performance liquid chromatography (HPLC) analysis of organic acids 258

7.11 Cell fractionation 259

8. Bibliography 260

Table of Figures

Figure 1.1 Schematic of the Proton Exchange Membrane (PEM) fuel cell. 6
Figure 1.2 Modes of glycolysis in prokaryotes. 12
Figure 1.3 Mixed acid fermentation in enteric bacteria results in H_2 production. Under fermentative conditions. 13
Figure 1.4 [Fe]-hydrogenase architecture. 17
Figure 1.5 [FeFe]-hydrogenase architecture 19
Figure 1.6 [NiFe]-hydrogenase architecture.. 21
Figure 1.7 Comparison of the active sites in standard O_2 sensitive [NiFe]-hydrogenases and a possible active site arrangement of the SH from *C. necator*. 32
Figure 1.8 The *E. coli* Hyd-1 isoenzyme. 35
Figure 1.9 The Hyd-2 isoenzyme from *E. coli*. 38
Figure 1.10 Hyd-3/ FHL of *E. coli*. 41
Figure 1.11 The formate regulon. 42
Figure 1.12 Respiratory Complex I and FHL share homology 43
Figure 1.13 Biosynthesis of the [NiFe] active site in *E. coli*. 49
Figure 2.1 Schematic of the Soluble Hydrogenase (SH) of *Cupriavidus necator*. 62
Figure 2.2 Comparison between predicted heterologous expression efficiency in *E. coli* of *C. necator* genes before and after optimisation. 65
Figure 2.3 Synthetic *hoxF-I*, *hypA2-X* and *hypA1-X* operons for expression in *E. coli*. 66
Figure 2.4 The synthetic operons *hoxF-I* and *hypA2-X* and *hypA1-X* operons produce protein products in *E. coli*. 68
Figure 2.5 The synthetic maturase operons can complement *E. coli hyp* mutants. 70
Figure 2.6 Towards purifying the SH complex heterologously expressed in *E. coli*. 72
Figure 2.7 Heterologously expressed SH shows hydrogenase activity *in vitro.* 74
Figure 2.8 Heterologously expressed SH exhibits hydrogen production *in vivo*. 76
Figure 2.9 The SH enzyme is not capable of rescuing fermentative growth in Δ*adhE* mutants. 79
Figure 2.10. Sequence homology between maturase enzymes in *E. coli* and *C. necato*r 83
Figure 2.11 The reductive pathways of mixed acid fermentation allow for NAD^+ regeneration. 92
Figure 3.1 Summary of RH-mediated regulation of gene expression. 97
Figure 3.2 Gene cluster encoding RH in *C. necator*. 99
Figure 3.3 Recruitment of the RH to act as an intracellular H_2 Biosensor. 101
Figure 3.4 Native *C. necator hoxABCJ** and *hypA1-X* genes lead to aberrant protein production in *E. coli.*. 103

Figure 3.5 *OPTIMIZER* estimations of native RH codon usage suitability in *E. coli.* 104
Figure 3.6 Genes cloned downstream of optimised *hoxJ** are not efficiently translated. 105
Figure 3.7 Optimisation of the *hox* operon allows for the full synthesis of the RH machinery in *E. coli.*. 107
Figure 3.8 Preliminary assessment of biosensor functionality in *E. coli*. 110
Figure 3.9 Live/die screen to examine RH biosensor functionality 113
Figure 3.10 Amplification of the RH signal using the tetrathionate two-component system from *S. enterica* 115
Figure 3.11 Live/die screen to assess amplification of the RH signal. 117
Figure 3.12 Hyd-2 as a biosensor. 120
Figure 3.13 Both operons encoding the Hyd-2 biosensor are fully expressed.. 121
Figure 3.14 The two HybO-HoxB constructs exhibit *in vitro* hydrogenase activity. 122
Figure 3.15 β-gal assays suggest Hyd-2 biosensor may not be functional. 123
Figure 3.16 Live/die screen to examine Hyd-2 biosensor functionality using MBHp.. 125
Figure 3.17 Live/die screen to examine Hyd-2 biosensor functionality using SHp. 127
Figure 3.18 Live/die screen to assess amplification of the Hyd-2 biosensor signal. 129
Figure 3.19 Sulfur-containing residues of the RH machinery. 133
Figure 3.20 Analysis of the translation efficiency of each gene in the optimised *CBAJ** operon as found in pUNI-RH using *RBS Calculator*. 135
Figure 3.21 Analysis of the translation efficiency of each gene in both Hyd-2 biosensor operons as found in pUNI-hybO^{long}AJ* and pUNI-hybO^{short}AJ*using *RBS Calculator*. 137
Figure 4.1 The ferredoxin-Hyd-3 fusion protein can be synthesised in the cell. 148
Figure 4.2 The Fd-Hyd-3 chimera exhibits H_2 evolution in the presence of PFOR. 149
Figure 4.3 Representative HPLC elution profiles to show organic acid content in spent fermentation broth. 151
Figure 4.4 The influence of the Fd-Hyd-3 fusion and PFOR on the *E. coli* metabolome. 152
Figure 4.5 Proposed mechanism by which the PFOR Hyd-3::Fd chimera generates H_2 production from pyruvate.. 156
Figure 4.6 Possible influence of the Fd-Hyd-3 enzyme on mixed acid fermentation. 160
Figure 5.1 Respiratory metabolism of glycerol in *E. coli*. 166
Figure 5.2 Glycerol fermentation can occur in specific conditions in *E. coli* 167
Figure 5.3 The thiosulfate reductase complex from *S. enterica.* 169
Figure 5.4 A Phs-Hyd-2 chimera to allow for H_2 production from the oxidation of glycerol in *E. coli*. 171
Figure 5.5 The design of various linker peptides between PhsB and HybO. 172

Figure 5.6 The co-production of proteorhodopsin to augment the yield of the Phs-Hyd-2 chimera in *E. coli*. 173
Figure 5.7 Phyre^2 predictive modelling of HybO-PhsB constructs allows for an estimate of [Fe-S] cluster distance. 177
Figure 5.8 Cell colour suggests production of proteorhodopsin. 178
Figure 5.9 Incubation of cultures to investigate light-augmented H_2 production from glycerol. 179
Figure 5.10 All three variants of the Phs-Hyd-2 chimeric metalloenzyme exhibit functionality *in vivo*. 180
Figure 5.11 Casamino supplementation leads to greater H_2 evolution in all three fusion constructs..... 181
Figure 5.12 L-Rhamnose-regulated constructs allow for production of PhsB-HybO fusion peptides. 183
Figure 5.13 Western immunoblots establish production of the PhsB-HybO fusion proteins. . 184
Figure 6.1 The Pdu BMC from *S. enterica*.. 202
Figure 6.2. Proposed co-localisation of SH and GAPDH in a BMC. 204
Figure 6.3 Co-production of PduD-SH and PduP-GAPDH with a BMC does not boost H_2 yield.205
Figure 7.1 Suicide Ligations..... 241
Figure 7.2 Fusion PCR..... 243
Figure 7.3 His-tag insertion schematic..... 245

Table of Tables

Table 7.1 Table of bacterial strains used in this study. 218
Table 7.2 Growth media used in this study. 220
Table 7.3 Media supplements and their concentrations. 220
Table 7.4 Antibiotics used in this study.. 221
Table 7.5 Buffers used in this study. 222
Table 7.6 Plasmids used in this study. 228
Table 7.7 PCR reaction mix used for GoTaq or Herculase II polymerase. 231
Table 7.8 Cyclic conditions for PCR reactions performed in this study 231
Table 7.9 Table of primers used in this study. 237
Table 7.10 Composition of the resolving and stacking gels for SDS-PAGE. 248

Acknowledgements

First and foremost I must thank my supervisor, Professor Frank Sargent. He has been a tremendous support for me, not just academically, but also as a calming presence during any of my concerns during my project. I have lost count of the amount of times I have felt reassured and re-motivated after one of our discussions. Not only have I found this project intellectually rewarding, but also I feel I have gained a broad range of skills that will serve me well in the future. I am hugely grateful to Frank for allowing me to study in his lab all these years; I hope I have repaid his goodwill.

I am indebted to the whole of the Molecular Microbiology division, not only for their technical assistance in the science-side of my project, but also for making the division an enjoyable place to work for the past four years. In particular, I am grateful to Dr. Ciarán Kelly and Dr. Constanze Pinske for their great support during my formative months in the lab; without them I would have been truly lost. In the subsequent years, the continued discussions of my work over a beer with Ciarán have also been a tremendous help, so thank you once again.

Thanks must also be extended to Dr. Jacqueline Heilbronn and all the support staff who ensure the lab runs smoothly. With this being the first lab in which I have ever worked, I feel I may have taken this for granted at times. It is only as I have spoken to people in labs elsewhere that I realise just how easy I have had it, and it is thanks to you.

I am grateful to Axis-Shield in general, and Dr. Jeff Brady in particular, for taking me on as an intern. It was an invaluable experience that has really helped me decide about my future career.

Last but not least I want to mention Mum and Dad. You have both have sacrificed so much to allow me to be in education for so long, and you have given me every opportunity so I could best decide what I want to do with my life. Though I might not always say it, please know that I am grateful beyond words for the unwavering amount of love and reassurance you have given me. It's been a long road but I'm almost there, and none of this would have been possible without you. I hope I have made you proud. I feel I should now make a vow to you that after this is over I will finally go and get a job!

My deepest gratitude to all of you.

Declaration

I declare that I am the author of this thesis and that, unless otherwise stated, all references cited have been consulted; that the work of which this thesis is a record has been performed by me, and that it has not been previously accepted for a higher degree: where the thesis is based upon joint research, the nature and extent of my individual contribution is defined.

Ciaran Mitchell Lamont

Abstract

Molecular hydrogen (H_2) is seen as an ideal replacement for fossil fuels; however the current methods of its synthesis are unsustainable and environmentally damaging. Research is therefore needed to devise new, more suitable modes of H_2 derivation. Biohydrogen – i.e. H_2 derived from cellular metabolism – is a particularly promising future fuel, owing to it being a truly renewable means to generate H_2 that would contribute to neither pollutant nor greenhouse gas emissions. The predominant enzymes responsible for microbial H_2 evolution are called hydrogenases. The model organism *Escherichia coli* produces H_2 during mixed acid fermentation by the action of it native hydrogenases. However, the natural level of H_2 produced is too low to meet current industrial demand for H_2 or any future uses as a fuel.

The context of the work presented in this Thesis was therefore towards the augmentation of *E. coli* H_2 yield. This was addressed through a number of specific aims that employed synthetic biology techniques. The first aim was to engineer *E. coli* to heterologously express genes that lead to the biosynthesis of a foreign NADH-consuming [NiFe]-hydrogenase, native to *Cupriavidus necator.* It was shown that this hydrogenase was assembled in *E. coli* and it exhibited activity both *in vitro* and *in vivo*. Serendipitously, it was found that the native *E. coli* maturase system, critical for biosynthesis of the [NiFe] cofactor, could assemble a functional enzyme. The converse was also found: that the *C. necator* maturase operons were able to complement *E. coli* mutants defective in hydrogenase biosynthesis.

A second approach to augment *E. coli* H_2 yield utilised in this Thesis was the generation of synthetic chimeric metalloenzymes that might allow for new substrates to be used. One such chimera, consisting of a fusion between *E. coli* Hyd-3 and a ferredoxin from *Thermotoga maritima*, was characterised and shown to exhibit *in vivo* H_2 evolution when co-produced with a heterologous pyruvate: ferredoxin oxidoreductase. This allowed pyruvate to be employed as a new electron donor for H_2 production. In addition, the further characterisation of a chimeric complex combining subunits of *E. coli* Hyd-2 and *Salmonella enterica* thiosulfate reductase was undertaken. This allowed H_2 production to be driven by respiratory electron donors such as glycerol 3-phosphate.

An additional aim of this work was to develop an intracellular H_2 biosensor in *E. coli*, with a view to obtaining a screening method that could be used to scan mutant libraries for increased H_2 production. The strategy was to utilise the H_2-sensing regulatory [NiFe]-hydrogenase (RH) from *C. necator* in *E. coli* to control reporter gene transcription. Synthetic operons were designed for optimum expression of RH-encoding genes, and the heterologous biosynthesis of

the RH apparatus was established. Various reporter gene constructs were also generated. However, the system was not found to be functional, and further experiments needed to address this are discussed.

Publications

Lamont, C., Sargent, F. (Accepted) Bioengineering a soluble, cytoplasmic [NiFe]-hydrogenase for biohydrogen technology. Submitted to Archives of microbiology.

Conferences

10th International Hydrogenase Conference, July 2013 (Szeged, Hungary).

- Poster Presentation 'Engineering the formate hydrogenlyase complex of *Escherichia coli.*' C. Lamont; J. McDowall; C. Hjersing; B. Murphy; F. Armstrong; F. Sargent.

Young Microbiologists Symposium, June 2014 (Dundee, Scotland).

Internship

Axis-Shield Diagnostics, Dundee (March to June 2015).

- A three month internship as part of my PhD, where I worked in both the manufacturing and on-market-support divisions. A notable achievement was my aid in developing a new assay to better assess enzyme concentration, which allowed for better lot-to-lot consistency in a product. I also gave input about how gene optimisation could be employed to improve protein yield. This placement helped foster new skills in enzymology and statistics, whilst also giving me a first-hand experience of working in an industrial setting. As such I now have an appreciation of commercial considerations and Good Manufacturing Practice.

Common Abbreviations

Å	Ångstrom (0.1 nm)
A	Absorbance
ADP	Adenosine diphosphate
Amp	Ampicillin
Apra	Apramycin
ATP	Adenosine triphosphate
$BioH_2$	Biohydrogen
BMC	Bacterial microcompartment
bp	Base pairs
BSA	Bovine serum albumin
BV	Benzyl viologen
^oC	Celsius
Casacids	casamino acids
Cml	Chloramphenicol
C-terminus	(protein) Carboxy-terminus
DNA	Deoxyribonucleic acid
DNase	Deoxyribonuclease
dNTP	Deoxynucleoside triphosphate
DTT	Dithiothreitol
E_0	Standard reduction potential
EDTA	Ethylenediaminetetraacetate
Fd	Ferredoxin
[Fe-S]	Iron-sulfur
FHL	Formate hydrogenlyase
FMN	Flavin mononucleotide
g	Gram
x *g*	Relative centrifugal force
gDNA	Genomic DNA
GTP	Guanosine triphosphate

h	Hour
H^+	Proton
H_2	Molecular hydrogen
HA-tag	(human influenza) Haemagglutinin epitope affinity tag
His-tag	Hexahistidine epitope affinity tag
Hyd-1	Hydrogenase-1 (*E. coli*)
Hyd-2	Hydrogenase-2 (*E. coli*)
Hyd-3	Hydrogenase-3 (*E. coli*)
Hyd-4	Hydrogenase-4 (*E. coli*)
IMAC	Immobilised metal-ion affinity chromatography
IPTG	Isopropyl β-D thiogalactopyranoside
Kan	Kanamycin
kb	Kilobase (1000 bp)
kDa	Kilodalton (1000 Da)
L	Litre
LB	Luria-Bertani medium
λ	Lambda (wavelength)
m	Milli (10^{-3})
M	Molar
MGD	Molybdopterin guanine dinucleotide
MMD	Membrane microdomain
µ	Micro (10^{-6})
min	Minute
mol	Mole
mRNA	Messenger RNA
MV	Methyl viologen
NAD^+	Nicotinamide adenine dinucleotide
NADH	Nicotinamide adenine dinucleotide (reduced)
$NADP^+$	Nicotinamide adenine dinucleotide phosphate
NADPH	Nicotinamide adenine dinucleotide phosphate (reduced)
N-terminus	(protein) Amino-terminus

n	Nano (10^{-9})
nm	Nanometre
O_2	Molecular oxygen
OD	Optical density
PAGE	Polyacrylamide gel electrophoresis
PCR	Polymerase chain reaction
PFOR	Pyruvate: ferredoxin oxidoreductase
Pi	Inorganic phosphate
pK_a	Acid dissociation constant
pmf	Proton motive force
psi	Pounds per square inch
RH	Regulatory hydrogenase (*C. necator*)
RNA	Ribonucleic acid
rpm	Revolutions per minute
SDS	Sodium dodecyl sulphate
SEM	Standard error of mean
SH	Soluble hydrogenase (*C. necator*)
Tat	Twin-arginine translocase
TBS	Tris-buffered saline
TEMED	N, N, N', N'-tetramethylethylenediamine
TM	Transmembrane (protein structure)
Tris	Tris(hydroxymethyl)aminomethane
tRNA	Transfer RNA
V	Volts
v/v	Volume per volume
w/v	Weight per volume

Amino-acid Abbreviations

Amino acid	Three letter abbreviation	One letter abbreviation
Alanine	Ala	A
Arginine	Arg	R
Asparagine	Asn	N
Aspartate	Asp	D
Cysteine	Cys	C
Glutamate	Glu	E
Glutamine	Gln	Q
Glycine	Gly	G
Histidine	His	H
Isoleucine	Ile	I
Leucine	Leu	L
Lysine	Lys	K
Methionine	Met	M
Phenylalanine	Phe	F
Proline	Pro	P
Pyrrolysine	Pyl	O
Selenocysteine	Sec	U
Serine	Ser	S
Threonine	Thr	T
Tryptophan	Trp	W
Tyrosine	Tyr	Y
Valine	Val	V
Any amino acid	-	X

1. Introduction

1.1 **The need for alternative fuels**

The world energy consumption (WEC) continues to rise at an ever-greater rate. Current forecasts predict that the WEC in 2040 will be 815 quadrillion British thermal units (Btu), a 48% increase from the 549 Btu WEC in 2012 (Energy Information Administration, 2016). Two main reasons account for this increased demand. First, the explosion in world population shows little sign of abating, with a conservative estimate of 8.5 billion people living by 2030 (UN Department of Economic and Social Affairs, 2015). This is only compounded by the second factor: that there is increasing *per capita* energy consumption as the standards of living, particularly of those in the traditionally-defined 'developing world', enjoy lifestyles more akin to that already experienced in the developed world. Clearly, a major issue for society is to address this insatiable demand for energy.

The current energy economy is undeniably hugely reliant on fossil fuels, for example in 2012 ~67% of energy was derived from these sources (Energy Information Administration, 2016), which only exacerbates this problem of trying to meet the future energy demand. The finite nature of fossil fuels means their long-term use is unsustainable economically. Resources are expected to be exhausted within the next century (Karp and Richter, 2011), so driving up price. Furthermore, fossil fuel reserves are concentrated in specific geographical locations, with 62% of oil and 45% of coal found in the Middle East, and the vast majority of extraction carried out by only a handful of companies (Umbach, 2010), which also has ethical implications. Perhaps the biggest issue with merely scaling up current fossil-fuel dominated methods of energy production to meet future demand is the environmental concerns, with as much as three quarters of CO_2 emissions derived from fossil fuel combustion (Energy Information Administration, 2016). Therefore, the seemingly paradoxical situation exists of trying to increase energy production on one hand but decreasing the undesirable by-products of such production on the other. One solution is to adopt new modes of energy evolution, preferably those that are renewable, sustainable and 'green' in nature.

1.2 **Biofuels**

It is not sufficient to merely find a renewable source of energy *generation* but also an effectively way to *store* said energy so it can be used at a later date. The myriad non-biological, renewable sources of energy derivation that have had relatively widespread adoption to date, such as wind, solar, hydro and tidal power, all produce electricity directly with varying degrees of efficiency. However, electrical energy itself cannot be easily stored. It must be converted into other forms for storage, before being converted back to electricity again at the point of energy usage. A problem arises in that these transductions incur energy loss; batteries, for example, are notoriously inefficient, and there is a great deal of research into developing technologies to address this issue (Luo *et al*., 2015). Fuels, on the other hand, are an efficient medium of energy storage and transportation, that are converted into usable energy when required (Hallenbeck and Benemann, 2010). It follows that biofuels are seen as an attractive green replacement for fossil fuels.

The original wave of biofuels adopted, the so-called 'first generation', such as biodiesel and bioethanol, are derived from the fermentation of plant derived sugars. They are recognisable by their ability to be mixed with conventional fossil fuels or in specially designed vehicles (Naik *et al*., 2010). Brazil has long been viewed as a case study into the successful integration of such alternative fuels into the energy economy, and they have been a mandatory component of fuel since the 1970s (Renewable Fuels Association, 2015). However such biofuels are often made from the growth of dedicated crops— sugar cane in the case of bioethanol in Brazil— and thus there is not only the risk of land use conflict with food-based crop growth, but also environmental risks brought about by increased land use for agriculture.

The 'second-generation' biofuels were developed in order to try to circumvent this land-use conflict. Instead of the raw materials being grown instead of food crops, these biofuels are derived from the waste products of agriculture (Karp and Richter, 2011). Utilising the abundant, cheap biomass comprising the inedible or unused plant material from agriculture

would represent an idea with strong ‘green’ credentials, as such organic waste is currently underutilised. However, the bulk of such material is composed of lignocellulose, and converting this into biofuels is currently prohibitively expensive; requiring prior treatment with enzymes, heat, or chemicals to release fermentable sugars (Chen, 2014).

1.3 **Hydrogen: the ideal fuel?**

Perhaps the most promising fuel for the future is molecular hydrogen (H_2). Unlike carbon based fuels, which are associated with greenhouse gas and pollutant emissions, H_2 combustion forms only water (Equation 1.1).

$$2H_2\,(g) + O_2\,(g) \longrightarrow 2H_2O\,(l) \qquad \Delta H^o_r = -572\ kJ\ mol^{-1}$$

Equation 1.1 The combustion of hydrogen is highly exothermic.

Furthermore, its small molecular size means it has a very high energy/mass ratio (Häussinger *et al.*, 2011), with combustion releasing 120 MJ kg^{-1} compared to 45 MJ kg^{-1} for oil (Vijayaraghavan and Mohd Soom, 2006) and makes it is an effective fuel vector, which would be central to transportation considerations. Indeed, it is because of these reasons that H_2 is for the fuel-of-choice for space craft propellant.

Despite the conventional combustion of H_2 releasing substantial energy, an even more desirable mode of consumption is *via* the direct conversion to electricity through the use of fuel cells. Fuel cells, specifically the archetypal Proton Exchange Membrane (PEM) fuel cells (Figure 1.1), convert hydrogen fuel and oxygen—which is present in the air—to water *via* redox reactions, and generate an electrical current in the process (Ball and Wietschel, 2009).

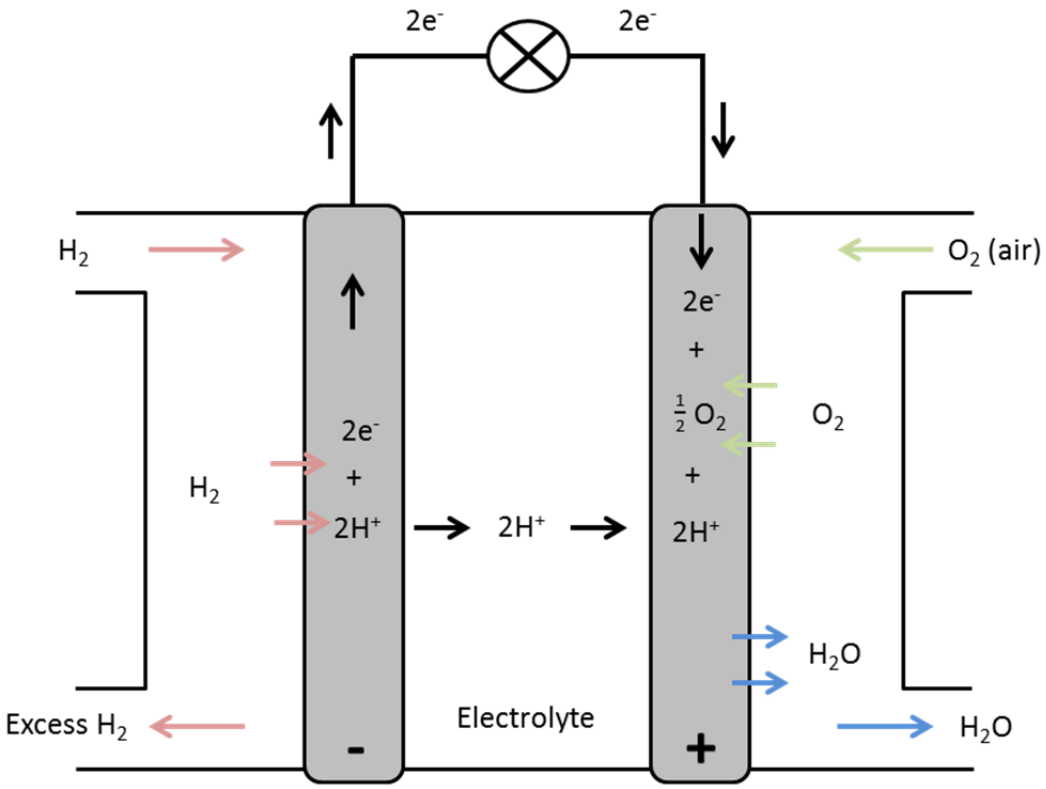

Figure 1.1 Schematic of the Proton Exchange Membrane (PEM) fuel cell. Hydrogen fuel is introduced to the anode where it is oxidised to H^+ and electrons. The H^+ ions are free to move through the eponymous selectively permeable membrane (not shown), present in the electrolyte, to the cathode. Meanwhile the electrons must travel to the cathode through the external circuit, which generates an electric current. Simultaneously, the cathode is supplied with oxygen, present in air, which is reduced to O^{2-}. The O^{2-}, H^+ and electrons react to from water, which is drained away from the fuel cell. Adapted from Ball and Wietschel (2009).

Unlike combustion, fuel cells avoid high temperatures that risk the production of pollutant nitrogen oxides, and they operate at two-to-three times the efficiency of standard internal combustion engines (Cracknell *et al*., 2008). However, despite these advantages, there are drawbacks to current fuel cell technology. In order to allow the reaction to occur at industrially viable rates, the electrodes are coated with precious metal catalysts, often platinum. Whilst these catalysts solve the problem of slow reaction rates, they themselves introduce new obstacles against the adoption of fuel cells, and thus hydrogen fuel, on a large scale. The first such caveat is the rarity of these metals. This means that they are not only prohibitively expensive, but perhaps means there is too little to permit worldwide adoption of such

technologies. The second is that these catalysts are highly sensitive to common impurities associated with H_2, such as carbon monoxide and hydrogen sulfide. As such the average lifespan of a PEM fuel cells is just 167 days, whereas that required for a commercially viable cell is estimated to be approximately five years (Aki *et al*., 2005). Whilst palladium is half the price of platinum, and has been shown to have higher catalytic properties than platinum in certain conditions (Antolini, 2009), it is still too expensive and rare to be used on any truly widespread basis.

Hydrogen is the most abundant element in the Universe; however a combination of its low density and high reactivity mean that very little is readily available on Earth. As such, hydrogen synthesis is required for industrial applications. At present the majority of H_2 production is for a feedstock to the Haber-Bosch process; an artificial nitrogen-fixation process to produce ammonia, which is an important industrial commodity that is required for fertiliser synthesis, amongst other products. Of the numerous chemical processes involved in industrial hydrogen production at present, the most prominent is the steam reformation of methane (Gallucci *et al*., 2006), a summary of which is shown in Equation 1.2.

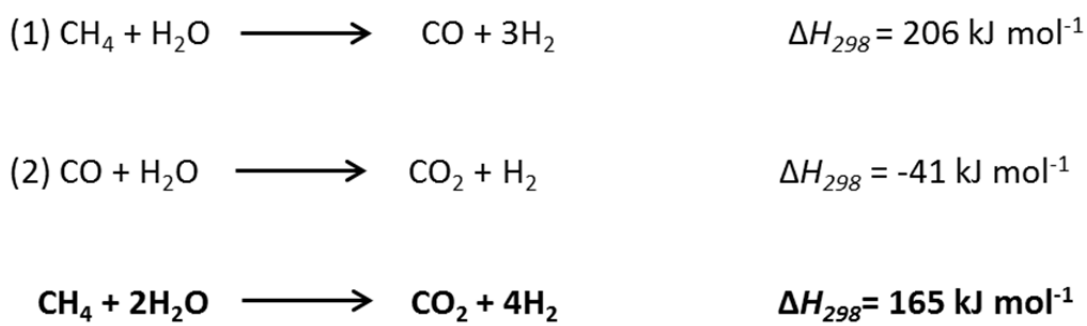

Equation 1.2 Steam Reformation of Methane. The steam reformation of methane is currently the predominant mode of synthesis for H_2 on an industrial scale, and can be split into two stages. The first step (1) involves the reaction of methane with steam to form carbon monoxide and hydrogen. This is an endothermic process, requiring heat of at least 850 ^{o}C in the presence of a metal catalyst (often nickel). The second step (2) allows for further H_2 liberation *via* reaction of the evolved CO with more steam in a mildly exothermic reaction. Overall (**bold**), the process yields 4 moles of molecular H_2 per mole of methane in an endothermic reaction.

However, if H_2 is to be used as a widespread fuel in the future, steam reformation is not the answer, with multiple facets of the requisite reactions making it unsuitable. The use of CH_4 as substrate means that, far from replacing fossil fuels, H_2 derived in this manner is actually dependent on them. Similarly, it can be seen from Equation 1.2 that steam reformation also results in CO_2 emissions, and thus it does not meet the desired green credentials required of a future fuel. Indeed, it has been estimated that this process, for the synthesis of ammonia alone, resulted in almost 200 million tons of CO_2 globally; 0.7% of total CO_2 emissions in 2009 (US Environemental Protection Agency, 2008). It has even been suggested that steam reformation of methane actually emits more CO_2 per mole of carbon than merely burning fossil fuels directly (Romm, 2004). The high temperatures and pressures also mean steam methane reformation is energy intensive. Whilst proof-of-principal attempts have been made to carry out this reaction at lower temperatures (Lazarus *et al*., 2009), they have problems with upscaling to industrial levels.

Effectively the reverse reaction of that which occurs in fuel cells, the electrolysis of water is another approach that could potentially be used to produce H_2 in a renewable manner (providing the electricity used was not derived from fossil fuels). However, yet again common objections to this are that it is too energy intensive to viable on the industrial scale. It is proposed that such commercial electrolysis would require 50 kWh to produce just 1kg of H_2, an efficiency of just 70% (Romm, 2004). Furthermore, if electrolysis were to be adopted as the sole means of H_2 fuel production, replacing just 50% of ground vehicle transportation fuels as predicted to be used by 2025 in the US with H_2 would require about as much electricity as the total amount used in the US at present (Romm, 2004). The process is also expensive, with the use of rare metals such a platinum as catalysts (Barreto *et al*., 2003), although more recently a nickel catalyst has been reported (Gong *et al*., 2014).

It is thus evident that the current state of the ‘hydrogen economy’ is critically hampered by the processes used in both the production and consumption of H_2 fuel. From the ultimate

continued reliance on fossil fuels, a lack of efficiency or the cost of materials, hydrogen could never be the solution to sate the planet's future energy needs if current technology was to be relied upon. Further research is needed to either improve these technologies or devise new ones.

1.4 **Biohydrogen**

It has hitherto been established in this Thesis that the current methods for hydrogen evolution and consumption are unsuitable for the further upscaling that would be required to make H_2 a widespread fuel. Instead of these aforementioned abiotic processes, perhaps the answer to permitting the worldwide adoption of H_2 as a fuel may lie with *biohydrogen* (henceforth bioH_2): i.e. molecular hydrogen derived from biological means.

3.6 billion years ago, at the dawn of life on Earth, hydrogen was abundant in the atmosphere (Tian *et al*., 2005). Aside from allowing the efficient formation of organic compounds vital for life, this highly-reducing atmosphere was also a source of energy for the primitive lifeforms living on the primeval planet. Along with H_2, carbon monoxide was also abundant in the early atmosphere. It is known that some extant species of Bacteria and Archaea can actually produce H_2 during autotrophy using CO as a carbon source (Sokolova *et al*., 2004); likely a relic from ancestral species. Intriguingly these facts have partly helped shape the search for extra-terrestrial life, as Mars is known to have an atmosphere similarly rich in H_2 and CO (Weiss *et al*., 2000). Indeed, relics of this ancient link with hydrogenases and energy derivation may be seen in present day species, such as *E. coli* (see Section 1.7.3).

Currently, bioH_2 evolution is observed in prokaryotic and eukaryotic microbes, and is generated by a variety of metabolic processes. One such process is through the biophotolysis of water by (oxygenic) photosynthetic organisms such as green algae and cyanobacteria (Gaffron and Rubin, 1942; Gest and Kamen, 1949). H_2 can also be generated by another route in some cyanobacteria, specifically as a consequence of nitrogenase enzyme activity during nitrogen fixation (Bothe *et al*., 2010). Another route to microbial biohydrogen production is photo-fermentation in (anoxygenic) photosynthetic bacteria, such as purple non-sulfur bacteria, which produce H_2 as a result of the assimilation of small organic compounds (Eroglu and Melis, 2011). It has been proposed that these organisms could be harnessed to produce H_2 for use as a biofuel. However, problems with performing these reactions on an industrial scale

are that most of these reactions are inhibited by oxygen, and so, with the exception of the anoxygenic photosynthesis in purple non-sulfur bacteria, H_2 yield will be adversely affected by one of the essential substrates for the reactions. Furthermore, it would be difficult to ensure such reactions would have maximal exposure to light to allow for maximum turnover if carried out on a large scale (say in an industrial-scale vat). Another problem is that the enzymes involved naturally operate at low efficiency in terms of H_2 evolution. For example, biophotolysis is estimated to transfer only 0.2% of light energy into the hydrogen evolved (Hallenbeck and Benemann, 2010). Because of these factors H_2 production may be too low *via* these processes to be industrially viable (McKinlay and Harwood, 2010).

A fourth source of bioH_2 is dark fermentation. A variety of bacteria such as Clostridia and the Enterobacteriaceae are able to evolve hydrogen under anaerobic conditions, without the need for light, during mixed acid fermentation. In such conditions, enteric bacteria derive ATP from glycolysis, where glucose or other carbon sources are oxidised to pyruvate by three main routes: primarily the Embden-Meyerhof-Parnas (EMP) pathway, but also the Entner-Doudoroff (ED) pathway and the Pentose Phosphate (PP) pathway (Figure 1.2) (Neidhardt *et al*., 1990). The latter pathway allows for re-direction of other metabolites to and from both the EMP and ED pathways. It is also essential in the generation of many essential metabolites, such as vitamins, nucleotides and several amino acids, as well as the production of the reducing equivalent NADPH (Romeo and Snoep, 2005; Neidhardt *et al*., 1990).

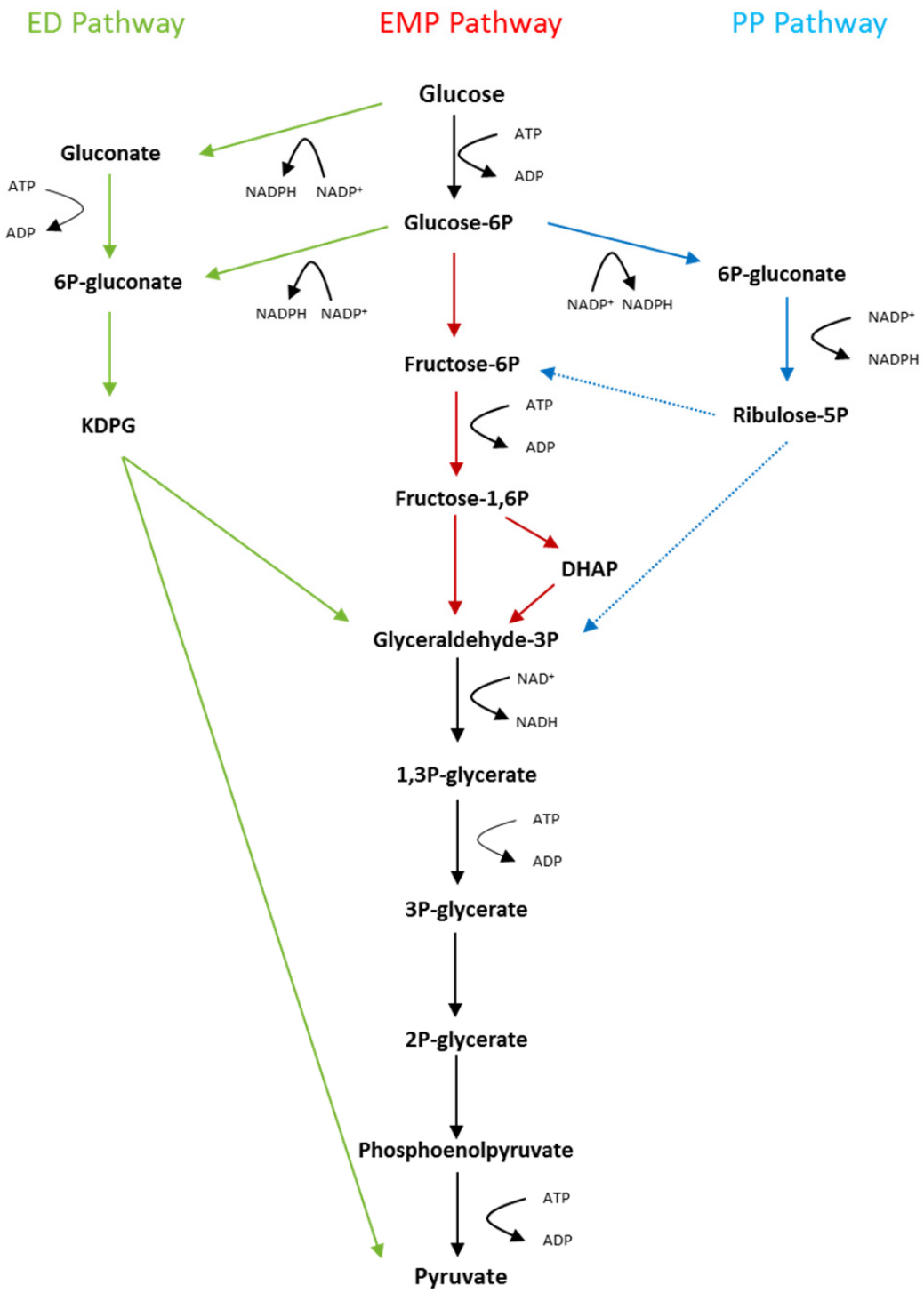

Figure 1.2 Modes of glycose catabolism in prokaryotes. Glycolysis leads to the generation of pyruvate from glucose or other carbon sources with the net generation of ATP. Reactions corresponding to the three main modes of glucose degradation in *E. coli* are colour-coded. Red: Embden-Meyerhof-Parnas (EMP) pathway; Green: Entner-Doudoroff (ED) pathway; Blue: Pentose Phosphate (PP) pathway (dashed arrows represent abridged reactions). Black arrows represent reactions common to all three glycolysis modes. Abbreviations: KDPG: 2-keto-3-deoxy-6-phosphogluconate; DHAP: Dihydroxyacetone-phosphate. Note: For each molecule of glucose entering the EMP pathway, two glyceraldehyde-3-phosphate molecules are converted to pyruvate, thus there is a net gain of 2 mol ATP and 2 mol NADH per mol glucose. Adapted from Chen *et al*. (2016).

The EMP pathway yields a net gain of 2 moles of ATP per mole of glucose oxidised to pyruvate, whilst the ED pathway only yields one (Flamholz *et al*., 2013). In producing this ATP, reducing equivalents are generated: 2 moles of NADH per mol glucose for the EMP pathway, and 1 mole of NADH and one mole NADPH per mol glucose for the ED pathway (Chen *et al*., 2016). In order to maintain redox balance and allow glycolysis to persist, the cell employs downstream reactions to recover NAD^+ (Figure 1.3). This yields a variety of end products, the majority of them organic acids, from where mixed acid fermentation derives its name. One such acid, formate, can subsequently be converted to H_2 by the action of the formate hydrogenlyase (FHL) complex, which will be discussed in more detail in Section 1.7.3.

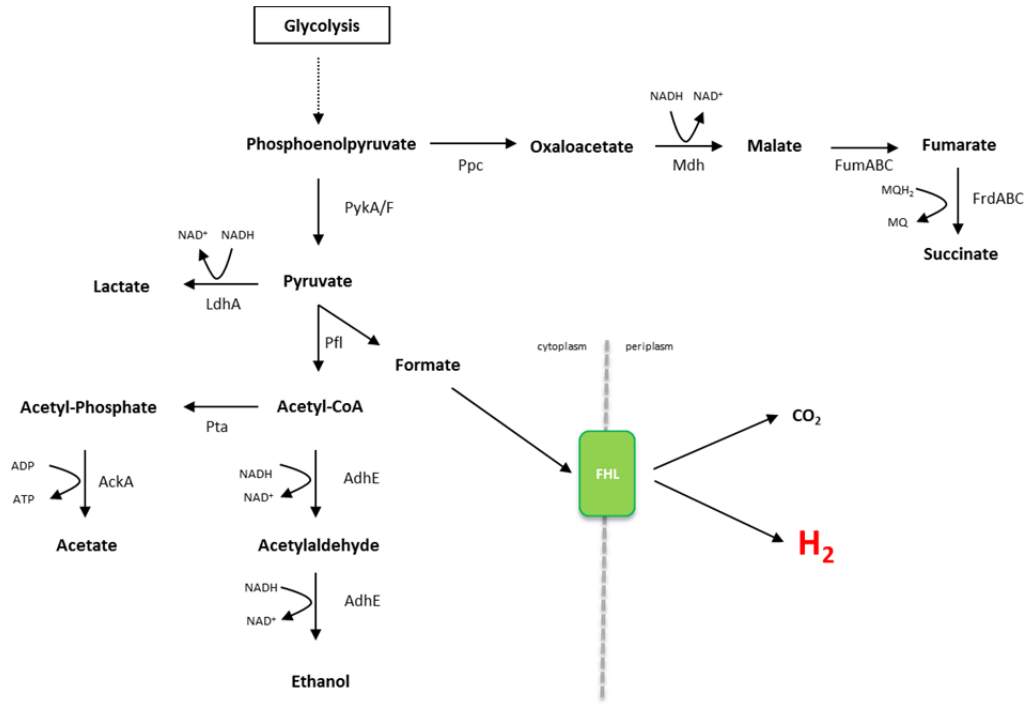

Figure 1.3 Mixed acid fermentation in enteric bacteria results in H_2 production. Under fermentative conditions *E. coli* degrades glucose to a variety of organic acids and ethanol. One such product, formate, can be further processed by the FHL complex to evolve H_2. For simplicity, only one mode of pyruvate generation is shown, specifically the Embden–Meyerhof–Parnas (EMP) Pathway, which is the predominant mode of glycolysis. However two other pathways also exist in *E. coli*: the Pentose Phosphate pathway, and the Entner-Doudoroff pathway. Enzyme abbreviations: Ppc: phosphoenolpyruvate carboxylase; Mdh: malate dehydrogenase; FumABC: fumarase; and FrdABC: fumarate reductase PykA/F: pyruvate kinase; LdhA: lactate dehydrogenase; Pfl: pyruvate formate lyase Pta: phosphotransacetylase; AckA: acetate kinase; AdhE: alcohol dehydrogenase. FHL: formate hydrogenlyase (containing Hyd-3).

The employment of dark fermentation is seen as a particularly appealing method of bioH_2 production due to the heterotrophic nature of the microbes involved. Their varied biochemistry permits them to utilise the large quantities of carbohydrate waste produced as a result of agriculture and other industries (Levin *et al*., 2007). This has important implications with regards to developing an environmentally-sustainable fuel as it would not only provide a green source of hydrogen, but it would assist in waste management; a pertinent consideration given the escalating cost of landfill (Bartelings *et al*., 2005). BioH_2 generated in this manner is derived from organic waste, and can therefore be seen as a second generation biofuel. Compared to the steam reformation means of H_2 generation, bioH_2 can be synthesised at ambient temperatures and does not produce pollutants or (net) greenhouse gasses. Indeed, it has been estimated that greenhouse gas emissions are reduced by as much as 73%, and energy expenditure reduced by 79% during bioH_2 generation compared to H_2 synthesis *via* the steam reformation of methane (Manish and Banerjee, 2008).

Unfortunately, as with the other methods of current bioH_2 generation previously discussed, the main caveat with dark fermentation at present is that these metabolic processes do not naturally run at the efficiencies required for industrial-scale H_2 production. Fermentation tends to have low yields due to incomplete substrate-to-product conversion, for example the maximum yield of H_2 from *E. coli* is bottle-necked to 2 mol per mol of glucose, or 4 mol H_2 per mol glucose in *Clostridia* (Hallenbeck and Ghosh, 2012).

1.5 **Hydrogenase enzymes**

From the previous section discussing the current methods of biohydrogen generation, it should be apparent that it is pertinent to better understand the processes entailed in microbial hydrogen metabolism if it is to become a viable method for industrial-scale synthesis of H_2. A key aspect to any such research will of course focus heavily on the enzymes catalysing such reactions, of which proteins known as hydrogenases are the predominant.

Despite their being a complex group of metalloenzymes, hydrogenases catalyse a very simple reaction: namely the reversible oxidation of molecular hydrogen to protons and electrons (Equation 1.3) (Lubitz *et al*., 2014). However, in physiological setting this often coupled to other electron donors/acceptors.

$$H_2 \longleftrightarrow 2H^+ + 2e^-$$

Equation 1.3 Hydrogenases catalyse the reversible oxidation of molecular hydrogen to protons and electrons.

Hydrogenases are pervasive in nature, and found not just in bacteria, but also in Archaea and even some eukaryotes. Examples of the latter include parasitic protozoa such as *Trichomonas vaginalis*; the anaerobic fungi e.g. *Neocallimastix frontalis*; and green algae such as *Chlamydomonas* spp. (Vignais and Billoud, 2007). In such cases they reside in organelles; either chloroplasts in green algae or in specialised hydrogen-metabolising structures known as hydrogenosomes in the case of the former two examples. In these instances hydrogenosomes replace mitochondria as the site of ATP generation; indeed they are themselves degenerate mitochondria (Muller, 1993; Vignais and Billoud, 2007).

Hydrogenases are classified into three distinct categories depending on the metal cofactors present in their active site. To date three such classes have been discovered: nickel-iron [NiFe], iron-iron [FeFe], and iron [Fe]-hydrogenases. Species often contain multiple hydrogenases,

usually of the same classification, but some may possess both [NiFe] and [FeFe]-hydrogenases (Vignais and Billoud, 2007). Similarly, methanogens contain four [NiFe]-hydrogenases and one [Fe]-hydrogenase (Thauer *et al*., 2010). Interestingly, it is believed that the three classes of hydrogenase arose separately and are thus examples of convergent evolution (Shima *et al*., 2008).

Hydrogenase research is crucial in allowing for the improvement in bioH_2 yields, i.e. the *in vivo* production of H_2. However the enzymes may also be recruited for *in vitro* applications for H_2-related technology, either in the production or consumption of H_2. For example, it has been proposed that a 'semi-artificial' device for the (sun)light-driven electrolysis of water could be possible, using anchored Photosystem II on one electrode to split water (Badura *et al*., 2006), and a Photosystem I/hydrogenase complex on the other to evolve H_2 (Lubner *et al*., 2010).

Similarly, proof-of-principal work has shown that hydrogenases can replace platinum as the catalyst in fuel cells, alleviating both the associated problems of expense and sensitivity to common impurities present in steam reformation-derived H_2, and without compromising activity (Cracknell *et al*., 2008; Jones *et al*., 2002; Lubitz *et al*., 2014).

1.5.1 [Fe]-hydrogenases

[Fe]-hydrogenases, which are alternatively called '[Fe-S] cluster free hydrogenases', are the least studied class (Vignais and Billoud, 2007). First discovered in *Methanothermobacter marburgenesis*, specifically the hydrogenase named 'Hmd' (hydrogen forming methylenetetrahydromethanopterin [methylene-H_4MPT^+] dehydrogenase), [Fe]-hydrogenases are only found in some methanogenic archaea and deviate from the archetypal characteristics found in [NiFe] and [FeFe]-hydrogenases. The enzymes harbour a unique single iron cofactor: Fe-guanylyl pyridinol (Fe-GP), and they contain no [Fe-S] clusters (Lubitz *et al*., 2014). [Fe]-hydrogenases exhibit a different mechanism-of-action in *lieu* of these electron-relay structures

that requires the simultaneous recruitment of the co-substrate methylene-H_4MPT^+, as well as H_2. Unlike, [NiFe] and [FeFe]-hydrogenases, where the active site conformation is static, buried in the protein, the binding of methylene-H_4MPT^+ opens the enzyme and allows H_2 to access the catalytic site directly, and so removes the need for electron relay (Shima *et al*., 2008). An illustration of the [Fe]-hydrogenase active site is shown in Figure 1.4A.

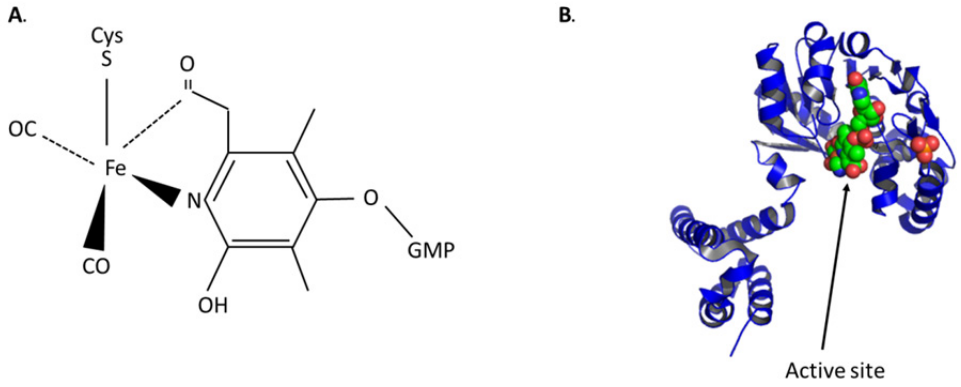

Figure 1.4 [Fe]-hydrogenase architecture. (**A**) The active site is centred on a single iron atom core, anchored into the enzyme via coordination to a cysteine residue. Non-protein ligands are carbonyl and cyanides, in additional to a novel FeGP cofactor (Thauer *et al*., 2010). (**B**) Crystal structure of the [Fe]-hydrogenase from *Methanocaldococcus jannaschii* shows the active site and an absence of [Fe-S] clusters in the monomeric holoenzyme (PDF file 3DAF) (Shima *et al*., 2008).

Another characteristic of [Fe]-hydrogenases that distinguishes them from the other classes of hydrogenases is that the oxidation of H_2 produces a proton and a hydride ion (H^-), as opposed to two protons and two electrons (Shima *et al*., 2008) and this is a crucial step in the formation of methane from carbon monoxide and hydrogen (Thauer *et al*., 2010). This unique mode-of-operation does not lend [Fe]-hydrogenases well for the utilisation of hydrogenases in technological applications due to there being no electron flow, and so no electrical current.

1.5.2 [FeFe]-hydrogenases

[FeFe]-hydrogenases are found predominantly in the Gram-positive Firmicutes, but also in the (Gram-negative) gamma and delta Proteobacteria (Vignais and Billoud, 2007). Furthermore they are the sole class of hydrogenases found in eukaryotes.

Intriguingly, [FeFe]-hydrogenase-like sequences have been identified in the genomes of higher eukaryotes, including the human genome, specifically genes encoding nuclear perlamin A recognition factor (Narf) proteins. Narf proteins possess two [4Fe-4S] clusters and show particularly close sequence identity to the H-cluster active site of [FeFe]-hydrogenases, although they do not contain the di-iron cofactor moiety, and resultantly exhibit no hydrogenase activity (Lubitz *et al*., 2014).

Although exceptions exist, [FeFe]-hydrogenases tend to be monomeric (Vignais and Billoud, 2007), containing the active site and [Fe-S] clusters. The consensus model of the active site consists of a di-iron core coordinated to CN^- and CO ligands and a di-sulfur bridge. Each Fe is linked to two separate CN^- ligands, and the same di-sulfur bridge in addition to the same CO ligand. The exact nature of the di-sulfur bridge has not been confirmed but is likely to be a CH_2, NH/NH_2^+, or O ligand (Mulder *et al*., 2011). One of the Fe ions, called the 'proximal Fe', has a unique ligand in the form of a [4Fe-4S] cubane cluster, linked via a cysteine residue. The proximal Fe is further linked to a CO ligand that is separate to the bridging CO ligand mentioned previously. The other Fe is instead coordinated by CO and CN ligands. (Mulder *et al*., 2011). This unique arrangement of the [FeFe] hydrogenase active site is called the 'H-cluster' (Ghirardi *et al*., 2007). The H-cluster configuration is shown in Figure 1.5A.

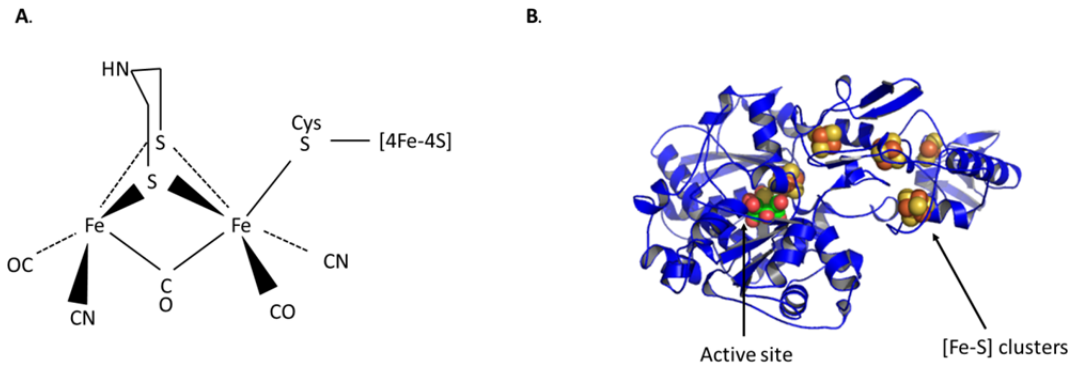

Figure 1.5 [FeFe]-hydrogenase architecture (**A**) The H-cluster active site of [Fe]-hydrogenases**.** The 2Fe sub-cluster core is coordinated by various cysteine residues, but also non-protein ligands. The proximal Fe is linked, by way of a cysteine, to a cubane [4Fe-4S] cluster (Ghirardi *et al*., 2007). (**B**) Structure of the monomeric [FeFe]-hydrogenase from *Clostridium pasteurianum* (PDB File 1FEH) (Peters *et al*., 1998).

This complex formation does not form spontaneously and requires a number of accessory proteins for proper assembly. Three such maturases (HydE, HydF and HydG) have been identified for this purpose. HydG belongs to the radical S-adenosylmethionine (SAM) family and is thought to use tyrosine to generate the CO and CN^- ligands and so help generate a $Fe_2S_2(CO)_4(CN)_2$ precursor to the H-cluster using an [4Fe-4S] cluster. This is transferred to HypF, which adheres the cubane [4Fe-4S] cluster to the proximal Fe atom. HydE generates the di-sulfur bridging ligand and this is incorporated into the forming H-cluster, likely involving the action of the C-terminal GTP-ase in HypF (Lubitz *et al*., 2014; Shepard *et al*., 2010). HydF then inserts the complete H-cluster into the HydA apoprotein forming the holoenzyme (McGlynn *et al*., 2007). HydF is known to contain a GTP-ase domain, and it is possible this is necessary for inducing interaction between HydE, HydG and HydF.

Some [FeFe]-hydrogenases contain no [Fe-S] clusters beyond the one present in the H-cluster, however in those that do contain extra cofactors the clusters are either [2Fe-2S] or [4Fe-4S] in nature and are called ‘F-clusters’ (Lubitz *et al*., 2014; Mulder *et al*., 2011). The cytoplasmic [FeFe] hydrogenase in *Clostridium pasteurianum*, the crystal structure of which helped first

elucidate the architecture of these enzymes, contains four such F-clusters: three [4Fe-4S] and one [2Fe-2S] (Peters *et al*., 1998) (Figure 1.5B).

[FeFe]-hydrogenases typically show a catalytic bias towards H_2 evolution (Mulder *et al*., 2011) although the *Desulfovibrio vulgaris* periplasmic [FeFe]-hydrogenase is known to be involved in H_2 oxidation physiologically (Caffrey *et al*., 2007).

1.5.3 [NiFe]-hydrogenases

[NiFe] hydrogenases are the most abundant and extensively studied of the three hydrogenase classes (Vignais and Billoud, 2007). Crystallography studies on enzymes from the *Desulfovibrio* genus were crucial in elucidating the general structure of [NiFe]-hydrogenases (Higuchi *et al*., 1997; Matias *et al*., 2001; Volbeda *et al*., 1995). Unlike [Fe] and [FeFe]-hydrogenases, all [NiFe]-hydrogenases consist of (at least) two subunits of different sizes: a large subunit which houses the active site and a smaller unit which contains a minimum of one [4Fe-4S] cluster for electron transfer, which sits near the active site and is called the 'proximal cluster' (Bleijlevens *et al*., 2004). In reality many [NiFe]-hydrogenases contain additional clusters. In the standard *D. gigas* type [NiFe]-hydrogenase, for example, three clusters are present in the small subunit, two [4Fe-4S] and one [3Fe-4S], and are bound *via* conserved cysteine and histidine residues (Volbeda *et al*., 1995) (Figure 1.6B).

The conserved [NiFe]-hydrogenase active site consists of a two-metal [NiFe] core that is found deep inside the large subunit, anchored to the protein *via* coordination by the sulfurs of four cysteine residues. Two of these thiolates coordinate Ni only, whilst the other two bridge between both the Ni and Fe. The Fe is further coordinated by three non-protein ligands: one carbonyl and two cyanides (Bleijlevens *et al*., 2004; Ohki *et al*., 2008). A further ligand is found in a bridging position between the Ni and Fe in the oxidised form of the enzyme - often an O, S

or OH – whereas in the reduced form this is replaced with a hydride (H^-) (Ohki *et al*., 2008). An illustration of the [NiFe]-hydrogenase active site is shown in Figure 1.6A.

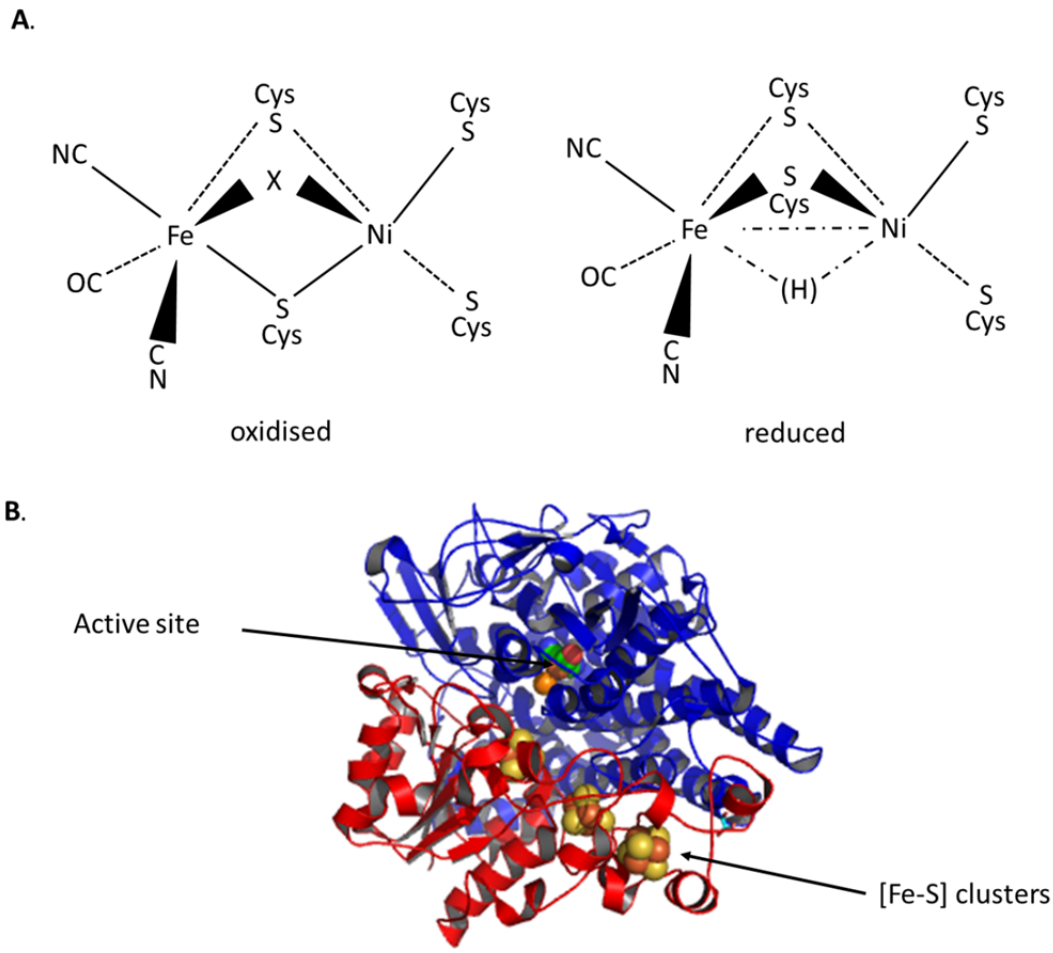

Figure 1.6 [NiFe]-hydrogenase architecture. (**A**) Consensus structures of the [NiFe]-hydrogenase active site in both oxidised and reduced forms**.** Four cysteines coordinate the NiFe core along with cyanide and carbonyl groups. The additional bridging atom is represented by 'X' in the oxidised form, which may either be an oxygen, sulfur or hydroxyl group. In the reduced form this is replaced by a hydride. (**B**) Holoenzyme structure of [NiFe]-hydrogenase for *Desulfovibrio gigas*. The large subunit, coloured blue, contains the active site, whilst the small subunit (red) possesses the three [Fe-S] clusters (PDB file 1YQ9) (Volbeda *et al*., 1995).

Unlike in [FeFe]-hydrogenases, where the CO ligands are derived from tyrosine, their source is uncertain in [NiFe]-hydrogenase biosynthesis. Recent research indicates CO_2 may be the source (Soboh *et al*., 2013), although other studies have proposed acetate (Roseboom *et al*.,

2005) and others have suggested atmospheric CO (Lenz *et al.*, 2007) or some other metabolic precursor instead of acetate are utilised (Burstel *et al*., 2011). The cyanide is synthesised from a carbamoyl phosphate (Sargent, 2016).

The distance between the Ni species and proximal [Fe-S] cluster is further than that found in the [FeFe]-hydrogenase H-cluster, at 11 Å compared to 4 Å, respectively (Lubitz *et al*., 2014). The large subunit also possesses a hydrophobic gas channel provides a route for H_2 to gain access to the buried active site from the protein surface (Fontecilla-Camps *et al*., 2007).

The [NiFeSe]-hydrogenases are a subclass of the [NiFe]-hydrogenases but differ in that one of the cysteine ligands coordinating the Ni is substituted with a selenocysteine (Fauque *et al*., 1988). These are widespread in sulfur-reducing bacteria such as *Desulfomicrobium baculatum* (Garcin *et al*., 1999). In this species, the [NiFeSe] enzyme has been shown to be remarkably resistant to product inhibition, maintaining H_2 evolution activity (*in vitro*) even in 100 % H_2. It has been postulated that is due to the Se-Cys residue selenol group having a more acidic pK_a (5.2) than the thiol group of a cysteine (8.0); allowing it to more readily be able to donate protons to the active site (Parkin *et al.* 2008). Furthermore, [NiFeSe] hydrogenases also exhibit O_2 tolerance, with activity persisting in 1% O_2 (Parkin *et al*., 2008). This has important biotechnological implications as both of these characteristics would be desirable in enzymes to maximise yield during the industrial-scale H_2 production.

The pervasiveness of [NiFe]-hydrogenases has resulted in a diverse range of physiological roles across species, although these can be grouped into five broad classes: (1) Uptake [NiFe]-hydrogenases; (2) Cyanobacterial uptake [NiFe]-hydrogenases and H_2 sensors; (3) Bidirectional heteromultimeric cytoplasmic [NiFe]-hydrogenases; (4) Membrane-associated, energy conserving and H_2-producing [NiFe]-hydrogenases; and (5) Actinobacterial, high-affinity H_2-oxidising hydrogenases (Constant *et al*., 2011; Greening *et al*., 2016; Vignais and Billoud, 2007).

1.5.4 Group 1: Uptake [NiFe]-hydrogenases

As exemplified by the extensively studied *Desulfovibrio* enzymes, hydrogenases in Group 1 are characterised by being periplasmically-orientated in Gram-negative bacteria and usually link H_2 oxidation to the reduction of quinones by way of association with a third subunit comprising a di-haem cytochrome complex, either cytochrome *b* or *c* (Pandelia *et al*., 2012). Group 1 enzymes are thus involved in respiration, and are a means of energy derivation from H_2, *via* the generation of a proton motive force (pmf). Often this is during anaerobic respiration, with final electron acceptors such as nitrate, fumarate or sulfate (Pandelia *et al*., 2012). In these cases the hydrogenases are often O_2 sensitive, however a subclass are O_2 tolerant, and have garnered interest due to their biotechnological implications, with examples being the *Cupriavidus necator* membrane bound hydrogenase (MBH) (Goldet *et al*., 2008), the *E. coli* Hyd-1 (Lukey *et al*., 2010) or HaseI from *Aquifex aeolicus* (Brugna-Guiral *et al.,* 2003). Intriguingly, in some O_2 tolerant hydrogenases the final electron acceptor is actually O_2, and thus there are instances of hydrogenases involved in aerobic respiration (Vignais and Billoud, 2007). Oxygen tolerance is discussed in more detail in Section 1.6.

The periplasmic orientation of these hydrogenases necessitates the export of the peptides across the inner membrane. Whilst many peptides are exported in an unfolded state *via* the general secretory (Sec) pathway, Group 1 [NiFe]-hydrogenases are translocated in a fully folded state *via* the twin-arginine translocation (Tat) pathway (Palmer and Berks, 2012). They are targeted to this pathway *via* a signal peptide present at the N-terminus of the small subunit that contains a Tat-motif; so named because of the twin-arginine residue pair present in the consensus sequence (**RR**XFXK). The hydrogenase large subunit does not contain a Tat signal peptide itself and is co-translocated *via* association with the small subunit; a phenomenon termed 'hitch-hiking' (Rodrigue *et al*., 1999). Thus, the presence of a long N-terminal signal peptide sequence containing a Tat motif is another characteristic of Group 1 [NiFe]-hydrogenases.

1.5.5 Group 2: Cyanobacterial uptake [NiFe]-hydrogenases and H_2 sensors

Unlike Group 1 [NiFe]-hydrogenases, Group 2 enzymes are located in the cytoplasm, owing to their not having a Tat-signal peptide and have characteristic deletions in their small subunits when compared to the enzymes in Group 1 (Vignais and Billoud, 2007). The Group 2 enzymes are further split into Group 2a, comprising uptake enzymes found in cyanobacteria that are induced during nitrogen fixation, and re-oxidise H_2 evolved by nitrogenase activity (Tamagnini *et al*., 2002), and Group 2b, which are so called 'regulatory hydrogenases'; sensing the presence of hydrogen and allowing for resultant expression of uptake hydrogenase genes. A prominent example of this is the regulatory hydrogenase (RH) native to *Cupriavidus necator*. The Group 2 [NiFe]-hydrogenases also exhibit oxygen-tolerance, although by a different method to that employed in the O_2-resistant subset of Group 1 enzymes. This will be discussed in more detail in Section 1.7.

1.5.6 Group 3: Bidirectional heteromultimeric cytoplasmic [NiFe]-hydrogenases

Group 3 [NiFe]-hydrogenases are well represented in Archaea and form complexes with additional subunits containing a variety of cofactors such a NAD^+, $NADP^+$ or cofactor F_{420} (8-hydroxy-deazaflavin). They exhibit bidirectional activity. An example in Archaea is the F_{420}-non-reducing hydrogenase (MvH) native to *Methanothermobacter marburgensis,* which links H_2 oxidation to heterodisulfide reduction, which is an important step in methanogenesis (Stojanowic *et al*., 2003). Again, an example of a Group 3 [NiFe]-hydrogenase in Bacteria is found in *C. necator*, specifically the Soluble Hydrogenase (SH); indeed this was the first identified NAD^+-dependent tetrameric [NiFe]-hydrogenase identified (Schneider and Schlegel, 1976).

1.5.7 Group 4: Membrane-associated, energy-conserving and H_2-producing [NiFe]-hydrogenases

Hydrogenases in Group 4 consist of more subunits than the other classes, at a minimum of six, and have a physiological role of removing excess reducing equivalents from the cell. Perhaps the archetypal enzyme of this group is Hyd-3 from *E. coli*, which forms part of the seven-subunit formate hydrogenlyase (FHL) complex and permits H_2 (and CO_2) evolution from the oxidation of formate, and thus acts as a preventative mechanism against low pH (Sawers, 2005). Hyd-3 is discussed in more detail in Section 1.9.3. Most Group 4 enzymes identified to date are found in Archaea, and an example is the membrane bound [NiFe]-hydrogenase of *Methanosarcina barkeri*, which generates H_2 from ferredoxin, which is firstly reduced *via* the oxidation of acetate to CO_2, thus conserving energy (Kunkel *et al*., 1998).

1.5.8 Group 5: Actinobacterial, high-affinity H_2-oxidising [NiFe]-hydrogenases

The most recent class of [NiFe]-hydrogenases to be identified – although potentially better described as a subclass of Group 1 (Greening *et al*., 2016) – enzymes in this class are characterised by exhibiting H_2-oxidative activity in very low H_2 conditions, akin to that in the atmosphere, with a K_m < 100ppm (Constant *et al*., 2010). Abundant in soil-dwelling Actinobacteria where they are expressed during periods of carbon and oxygen limitation (Berney and Cook, 2010), these enzymes are thus conducive to the utilisation of atmospheric H_2 as an energy source. Indeed, this activity is thought to account for much of the soil-based uptake of H_2, which is the main sink for atmospheric hydrogen (Constant *et al*., 2009). Whilst abundant in the eponymous Actinobacteria, this class of hydrogenase has also been found in Proteobacteria. The Actinobacterial Hydrogenase (AH) from *Cupriavidus necator*, for example, was the first hydrogenase of this type characterized biochemically in its purified form (Schafer *et al*., 2016). It has been reported that the AH maintains activity even in the 70 % oxygen

conditions, leading to the conclusion that the enzyme is oxygen insensitive. It is also highly tolerant to pH and temperature fluctuations (Schafer *et al*., 2016). However unlike other Group 5 enzymes, the AH exhibits a low rate of catalysis.

1.6 **Hydrogenase inhibitors, and adaptations to counter these**

Considering the complex nature of hydrogenases, from their intricate architecture to the multitude of maturase proteins required for proper assembly (see Section 1.8), it should be no surprise that their catalytic activity is sensitive to a broad range of compounds. H_2 evolution is rapidly inhibited by formaldehyde in [FeFe]-hydrogenases, although the reverse reaction is inhibited to a far lesser degree, and interestingly the formaldehyde also acts as a protectant against the stronger H_2-oxidation inhibitors of CO and O_2. By way of contrast, formaldehyde only weakly affects [NiFe]-hydrogenase activity (Wait *et al*., 2011). Examples of [NiFe]-hydrogenase inhibitors include diphenylene iodonium, (Magnani *et al*., 2000), azide, heavy metals (copper and mercury) and *N*-bromosuccinimide (Sawers and Boxer, 1986).

Numerous gases may also inactivate hydrogenases. For example, nitric oxide abolishes [NiFe]-hydrogenase activity by way of interactions with both the active site and the [Fe-S] clusters (Ceccaldi *et al*., 2016). Likewise the inhibitory effects of carbon monoxide of hydrogenases has been long known (Purec *et al*., 1962). However, when viewed from the standpoint of trying to maximise H_2 yield for industrial-scale production, the most important inhibitor of hydrogenases is undoubtedly O_2.

1.6.1 O_2 tolerance in hydrogenases

The fixation of energy into bioH_2 by microbes is potentially rather high. For example, it has been estimated that as much as 10% of the energy in sunlight could be captured by the biophotolytic method of H_2 production (Liebgott *et al.*, 2011). Unfortunately this level is unable to be achieved using native hydrogenases due to their sensitivity to O_2. As the other product of biophotolysis is O_2, the process is severely product-inhibited. Even if dark fermentation was to be used as the mode of H_2 production, the use of batch cultures or even continuous flow

cultures would mean transient exposure to oxygen that could at least temporarily impede hydrogenase activity.

Addressing oxygen sensitivity in hydrogenases is therefore a crucial measure with the long term aim of the industrial-scale production of bioH_2. Different hydrogenases show different sensitivities towards oxygen, with some being irreversibly inactivated upon exposure to O_2. Examples of these are the [FeFe]-hydrogenases, where O_2 induces H-cluster degradation (Lambertz *et al*., 2011). Others, indeed the majority of [NiFe]-hydrogenases, are only transiently inactivated, and removal of O_2 and replacement with H_2 or other reducing agents such as DTT allow for the resumption of activity over the course of hours. So-called O_2-tolerant hydrogenases exhibit a similar transient inactivation by O_2; however they can resume function in a far shorter time-frame (minutes). Last, some enzymes may be truly oxygen-resistant and show no decrease in activity during aerobic conditions. By understanding the mechanisms that for allow O_2 tolerance, so it is hoped that the same principles could be used to engineer tolerance in industrially relevant hydrogenases. This is particularly important as naturally O_2 tolerant hydrogenases are usually less active than their O_2-sensitive counterparts; with H_2 oxidation activity reduced by approx. five times (Liebgott *et al*., 2011). By such engineering it would be hoped that naturally O_2 sensitive hydrogenases would maintain higher activity, but have tolerance built in.

1.6.2 Unusual redox potentials and enzyme kinetics

Oxygen tolerance in the Group 1 [NiFe]-hydrogenases is conferred by way of an unusual proximal [Fe-S] clusters, as found in the *C. necator* MBH (Fritsch *et al*., 2011) and *E. coli* Hyd-1 (Volbeda *et al*., 2012). Normally the proximal cluster has [4Fe-4S] architecture, and is coordinated to the small subunit by four cysteine residues. However in the case of O_2-tolerant Group 1 enzymes the proximal cluster is [4Fe-3S] and is anchored to the polypeptide by two

additional, or 'supernumerary', cysteines that are replaced by glycines in O_2-sensitive proteins (Lukey *et al*., 2011).

The proposed model is that in normal O_2-sensitve hydrogenases exposure to O_2 necessitates the expenditure of four electrons, otherwise required for catalytic activity, in order to prevent the formation of reactive oxygen species, which could damage or block the active site (Cracknell *et al*., 2008). The resultant electron deficiency about the active site after O_2 attack means that, on return to more reducing conditions, it takes time for the enzyme to revert to functionality. Supernumeric cysteines are thought to be important due being able to more quickly allow for donation of electrons to the active site after inactivation. Indeed, the additional cysteine was found to be particularly pertinent for O_2-tolerance when it coordinated the [Fe-S] cluster at the side adjacent to the active site, supporting this model (Lukey *et al*., 2011).

Electron paramagnetic resonance (EPR) spectroscopy studies had revealed a correlation between these kinetics in response to oxygen presence and specific active site redox states. The state exhibited by O_2-sensitive [NiFe]-hydrogenases after O_2 exposure, where in reducing conditions reactivation of the enzyme is slow, is termed Ni-A or the 'unready state' (Volbeda *et al*., 2005). Conversely, the redox state adopted by O_2 tolerant hydrogenases on exposure to oxygen, allowing for quick resumption of activity on return to reducing conditions was termed the Ni-B or 'ready' state (Volbeda *et al*., 2005). There has been some debate as to the exact chemical differences underpinning the difference between Ni-A and Ni-B states, but it has been suggested that the Ni-A state possesses a di-oxygen ligand, possibly hydro-peroxide, (Volbeda *et al*., 2005), or a mono-oxygen ligand (Barilone *et al*., 2015) that Ni-B states do not.

The Regulatory Hydrogenase (RH) from *Cupriavidus necator* exhibits another deviation from the canonical [Fe-S] architecture that has been suggested to be involved in conferring O_2 tolerance. Instead of the standard configuration of two [4Fe-4S] and one [3Fe-4S] clusters, the RH small subunit (HoxB) instead possesses three [4Fe-4S] clusters (Shafaat *et al.*, 2013).

The aforementioned O_2 tolerance exhibited by [NiFeSe] hydrogenases has been hypothesised to be due to the weaker interactions between the selenol functional group and oxygen compared to those seen in interactions between thiol groups and oxygen. As such the Se-O bond in any inactive [NiFeSe] active site state may be easier to reduce (and so restore activity) compared to the equivalent situation in [NiFe] hydrogenases (Parkin *et al.* 2008).

1.6.3 Modifications to gas channels

A second adaptation to confer O_2 tolerance in hydrogenases is exemplified by the Group 2 regulatory hydrogenases such as the RH from *C. necator* and HupUV from *Rhodobacter capsulatus* (Buhrke *et al*., 2005a; Duche *et al*., 2005) and consists of modifications to the gas channel spanning between the large subunit protein surface and the buried active site (Vignais and Billoud, 2007).

In O_2 sensitive hydrogenases the gas channel is composed of residues with relatively small side-chains, however in O_2 tolerant cases these may be replaced with 'bulkier' residues, which can impede O_2 molecule movement by steric hindrance, but still permit the passage of the smaller H_2 molecules (Liebgott *et al*., 2011). For example, replacing the relatively large phenylalanine and isoleucine residues normally present at the end of this channel in the *C. necator* RH with the smaller valine and leucine (as found at the same locations in the O_2 sensitive hydrogenase from *D. gigas*) made the RH sensitive to oxygen (Buhrke *et al*., 2005a).

An attempt was made by Liebgott *et al.* (2011) to engineer tolerance in the normally O_2 sensitive [NiFe] hydrogenase of *Desulfovibrio fructosovorans via* replacement of Valine 74 and Leucine 122 with residues that had larger side-chains. Some reduction in O_2 diffusion was seen, but O_2 movement was found to also be disrupted when residues of similar volumes but different chemical properties to Val and Leu, such as polarity and hydrophilicity, were introduced (Liebgott *et al*., 2011). For example, a V74D substitution slowed diffusion rates by a

factor of 40, despite aspartate having a volume 40% smaller than valine (Liebgott *et al*., 2011) These findings therefore demonstrate that molecule diffusion rate through the channel is not merely dependent steric hindrance, but may also be influenced by the chemical nature of the channel-forming residues as well.

The replacement of the two residues with methionines resulted in even greater O_2 tolerance, inactivating slower and reactivating quicker on exposure to oxygen (Liebgott *et al*., 2011). Steric hindrance still contributed, however the quicker reactivation rate was due to the chemical properties of methionine. The sulfur found in this amino acid is known to participate in oxidative stress responses due to its ability to form S-O bonds on exposure to reactive oxygen species (Chakrabarti and Pal, 2001). Thus, it could be that methionine can allow for an arrangement of oxygen bound to the active site that made it easier to protonate, and thus be removed. This would account for why the methionine substitutions result in a quicker reactivation after O_2 exposure in addition to a slower inactivation.

1.6.4 Additional maturation proteins

Another route to O_2 tolerance is exemplified in the soluble hydrogenase (SH) from *C. necator*. This Group 3 [NiFe]-hydrogenase operates under aerobic conditions to generate NADH; i.e. to allow the reduction of NAD^+ to NADH through the oxidation of H_2. Normally the proper formation of the active site of [NiFe] hydrogenases requires a minimum of six accessory proteins, HypA-F. However, the formation of the SH active site necessitates an additional maturation protein known as HypX. This maturase may allow for additional cyanide ligand coordination to the Ni and Fe; features not seen in O_2 sensitive [NiFe]-hydrogenases (Figure 1.7) (Bleijlevens *et al*., 2004) (Happe *et al*., 2000). However, other spectroscopic studies contradict this, suggesting these additional ligands do not exist, and that the SH active site has a standard [NiFe] arrangement (Horch *et al*., 2010; Lauterbach *et al*., 2011).

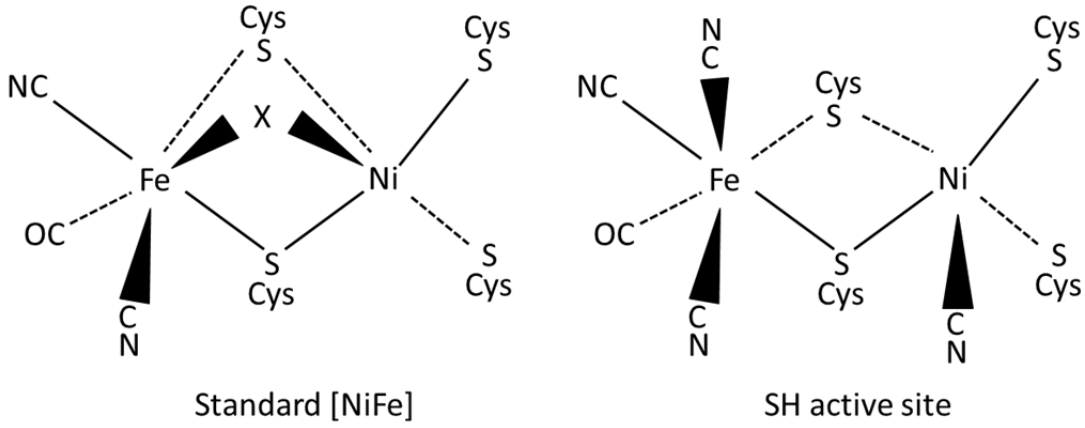

Figure 1.7 Comparison of the active sites in standard O_2 sensitive [NiFe]-hydrogenases and a possible active site arrangement of the SH from *C. necator*. The standard [NiFe]-hydrogenase active site is based on the crystal structure obtained from *Desulfovibrio gigas* (Volbeda *et al*., 1996) compared to that predicted in SH (Van der Linden *et al*., 2004).

1.7 **The hydrogenases of *E. coli***

The enteric bacterium *Escherichia coli* has long been a model organism in both microbiology and biotechnology, but in more recent times the [NiFe]-hydrogenases it possesses have become paradigms themselves in hydrogenases research (Sargent, 2016). Furthermore, with the possibility of dark fermentation being an industrially-relevant mode of bioH_2 production in the future, the understanding of such Enterobacteriaceae hydrogenases may in fact have direct biotechnological implications.

E. coli possesses genes encoding four [NiFe]-hydrogenase enzymes (Andrews *et al*., 1997; Sawers, 1994). Expressed under different conditions, Hyd-1, Hyd-2 and Hyd-3 are inner membrane-anchored proteins that have been confirmed to exhibit hydrogenase activity in a physiological setting (Ballantine and Boxer, 1985; Sawers *et al*., 1985). Hyd-1 and Hyd-2 are Group 1 [NiFe]-hydrogenases, periplasmically orientated (and thus requiring export *via* the Tat pathway) and perform H_2 oxidation, coupling it to quinone reduction. On the other hand, Hyd-3 is located on the cytoplasmic side of the inner membrane and, functioning as part of the FHL complex, undertakes H_2 evolution (Bohm *et al*., 1990).

1.7.1 Hyd-1

Hyd-1 is encoded by the *hyaABCDEF* operon (Menon *et al*., 1991) (Figure 1.8A). The large subunit is encoded by *hyaB* and contains the [NiFe] active site. The small subunit, encoded by *hyaA*, possesses a C-terminal transmembrane helix anchor as well as three [Fe-S] clusters, a proximal [4Fe-3S], medial [3Fe-4S] and distal [4Fe-4S] (Lukey *et al.* 2010; Volbeda *et al*., 2012). HyaA also possesses an N-terminal Tat signal peptide to allow for translocation of the fully folded protein, in conjunction with the associated HyaB, over the inner membrane and into the periplasm. An associated transmembrane cytochrome *b* subunit encoded by *hyaC* couples hydrogen oxidation in the periplasm to quinone reduction at the cytoplasmic side of the

membrane (Figure 1.8B) (Sargent, 2016). This implicates Hyd-1 as a scalar proton pump that could generate a proton electrochemical gradient that could be used for ATP synthesis (Menon *et al.* 1991). When this is considered in conjunction with its high expression in the stationary phase, the likely conclusion is that Hyd-1 is a 'hydrogen scavenger': utilising extracellular hydrogen for respiration in low nutrient environments. Indeed, it has been proposed many times that Hyd-1 may actually function to partly recycle the hydrogen produced by Hyd-3 during fermentation (Zbell and Maier, 2009). Although Hyd-1 was originally described as being bidirectional *in vitro* (Sawers and Boxer, 1986), more recent electrochemical work suggests that Hyd-1 is unidirectional, showing only H_2-oxidising activity (Lukey *et al*., 2010). This unidirectionality may be important when it is considered that Hyd-1 is likely involved in energy conservation. This is because H_2 production by reverse electron transport through Hyd-1 would collapse the pmf. Whilst Figure 1.8B shows Hyd-1 as an isolated trimer, from crystallography studies it is hypothesised that the enzyme is in fact physiologically active as $(HyaABC)_2$ dimer of trimers (Volbeda *et al*., 2012).

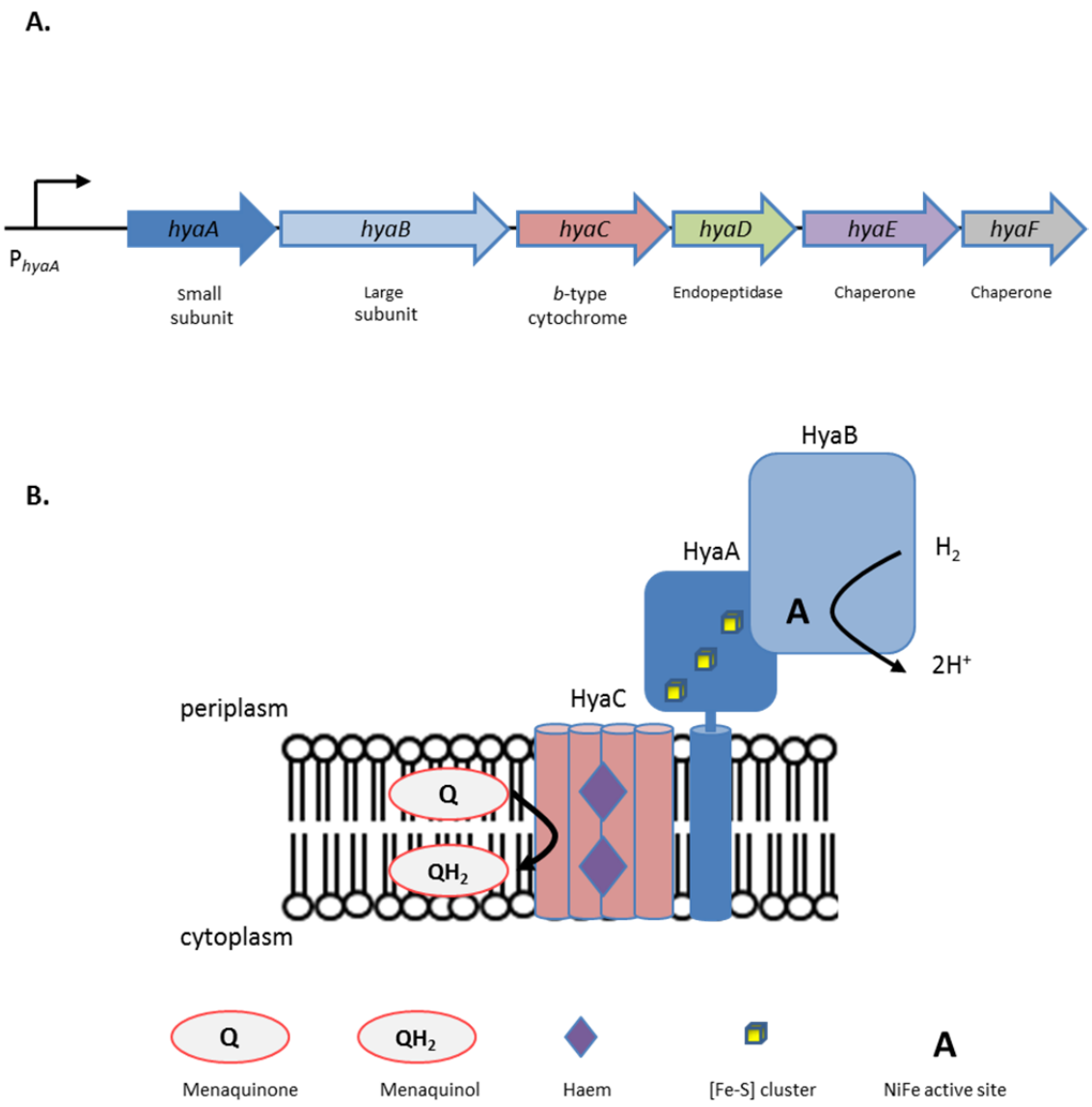

Figure 1.8 The *E. coli* Hyd-1 isoenzyme. (**A**) Hyd-1 is encoded by the *hyaABCDEF* operon. The *hyaABC* genes encoded the structural components of the enzyme, whereas *hyaDEF* encode proteins involved in the proper assembly of the complex. (**B**) Illustration of the trimeric Hyd-1 complex. Orientated towards the periplasm, the active site-containing large subunit, HyaB, associates with HyaA, the small subunit, which possesses three [Fe-S] clusters. This allows for electron relay between the active site and the cytochrome *b*-type membrane subunit HyaC, which ultimately allows for the H_2 dependent replenishment of the quinone pool.

While *hyaABC* encode the structural proteins of Hyd-1, the products of *hyaDEF* are required for proper assembly of the enzyme. The *hyaD* gene encodes a Hyd-1 specific protease that cleaves the C-terminal domain of HyaB after active site insertion (Bock *et al.*, 2006). HyaE is a chaperone protein that associates with HyaA in the cytoplasm preventing premature Tat

translocation, a process termed ‘proof-reading’ (Dubini and Sargent, 2003). Intriguingly, HyaE is not essential for the production of functional Hyd-1 during anaerobiosis (Dubini *et al*., 2002); and the same result has been noted in homologues in other species that encode O_2-tolerant, Group 1 [NiFe]-hydrogenases (Manyani *et al*., 2005; Schubert *et al*., 2007). It has been speculated that HyaE and its homologues may therefore be important in ensuring the proper insertion of the [3Fe-4S] proximal cluster, which is known to confer the O_2-tolerace in this class of hydrogenases (Sargent, 2016).

The role of HyaF is unclear, despite the availability of a crystal structure of a homologue to scrutinise (Parkin and Sargent, 2012). It was once thought that HyaF was involved in active site nickel incorporation (Menon *et al*., 1991), however later work suggested this was not the case (Dubini *et al*., 2002). However homologues in other species have suggested it may play a role as a chaperone during Tat translocation, and thus a similar role to HyaE (Schubert *et al*., 2007). A further similarity between the proteins is that, like HyaE, HyaF was not found to be essential for Hyd-1 assembly (Dubini *et al*., 2002).

The *hya* operon is induced by the anaerobic regulators, AppY and ArcA/ArcB transcriptional regulatory system, with Hyd-1 most abundant during stationary phase, and in the presence of formate (Atlung *et al*., 1997; Richard *et al*., 1999; Sawers and Boxer, 1986). The transcriptional regulator FNR (fumarate and nitrate reductase) is known to be required for Hyd-1 activity (Sawers *et al*., 1985), but this is not down to FNR-mediated induction of the *hya* operon, but rather some *nik* and *hyp* operon genes encoding essential maturases (Messenger and Green, 2003). FNR is a cytoplasmic regulator that acts to inhibit aerobically-associated and induce anaerobically-associated gene expression, and senses oxygen by way of a labile [4Fe-4S] that is converted to [2Fe-2S] in the presence of O_2 (Khoroshilova *et al*., 1997).

Expression of the genes encoding Hyd-1 and Hyd-2 is inhibited by IscR, which is the (negative) transcriptional regulator of [Fe-S] cluster biosynthesis (Giel *et al*., 2006). Hyd-1 and Hyd-2 synthesis is also repressed in the presence of nitrate *via* the action of the dual regulators NarP

and NarL (Richard *et al*., 1999). It has been proposed that this occurs because the cell may preferentially utilise intracellular formate during the anaerobic respiration of nitrate as opposed to gaseous H_2 (Sargent, 2016).

1.7.2 Hyd-2

The second hydrogenase found in *E. coli*, Hyd-2, is encoded by the *hyb* operon (Figure 1.9A) and its predicted structure is shown in Figure 1.9B. The *hybC* gene encodes the large, active site-containing subunit; *hybO* codes for the small subunit; while *hybA* encodes a ferredoxin-type component that possesses [Fe-S] clusters, relaying electrons released by H_2 oxidation through the integral membrane proteins, HybB so quinone reduction can take place (Dubini *et al*., 2002). Thus, despite being classed as a Group 1 [NiFe]-hydrogenase, Hyd-2 deviates from the archetypal structure (large and small hydrogenase subunits in conjunction with a cytochrome) in that it is probably tetrameric (Vignais and Billoud, 2007). The *hyb* operon contains genes encoding accessory proteins; specifically *hybDEFG*. Two of the gene products, HybF and HybG, are homologues of the general maturase proteins encoded in the *hyp* operon, HypA and HypC, respectively (Blokesch *et al*., 2001; Blokesch *et al*., 2004). Like HyaD for Hyd-1, a protein with which it shares a high degree of similarity, HybD is an endopeptidase required for proper assembly of the Hyd-2 enzyme *via* its cleaving of the C-terminal peptide sequence of the HybC large subunit (Fritsche *et al*., 1999). HybE is a Hyd-2 specific Tat proof-reading chaperone protein, binding specifically to the precursor form of HybO, but not the final, fully folded and [Fe-S]-bearing form of the protein (Dubini and Sargent, 2003; Jack *et al*., 2004).

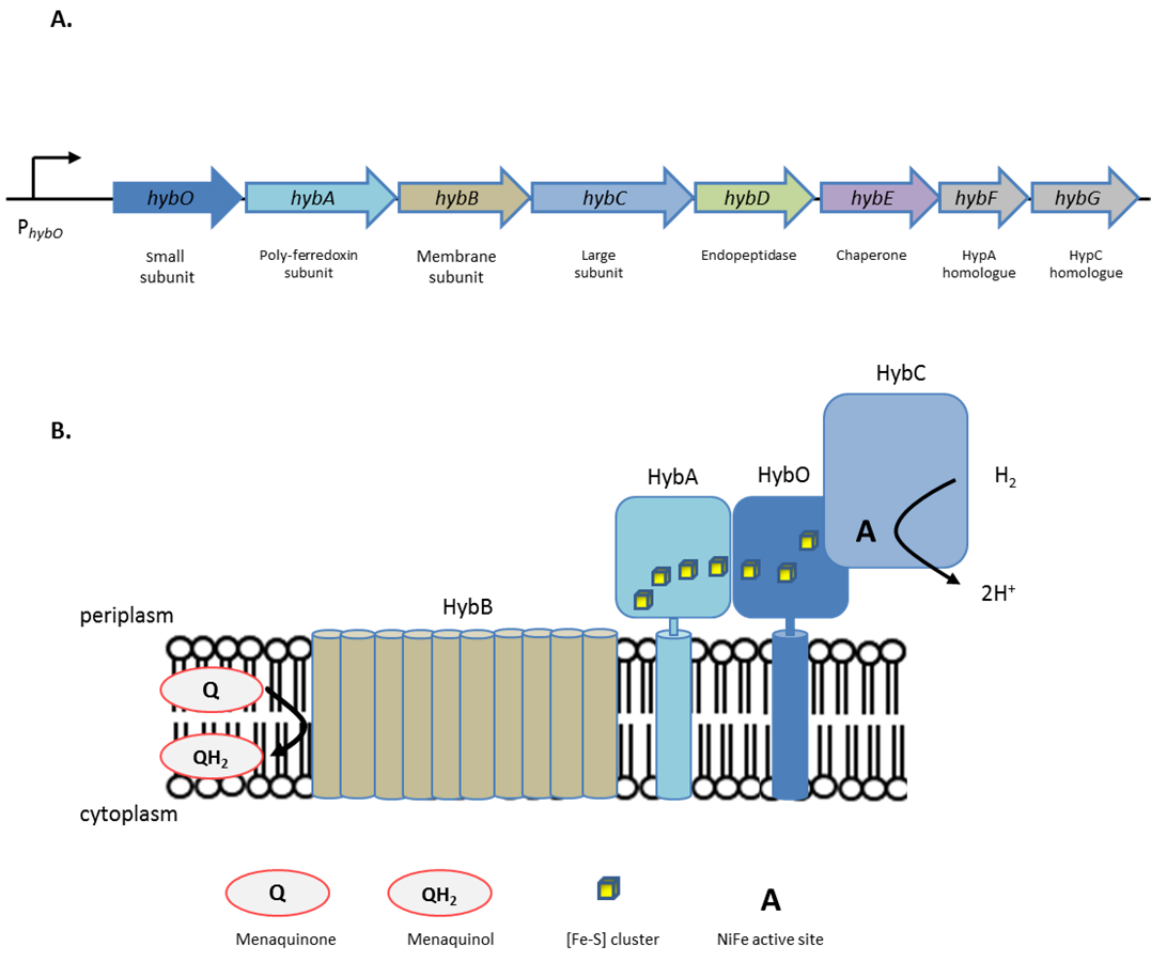

Figure 1.9 The Hyd-2 isoenzyme from *E. coli*. (**A**) Hyd-2 is encoded by the *hybOABCDEFG* operon. The *hybOABC* genes encode the structural components of the complex itself, whilst *hybDEFG* encode proteins involved in enzyme assembly. (**B**) The large subunit, HybC, contains the [NiFe] active site and is associated with the membrane-bound small subunit, HybO, which contains three [Fe-S]. In turn, this interacts with a second membrane-bound ferredoxin protein, HybA, which is predicted to contain four [Fe-S] clusters. The final subunit is HybB, a 10 transmembrane domain protein that helps anchor Hyd-2 to the inner membrane .Note: whilst not illustrated in the figure, it may be that quinone pool reduction occurs at HybA instead.

The genes encoding Hyd-2 are most highly expressed during anaerobic respiration with glycerol and fumarate (Ballantine and Boxer, 1985). Whilst this correlates with an increase in levels of FNR (Sawers *et al*., 1985), there is no FNR site in the in the *hyb* promoter region (Richard *et al*., 1999). Thus, as for Hyd-1, this correlation is due to the FNR-dependent expression of the *hyp* maturase and *nik* nickel transporter operons (Lutz *et al*., 1991; Messenger and Green, 2003). Another similarity of Hyd-2 synthesis with that of Hyd-1 is that it is completely repressed by the presence of nitrate (Richard *et al*., 1999). Unlike the *hya*

operon, expression of the *hyb* operon is not influenced by AppY (Richard *et al*., 1999). Another deviation from Hyd-1 is that Hyd-2 does not exhibit O_2 tolerance (Lukey *et al*., 2010). The reduction of the quinone pool by Hyd-2 is known to be essential for the activity of fumarate reductase during fumarate respiration (Dubini *et al*., 2002). In low-potential - and so anaerobic - conditions Hyd-2 has been shown to function as a respiratory uptake enzyme (Laurinavichene *et al*., 2002). Hyd-2 has been shown to be capable of bidirectional activity *in vitro*, with speculation that any such *in vivo* activity may allow the enzyme to act as an 'electron release valve', catalysing the reverse reaction if the quinone pool becomes over-reduced (Lukey *et al.* 2010). More recently this supposition was confirmed, with Hyd-2 being shown to be a *bona fide* bidirectional enzyme physiologically, with the 'reverse reaction' of H_2 evolution from the oxidation of (mena)quinol being driven by the pmf (Pinske *et al*., 2015a).

1.7.3 Hyd-3

H_2 production in *E. coli* occurs during anaerobic conditions and in the absence of external electron acceptors (i.e. during fermentation). Such mixed acid fermentation of sugars results in a number of products such as ethanol, lactate and formate. These are normally transported outside of the cell to prevent intracellular pH from falling. Formate is exported by the FocA channel (Doberenz *et al*., 2014; Suppmann and Sawers, 1994). It can then be oxidised extracellularly by formate hydrogenases O or N provided there are electron acceptors available. However, under fermentative conditions where no such external electron acceptors are present, formate is transported back into the cell. Here the H_2-evolving formate hydrogenlyase complex (FHL)—which includes Hyd-3— disproportionates formate to hydrogen and carbon dioxide (Sawers, 2005). Such activity is thought to protect the cell from acidic pH (Sawers *et al*., 1985). Formate hydrogenlyase is a membrane-bound, cytoplasm-orientated enzyme comprised of seven subunits (Figure 1.10B). Being the hydrogenase responsible for the

majority of H_2 evolution in *E. coli*, any work aimed at the augmentation of biohydrogen yield will have a strong focus on Hyd-3.

A Group 4 [NiFe]-hydrogenase, Hyd-3 is encoded by the *hycABCDEFGHI* operon (Figure 1.10A), with *hycBCDEFG* encoding the structural subunits. The active site-containing large subunit is encoded by *hycE*, whilst the (probable) small subunit is the product of *hycG* (Rossmann *et al*., 1994; Sauter *et al*., 1992). HycB and HycF are small [Fe-S] cluster-containing proteins (Sauter *et al*., 1992), whilst HycCD comprise membrane proteins anchoring the complex to the inner membrane. Together with formate dehydrogenase H, encoded by *fdhF* (Sawers *et al*., 1985), which is present elsewhere on the chromosome, these proteins associate to form the FHL complex (Figure 1.10B). The proteins produced from *hycAHI* are accessory proteins. HycA is a regulatory gene that acts antagonistically to FhlA, repressing *hyc* operon transcription (Sauter *et al*., 1992). HycI is the endopeptidase required for C-terminal processing of HycE to form the mature enzyme (Rossmann *et al*., 1995; Sauter *et al*., 1992). The role of HycH is currently unknown, however there are indications that it may involve some interaction with HycE and/or HycC, particularly *in lieu* of HycG (McDowall *et al*., 2015).

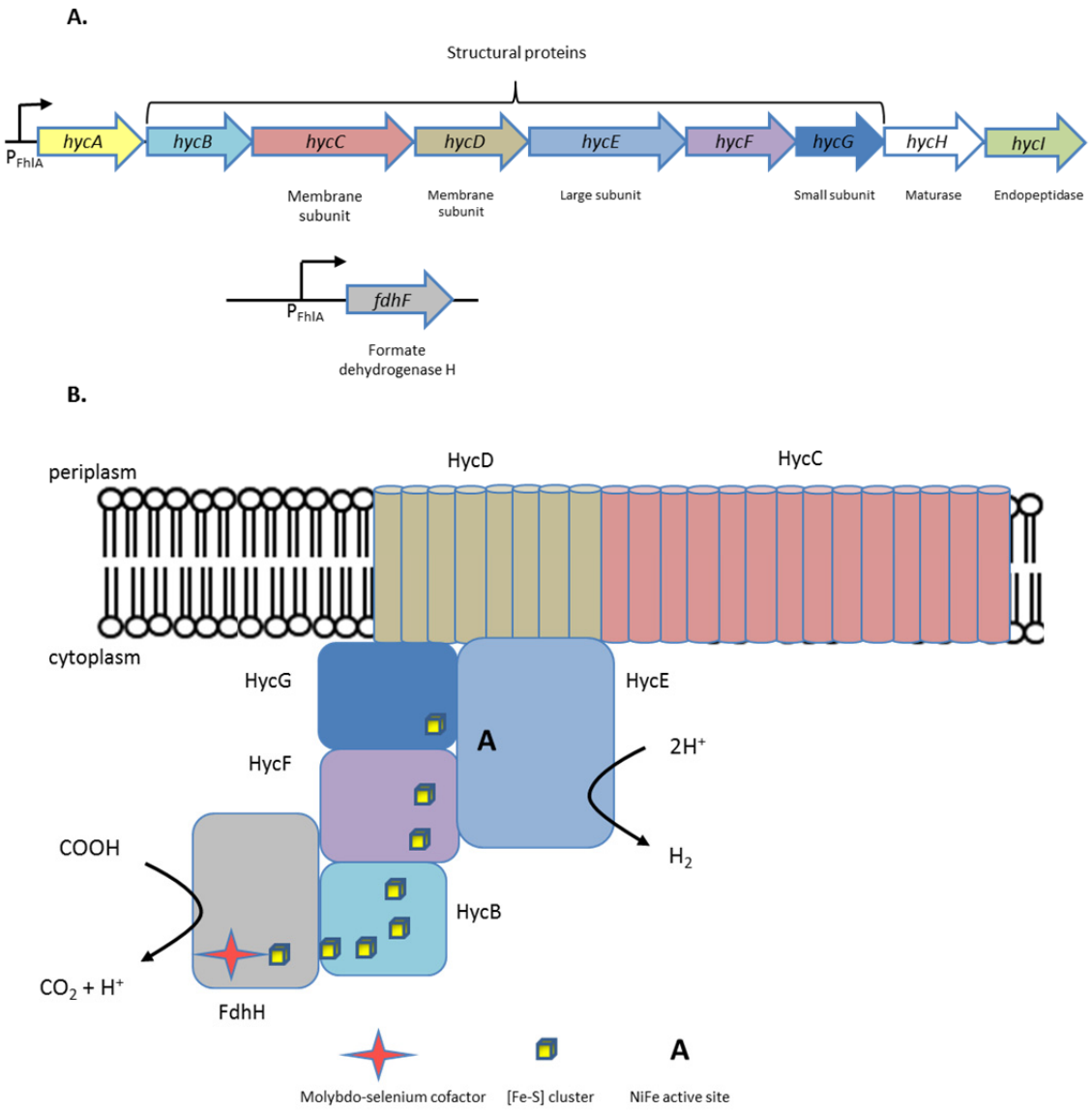

Figure 1.10 Hyd-3/ FHL of *E. coli*. (**A**) Hyd-3 is encoded by the *hycABCDEFGHI* operon. Whilst *hycAHI* are accessory genes involved in both gene transcription and enzyme assembly, *hycBCDEFG* encode the structural components of Hyd-3. Together with formate dehydrogenase H, which is encoded by *fdhF* located elsewhere in the genome, these form the formate hydrogenase lyase (FHL) complex. (**B**) Physiologically, Hyd-3 associates with formate dehydrogenase H to form the FHL complex. This seven subunit complex comprises two membrane-bound proteins HycC and HycD. The soluble domain is orientated in the cytoplasm, and consists of formate dehydrogenase H, which catalyses the oxidation of formate. The electrons released by this process are relayed through [Fe-S] clusters present in HycB, HycF and HycG to the Hyd-3 large subunit, HycE, where they are utilised by the [NiFe] active site to reduce protons to H_2.

The expression of the *hyc* operon is controlled by the positive transcriptional regulator FhlA, a functional homotetramer that shares some resemblance to NtrC regulators but is not modulated by phosphorylation (Vignais and Billoud, 2007). Instead FhlA functions in the

presence of formate (Sawers, 2005). Similarly, *fdhF* and the maturase encoding *hyp* operon are also regulated in this manner (Sawers, 2005). This so-called 'formate regulon' is illustrated in Figure 1.11. Additional control of the *hyc* operon is performed by the transcription factor ModE, is involved in the operation of molybdenum-related genes (Self *et al*., 1999).

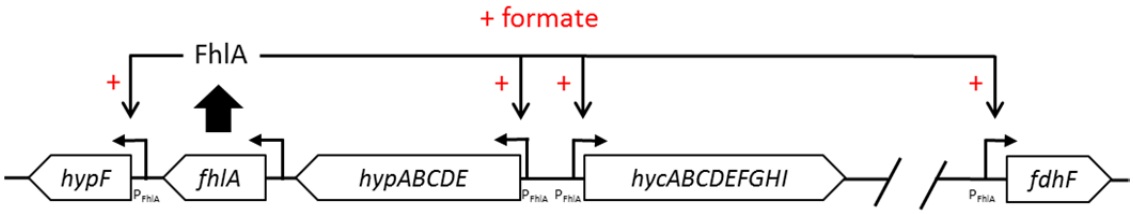

Figure 1.11 The formate regulon. *fhlA* is constitutively expressed to produce the positive transcriptional regulator FhlA. In this presence of formate, this then acts to in turn induce expression of both the operons encoding the FHL complex (*hycABCDEFGHI* and *fdhF*) and also the maturases required for [NiFe] active site formation (*hypABCDE* and *hypF*). Adapted from Sawers(2005).

An intriguing similarity exists between the both the genetic sequences (Bohm *et al*., 1990) and protein structures (Efremov and Sazanov, 2012) of FHL and respiratory Complex I (NADH: quinone oxidoreductase). A crucial component of the electron transport chain, Complex I couples NADH oxidation to the reduction of quinones, and in doing so pumps H^+ ions across the membrane. Indeed Complex I is responsible for 40% of the proton gradient (Efremov and Sazanov, 2012). The resultant pmf can be used by ATP synthase to generate ATP. All subunits of the FHL complex exhibit homology with subunits of Complex I; with HycE, HycG, HycF, HycB, FdhH, HycC and HycD sharing sequence identity with the *E. coli* Complex I subunits of NuoC & D, NuoB, NuoI, NuoG N-terminus, NuoG C-terminus, NuoL and NuoH respectively (Efremov and Sazanov, 2012) (Figure 1.12).

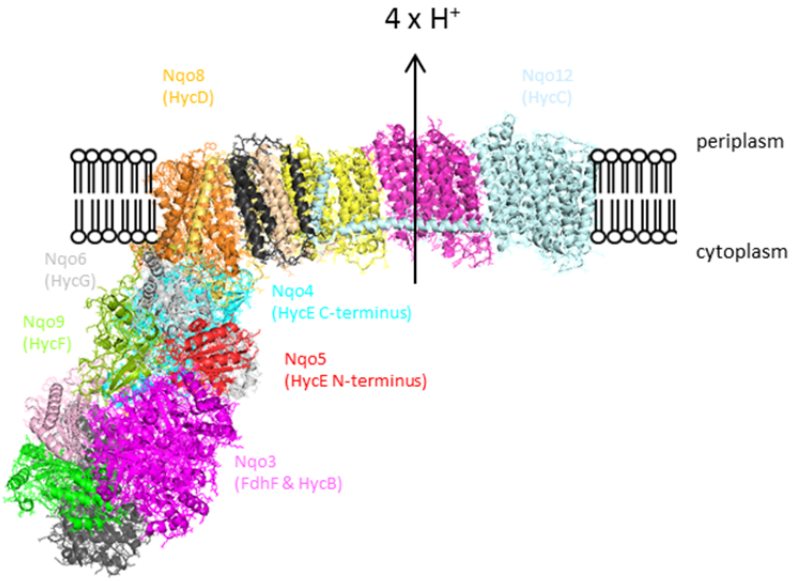

Figure 1.12 Respiratory Complex I and FHL share homology. The crystal structure of Complex I from *Thermus thermophilus* (PDB File: 4HEA) (Baradaran *et al*., 2013) is shown and colour coded by subunit. Subunits which share homology to subunits in FHL, as described in Efremov and Sazanov (2012) are labelled. Complex I is known to be involved in proton pumping across the membrane, and this has led to speculation that FHL is capable of a similar activity.

The homology of the FHL membrane proteins, HycC and HycD, to their proton pumping homologues in Complex I has led to speculation that FHL may also be capable of proton pumping. Whilst HycC potentially lacks an amphipathic helix that is implicated in proton pumping in its homologue in Complex I (Efremov and Sazanov, 2012), it has been suggested that proton translocation can indeed be carried out by FHL (Hakobyan *et al*., 2005). Related Group 4 [NiFe]-hydrogenases, such as those from *Methanosarcina barkeri* or *Rhodospirillum rubrum* are known to undertake proton translocation (Fox *et al*., 1996; Kunkel *et al*., 1998).

The similarities to elements of Complex I have also been noted in other [NiFe]-hydrogenases, such as the *C. necator* SH (Pilkington *et al*., 1991) and also [FeFe]-hydrogenases as in *D. fructosovorans* and *Thermotoga maritima* (Malki *et al*., 1995; Verhagen *et al*., 1999). As such there is a suggestion that the evolutionary history of modern hydrogenases can be traced right back to the origin of life.

Hyd-3 is unusual amongst [NiFe]-hydrogenases in that it is only weakly product inhibited, which is more akin to the activity exhibited by [FeFe]-hydrogenases (McDowall *et al*., 2014). Furthermore, whilst it has long been known that Hyd-3 can perform H_2-dependent redox dye reduction *in vitro* (Sawers *et al*., 1985), and more recently FHL has been shown to be able to perform the reverse reaction in high H_2 and CO_2 concentrations at an alkaline pH *in vivo* (Pinske and Sargent, 2016), neither of these conditions are likely to be encountered by the cell. As such it may be said that FHL shows unidirectional, H_2-evolving, activity in physiological conditions. Both of these are desirable characteristics for any enzyme that would be used in the industrial-scale production of BioH_2, where H_2 levels would be high. These features, in conjunction with FHL being by far the most predominant method of H_2 production in *E. coli*, make Hyd-3 a particularly important enzyme in the field of BioH_2 research.

1.7.4 Hyd-4

Besides the three functional enzymes discussed so far, *E. coli* also possesses genes encoding a putative fourth [NiFe]-hydrogenase, Hyd-4. The *hyfABCDEFGHIJRfocB* operon encodes a similar enzyme to Hyd-3, both in terms of complex architecture and sequence homology (Andrews *et al*., 1997). Like Hyd-3, Hyd-4 appears to be a Group 4 hydrogenase, with subunits again sharing homology to those in Complex I (Marreiros *et al*., 2013). However, one deviation is Hyd-4 has substantially more transmembrane domains. Where Hyd-3 only has two membrane subunits, HycC and HycD, the *hyf* operon encodes five such subunits: HyfB, HyfC, HyfD, HyfE and HyfF (Andrews *et al*., 1997). The other structural subunits HyfG (the large subunit), and the [Fe-S] containing HyfI, HyfH and HyfA are soluble subunits present in the cytoplasm, again similar to the counterparts in Hyd-3. In forming a putative second FHL complex, called FHL-2, the Hyd-4 enzyme would either also associate with formate dehydrogenase H like FHL, or perhaps associate with a FdhF homologue called YdeP (Sargent, 2016).

The other genes in this operon *hyfJ*, *hyfR* and *focB* encode non-structural proteins. HyfJ is homologous to the protein of unconfirmed function HycH that has been implicated in Hyd-3 maturation (Rossmann *et al*., 1994; Sargent, 2016). HyfR seems to be a formate-dependent transcriptional regulator of the *hyf* operon in an analogous manner to FhlA (Skibinski *et al*., 2002). Similarly, FocB seems to be a formate channel analogous to FocA (Sargent, 2016). Despite these accessory genes being present, the *hyf* operon in *E. coli* K-12 does not encode a specific endopeptidase that is normally required for maturation of the large subunit (Andrews *et al*., 1997). Interestingly, in other Enterobacteriaceae species such a Hyd-4 endopeptidase is present. Quite why it is not present in the lab strain is unknown.

1.8 **[NiFe] active site formation**

The complex active site architecture of [NiFe]-hydrogenases necessitates a suite of dedicated maturation proteins (maturases) to assist in proper formation. Aside from the previously discussed dedicated maturases specific to Hyd-1, Hyd-2 and Hyd-3 that are encoded by their respective operons, six additional proteins involved in maturation are encoded elsewhere in the *E. coli* genome. Five of these are present in one operon: *hypABCDE*, which is found upstream of the *hyc* operon, on the opposite strand, and adjacent to *fhlA*. The gene encoding HypF is found on the same strand, further downstream. Both *hypABCDE* and *hypF* can be induced in the presence of formate by FhlA (Sawers, 2005).

The initial stage of active site biosynthesis involves the recruitment of the Fe centre by a HypC/ HypD complex from which the nascent active site is built around (Sargent, 2016) (Figure 1.13). The next step is the generation of the unusual non-proteinaceous ligands that coordinate the Fe: CN^- and CO. The cyanide is derived from carbamoyl phosphate. This is done initially by the carbamoyltransferase, HypF, which transfers the carbamoyl group from carbamoyl phosphate to HypE in an ATP-dependent manner (Reissmann *et al*., 2003; Shomura and Higuchi, 2012). HypE then further modifies this carbamoyl group to a cyanide precursor, either thiocyanate or isothiocyanate, again in an ATP-dependent manner (Stripp *et al*., 2015; Tominaga *et al*., 2013). From this, CN^- ligands are than able to be donated to the Fe bound to HypC/ HypD. The origin of the CO ligand is less understood. It may be derived from atmospheric CO or CO_2, acetate or some other metabolic precursor (Burstel *et al*., 2011; Roseboom *et al*., 2005; Soboh *et al*., 2013). Nonetheless, the CO ligand added to the HypD/ HypC bound Fe, either before (Soboh *et al*., 2013) or after (Burstel *et al*., 2012) addition of the CN^- ligands.

Next, delivery of the $Fe(CN)_2CO$ moiety is performed by HypC, which interacts directly with the large subunit apoprotein. This is specifically the case during Hyd-3 maturation. For Hyd-2, the HypC homologue HybG is required, and either of these proteins can assist in Hyd-1 maturation (Blokesch *et al*., 2001; Hartwig *et al*., 2015).

Ni is then inserted into the active site *via* the action of HypA and HypB in a GTP-dependent manner (Blokesch *et al*., 2002; Dias *et al*., 2008), although these proteins are actually redundant in high Ni concentrations (Lutz *et al*., 1991; Waugh and Boxer, 1986). In some species, such as *E. coli*, an additional protein called SlyD is required (Chung and Zamble, 2011). Indeed, it has more recently been shown that in *E. coli* that SlyD is essential for proper maturation of Hyd-1, Hyd-2 and Hyd-3 during stationary phase cells in conditions of non-enrichment with nickel (Pinske *et al*., 2015b). In E*. coli* Hyd-2 biosynthesis, HybF can perform the same function as HypA (Blokesch *et al*., 2004).

Cleavage of the C-terminal region of the large subunit completes the process, forming a mature holoprotein that can now associate with the small subunit for translation by the Tat pathway, if appropriate. In *E. coli*, this cleavage of the C-terminal region is performed by HyaD for Hyd-1, HybD for Hyd-2 and HycI for Hyd-3 (Menon *et al*., 1994; Menon *et al*., 1991; Rossmann *et al*., 1995).

The active site formation in *E. coli* is a paradigm for [NiFe]-hydrogenases, though modifications exist in different species. In *C. necator* for example, the O_2-tolerant Membrane Bound Hydrogenase (MBH) requires additional proteins. HoxV and HoxL thought to act as a scaffold and chaperone respectively during $Fe(CN)_2CO$ insertion that can shield the active site from O_2 (Ludwig *et al*., 2009).

Nickel transport into the cell is catalysed by the Nik machinery under anaerobic conditions, encoded by *nikABCDER* (Wu *et al*., 1989). The transporter itself is an ATP-binding cassette transporter consisting of NikABCDE. NikA is a periplasmic Ni-binding protein, whilst NikB and NikC encompass the membrane channel subunits. NikD and NikE comprise the ATP binding domains to power the import process. NikR represses the *nik* operon, and so helps homeostasis between Ni transport and hydrogenases synthesis. In high nickel concentrations, the *nik* transport system can be bypassed, with Ni instead imported *via* the magnesium transport system (Wu *et al*., 1989). The mechanism for *E. coli* Fe uptake is less clear, however it

has been hypothesised that perhaps a Mn/Fe symporter (Makui *et al*., 2000) or dedicated Fe^{2+} importer (Cartron *et al*., 2006) is used.

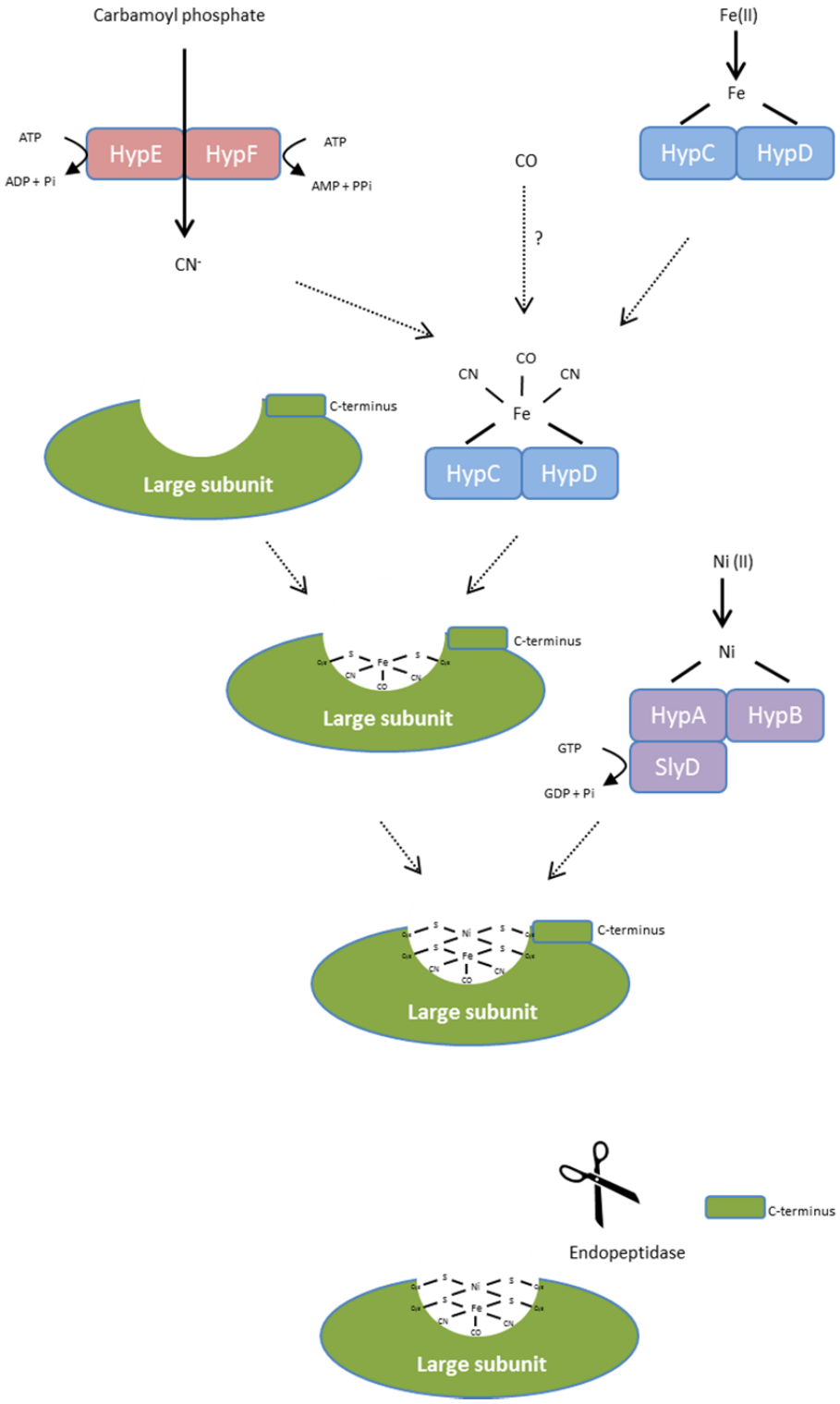

Figure 1.13 Biosynthesis of the [NiFe] active site in *E. coli*. The first stage of active site biosynthesis involves the binding of Fe to a HypC/HypD scaffold. The CN^- ligands are synthesised from carbamoyl phosphate *via* the action of HypE and HypF. These, along with the CO ligand which is derived from a still-unknown process, are then coordinated to the Fe, forming a nascent $Fe(CN)_2CO$ moiety. This is then transferred to the hydrogenase large subunit and inserted, via a process that involves direct association of HypC with the apoprotein. Ni is then sequestered by a HypA/ HypB complex, in addition to the action of SlyD in *E. coli*. This is then inserted into the protein, thus completing the active site. The large subunit C-terminal peptide is then cleaved to form the mature holoprotein.

1.9 **[Fe-S] biosynthesis**

Whilst the large subunit of [NiFe]-hydrogenases necessitates the insertion of the active site for proper function, so the small subunit also requires cofactor incorporation. [Fe-S] clusters are essential for electron relay to/from the active site. Furthermore, [Fe-S] clusters are also found in hydrogenase–associated machinery, such as in the HypD maturation protein, and in the anaerobic transcriptional activator, FNR (Vignais and Billoud, 2007).

In *E. coli* two pathways are responsible for [Fe-S] synthesis: the 'isc' (iron sulfur cluster) and 'suf' (sulfur formation) pathways, which are encoded by the *iscRSUA* and *erpA*, and *sufABCDSE* and operate under normal or oxidative conditions respectively (Roche *et al*., 2013). Whilst the suite of Suf proteins is not required for proper hydrogenase assembly in *E. coli*, the Isc machinery is (Pinske *et al*., 2013; Pinske and Sawers, 2012). In particular, the proteins involved in delivery of newly synthesised [Fe-S] clusters to target proteins, the A-type carrier (ATC) proteins IscA and ErpA, are both essential for proper hydrogenase formation, specifically in the delivery of [Fe-S] clusters to the hydrogenase small subunits.

The presence of a scaffold protein involved directly in [Fe-S] cluster synthesis, IscU, was found to be a requisite for proper formation of the [4Fe-4S]-containing maturase HypD, and also FNR (Pinske *et al*., 2013; Pinske and Sawers, 2012). The absence of FNR decreases H_2 evolution in a number of ways. Not only is it required for complete Hyp maturase production, but also nickel transport (Messenger and Green, 2003). Furthermore, FNR is required for pyruvate formate-lyase (PflB) synthesis (Sawers and Suppmann, 1992). The lack of FNR thus leads to a decrease in formate production, with a knock-on effect of less H_2 evolution by FHL (Pinske *et al*., 2013).

IscR acts as a repressor of the *isc* operon, and thus inhibits its own expression. Itself containing a [2Fe-2S] cluster, so production of the holoprotein acts to sense [Fe-S] biosynthesis and so help keep the process in homeostasis (Giel *et al*., 2006). As such, overexpression of hydrogenases may be limited in strains with a functional *iscR*, due to a limit of [Fe-S]

production. This problem might only be accentuated in that IscR also seems to repress the hya and *hyb* operons, at least aerobically (Giel *et al*., 2006). Anaerobically the IscR binding site may be occluded by the anaerobic transcriptional activator proteins FNR, AppY and ArcA.

1.10 **The hydrogenases of *C. necator***

The β-Proteobacterium *Cupriavidus necator* is found in soil and water and as such is exposed to a changeable environment that is susceptible to transient anoxia and low nutrient availability. In response to this, the species has evolved facultative lithoautotrophy, where it can utilise CO_2 and H_2 as the sole carbon and energy sources respectively; the latter feature leading *C. necator* to be described as a 'Knallgas' bacteria (Pohlmann *et al*., 2006). Originally named *Alcaligenes eutrophus* and then *Ralstonia eutropha*, *C. necator* was recently reclassified in a novel genus *Wauterisia* gen.nov. (Vaneechoutte *et al*., 2004). However it was subsequently discovered that *Wauterisia eutropha*, the species the taxonomic name is derived from, was the same as an earlier described species, *Cupriavidus necator* (Vandamme and Coenye, 2004).

C. necator has garnered great interest in the field of biotechnology for a number of reasons. In carbon-abundant, but otherwise nutrient-deprived conditions, *C. necator* is naturally capable of producing and accumulating energy and carbon rich compounds called polyhydroxyalkanoates (PHA) (Verlinden *et al*., 2007). Whilst PHAs exhibit properties similar to polypropylene (Braunegg *et al*., 1998), unlike such oil-derived plastics in prevalent use today, they are not an ecological risk as they are biodegradable and derived by renewable means (Mergaert *et al*., 1992).

C. necator is also of biotechnological interest in terms of $BioH_2$ production as it produces a suite of oxygen tolerant hydrogenases, from across the various [NiFe]-hydrogenase groups, which carry out different physiological roles. *C. necator* possesses four hydrogenases in total. The genome of *C. necator* consists of three replicons: chromosome 1 (4.1 Mb), chromosome 2 (2.9 Mb) and the 450 kb megaplasmid pHG1 (Schwartz and Friedrich, 2001), and the latter of these contains the genes encoding all four hydrogenases (Burgdorf *et al*., 2005a; Schafer *et al*., 2013).

The first, the Membrane Bound Hydrogenase (MBH) is an oxygen tolerant Group 1 [NiFe]-hydrogenase, that is orientated in the periplasm. In a structure very similar to *E. coli* Hyd-1, it consists of a large subunit, HoxG, bound to the small subunit HoxK. The trimeric complex is completed by the di-haem cytochrome *b* protein, HoxZ, allowing the MBH to reduce the quinone pool by H_2 oxidation (Bernhard *et al*., 1997; Schink and Schlegel, 1979).

The Soluble Hydrogenase (SH) couples H_2 oxidation to NAD^+ reduction. As a Group 3 hydrogenase it functions primarily as an H_2 uptake enzyme physiologically. The SH consists of at least four subunits, with HoxHY forming the large and small subunits of a hydrogenase domain, which is linked to a diaphorase domain comprising HoxFU (Burgdorf *et al*., 2005a). A fifth protein, HoxI, is also implicated in enzyme function, acting as a docking site for the diaphorase substrates (Burgdorf *et al*., 2005b).

The Regulatory Hydrogenase (RH) is a Group 2 sensory hydrogenase. Because *C. necator* will preferentially grow in a heterotrophic manner, the MBH and SH genes are not constitutively expressed. Rather they are induced in response to H_2 or when organic carbon is scarce (Lenz and Friedrich, 1998b). This is done through the action of the RH, which couples H_2 oxidation to gene transcription. The RH consists of large and small subunits, HoxCB respectively, associated to a histidine kinase, HoxJ, which modulates the phosphorylation of a DNA binding protein, HoxA. Upon H_2 degradation by the HoxBC module, the activity of HoxJ is altered. HoxA is resultantly no longer phosphorylated and downstream transcription of the MBH and SH genes is induced.

The fourth hydrogenase in *C. necator*, the Actinobacterial-type Hydrogenase (AH) is a Group 5/ Group 1h enzyme that exhibits O_2 resistant activity in even low levels of H_2, comparable to that found in air (Schafer *et al*., 2016). Consisting of only two subunits: the large subunit, HofG (67 kDa) and the small HofK (37 kDa), the enzyme is encoded by an operon on the pHG1 megaplasmid, which also contains genes encoding for maturases (HypF3C2D2E2A3B3), a specific endopeptidase (HupD) and four proteins of unknown function (Schafer *et al*., 2013). As

well as the remarkable O_2 resistant activity, the enzyme is also highly stable to pH and temperature fluctuations; a feature thought to be due to the large contact are between the large and small subunits, which is almost twice as much as Group 1 hydrogenases (Greening *et al*., 2016; Schafer *et al*., 2013).

1.11 **Hydrogenases: beyond biofuels**

Hydrogenase research also has implications beyond biofuels. Another potential biotechnological application of hydrogenases is in bioremediation; i.e. to assist in the removal of pollutants from the environment (Vignais and Billoud, 2007). Whilst heavy metals are biohazards, they occur naturally at concentrations low enough for their toxic effects to be negligible. However, industrial processes can lead to increased levels such that a risk is posed to the environment. One such toxic heavy metal is chromium. Chromium, like many heavy metals, is less soluble when reduced than when in an oxidised state. Whilst Cr(III) is not a significant health hazard, the more oxidised Cr(VI) is a potent carcinogen (Norseth, 1981). The action of hydrogenases in the sulfur-reducing bacteria *Desulfovibrio vulgaris* str. Hildenborough is involved in the conversion of Cr(VI) to Cr(III), so precipitating this toxic pollutant and making it less bioavailable (Goulhen *et al*., 2006).

Another class of chemicals which pose a risk to ecological systems is the chlorocarbons, such as the powerful industrial solvent tetrachlorethene. These can similarly be removed from the environment by the action of hydrogenases. The obligate anaerobe *Dehalobacter restrictus* can make use of such powerful oxidising agents during ATP synthesis, employing them as electron acceptors during anaerobic respiration with H_2 oxidised *via* a membrane-bound, quinone-pool linked uptake hydrogenase (Holliger *et al*., 1998).

Hydrogenase enzymes also have ramifications for medicine. The microbiota of the human digestive tract, exposed to a nutrient-rich and oxygen-limited environment, evolve appreciable levels of molecular hydrogen (Olson and Maier, 2002). This can be used as an energy source by pathogenic bacteria, such as *Salmonella enterica* (Zbell and Maier, 2009) and *Helicobacter pylori* (Kuhns *et al*., 2016; Olson and Maier, 2002). The significance of this H_2, and by extension the hydrogenases by which it is produced, has been shown in *S. enterica* as mutants with abolished hydrogenase activity have compromised virulence (Maier *et al*., 2004). As our understanding of hydrogenases increases, particularly with regards to the structural make-up

of the enzymes, so it is possible that they can be used as drug targets to combat infection. This is a salient implication as antimicrobial resistance is a major threat to global health presently. Misuse of antibiotics has led to the evolution of pathogens with resistance to multiple drugs to which they were previously susceptible, such as Mycobacterium *tuberculosis*, *Campylobacter jejuni*, and *Clostridium difficile* (Davies and Davies, 2010). As such, there is a constant drive to find new drugs to combat infection.

1.12 **Synthetic biology**

As was discussed in Section 1.4, the natural rates of hydrogenase activity are not sufficient for bioH_2 to be an industrially-viable source of hydrogen currently. Research into engineering these enzymes to augment their activity is required. Such genetic modification of gene products fits into the new and blossoming field of synthetic biology, which entails taking an engineering approach to biology.

Synthetic biology comes in two broad flavours. One employs unnatural molecules (such as unnatural amino acids (Liu and Schultz, 2010)) to generate novel behaviours in natural biology, with an ultimate goal of creating artificial life. One prominent group working towards this end is that at the James Venter Institute, where recent work has led to the generation of the partially synthetic species, *Mycoplasma laboratorium* (Hutchison *et al*., 2016). The second approach utilises parts from natural biology to assemble into systems that function unnaturally (Benner and Sismour, 2005). The ever-increasing computational power of bioinformatics technology to analyse and understand the molecular basis of biological systems, combined with the ever-decreasing cost of DNA synthesis and assembly (Carlson, 2009), has led to synthetic biology becoming an ever-growing area of research, that will only increase further over time.

One important feature of synthetic biology is a drive to standardise biological parts to allow for quick and easy integration by different research groups to create new constructs. A prominent example of this is the 'Biobrick' standard for DNA sequences, be they genes or gene expression-related sequences such as ribosome binding sites, promoters or terminators (Shetty *et al*., 2008). *E. coli* is the common host organism, or 'chassis' for these circuits, due to its biochemistry being particularly well understood (Cameron *et al*., 2014).

Whilst in its infancy, synthetic biological approaches have begun to be used in the field of hydrogenase research in order to develop new avenues of hydrogen metabolism in *E. coli.* For

example, heterologous expression of [FeFe]-hydrogenases has led to novel reaction pathways to generate cysteine in the cell (Barstow *et al*., 2011). A way to link H_2 generation to NADH, and so integrate BioH_2 production directly into the cell's central metabolism, was also developed (Kelly *et al*., 2015). Similar approaches will be used in the work presented in this Thesis.

1.13 **Aims**

The broad aim of the work is to engineer additional hydrogenase activity, and specifically hydrogen production activity, into *Escherichia coli*. This will entail the use of molecular biology techniques to either heterologously express non-native enzymes in the cell, or to engineer the native hydrogenase enzymes in an attempt to perform new functions. Four specific objectives will be addressed:

1. Heterologous production of an active NADH-linked SH from *C. necator* in *E. coli* (Chapter 2).
2. Towards the construction of a H_2 biosensor in *E. coli* based on the *C. necator* RH (Chapter 3).
3. Engineering *E. coli* Hyd-3 for a novel route to H_2 production from pyruvate (Chapter 4).
4. Engineering *E. coli* Hyd-2 for a novel route to H_2 production from glycerol (Chapter 5).

2. Heterologous production of an NADH-linked [NiFe]-hydrogenase in *Escherichia coli*

2.1 **Introduction**

2.1.1 Heterologous hydrogenase production could augment H_2 yield

For biohydrogen to become commercially viable, H_2 yield will need to be substantially increased. One possible approach to achieving this is the engineering of heterologous systems into a host cell. A number of hydrogenases from other species have been successfully transplanted into an *E. coli* host cell and exhibited activity, from the related γ-Proteobacteria such as *Thiocapsa roseopersicina* (Weyman *et al*., 2011); fellow eubacterial species such as *Hydrogenovibrio marinus* (Kim *et al*., 2011); to organisms from another taxonomic domains such as the archaeon *Pyrococcus furios*us (Sun *et al*., 2010).

In *E. coli*, the predominant mode of H_2 production is *via* the oxidation of a single metabolite; specifically formate, by the FHL complex. It can therefore be supposed that modifying the cell to utilise different substrates may help augment H_2 yield. It is of particular interest in the field to heterologously express hydrogenase activities that can be integrated into existing *E. coli* metabolic networks. NADH is seen as an especially desirable electron donor to employ, due to it being a major redox agent in the cell, and is in relatively high abundance during fermentation. Some prokaryotes produce metalloenzymes that can couple NADH oxidation directly to proton reduction *via* hydrogenase domains. In this Chapter, it was attempted to engineer an active NADH-dependent [NiFe]-hydrogenase into the central anaerobic metabolism of *E. coli*. To this end, a hydrogenase from *Cupriavidus necator* was chosen for experimentation.

2.1.2 Linking NADH to H_2: The Soluble Hydrogenase from *Cupriavidus necator*

The 'knallgas' bacterium *Cupriavidus necator* (still commonly known by its previous name, *Ralstonia eutropha*) contains four different [NiFe]-hydrogenases (Burgdorf *et al*., 2005a;

Schafer *et al*., 2016), which are encoded by various clusters on the self-transmissible megaplasmid, pHG1 (Schwartz *et al*., 2003). One of them, a soluble cytoplasmic enzyme that links NAD^+/NADH to hydrogen metabolism, is called the soluble hydrogenase (SH). The SH resembles the peripheral arm of Complex I both structurally and functionally, and so in turn shares aspects with Hyd-3 in *E. coli* and other group 4 membrane-bound [NiFe]-hydrogenases, although the SH is classed a Group 3 hydrogenase (Albracht and Hedderich, 2000; Marreiros *et al*., 2013; Vignais and Billoud, 2007).

The SH is encoded by the nine gene *hoxFUYHWI-hypA2B2F2* operon (Schwartz *et al*., 1998). The first four genes encode for the structural proteins of the enzyme complex, with HoxFU representing the diaphorase half of the enzyme, and HoxHY the [NiFe]-hydrogenase half (Figure 2.1). HoxI has been implicated in the activation of the complex by acting as a docking site for NAD(P)H, at least *in vitro* (Burgdorf *et al*., 2005b) HoxW is an endopeptidase involved in the C-terminal processing of HoxH, and is thus involved in hydrogenase maturation along with HypA2, HypB2 and HypF2. Further maturases required for proper assembly of SH are found outwith this operon, with HypC1, -D1, -E1, and -X encoded by another gene cluster on the pHG1 megaplasmid (Schwartz *et al*., 2003).

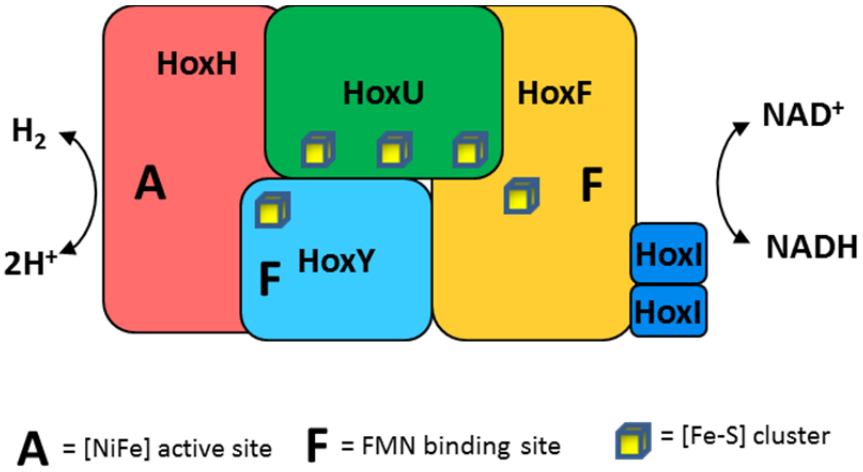

Figure 2.1 Schematic of the Soluble Hydrogenase (SH) of *Cupriavidus necator*. The SH is capable of the reduction of protons to H_2 *via* the oxidation of NADH to NAD^+, and the reverse reactions. Electrons are predicted to be relayed between the hydrogenase HoxHY and diaphorase HoxFU components of the complex by way of the [Fe-S] clusters.

2.2 **Aims**

This Chapter describes the attempt to heterologously produce a functional NADH-linked soluble [NiFe]-hydrogenase in an *E. coli* host. The work employed a synthetic biology approach by the design and construction of synthetic operons to optimally express the *hox* genes encoding the structural proteins, and the *hyp* genes encoding the associated maturases, from *Cupriavidus necator*. Both *in vivo* and *in vitro* functional characterisation of the resultant, active, soluble hydrogenase (SH) complex is reported.

2.3 **Results**

2.3.1 The design and expression of synthetic operons encoding the *C. necator* soluble hydrogenase and its maturases

The *C. necator* soluble hydrogenase (SH) is encoded by the *hoxFUYHWI* operon. The project began with the *in silico* design of a new synthetic operon designed to optimise transcription and translation in an *E. coli* host. The primary amino acid sequence for each protein in the SH complex was back translated into DNA sequence, which was then codon optimised to allow for the ideal translation efficiency in an *E. coli* K-12 chassis. This was done using the online software, OPTIMIZER (Puigbo, 2007), which produces a DNA sequence, and therefore a transcribed mRNA sequence, that will be recognised by the most abundant tRNAs in the host cell; in this case *E. coli* K-12.

In order to help with later cloning and characterisation of the synthetic operon, the new DNA sequence was then analysed for the sites recognised by the common restriction enzymes used for cloning (*BamH*I, *Bgl*II *Eco*RI, *Hind*III, *Sal*I, *Sph*I, *Sma*I, *Xba*I, *Cla*I, *Nde*I, *Nhe*I, *Mun*I, *Xho*I, *Kpn*I, *Pst*I, *Rca*I, *Eco*RV, *Nco*I). These were then removed by changing the codon usage at these points. OPTIMIZER gives a score between 0 and 1 representing the predicted degree of translation efficiency of a DNA sequence in *E. coli* (or more specifically the mRNA transcript derived from it), with 1.0 being the highest and 0.3 being a minimum threshold for efficient translation. After restriction site removal this new synthetic operon scored 0.971, giving initial confidence that all gene products should be produced with a high degree of efficiency. The 'CAI' scores for expression in *E. coli* for the wild-type sequences and the final optimised sequences of each gene in the SH operon, as well as the associated maturase genes, are shown in Table 2.1. It can be seen here that the wild-type *C. necator* gene sequences are likely to all permit a degree of expression in *E. coli*, however the optimisation procedure is clearly predicted to result in far more efficient expression.

Gene	Unoptimised CAI	Final Optimised CAI
hoxF	0.380	0.982
hoxU	0.431	0.953
hoxY	0.462	0.985
hoxH	0.459	0.958
hoxW	0.389	0.986
hoxI	0.387	0.958
hypA1	0.383	0.866
hypB1	0.459	0.954
hypF1	0.442	0.953
hypC1	0.489	0.944
hypD1	0.441	0.978
hypE1	0.445	0.977
hypX	0.442	0.963
hypA2	0.527	0.922
hypB2	0.558	0.979
hypF2	0.472	0.967

Figure 2.2 Comparison between predicted heterologous expression efficiency in *E. coli* of *C. necator* genes before and after optimisation. The CAI score computed by the OPTIMZER software indicates the efficiency of gene expression in an *E. coli* chassis, from 0 to 1, with 0.3 regarded as the minimum cut-off for successful expression.

Next, an artificial ribosome binding site and spacer (5'-AGGAGGAAAAAAAA-3') was placed at the beginning of each gene in the operon and a double stop codon (5'-TAATAA-3') at the end of each gene to further enhance translation efficiency and ensure the prevention of read-through. A single *Bam*HI site was placed at the 5' end of the operon along with unique *Hind*III and *Sal*I sites at the 3' end to allow for facile cloning of the entire 5.8 kbp gene cluster. The final step in the *in silico* design was to 'bookend' each individual gene in the operon with a dedicated restriction site, to allow for the construction of in-frame deletions of each gene and so allow for protein production to be monitored by ^{35}S-Methionine radiolabelling (Figure 2.4).

The complete optimised *hoxFUYHWI* operon was then synthesised by the company BIOMATIK, and cloned into pUNI-PROM to generate pUNI-SH.

C. necator possesses three operons encoding maturase proteins required for activation of its various hydrogenases: *hypA1B1F1C1D1E1X* and *hypA2B2F2* and *hypF3C2D2E2A3B3*. It has been reported that *hypA2B2F2* are required for SH assembly specifically (Schwartz *et al*., 1998), and it is assumed that *hypC1D1E1X* of the alternative operon would also have a role in SH assembly. Therefore, two slightly different synthetic *hyp* operons were designed and optimised for expression in *E. coli*. Firstly, a synthetic *hypA1-X* operon was made in the same manner as described for *hoxF-I*. This was then modified to *hypA2-X* by excising *hypA1B1F1*, and inserting optimised synthetic *hypA2B2F2* sequence. A schematic illustrating the design of the *hoxF-I*, and *hypA2-X* and *hypA1-X* synthetic operons is shown in Figure 2.3.

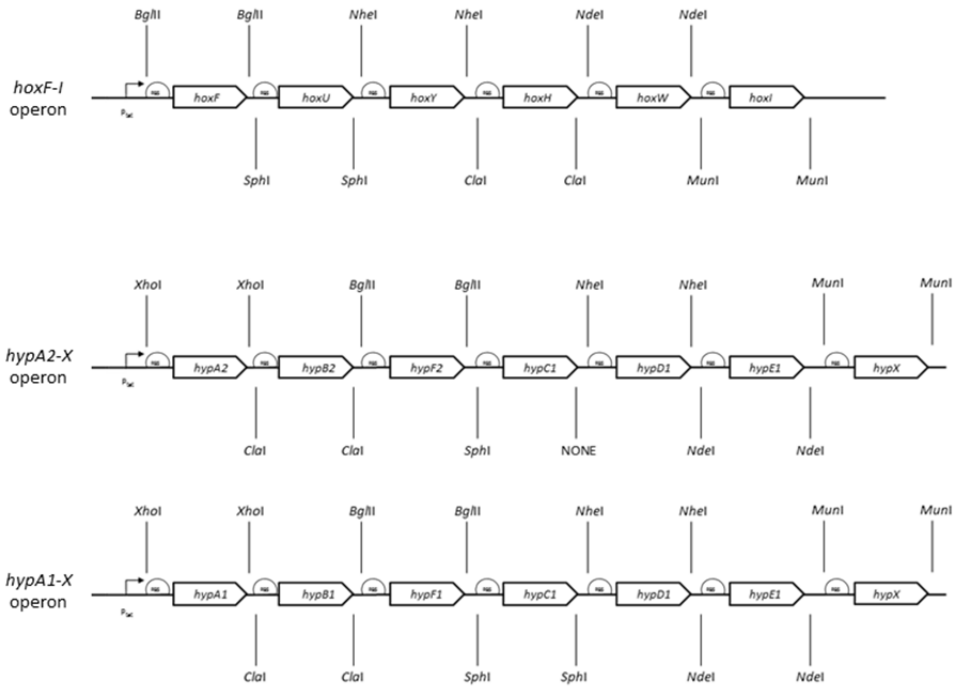

Figure 2.3 Synthetic *hoxF-I*, *hypA2-X* and *hypA1-X* operons for expression in *E. coli*. The two operons encoding the SH complex and the associated maturases, *hoxF-I* and *hypA2-X* respectively, along with the other maturase operon *hypA1-X*, were designed for optimal expression in *E. coli*. The operons were initially cloned under the control of the constitutive *tat* promoter. Synthetic ribosome binding sites (RBS) were placed before each gene sequence. Restriction sites bookend each synthetic gene to allow in-frame, single gene deletions to be constructed.

^{35}S-Methionine radiolabelling was used to confirm the production of gene products from the three synthetic operons in *E. coli* (Figure 2.4). The vectors pUNI-SH, pUNI-A1-X and pUNI-A2-X were used as here the operons are under the control of a T7 promoter, an essential pre-requisite for radiolabelling as the protocol utilises a T7 polymerase produced by the vector pGP1-2 (Tabor and Richardson, 1985). In-frame deletions of single genes using the bookending restriction enzymes were then performed to generate a suite of vectors with incomplete operons, so that protein production could be determined by comparison of the protein bands observed by SDS-PAGE. The exception to this was *hypC1* in the *hypA2-X* vector, which could not be deleted as the *Sph*I site at the end of the gene was modified by QuickChange (Section 7.5.6) so that the other *Sph*I site at the beginning of *hypC1* could be used to excise *hypA1B1F1* prior to replacement with *hypA2B2F2* to construct *hypA2-X*.

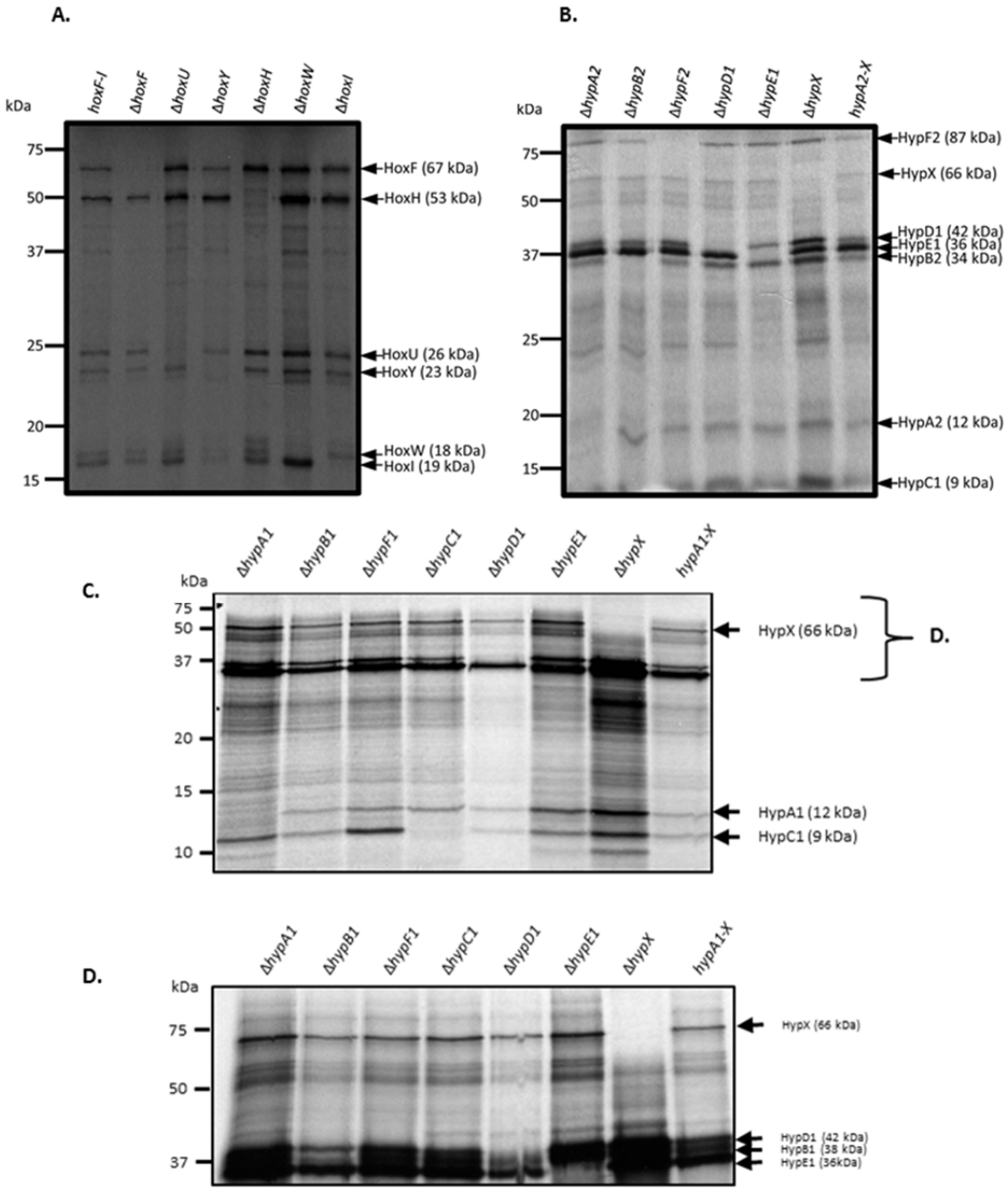

Figure 2.4 The synthetic operons *hoxF-I* and *hypA2-X* and *hypA1-X* operons produce protein products in *E. coli*. ^{35}S-Methionine radiolabelling was carried out in *E. coli* K38 cells carrying the vector pGP1-2 in addition to either (**A**) pUNI-SH, (**B**) pUNI-A2-X or (**C**) pUNI-A1-X to examine protein production of the SH structural proteins and both suites of maturases respectively. (**D**) Shows the same samples as in (**C**) but on a lower acrylamide gel to better resolve the proteins bands ~ 40 kDa in mass. Single gene deletions were carried out and the resultant protein banding patterns compared, therefore allowing for identification of each gene product. HypF1 (40 kDa) is not able could not be confirmed. Labelling of plasmid-encoded proteins was carried out in whole cells before samples were then separated by SDS–PAGE (12% or 7.5% w/v polyacrylamide), fixed with methanol and acetate, and visualised by autoradiography. Note that *hypC1* cannot be excised from the *hypA2-X* operon due to the cloning procedure used; however it can be confirmed in (**C**) that HypC1 is produced.

2.3.2 The synthetic maturase operons are functional and can activate endogenous *E. coli* [NiFe]-hydrogenases

It had now been ascertained that the synthetic *hypA2-X* operon and the synthetic *hypA1-X* operon were capable of producing fully synthesised protein products. The next step was to examine the functionality of the recombinant maturases. The chosen approach was to attempt genetic complementation of *E. coli* mutant strains compromised in [NiFe] cofactor biosynthesis. First, the *E. coli* BEF314 strain was examined, which carries a deletion of the *hypBCDE* maturase genes and as a result is completely devoid of hydrogenase activity (Jacobi *et al*., 1992). The *E. coli* BEF314 (Δ*hypB-E*) strain was transformed with pSU-A1-X or pSUA2-X; plasmids carrying the synthetic operons encoding HypA1-X and HypA2-X under the control of the constitutive *tat* promoter, respectively (Plasmid Table 7.6). Gas chromatography was then used to measure the resultant *in vivo* H_2 production (Figure 2.5A). In both cases, fermentative hydrogen production was restored indicating that, at a minimum, the *E. coli* Hyd-3 system can be properly assembled by both of the synthetic operons.

Next, individual mutant strains in each of the *hypA-E* and *hypF* genes were examined to determine which specific *E. coli* maturases could be substituted for by the *C. necator* counterparts. The mutant strains to be tested were taken from the Keio collection (a bank of several thousand in-frame, non-lethal, deletion mutants (Baba *et al*., 2006)) and transformed with vectors encoding HypA1-X or HypA2-X, before fermentative H_2 production was assayed by GC (Figure 2.5B). The first observation to note from these data is that some individual mutations, namely Δ*hypA,* Δ*hypB and* Δ*hypC*, do not abolish the H_2-evolving capability of the cell, but merely diminish it. Conversely, strains carrying the Δ*hypD*, Δ*hypE* or Δ*hypF* alleles exhibit no detectible H_2 production. In most cases, addition of either the HypA1-X or HypA2-X suite of maturases recovers the ability of the strains to produce H_2. The exception to this is in the example of Δ*hypF*, where only HypA2-X restores H_2 evolution, and not HypA1-X.

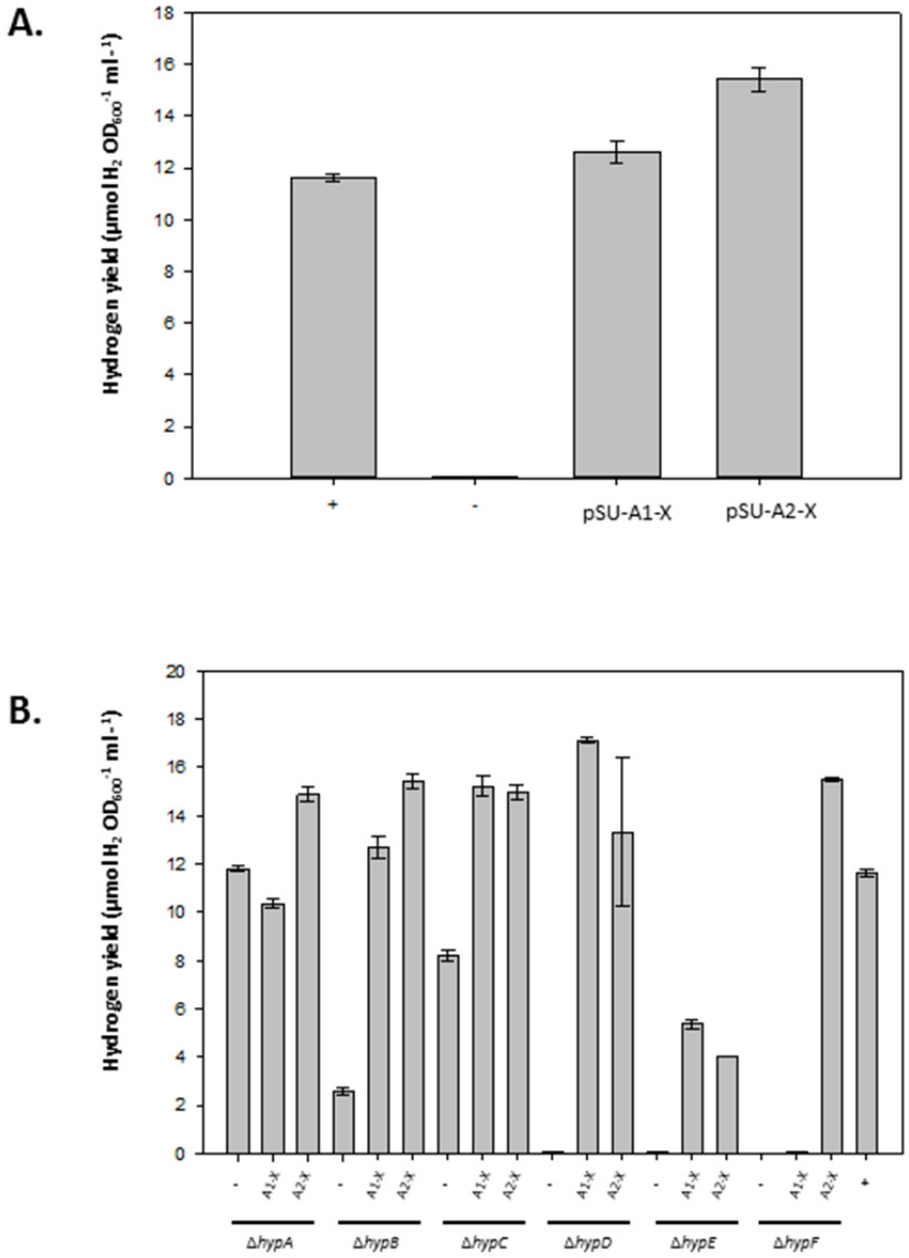

Figure 2.5 The synthetic maturase operons can complement *E. coli hyp* mutants. (A) *E. coli* strain BEF314 (Δ*hypBCDE*) was transformed with a pSU-PROM vector control (-) or vectors encoding the *hypA1-X* synthetic operon (pSUA1-X) or synthetic *hypA2-X* operon (pSUA2-X). (**B**) The Keio collection version of single *E. coli* deletion mutants in each of *hypA*, *hypB*, *hypC*, *hypD*, *hypE* and *hypF* operon were transformed with either empty vector (-) or pUNI-PROM-based vectors encoding the *hypA1-X* synthetic operon (A1-X) or synthetic *hypA2-X* operon (A2-X). In all cases, strains were grown fermentatively at 37 ^{o}C for 48 hours in M9 minimal media supplemented with 0.8% (w/v) glucose before gas chromatography was used to quantify any H_2 accumulated in the headspace. The hydrogen produced is therefore attributable to activation of Hyd-3, which is part of the FHL complex. The positive control (+) is the *E. coli* strain MC4100. Error bars represent SEM (n=3).

2.3.3 Attempts to purify the SH complex

Having explored the production and activity of the *C. necator* maturases operons in *E. coli*, the next phase was to explore the activity of the heterologously-expressed SH in an *E. coli* host. In order to help assess the functionality of the heterologously expressed SH *in vitro*, it was endeavoured to purify the complex, of which two approaches were taken. In the first instance, the HoxF diaphorase subunit was modified with an N' terminal polyhistidine-tag, mirroring an approach that had previously been used to successfully purify the complex, albeit in *C. necator* (Lauterbach and Lenz, 2013). Unfortunately, purification of the SH was not achieved in this instance. Therefore, a second strategy was chosen, this time placing an N-terminal polyhistidine-tag on the hydrogenase small subunit, HoxY. This method of tagging the small subunit has been previously successful for the purification of other hydrogenases by immobilised metal affinity chromatography (IMAC).

The strain FTD147 was transformed with pSU-*hypA2-X* together with pQE80-SH-HoxY^{HIS}, a vector allowing for the IPTG-inducible overproduction of the SH complex proteins including the tagged HoxY. Cells were grown aerobically with shaking in 5 L LB media supplemented with 0.4% (w/v) glucose and appropriate antibiotics for ~17 hours, with IPTG added to a final concentration of 2 mM, approximately half way through this incubation phase when OD_{600} = 0.6. After the 17 hours had elapsed the cells were harvested and then lysed by cell disruption. The resultant crude cell extract was loaded onto a Ni^{2+} Sepharose™ high performance column (GE Healthcare), washed and bound proteins eluted by the application of an imidazole gradient. Eluted fractions were noted to be brown in colour, suggesting the presence of [Fe-S] clusters as would be expected if HoxY (and other associated subunits in the SH) were purified.

Presence of HoxY^{HIS} was confirmed by western immunoblotting using a αHIS antibody (Roche) (Figure 2.6). Peak fractions were then concentrated before being assayed for hydrogenase activity *in vitro* utilising the redox dye methyl viologen (MV), however no activity was observed.

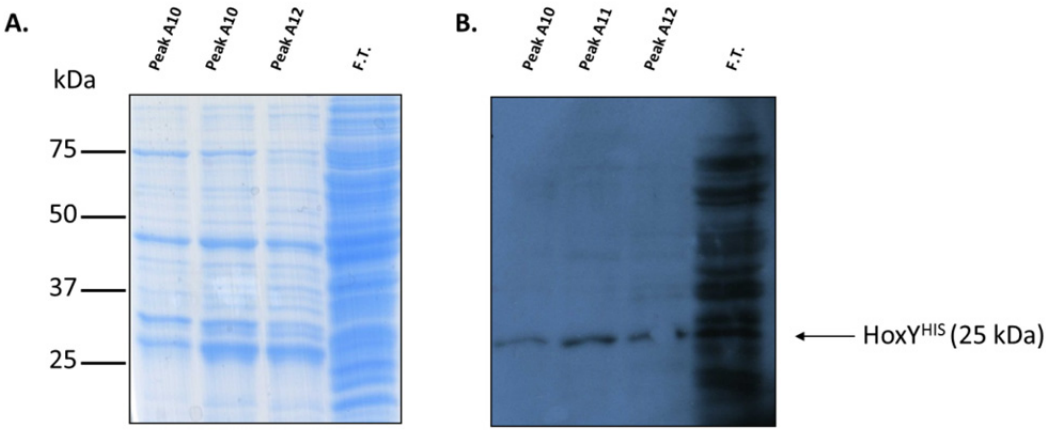

Figure 2.6 Towards purifying the SH complex heterologously expressed in *E. coli*. Overexpression of the *hoxF-I* operon (modified to produce $HoxY^{HIS}$) was performed aerobically in FTD147 before an attempt to purify the SH complex was made by Ni^{2+} IMAC. (**A**) The three eluted peak fractions from the IMAC procedure: A10, A11 and A12, along with the flow through (F.T.) were examined for prominent protein bands by SDS-PAGE. (**B**) These same fractions were then subjected to a Western immunoblot using αhexahistidine (αHis) antibody to establish the presence of the SH hydrogenase small subunit, HoxY.

2.3.4 Production of an active SH in *E. coli*

Attempts were made to measure SH functionality without the use of purification, relying instead on crude extract from lysed cells. In order to be able to test SH function in this way a new *E. coli* strain was generated based on IC011 (Δ*hyaB*, Δ*hycE*, Δ*hybOA*) (Strain Table 7.1). This strain was further modified by the inclusion of a Δ*iscR* allele; a mutation which has previously been found to be beneficial for heterologous production of metalloenzymes (Kelly *et al*., 2015), owing to the resultant de-regulation of [Fe-S] cluster formation. The addition of the Δ*iscR* allele to IC011 yielded strain HJ001 strain. Finally, a Δ*adhE* allele was engineered into the new strain with a view to assessing the physiological activity of the NADH-dependent SH in *E. coli*. The final *E. coli* host strain resulting from these modifications was named HJ002 (Δ*hyaB*, Δ*hybOA*, Δ*hycE*, Δ*iscR*, Δ*adhE*).

To test activity of the SH encoded by the synthetic operon, the HJ002 host strain was first transformed with a pSU-A2-X. Next, the strain was co-transformed with pQE80-SH or pUNI-SH, grown under anaerobic conditions in 500 mL LB media supplemented with 0.4 % fumarate, 0.5 % glycerol and appropriate antibiotics, and resultant (anaerobically prepared) crude extracts assayed for hydrogen-dependent MV reduction activity (Figure 2.7). The use of the pUNI-SH vector, which produces SH from the constitutive *tat* promoter, resulted in clear MV-linked hydrogenase activity in the crude extract (Figure 2.7). Crude extracts from cells possessing pQE80-SH exhibited activity even when no IPTG was added, suggesting the pQE80 *lac* operated promoter is “leaky”. This non-induced activity is comparable to that seen for pUNI-SH (Figure 2.7). Addition of increasing concentrations of IPTG to the cultures can be seen to confer an increase in hydrogenase activity in the crude extract (Figure 2.7). This assay demonstrated the [NiFe]-hydrogenase half of the SH had been fully assembled and was functional.

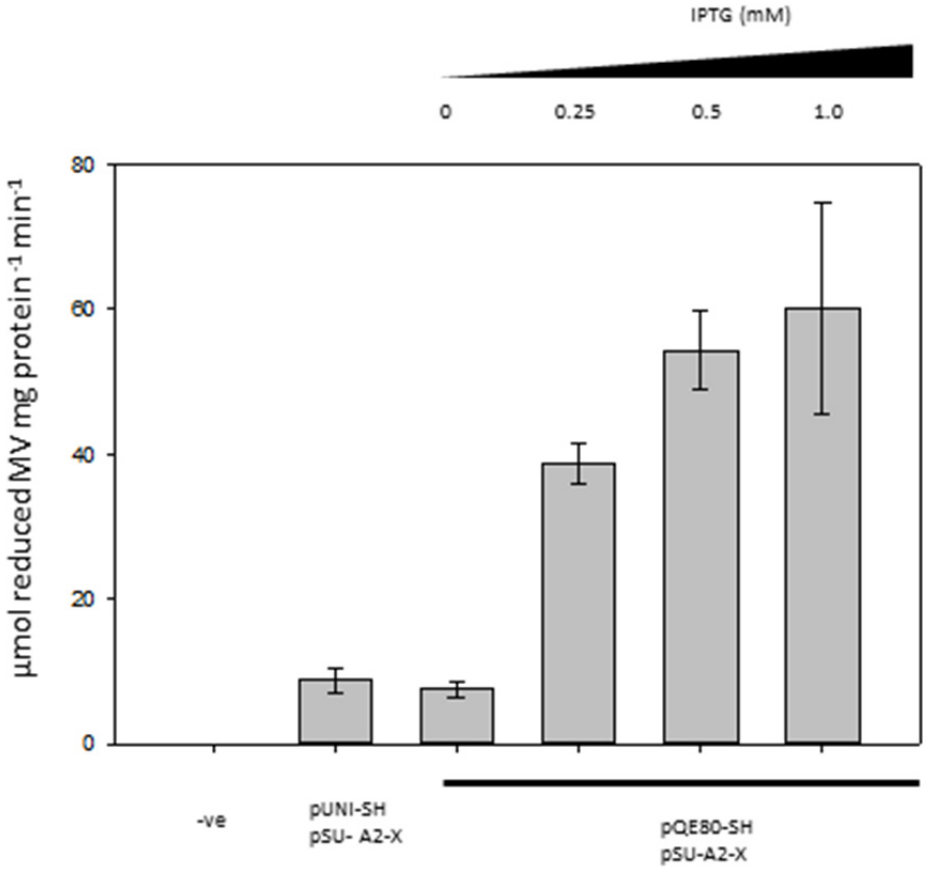

Figure 2.7 Heterologously expressed SH shows hydrogenase activity *in vitro.* *E. coli* host strain HJ002 (Δ*hyaB*, Δ*hybOA*, Δ*hycE*, Δ*iscR*, Δ*adhE*) was transformed with pUNI-PROM / pSU-PROM (-ve control); pUNI-SH / pSU-A2-X for constitutive level expression of SH, or pQE80-SH pSU-A2-X. The latter enables IPTG-dependent overexpression of the SH complex. Four concentrations of IPTG were used: 0 mM, 0.25mM, 0.5 mM, 1 mM IPTG. Cultures were incubated without shaking overnight at 37 °C in 500 mL LB media supplemented with 0.4 % fumarate, 0.5 % glycerol and appropriate antibiotics. Cells were harvested, washed, broken and crude extracts assayed for rates of hydrogen-dependent reduction of methyl viologen. Error bars represent SEM (n=3).

Attempts were also made to measure the activity of the diaphorase component of the SH *in vitro* using spectrophotometric assays; either measuring at a λ of 340 nm to measure NADH oxidation directly, or linking this to the reduction of the redox dye benzyl viologen (BV) and measure at λ= 600 nm. These procedures have previously been employed to assess the activity of the SH enzyme when purified from *C. necator*, giving an activity of 104 U mg^{-1} protein (Lauterbach and Lenz, 2013), however no diaphorase activity was detected here.

The ability of the SH to produce H_2 *in vivo* was then assessed. The HJ002 strain was transformed with either pQE80-SH or pUNI-SH together with either a control plasmid (pSU-PROM) or a plasmid allowing for constitutive expression of the *hypA1-X* or *hypA2-X* operon. Successful transformants were grown aerobically overnight at 37 ^{o}C in 5 mL M9 media supplemented with 0.8 % glucose, 0.2 % casacids, 100 µM $FeCl_3$ and appropriate antibiotics. The next day, the same media was made up and sparged with N_2 for 1.5 hours to remove dissolved O_2. Then, in an anaerobic cabinet, Hungate tubes were filled with containing 5 mL of this anaerobic media and sealed, before inoculation with 50 µL of the overnight culture. The Hungate tubes were inverted and incubated at 37 ^{o}C without shaking for 24 hours, after which the H_2 in the headspace was determined by gas chromatography in a single end-point assay (Figure 2.8).

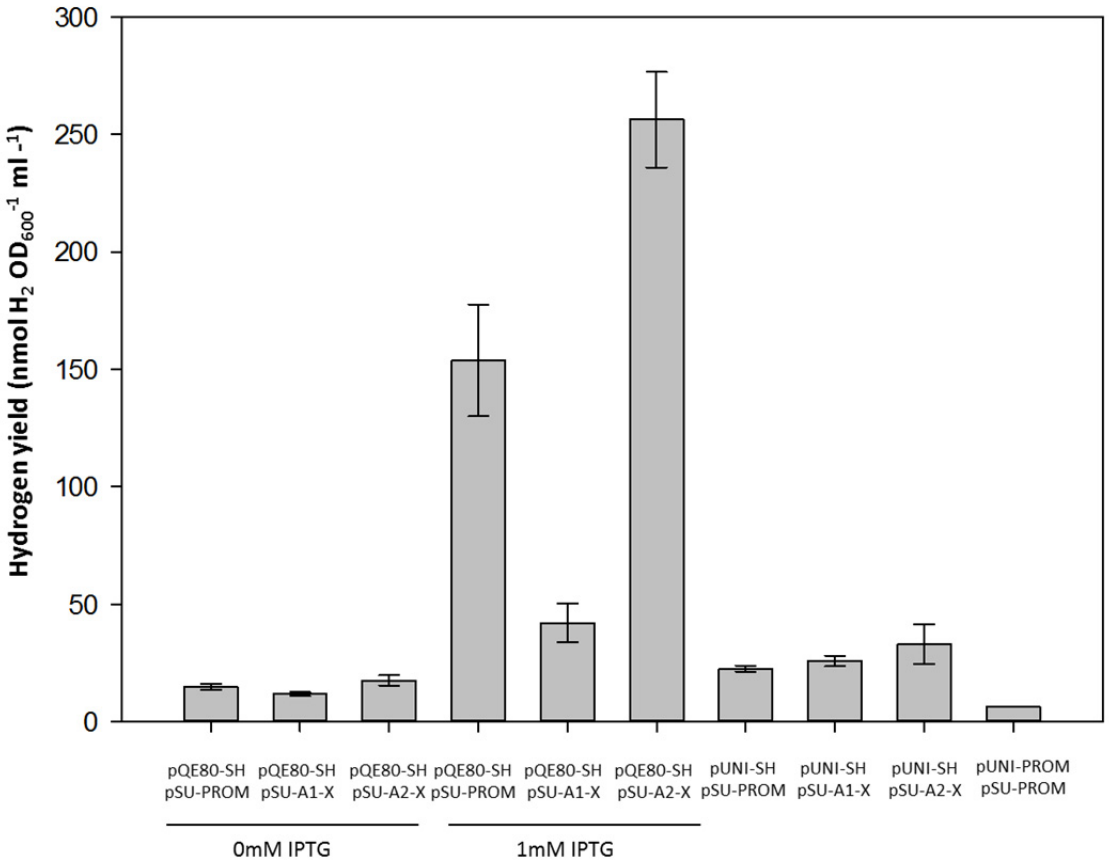

Figure 2.8 Heterologously expressed SH exhibits hydrogen production *in vivo*. *E. coli* strain HJ002 was transformed with either pQE80-SH or pUNI-SH together with either a control plasmid (pSU-PROM) or a plasmid carrying the synthetic *hypA1-X* operon or the *hypA2-X* operons (pSU-A1-X or pSU-A2-X respectively). Successful transformants were grown aerobically overnight at 37 ^{o}C in 5 mL M9 media supplemented with 0.8 % glucose, 0.2 % casacids, 100 µM $FeCl_3$ and appropriate antibiotics. The next day, the same media was made up and sparged with N_2 for 1.5 hours to remove dissolved O_2. Then, in an anaerobic cabinet, Hungate tubes were filled with containing 5 mL of this anaerobic media and sealed, before inoculation with 50 µL of the overnight culture. The Hungate tubes were inverted and incubated at 37 ^{o}C without shaking for 24 hours, after which the H_2 in the headspace was determined by gas chromatography in a single end-point assay Error bars represent SEM (n=3).

A number of points can be inferred from these data. Firstly, the pQE80-SH vector, when induced with 1 mM IPTG, resulted in a clear increase of H_2 production. This recapitulates the *in vitro* data presented in Figure 2.7 where a similar increase in activity was observed upon induction with IPTG.

Another conclusion drawn from the data presented in Figure 2.8 is that there is H_2 production levels from strain HJ002 carrying pQE80-SH/pUNI-SH even without the specially designed synthetic operons encoding the *C. necator* maturases. The native *E. coli* maturases are clearly able to assemble an active SH (Figure 2.8), thus partly corroborating the reciprocal experiment where the *C. necator* maturases were able to activate *E. coli* hydrogenase activity (Figures 2.5). The presence of the HypA1-X apparatus also allows for formation of functional SH (Figure 2.8). This finding corroborates previous reports that HypA1B1F1 can substitute for HypA2B2F2 (Wolf *et al*., 1998).

It was hypothesised that a functional SH, evolving H_2 *via* oxidation of NADH, would help replenish the NAD^+ pool and so confer a fitness advantage to a cell undergoing fermentation, especially in a Δ*adhE* mutant such as HJ002. Indeed, this has recently been reported where a plasmid carrying the native *hox* operon for the SH was able to induce a low level of anaerobic growth to an *E. coli adhE* mutant (Ghosh *et al*., 2013). In this work, however, no discernible difference in OD_{600} was found between the different strains when expressing the pUNI-SH vector or any of the others, implying that the functional SH developed here conferred no fitness advantage to a Δ*adhE* strain over a long timescale (Figure 2.9). This could be explained by the relatively low level of SH activity in this system.

Whilst it has been demonstrated here that the *E. coli* Hyp machinery is sufficient for proper SH assembly, it is apparent from Figure 2.9 that the presence of the putative HypA2-X suite of maturases result in quicker initial growth of cells that also constitutively express the SH, even outgrowing the wild type strain MC4100 (Figure 2.9). It may be possible that over a short time (until approximately 12 hours), the HypA2-X proteins do in fact allow for greater SH assembly compared to the *E. coli* Hyp proteins, and that there is a corresponding short term increase in fitness for *adhE* mutants.

It is also interesting to note that overproduction of the SH, *via* pQE80-SH, seemed to inhibit growth (Figure 2.9), suggesting that the synthesis of large quantities of SH actually conferred a

fitness disadvantage over any advantage gained by the [NAD^+] increase due to more SH being present.

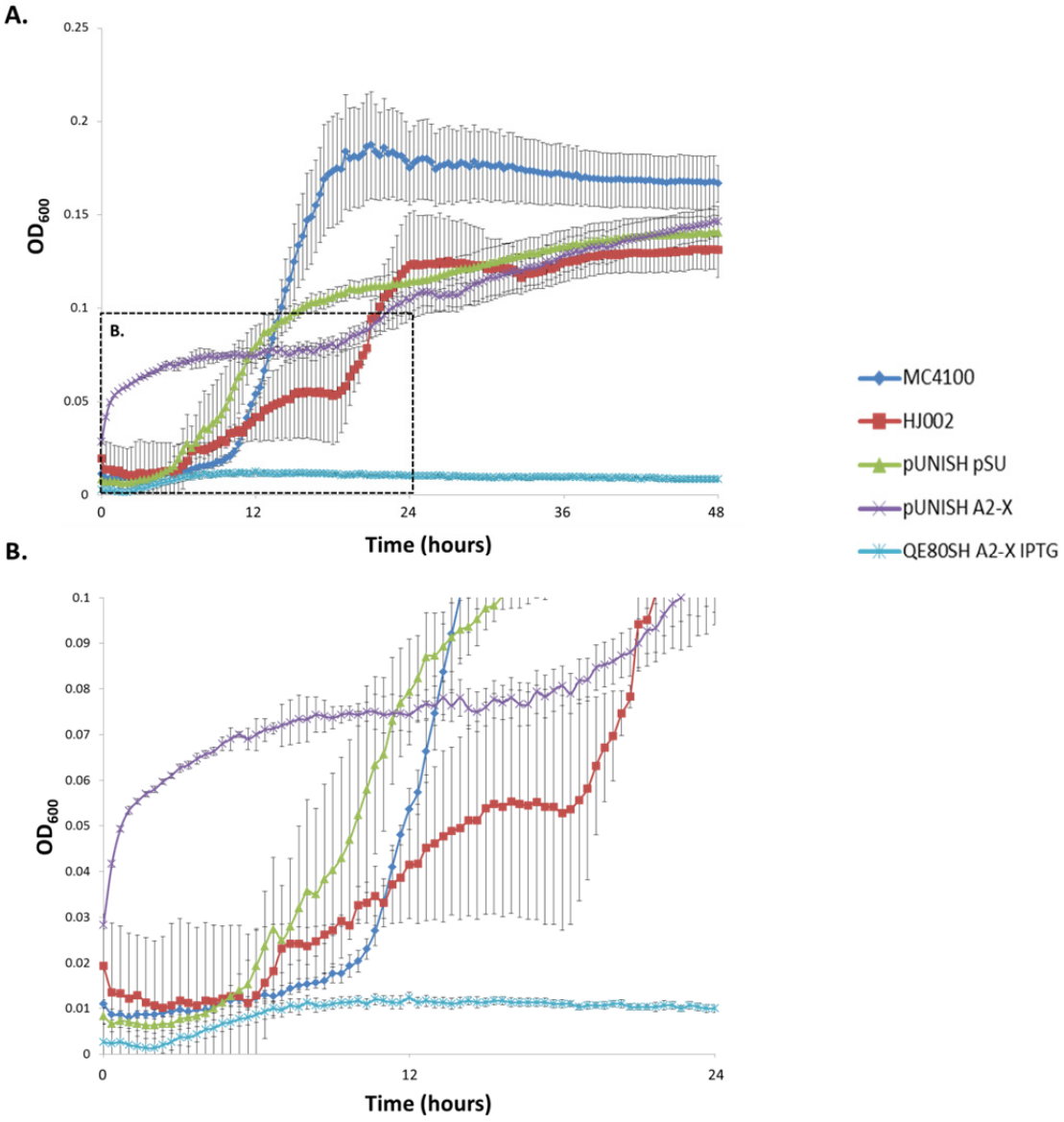

Figure 2.9 The SH enzyme is not capable of rescuing fermentative growth in Δ*adhE* mutants. (**A**) *E. coli* HJ002 cells (deficient in *adhE*) transformed with various vectors, or MC4100, were grown anaerobically in M9 media supplemented with 0.8% (w/v) glucose, 0.2% (w/v) casamino acids and appropriate antibiotics at 37 ^{o}C without shaking for 72 hours in a plate reader, which measured OD_{600} at 20 minute intervals.(**B**) shows the same data in (**A**) from time points between 0 and 24 hours. '**MC4100**': *E. coli* growth positive control. '**HJ002**': negative control. '**pUNISH pSU**': HJ002 constitutively expressing SH, and using the native *E. coli* maturases for proper assembly. '**pUNISH A2-X**': HJ002 cells constitutively expressing SH and the dedicated SH maturase proteins as identified by (Ghosh *et al.*, 2013). '**QE80SH A2-X +IPTG**': HJ002 overexpressing the *hoxF-I* operon to produce an overabundance of SH, with constitutive levels of the dedicated HypA2-X machinery.

2.4 **Discussion**

2.4.1 Complementation by the *C. necator* maturases

As was shown in Figure 2.5, the *C. necator* maturation machinery is able to complement *E. coli hyp* mutants, and Figure 2.8 showed that the *E. coli* Hyp proteins could assemble an active SH. Each maturation protein has a distinct role in hydrogenase assembly and so the nature of this complementation varied from maturase to maturase. First it was seen that, as previously reported (Jacobi *et al*., 1992), the *E. coli hypA* mutant retained some hydrogenase activity (Figure 2.5B). This suggests that HypA, a nickel-binding protein active in the last steps of cofactor insertion (Bock *et al*., 2006), is clearly not critically required under the conditions tested. Indeed, it can be seen that under these growth conditions the *hypA* mutant was able to accumulate hydrogen to the same level as the control strains.

HypB is a nickel-binding GTPase the role of which can be by-passed by increasing the amount of nickel salts in the growth medium (Bock *et al*., 2006). The fermentative H_2 production by the *E. coli* Δ*hypB* strain was low (Figure 2.5B) but this was restored to native levels by introduction of either HypA1-X or HypA2-X (Figure 2.5B), suggesting the *C. necator* HypB1 and HypB2 maturases can substitute for the *E. coli* HypB protein.

HypC is a small protein that acts as a bridge between the initial [NiFe] cofactor biosynthesis proteins and the empty apoenzyme (Bock *et al*., 2006), in particular making direct contact with the catalytic subunit of Hyd-3 (Drapal and Bock, 1998). In the hydrogen production assay here utilised, the Δ*hypC* mutant demonstrated significant hydrogenase activity (Figure 2.5B). This may be a consequence of the HypC homologue HybG contributing to cellular hydrogenase activity (Blokesch *et al*., 2001). Nevertheless, co-expression of HypA1-X and HypA2-X restored hydrogen evolution back to native levels (Figure 2.5B), suggesting that *C. necator* HypC1 can substitute for *E. coli* HypC. This is an interesting finding, since it implies that some previously unsuspected promiscuity may exist between cofactor insertion proteins from different

biological systems. Indeed, the HypC protein from *Dehalococcoides mccartyi* was also recently shown to be able to activate the *E. coli* [NiFe]-hydrogenases (Hartwig *et al*., 2015).

The operons encoding HypA1-X and HypA2-X can also rescue a Δ*hypD* mutant (Figure 2.5B), which encodes a protein that acts an initial scaffold for the first stages of cofactor biosynthesis (Bock *et al*., 2006).

Unlike the maturases previously discussed, the complementation of *E. coli hypE* and *hypF* mutants, which encode two proteins that interact extensively (Stripp *et al*., 2015), is less compelling (Figure 2.5B). The *C. necator* HypE1 protein (which is identical in both *hypA1-X* and *hypA2-X* plasmids) is able to complement a Δ*hypE* mutation, although hydrogenase activity is clearly reduced (Figure 2.5B). However, in the absence of endogenous *E. coli hypF*, it is clear that *C. necator hypF1* was completely inactive in this assay (Figure 2.5B).

The findings in this Chapter that maturase proteins are complementary between *E. coli* and *C. necator* systems contrasts with the consensus in the literature that dedicated system-specific Hyp machinery was required for proper SH assembly, although it has been previously suggested that *E. coli* maturases can aid SH maturation to some degree (Schiffels *et al*., 2013). Indeed, sequence homology between the suite of proteins from *C. necator* and their counterparts in *E. coli* show a high degree of similarity (Figure 2.10).

It can be seen that the truncated HypF1 shares least homology with the *E. coli* homologue, and so corresponds with the data obtained implying that it could not complement a *hypF E. coli* mutant. An alternative explanation, given credence by the difficulty in identifying HypF1 by radiolabelling (Figure 2.4), is that there is a problem with HypF1 biosynthesis in the cell, despite the sequence of *hypF1* being correct. Unlike HypF1, the non-truncated HypF2, which is normally co-produced with the SH itself, more closely resembles the native *E. coli* protein (Wolf *et al*., 1998), and can complement a Δ*hypF E. coli* mutantion accordingly. This homology is perhaps not unsurprising, considering *E. coli* and *C. necator* are not too distantly related,

with both being members of the Proteobacteria phylum, although belonging to different classes with *E. coli* being ranked taxonomically as a γ-Proteobacterium and *C. necator* a β-Proteobacterium. The result that the presence of HypA1-X suite of maturases resulted in less H_2 evolution than the *E. coli* maturases when the SH operon was over-expressed (Figure 2.8) is interesting. This is hard to explain, as the *E. coli* maturases were still present when the cell contained the pSU-A1-X vector. As such, it would be assumed that if the HypA1-X set were merely unable to successfully synthesise the SH, the *E. coli* suite would perform this role, and so the amount of H_2 evolution seen would be the same as that observed in the 'pSU-PROM' sample. Clearly this is not the case, and so something else must be occurring.

One hypothesis could be that the potentially problematic HypF1 protein is interfering with the *E. coli* suite of maturases from functioning efficiently. It is known that HypE and HypF (and homologues) interact during active site formation, and so if the HypF1 protein does indeed show aberrant function as previously supposed in this Chapter, so it could be preventing the functional *E. coli* HypF from interacting properly with HypE.

Nonetheless, this possible problem with the HypA1-X maturases is only seen during overexpression; it can be seen that when the SH operon is only constitutively expressed, there is no significant difference in H_2 evolution when the HypA1-X, HypA2-X, or the native *E. coli* maturases are present (Figure 2.8).

***E. coli* v *C. necator* maturases**	**Sequence Identity**	**Sequence Similarity**	**Gaps**
HypA vs HypA2	40/116 (34.5%)	62/116 (53.5%)	3/116 (2.6%)
HypA vs HypA1	36/120 (30%)	53/120 (46.7%)	5/120 (4.2%)
HypB vs HypB2	161/335 (48.1%)	190/335 (56.7%)	60/335 (17.9%)
HypB vs HypB1	165/372 (44.4%)	198/372 (53.2%)	93/372 (25.0%)
HypF vs HypF2	340/837 (40.6%)	451/837 (53.9%)	117/837 (14.0%)
HypF vs HypF1	145/790 (18.4%)	193/790 (24.4%)	436/790 (55.2%)
(if discounting truncation)	145/412 (35.2%)	193/412 (46.8%)	58/412 (14.1%)
HypC vs HypC1	25/96 (26.0%)	46/96 (47.9%)	12/96 (12.5%)
HypD vs HypD1	176/391 (45.0%)	240/391 (61.4%)	30/391 (7.7%)
HypE vs HypE1	160/355 (45.1%)	208/355 (58.6%)	37/355 (10.4%)

Figure 2.10. Sequence homology between maturase enzymes in *E. coli* and *C. necator*. Protein sequences were analysed using the EMBOSS Needle software (http://www.ebi.ac.uk/Tools/psa/emboss_needle/). 'Sequence Identity' indicates identical residues; 'Sequence Similarity' indicates residues with R-groups of the same chemical properties. Compared to HypF, HypF1 appears truncated at the N-terminus, with no sequence homology occurring until residue 379 of HypF. '**(if discounting truncation)**': shows sequence comparison of HypF from residue 379 to the end of the peptide, and the whole of HypF1.

HypX has been postulated by some to permit the coordination of an additional cyanide ligand to the Ni in the active site of SH and MBH (but not the RH) of *C. necator*, which confers O_2 resistant activity (Bleijlevens *et al*., 2004; Buhrke *et al*., 2001; Buhrke and Friedrich, 1998). It therefore follows that there is no homologous HypX protein in *E. coli*, given that no similar

oxygen resistant hydrogenases occur in this species, although O_2-tolerance does occur in Hyd-1 based on alternative chemistry (Lukey *et al*., 2010).

2.4.2 Comprehensive design of operons for expression and characterisation of the SH

This study reports the construction of two synthetic operons for heterologous expression of SH from *C. necator* in *E. coli*. Codon optimisation, in addition to the engineering of artificial, strong 16s rRNA binding sites and spacers in front of each gene, was performed in an effort to maximise gene expression, and was shown by the ^{35}S-methionine radiolabelling data to be successful. Both the *hoxF-I* and *hypA2-X* operons designed were polycistronic in nature; with only one promoter controlling expression of the whole operon, and so only one long mRNA product transcribed. It is therefore perhaps surprising that no problems with protein synthesis were found, as previously it has been reported that such design may give rise to problematic mRNA secondary structure and translation, particularly with genes further away from the promoter (Kim *et al*., 2004).

An attempt to purify the SH complex was carried out, in part to help with the *in vitro* characterisation of the heterologously expressed enzyme (Figure 2.6). Whilst activity was detected in the crude extracts of anaerobically-grown cells (Figure 2.7), no activity was observed in the purified enzyme obtained from aerobically-grown cells. This correlates with previous findings of purified SH, where aerobically purified SH was found to be inactive and required reductive treatment in order to activate the enzyme (Burgdorf *et al*., 2005b). The purification procedure would ideally be carried out as described by Burgdorf *et al*. (2005b). Indeed, the authors here explicitly state that affinity chromatography does not lead to the production of a stable functional enzyme, which was the method used in the work described in this Chapter (Section 2.3.3). Mass spectroscopy ought to have been performed on the purified protein fractions to ensure the complete SH apparatus was present.

SH diaphorase activity was not detected *in vitro* at all in this work, why this was the case could be explained as follows. The SH enzyme contains two flavin mononucleotide (FMN) cofactors, one in HoxF, which is ever-present and termed FMN-b, and another transiently present in HoxY named FMN-a, which may be dissociate from the complex upon reduction by NADH (Burgdorf *et al*., 2005b).

It has been proposed that FMN-a is responsible for the O_2 tolerance of SH; its location near to the [NiFe] active site allowing for rapid transfer of charges to the adjacent [Fe-S] cluster and on to the diaphorase component of the enzyme (Burgdorf *et al*., 2005b). However, this releasing of the FMN has been suggested to interfere with the *in vitro* measurement of diaphorase activity of the enzyme, but not the hydrogenase activity. This is likely the reason why no diaphorase activity was detected *in vitro* in Section 2.3.4; however it has been reported that this problem can be overcome with the addition of excess FMN to the assay buffer. The decision was taken to not proceed with trying this as the more physiologically relevant in *vivo* data had already been gathered showing the SH was functional.

Another reason for the lack of activity seen in the diaphorase assays compared to that reported in Lauterbach and Lenz (2013) is that here crude extracts were used. In that paper, purified enzyme was assayed, produced by its native species no less. However, this was impossible to test in this report due to the aforementioned problems with purification. As a result, any activity would be far lower, perhaps beyond levels of detection. Note well, however, that the *in vivo* GC-based data shows that H_2 is being evolved so implying that the diaphorase half of the SH could be functional in the cell. There is no other obvious route to the hydrogenase component receiving electrons.

2.4.3 Possible routes to improve SH functionality

Despite the genetic optimisation performed in this study, the activity of this heterologously produced SH in *E. coli* is much lower than that reported by others (Ghosh *et al*., 2013; Schiffels *et al*., 2013). For example, in terms of the *in vivo* data, a noticeable discrepancy exists between the H_2 yield from the heterologous SH production described in this Thesis and the yield reported by Ghosh *et al.* 2013. There, it was found that a maximum of 2.1 mol H_2 was evolved per mole glucose, which is often regarded as the theoretical maximum during mixed acid fermentation (Ghosh *et al*., 2013). Whilst the absolute theoretical maximum yield is 12 of mol H_2 per mol of glucose (as complete hydrolysis of glucose is $C_6H_{12}O_6 + 6H_2O \rightarrow 12\ H_2 + 6\ CO_2$) (Davila-Vazquez *et al*., 2008) the theoretical maximum for microbial reactions seems to be 2-4 mol H_2 per mol glucose (Davila-Vazquez *et al*., 2008).

In the data presented in this Chapter, the highest yield of H_2 was found (HJ002 with pQE80-SH + pSU-A2-X + 1mM IPTG) to be only 0.7 mmol H_2 per mole glucose (Figure 2.8). Interestingly, MC4100 was used as a positive control for that GC experiment and yielded only 0.63 moles H_2 per mole of glucose. Therefore, the heterologous expression of the SH by Ghosh *et al.* 2013 actually outperformed the wild-type *E. coli* in our hands. This finding is doubly interesting because in Ghosh *et al.* (2013) the media contained only 0.4 % (w/v) glucose, whereas the media in this Thesis was more highly enriched in terms of carbon, with 0.8 % (w/v) glucose in the M9 media, in addition to 0.2% (w/v) casamino acids. The large discrepancy in terms of heterologous SH activity may be as a result of other additives used in Ghosh *et al.* (2013) that were not used here, e.g. the additional Ni (II) added in the Ghosh *et al*. (2013) protocol. There, the nickel salt concentrations in the growth media was reportedly 25 µM, whereas in this Chapter no additional nickel was added beyond that in the trace element supplementation and thus came to final concentrations of only 1 µM. These concentrations were evidently sufficient for formation of both the heterologously produced SH and also the native *E. coli* hydrogenases,

but may not be sufficient for optimal assembly of the SH holoenzyme. However, a recent study suggested 1 µM of Ni aided SH production, albeit in *C. necator* (Jugder *et al*., 2016).

It was hypothesised that this possible lack of Ni(II) ions could be responsible for the inclusion bodies observed during SH overproduction, and why no fitness advantage was conferred to Δ*adhE* mutants in this Chapter (Figure 2.9). However, when the *in vivo* GC assay was repeated using this elevated Ni concentration (25 µM), growth was severely diminished, with OD_{600} of only 0.05 after 72 hours incubation. This suggests that this Ni(II) concentration was toxic, which correlates to the literature, where Ni(II) is known to be toxic when in high abundance, especially in minimal media (Wu *et al*., 1994). The toxic concentration reported in Wu *et al.* (1994) was 300 µM, however this was in a strain with a deletion in the nickel transporter-encoding *nik* operon. With a functional nickel transporter, such as in HJ001/HJ002 used in this Thesis, the Ni(II) concentration leading to toxicity would be much lower. On the other hand, Ni(II) levels can be as high as 600 µM without negative impact on fitness in rich media, where presumably there are more compounds to help chelate Ni(II) (Waugh and Boxer, 1986).

An alternative explanation as to why this high Ni(II) concentration was necessary for SH function as reported in Ghosh *et al*. (2013) is that the unoptimised HypA2 and HypB2 proteins used in that study were non-functional in *E. coli*. These maturases are involved in nickel insertion into the active site, but at high Ni(II) levels the metal may integrate spontaneously, and thus HypA2 and HypB2 become redundant. However, it would be supposed that the native *E. coli* HypAB would be able to produce functional SH in lower Ni(II) concentrations, as was intimated by the data presented in this Chapter (Section 2.3.2). Utilising the additional *C. necator* gene, *hoxN1*, which encodes a high affinity nickel transporter, may also help synthesis of functional SH at lower concentrations of Ni(II) (Schiffels *et al*., 2013). With this additional transporter biosynthesised in tandem, 1 µM Ni(II) was sufficient for proper assembly of the SH; indeed levels any higher than 1 µM actually compromised cell fitness, likely due to the

intracellular levels of Ni reaching toxic levels (Friedrich *et al*., 1981a), where it reportedly inhibits the action of fructose-1,6-bisphosphate aldolase (Macomber *et al*., 2011).

Other modifications to the growth conditions protocol as used in this Thesis could also be performed in an attempt to boost SH activity. For example, it has previously been reported that lowering the incubation temperature to 22- 25 ^{o}C aids in heterologous SH production in *E. coli* (Schiffels *et al*., 2013). This study recapitulated the protocol of Ghosh *et al*. (2013) in terms of supplementation with Ni(II) (albeit to a final concentration of only 1 μM $NiCl_2$) being optimal. Intriguingly, the study also suggested the addition of 1 μM riboflavin to the growth media was also required, to allow for optimal FMN formation. This is surprising, as *E. coli* can naturally produce riboflavin and other flavin cofactors, including FMN, in M9 minimal media (Pedrolli *et al*., 2015). Indeed, because *E. coli* contains no riboflavin importers (Hemberger *et al*., 2011), presumably addition of riboflavin to the media ought to confer no benefit to SH biosynthesis.

Under standard conditions (1 M of each compound, pH 7, 25 °C), the standard reduction potentials of the $NAD^+ + H^+ + 2e \rightarrow NADH$ and $2H^+ + 2e \rightarrow H_2$ half reactions are -320 mV and -420 mV, respectively (Thauer *et al*., 1977). Therefore, under standard conditions, it would be thermodynamically favourable for the SH system to catalyse the H_2 dependent reduction of NAD^+; that is, the direction of catalysis as found physiologically for the SH in *C. necator*, and the opposite of the direction investigated for the heterologous SH biosynthesis investigated in this Chapter. Whilst the cytoplasm of a fermentative *E. coli* cell is not under standard conditions, with an acidic pH and a high $NADH/NAD^+$ ratio, this thermodynamic bias of the system will nonetheless be expected to put a fundamental limit on the maximum yield of H_2 that can be evolved by the SH. In nature, hydrogenases that catalyse H_2-evolution using NADH as a substrate are normally bifurcating enzymes: that is they take electrons from two different sources. For example, the [FeFe]-hydrogenase from *Thermotoga maritima* requires the co-oxidation of reduced ferredoxin (E_m -500 mV) to 'power' the NADH-linked formation of H_2

under physiological conditions (Schut and Adams, 2009). Therefore, it is difficult to envisage how the SH enzyme alone could allow for H_2 evolution levels approaching the theoretical maximum.

2.4.4 Was SH codon optimisation required?

Another possible explanation for the heterologous SH activity seen in this Chapter being lower than previous attempts could be that the codon optimisation actually resulted in poorer enzyme biosynthesis. A completely codon optimised gene would mean that, due to the abundance of the corresponding tRNA, translation would be expected to occur at the maximum possible rate. Indeed, it could be supposed that this would be at a higher rate than is 'natural' in *C. necator*. It is feasible to hypothesise that the formation of the nascent peptide may become desynchronised with the cofactor insertion processes, as has previously been proposed (Hurley and Dunlap, 2013). Whilst the radiolabelling performed in this Chapter confirmed that the full suite of proteins were fully synthesised, it says nothing about whether the proteins are properly folded and contain all requisite cofactors. This may account for the lesser H_2 evolution seen here compared to other attempts at heterologous production of the SH in *E. coli* (Ghosh *et al*., 2013; Schiffels *et al*., 2013).

A more effective codon optimisation strategy may be to match the codon preference in the synthetic operons to that seen in the wild-type sequences. In other words, analysis should be carried out to see which codons in the native sequences correspond to abundant/rare tRNAs in *C. necator*, and match these codons to abundant rare/ tRNAs for *E. coli*. Similarly, the mRNA produced by the synthetic operons may not be conducive to optimal translation. One of the previous approaches to heterologously produce SH in *E. coli* employed a different strategy to improve gene expression (albeit of the native *C. necator* genes) (Schiffels *et al*., 2013). There, individual promoters and terminators were inserted to bookend each gene; a move taken to

counteract problems with translation of polycistronic mRNA (Schiffels *et al*., 2013). This contrasts to the strategy employed in the work described in this Chapter, where one promoter (the *tat* promoter) was present at the beginning of the operons. Perhaps employing this alternative approach could yield better SH heterologous biosynthesis.

Unlike Ghosh *et al.* (2013), the work presented in this Thesis included *hypX* in the maturase operon construction. It has previously been reported in the literature that HypX is needed for O_2 tolerance (Bleijlevens *et al*., 2004; van der Linden *et al*., 2006) and its absence has been seen to reduce the activity of SH in *C. necator* by as much as 50% (Buhrke and Friedrich, 1998). Conversely, the data presented in this Chapter has shown that the lack of the other *C. necator* maturase genes (*hypC1E1D1*) in their SH operon ought not to be relevant, as again the *E. coli* counterparts to these maturases can complement their absence.

Although SH retains functionality in the presence of oxygen (Bleijlevens *et al*., 2004), and aerobic growth may help for purification due to increased biomass and thus protein yield, SH had to be heterologously expressed in *E. coli* anaerobically in this study. This is because the nickel transporter machinery in *E. coli*, encoded by the *nikABCDER* operon (Navarro *et al*., 1993), is modulated by the FNR transcriptional activator and thus requires anaerobiosis for expression. Therefore, for SH to be aerobically expressed, either this FNR dependence must be abolished in the *E. coli* nickel transporter, or another nickel transporter used, such as HoxN1 from *C. necator* (Eberz *et al*., 1989; Wolfram *et al*., 1995).

2.4.5 SH activity cannot rescue fermentative growth of an Δ*adhE* mutant.

Under anaerobic conditions, *E. coli* can employ exogenous electron acceptors other than O_2 to carry out anaerobic respiration, and thus still utilise oxidative phosphorylation for ATP generation and NAD^+ regeneration. One example of a non-O_2 respiratory electron acceptor in *E. coli* is fumarate, which is reduced to succinate during fumarate respiration (Unden and

Bongaerts, 1997). However, in the absence of such external acceptors, an anaerobic cell must undergo fermentation. Here, ATP generation is limited to substrate-level phosphorylation during glycolysis, and is thus an inferior method of energy derivation. Furthermore, NAD^+ regeneration is compromised by the lack of oxidative phosphorylation. In order to overcome this, and thus allow glycolysis to continue, *E. coli* utilises mixed acid fermentation, where pyruvate and its derivatives are reduced to a variety of acids and ethanol (Figure 2.11).

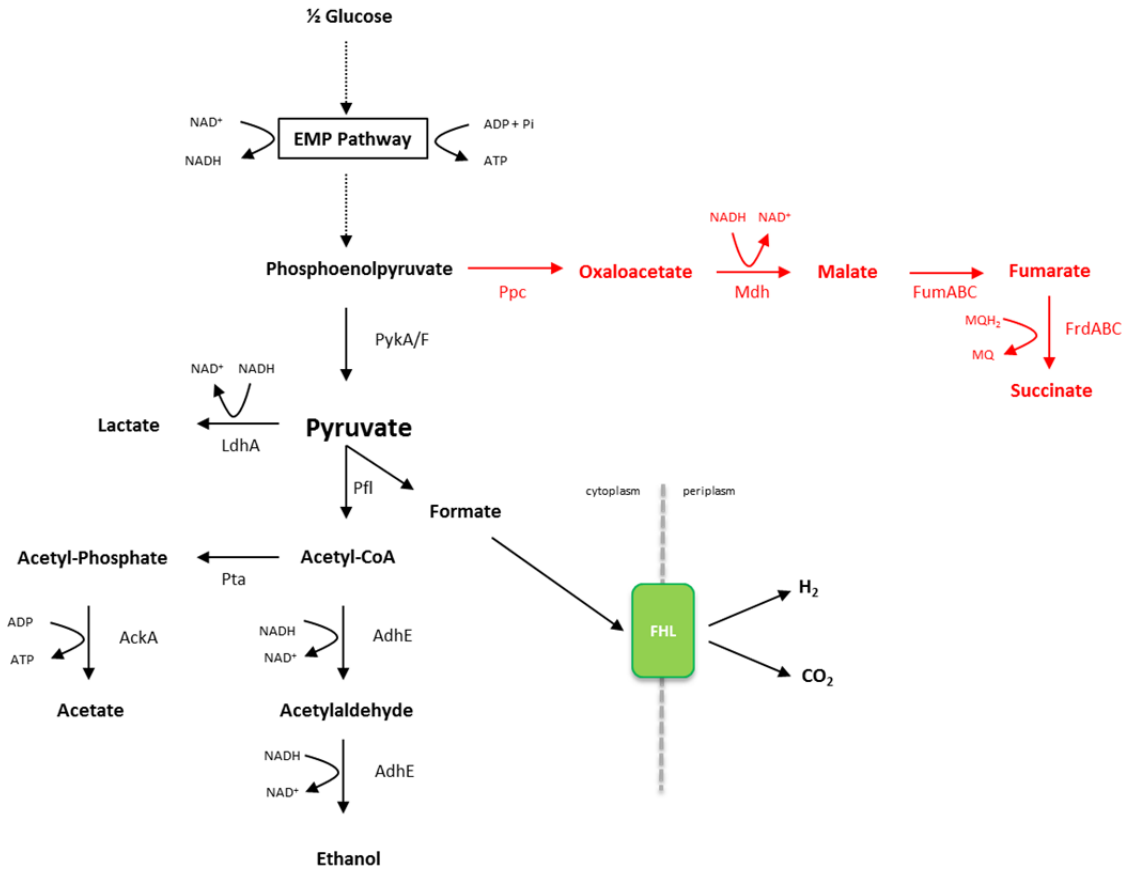

Figure 2.11 The reductive pathways of mixed acid fermentation allow for NAD^+ regeneration. Enzyme abbreviations: Ppc: phosphoenolpyruvate carboxylase; Mdh: malate dehydrogenase; FumABC: fumarase; and FrdABC: fumarate reductase PykA/F: pyruvate kinase; LdhA: lactate dehydrogenase; Pfl: pyruvate formate lyase Pta: phosphotransacetylase; AckA: acetate kinase; AdhE: alcohol dehydrogenase. FHL: formate hydrogenlyase (containing Hyd-3). EMP Pathway: Embden–Meyerhof–Parnas Pathway. Red text comprises part of the TCA cycle (reductive direction) which, although it regenerates NAD^+, is not sufficient itself for anaerobic growth on sugars. Furthermore, the low availability of required electron donors required for fumarate reductase operation will minimise this mode of NAD^+ regeneration.

Despite the various reduced end products produced, a cell undergoing mixed acid fermentation will still have a low [NAD^+] to [NADH] ratio. Therefore, any process that further increases this ought to increase cell fitness, and this would only be accentuated should any of the native NAD^+-regenerating pathways be abolished. Such was the rationale behind utilising SH in a Δ*adhE* mutant. However, it was demonstrated in this chapter that SH made no difference to fitness; the activity was at too low a level to significantly impact cell growth. A new strain HJ004, deficient in *ldhA,* has been generated from HJ002 in an attempt to further

impair NAD^+ regeneration and thus try to confer a bigger fitness advantage of the functional SH, but this has not yet been tested. Similarly, a Δ*arcA* allele, to de-repress the synthesis of the TCA cycle during anaerobiosis, might help boost the SH activity further. Indeed, this is a another possible explanation for the discrepancy in activity seen here and that reported in (Ghosh *et al*., 2013).

It would be desirable to have the SH activity at a basal level that gave some fitness advantage, as it would then mean that directed evolution could be performed to further optimise the activity. Of course, for such a technique to be feasible, a screening method to efficiently analyse a mutant library resulting from such random mutagenesis would need to be devised. The attempt to develop one such screen for improved hydrogen production is discussed in Chapter 3.

3. Towards the construction of an intracellular hydrogen biosensor in *Escherichia coli*.

3.1 **Introduction**

3.1.1 The need for a genetic screen for increased hydrogen production

At present the predominant method for modifying hydrogenases for improved activity is targeted protein engineering. A major drawback of this is the prerequisite for protein structures for optimum design. For example, this is a problem for the rational modification of FHL, which is the main source of H_2 evolution in *E. coli.* The FHL complex is difficult to purify and has not been crystallised to date. Indeed, it could be argued that researchers in the field could view the development of a genetic screen to measure H_2 production levels as a priority. This would remove the reliance on rational engineering, and allow the construction of mutant libraries that could then be screened for improved hydrogenase activity or hydrogen production.

Such libraries could consist of mutant strains generated by transposon mutagenesis, or banks of mutant genes constructed by error-prone PCR (epPCR), or metagenomic libraries, where DNA from whole communities in an environmental sample could be analysed. Of course, such a hydrogen production genetic screen could also allow directed evolution to be performed on engineered hydrogenases; honing the enzyme activity to the levels required for industrial-scale biohydrogen production.

3.1.2 The Regulatory Hydrogenase (RH) of *C. necator*

C. necator is found in habitats susceptible to transient anoxia and can switch between a heterotrophic lifestyle and lithoautotrophy. In the latter case it is able to utilise CO_2 as its sole carbon source and H_2 as its energy source (Pohlmann *et al*., 2006). To make use of this molecular hydrogen during lithoautotrophic growth*, C. necator* possesses three [NiFe]-hydrogenases: the Soluble Hydrogenase (SH), Membrane-Bound Hydrogenase (MBH) and

Actinobacterial Hydrogenase (AH) (Schafer *et al*., 2016). The SH and MBH enzymes are not constitutively expressed; their transcription is instead induced in the presence of H_2 and/or the scarcity of organic carbon sources (Lenz and Friedrich, 1998). This expression is controlled by the action of a fourth [NiFe]-hydrogenase found in the cell: the so-called Regulatory Hydrogenase (RH). Like the other *C. necator* hydrogenases, the RH exhibits resistance to O_2 attack. The mechanism of this tolerance is due to the presence of hydrophobic gas channels leading to the active site, which result in steric hindrance of O_2 molecule ingress but not the smaller H_2 molecules (Buhrke *et al*., 2005a). Additionally the RH possesses a non-canonical [Fe-S] cluster of the form [4Fe-3S-3O] (Buhrke *et al*., 2005b).

The RH is comprised of four proteins: the large and small subunits of the hydrogenase itself (HoxC and HoxB, respectively) in complex with a histidine kinase, HoxJ, which mediates the phosphorylation of a DNA binding protein, HoxA. A simplified schematic of how the RH operates is shown in Figure 3.1. In reality HoxBC forms a 'double dimer', which is in turn associated with a HoxJ tetramer (Buhrke *et al*., 2004). Whilst the mechanism of induction of HoxJ by HoxBC is not entirely understood, it is known that HoxJ contains a PAS domain; likely the input module for the redox potential signal from the hydrogenase component (Buhrke *et al*., 2004; Taylor and Zhulin, 1999).

It has been hypothesised that the reduction of the HoxB [Fe-S] cluster somehow causes a conformational change in the HoxCBJ complex and affect the phosphorylation activity (Buhrke *et al*., 2005b). HoxB is unusual for [NiFe]-hydrogenase small subunits in that it does not seem to contain three true [Fe-S] clusters, but rather only two plus a third cofactor, possibly [4Fe-3S-3O] (Buhrke *et al*., 2005b). This altered Fe-S cluster is also found in the ATCC 27774 [NiFe]-hydrogenase native to *Desulfovibrio desulfuricans* (Matias *et al*., 2001).

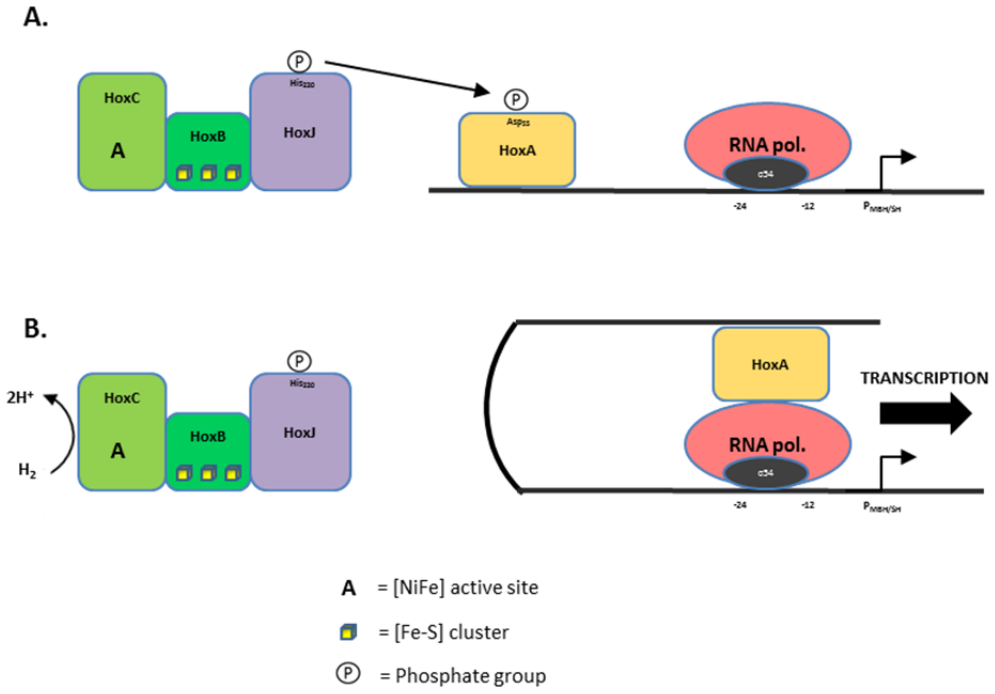

Figure 3.1 Summary of RH-mediated regulation of gene expression. Two genes, *hoxB* and *hoxC* code for the small and large subunits of an H_2-oxidising hydrogenase moiety of the RH respectively. This controls the activity of an associated third component: the histidine kinase, HoxJ. The fourth subunit, HoxA, sits on the chromosome upstream of the MBH and SH operons and mediates transcription in concert with a σ^{54} RNA polymerase complex. (**A**) In the absence of H_2, HoxJ phosphorylates HoxA, preventing interaction with the RNA complex and thus inhibiting MBH/SH gene expression. (**B**) However in the presence of H_2, HoxBC exhibits a low hydrogenase activity and, by a process still not entirely understood, causes HoxJ to cease its kinase activity. HoxA is then free to interact with the RNA polymerase and transcription ensues.

HoxA is a member of the NtrC family of transcriptional activators and is expected to work in tandem with an NtrA (σ^{54})-RNA polymerase complex (Eberz and Friedrich, 1991). It is thought that activated HoxA first binds to an enhancer sequence located upstream (typically ~100 bp) of the promoter. The still-bound protein then initiates transcription by direct interaction with the RNA polymerase, so contorting the DNA molecule (Su *et al*., 1990). Unlike the mechanism-of-action for other sigma factors, the σ^{54}:RNA polymerase holoenzyme sits intact on the promoter sites awaiting activation (Bonocora *et al*., 2015). The RH system operates contrary to typical two-component systems, in that it is the non-phosphorylated form of HoxA that activates transcription (Burgdorf *et al*., 2005a). It is therefore hypothesised that the histidine kinase HoxJ must be initiated/the de-phosphorylation of HoxA initiated in the presence of H_2.

Interestingly, the *hoxJ* wild type sequence from *C. necator* H16 produces a HoxJ with aberrant histidine kinase activity, whilst the closely related species *Alcaligenes hydrogenophilus* shows improved kinase capability (Lenz and Friedrich, 1998). This was understood to be due to a single residue mutation where *C. necator* H16 possesses a serine at position 422, where *A. hydrogenophilus* has a glycine. Subsequently in this chapter, this inactive native form of *C. necator hoxJ* sequence will be referred to as '*hoxJ*', and a modified version of the gene encoding the S422G substitution to allow for H_2-mediated transcription will be called '*hoxJ*'*.

The genes encoding the RH machinery are found on the 450 kb pHG1 megaplasmid, located in a gene cluster flanked by the genes encoding both the MBH and SH hydrogenases it controls (Burgdorf *et al*., 2005a) (Figure 3.2A). The genes encoding the maturases required for RH assembly, *hypA1-X*, are found upstream of the *hoxABCJ* genes (Figure 3.2B). Unusually, the RH large subunit does not require C-terminal processing, and has been said to have the simplest system for [NiFe] maturation (Lenz *et al*., 2015).

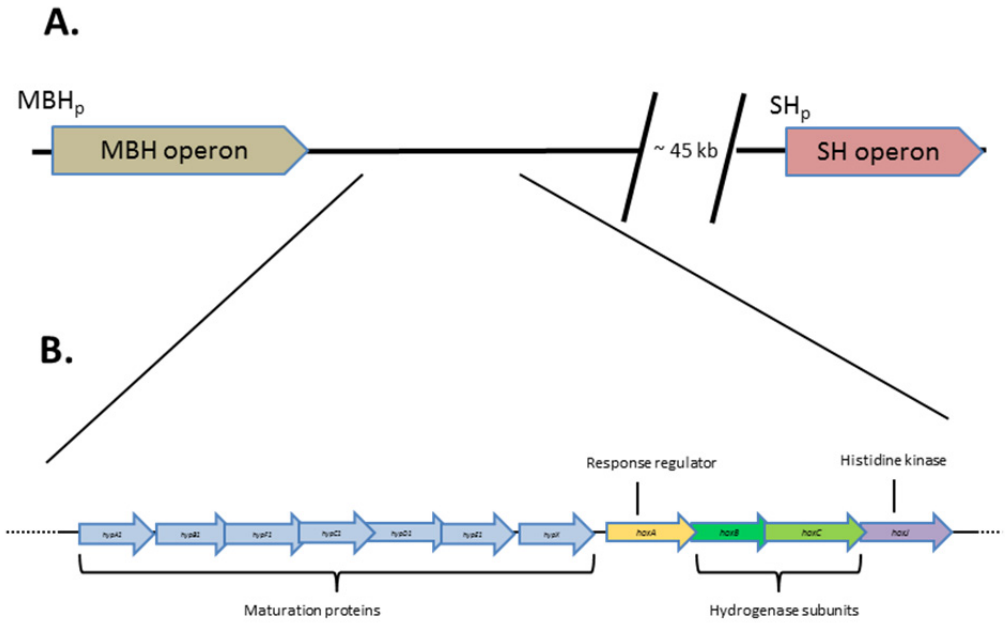

Figure 3.2 Gene cluster encoding RH in *C. necator*. (**A**) A broad view of a section of the pHG1 megaplasmid in *C. necator*. The genes encoding the RH are located on the pHG1 megaplasmid between those encoding the MBH and the SH (Friedrich *et al*., 2005). 'MBHp' and 'SHp' represent the promoters controlling expression of the MBH and SH operons respectively that are controlled by RH in response to H_2. (**B**) A 'zoomed-in' version of the region indicated shows that the RH *hox* genes lie downstream of the *hyp* operon coding for maturation proteins essential for proper [NiFe] active site assembly (Lenz *et al*., 2007). Adapted from Schwartz *et al*. (1999).

Interestingly, the RH encoding genes, *hoxABCJ*, belong to the same operon as the MBH and maturase suite of genes. Whilst *hoxA* expression is independent of the hydrogenase expression, it is nevertheless greatly enhanced by the presence of H_2, and this is due to the distal MBH promoter (Schwartz *et al*., 1999). Therefore, the RH is effectively transcribed by a positive feedback loop during lithoautotrophic growth (at least in the species with a fully functional HoxJ*), which induces the expression of ever more copies of the RH machinery (and MBH and HypA1-X maturases). This phenomenon also means that an extremely long mRNA transcript is produced from the MBH promoter, approximately 17 kbp long (Schwartz *et al*., 1999). Moderate constitutive promoters from within the MBH operon ensure that there is always a low level of RH synthesised in the cell, allowing it to be able to rapidly respond to H_2 levels (Lenz *et al*., 2015).

The RH system can be seen as a naturally occurring example of a transducer, converting one form of a signal — in this case a chemical signal H_2 — into another form, specifically a transcriptional one.

3.2 **Aims**

The main aim of the work presented in this chapter was to harness the RH system to act as an intracellular biosensor for H_2 in *E. coli*, allowing for the quantitative expression of reporter genes in response to various levels of H_2 (Figure 3.3). To achieve this, a functional RH will have to be assembled in an *E. coli* host and suitable reporter systems will be tested when coupled to RH-dependent promoter sequences. A secondary aim of this chapter was to harness *E. coli* Hyd-2 as an alternative to the RH to act as the hydrogenase in the biosensor.

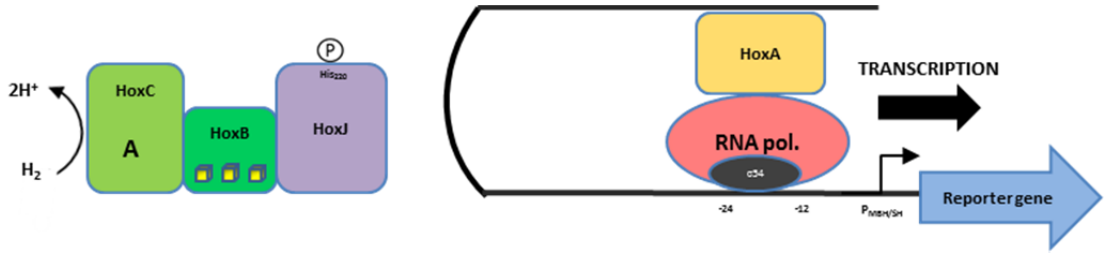

Figure 3.3 Recruitment of the RH to act as an intracellular H_2 Biosensor. It is envisaged that the a modified RH system could be recruited in *E. coli* to measure H_2 levels, with a view to becoming screening method. A reporter gene, such as *lacZ* or an antibiotic resistance gene, would be put under the control of the SH/MBH promoter, permitting its transcription in response to H_2 in a quantitative manner, and therefore meaning H_2 levels could be inferred by the magnitude of the reporter gene output signal seen.

3.3 **Results**

3.3.1 Initial attempts at RH heterologous production

The original strategy for generating an active SH in *E. coli* was simply to amplify and clone the native *C. necator hoxAJ* (albeit with HoxJ containing the mutation S422G to allow for functionality) and *hypA1-X* operons into expression vectors. First, *hoxAJ*, cloned from *C. necator* H16 genomic DNA, was inserted into the T7-possessing vector, pUNI-PROM. Site-directed mutagenesis (using the QuickChange protocol, Section 7.5.6) was then performed to introduce the S422G mutation required for RH functionality in *hoxJ*, thus forming *hoxJ**. The resultant vector construct was named pUNIR1-hoxAJ* (Plasmid table 7.6). The *C. necator* wild-type genes encoding the other half of the RH system, *hoxCB*, were then inserted in one multi-cloning site (MCS) of the commercially available two-MCS vector, pACYCDuet-1 (Novagen). Similarly, the operon encoding the maturases required for RH assembly, *hypA1-X* (Buhrke *et al*., 2001) were cloned into the other MCS of the same vector. The generated construct was called phypA1-X/hoxBC (Plasmid Table 7.6). Like pUNI-PROM, both MCSs of pACYCDuet are also under the control of a T7 promoter. All of this cloning was done by Dr Constanze Pinske.

Next, ^{35}S-Methionine radiolabelling was carried out to examine the production of the RH and associated Hyp proteins encoded by these new vectors (Figure 3.4). The *E. coli* strain K38 was transformed with either pUniR1-hoxAJ* or phypA1-X/hoxBC along with the vector pGP1-2 encoding T7 polymerase.

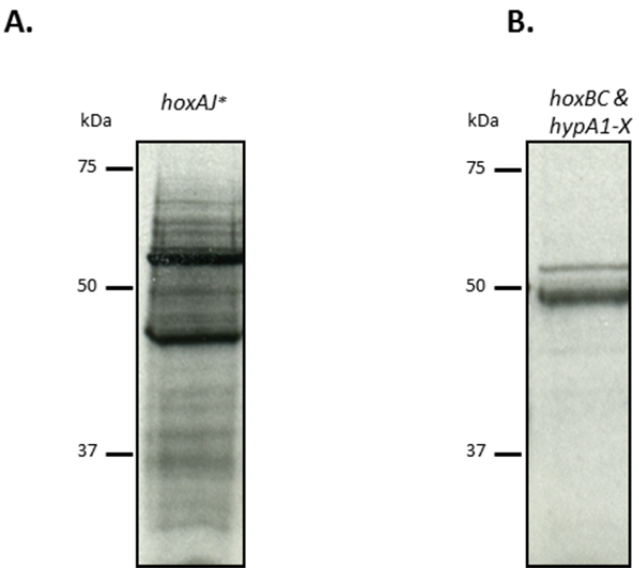

Figure 3.4 Native *C. necator hoxABCJ and *hypA1-X* genes lead to aberrant protein production in *E. coli.*** K38 [pGP1-2] cells were transformed with (**A**) pUniR1-hoxAJ* or (**B**) phypA1-X/hoxBC, to examine expression of the genes encoding the RH and associated maturases as found in *C. necator* H16 (including the S422G mutation in *hoxJ* allowing for functionality). ^{35}S-methionine radiolabelling was then performed to examine protein production from these genes.

It can be seen that there were problems with the heterologous production of the full suite of RH proteins from the native *C. necator* gene sequences. Two proteins were expected in Figure 3.4A corresponding to HoxA (54 kDa) and HoxJ* (51 kDa). The autoradiogram revealed two clear protein products from this experiment, however one had an apparent molecular mass by this method of (~55 kDa) and the second had an apparent mass of ~45kDa (Figure 3.4A). This led to the conclusion that the expression of one of these genes may be compromised, perhaps with incorrect initiation or a premature stop in translation for one or both genes. Similarly, in Figure 3.4B nine bands were expected corresponding to the structural proteins HoxB (36 kDa) and HoxC (52 kDa) and the seven maturases. That only two clear protein bands can be seen again suggests problems with gene expression. In an attempt to rectify this, genetic optimisation was performed on both the *hox* and *hyp* operons.

3.3.2 Design and optimisation of a synthetic *hoxABCJ** operon

To ensure efficient production of the RH in *E. coli* an optimized semi-synthetic operon was designed. The first stage of this was to determine whether the codon usage of the native RH genes from *C. necator* H16 was suitable for *E. coli* expression. This was done using the *OPTIMZER* web server utility, which gives codon adaptation indices 'CAI' scores to indicate codon usage compatibility, with 0 meaning no compatibility, and 1 being perfect expression using the host organism's preferred codons. The CAI scores of each native gene in the *C. necator hox* operon (bar the *hoxJ** modification) are shown in Figure 3.5.

Gene	CAI Score
hoxA	0.447
*hoxJ**	0.422
hoxB	0.404
hoxC	0.415

Figure 3.5 *OPTIMIZER* estimations of native RH codon usage suitability in *E. coli*. Each gene in the *C. necator* H16 *hox* operon was given a CAI score between 0-1 depending on how well the codon usage matches that optimal for *E. coli*, with 1 being a perfect match.

When using *OPTIMIZER* a threshold value of 0.3 is normally applied above which it can be assumed that codon usage is suitable for translation. Because each gene in the *hox* operon had CAI values >0.4, it was decided that it was not necessary to codon optimise the entirety of each gene. Instead, optimisation was done by concentrating on the first 20 codons only and leaving the remainder of each gene as wild type sequence. In addition, synthetic Shine-Dalgarno and linker sequences (5'-AGGAGGAAAAAAA-3') were also inserted before each gene in the operon. Optimised genes were amplified by PCR and sequentially inserted into the pUNI-PROM vector using suicide ligations (see Section 7.5.11), leading to the construction of four vectors in total: pUNI-hoxA; pUNI-hoxAJ*; pUNI-hoxAJ*B; and pUNI-hoxAJ*BC. Radiolabelling was then

performed using each of these vectors to examine synthesis of RH proteins *in vivo*. The results are shown in Figure 3.6.

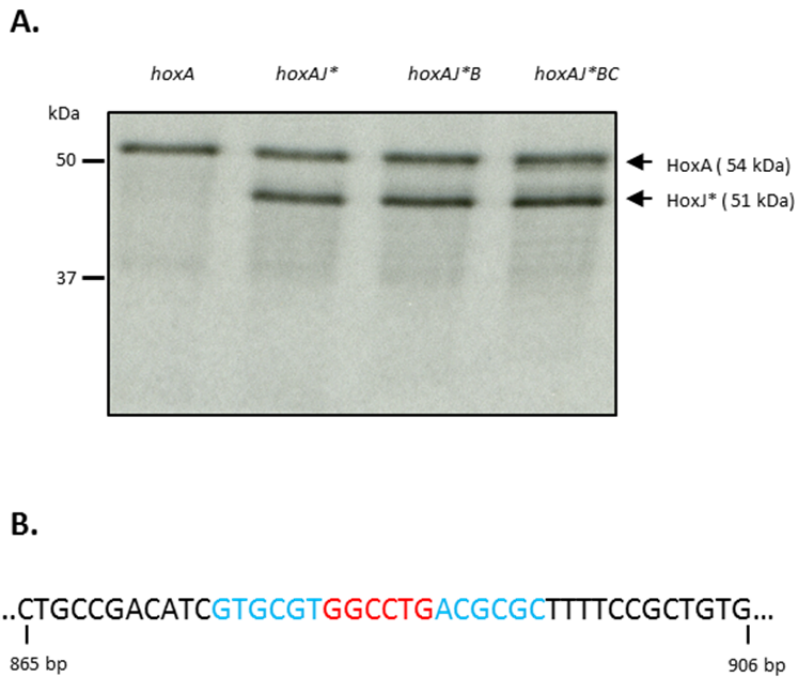

Figure 3.6 Genes cloned downstream of optimised *hoxJ are not efficiently translated.** (**A**) ^{35}S-methionine radiolabelling was performed using cells possessing various combinations of the optimised genes encoding for the RH structural proteins, HoxA, -J*, -B and –C, under the control of a T7 promoter. The specific vectors used were pUNI-hoxA, pUNI-hoxAJ*, pUNI-hoxAJ*B, pUNI-hoxAJ*BC, were constructed through sequential insertion of genes by suicide ligations. (**B**) Analysis of the *hoxJ** sequence with the terminator-predicting software, *ARNold*, showed the presence of a sequence leading to a stem loop structure in RNA towards the end of the 1413 bp *hoxJ** gene (between bases 865 to 906).

It appeared that there were problems with the production of the entire RH apparatus (Figure 3.6). Whilst the regulator and kinase components, HoxA and HoxJ*, were apparently correctly synthesised, there was no indication of the same for the two hydrogenase components HoxB and HoxC (Figure 3.6A). As *hoxJ* is naturally the last gene in the operon as found in *C. necator*, it was hypothesized that there may be an intrinsic terminator present preventing any expression of downstream genes. Indeed, using the online software *ARNold* (Naville *et al*., 2011), it was found that mRNA transcribed from *hoxJ** is predicted to exhibit a stem-loop secondary structure (Figure 3.6B). As such, it may be that rho-independent transcriptional

termination is occurring after *hoxJ* and so preventing transcription of *hoxBC.* This could perhaps be working in conjunction with the poly-A sequence present in the engineered RBS and linker sequence upstream of *hoxB* to give full termination through polymerase dissociation with the DNA (though at 501 bp this is admittedly quite far downstream from the hairpin to be likely). Alternatively the hairpin may be sufficient to stall the polymerase and interfere with the radiolabelling procedure, but without necessarily causing termination.

To circumvent this, the order of the engineered operon was then altered to *hoxCBAJ**, built up once again *via* suicide ligations, to sequentially produce a complete RH *hox* operon under the control of the constitutive *tat* promoter in the vector pUNI-RH (Table 7.6). In doing this, the cloning was first done in the vector pT7.5-litmus. This was because the cloning of *hoxC* alone into pUNI-PROM was not possible, perhaps due to the sole constitutive expression of a hydrogenase large subunit being toxic to the cells.

Radiolabelling confirmed proper synthesis of all four proteins (Figure 3.7). The initial vector, plitmus-hoxC, encoding only the optimised HoxC, clearly produced protein product of the expected size (52 kDa), although there was some evidence of breakdown products at approximately 40 and 30 kDa (Figure 3.7). When the optimised *hoxB* gene was cloned in isolation into the plitmus-hoxB vector a clear, stable product of expected size (36 kDa) was observed (Figure 3.7). Cloning of *hoxB* downstream of *hoxC* (yielding the vector plitmus-hoxCB) allowed the co-production of both proteins, although fragmentation of HoxC seemed to be exacerbated in this system (Figure 3.7). Furthermore, the expression of *hoxA* and *hoxJ** from the previously constructed pUNI-hoxAJ* yielded bands of expected size for HoxA and HoxJ* as seen before (Figure 3.6). Interestingly, the cloning of *hoxAJ** downstream of *hoxBC* to yield the vector plitmus CBAJ* stabilised the HoxC protein (Figure 3.7). Unfortunately, only a faint band corresponding to HoxB could be detected in the final system producing all proteins (Figure 3.7), however this was considered suitable to continue.

This new *hoxCBAJ** operon was then moved into pUNI-PROM yielding the vector pUNI-RH. This could then be used in conjunction with the requisite maturase operon encoding *hypA1-X* (Chapter 2) in an attempt to synthesise a functional RH system heterologously in *E. coli*.

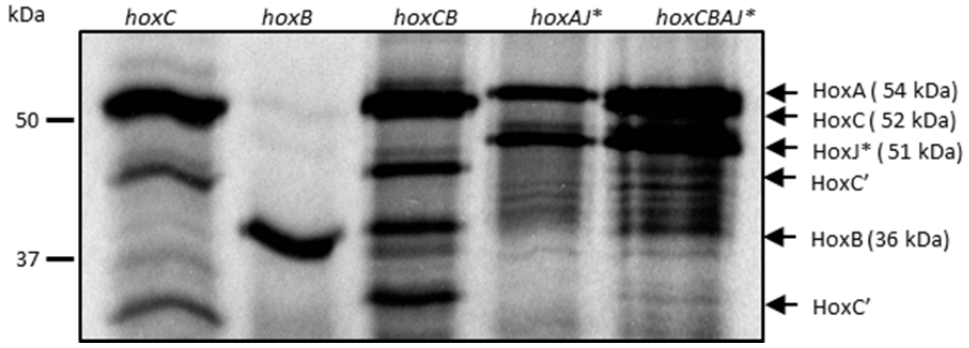

Figure 3.7 Optimisation of the *hox* operon allows for the full synthesis of the RH machinery in *E. coli.* K38 [pGP1-2] cells were transformed with plitmus-hoxC, plitmus-hoxB, plitmus-hoxCB, pUNI-hoxAJ* or plitmus-hoxCBAJ*, after which ^{35}S- Methionine radiolabelling was performed to analyses protein production. Samples were then separated by SDS–PAGE (12% w/v polyacrylamide), fixed, and visualised by autoradiography.

3.3.3 Initial attempts to assess biosensor functionality

Now having evidence that the RH proteins were synthesised in *E. coli*, the next step was to assess whether the RH could be used to induce reporter gene expression in an H_2-dependent manner. Initially, a strain was constructed (by Dr Constanze Pinske) from an IC011 background carrying reporter gene *lacZ* under the control the MBH promoter region as found in *C. necator* (operated by RH) at the λ attachment site (*attB*). This strain was called 'IC011 λMBH$_p$-lacZ' (Strain Table 7.1). This strain was then used to perform various assays to assess whether the semi-synthetic *hox* and synthetic *hyp* operons could give rise to a functional RH in *E. coli* (Figure 3.8). Because this strain is kanamycin resistant, the *hypA1-X* operon was cloned into a chloramphenicol resistant vector to allow for constitutive expression of the genes, in this case pSU18, yielding the vector pSU18-hyp (Plasmid Table 7.6).

IC011 λMBH$_p$-lacZ was transformed with pSU18-hyp and then with one of four different vectors to test how the complete biosensor system, or partial components of it, would affect

lacZ transcription in response to H_2 (Figure 3.8). The vectors used were pUNI-hoxA, pUNI-hoxAJ*, pUNI-RH or the negative control pUNI-PROM. First a 'blue plate assay' was performed where plates were supplemented with X-gal reagent (Figure 3.8B). Transformants were first cultured overnight in 5 mL LB and appropriate antibiotics, before a loop was taken and streaked onto LB agar containing 0.5 % (w/v) glucose, 20 μg mL^{-1} X-gal and appropriate antibiotics. These were then incubated for 24 hours at 37 ^{o}C in either aerobic atmospheric conditions or in a 100% H_2 atmosphere. All four transformants were observed to result in blue colonies on X-gal plates under aerobic conditions, however when incubated under anaerobiosis in the presence of H_2, no blue colour was observed in the growth tests (Figure 3.8B).

These data suggested that the biosensor may not be functioning as desired. Further assessments were undertaken in the form of β-gal assays, which have the benefit of giving a more quantitative data output than the X-gal assay, allowing for detection of more subtle differences in activity. In this case transformants containing either pUNI-PROM or pUNI-RH (and pSU18-hyp) were cultured overnight at 37 ^{o}C in LB with appropriate antibiotics; before subcultures were set up to test for how aerobic and 100 % H_2 atmospheres would affect the biosensor system. For the aerobic condition, cells were subcultured in 5 mL LB supplemented with 0.5 % (w/v) glucose and appropriate antibiotics in a universal tube and grown with shaking at 37 ^{o}C for six hours.

For the H_2 conditions, the same media was pre-bubbled in a sterile manner with H_2, after which the 20 mL was used to fill a universal tube and inoculated. These cultures were then incubated at 37 ^{o}C for six hours as well, but without shaking. After the six hours incubation, cells were harvested and run in the β-gal assay (See Chapter 7, Section 7.9.2) (Figure 3.8C). The data show that there is no difference between the RH system and the negative control in the absence of H_2 (Figure 3.8C). Producing HoxA by itself was found to give higher expression through the MBH promoter than when present with HoxJ* or even the complete apparatus in

the aerobic condition (Figure 3.8C). However, statistical analysis of the data by t-test showed that there was no significant difference between the value obtained for the complete RH system and the negative control (p value = 0.065). It should also be noted that the β-gal activity measurements recorded here are about 2 to 3 orders of magnitude lower than might be normally expected from a single copy reporter in *E. coli*. For example, single copy *lacZ* fusions to the *tat* promoter in *E. coli* MC4100 gave β-gal activity of 860 Miller units when grown in glucose and oxygen (Jack *et al*., 2001). Thus, it is apparent that further work could be done to try and boost the signal. In hindsight, this should have been taken to be an indication that perhaps the system was not functioning properly. However, at the time these data led to the tentative conclusion that the RH was perhaps weakly functional. It was also decided at this time that the LacZ-based method to assess the biosensor functionality was unsuitable, and a new method to analyse the biosensor was devised.

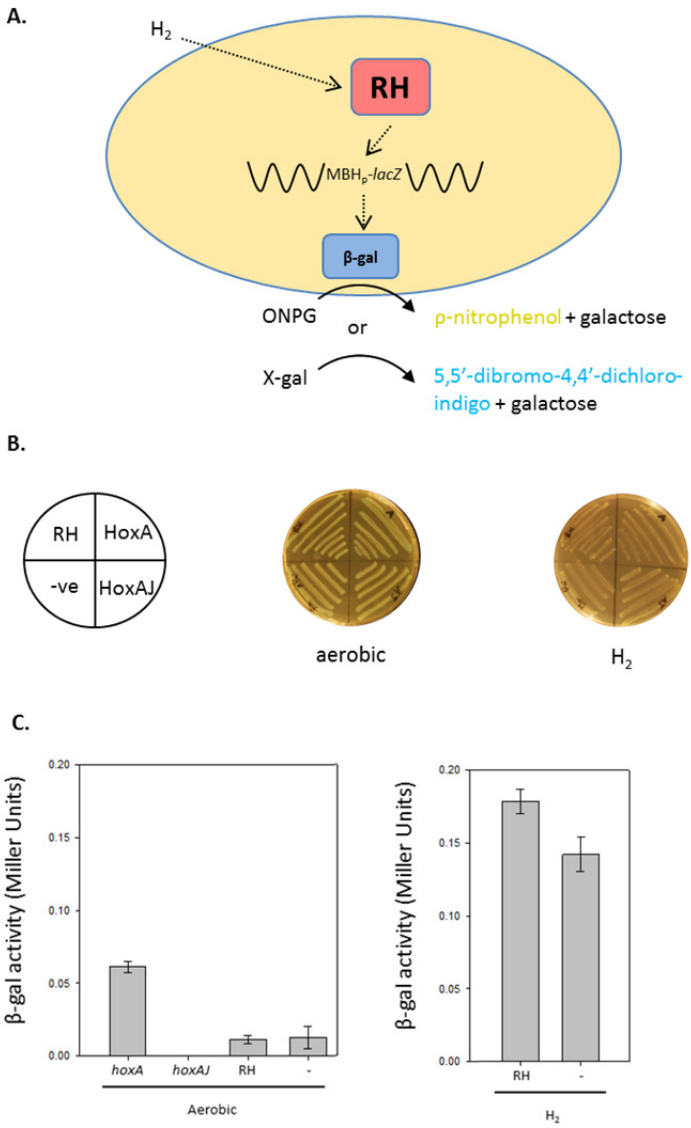

Figure 3.8 Preliminary assessment of biosensor functionality in *E. coli*. (**A**) Schematic to illustrate how a functional RH system should cause H_2 mediated transcription of *lacZ* in IC011 λMBH$_p$-lacZ. Any *lacZ* expression could then be monitored in either a blue plate assay or β-gal assay using X-gal or ONPG as substrates respectively. Any H_2 present, produced endogenously by FHL or artificially introduced into the atmosphere, is detected by RH and results in transcription of the reporter gene *lacZ*, present on the chromosome under the control of the MBH promoter. Of course IC011 (Δ*hyaB*, Δ*hybOA*, Δ*hycE*) will not produce any endogenous H_2. (**B**) Blue plate test to assess H_2-dependent expression of *lacZ*. IC011 λMBH$_p$-lacZ cells transformed with pSU18-hyp and vectors allowing for constitutive expression of *hoxA*, *hoxAJ**, the complete RH apparatus *hoxCBAJ**, or the negative control pUNI-PROM were plated on LB agar supplemented with 0.5 % glucose, appropriate antibiotics and 20 µg mL $^{-1}$ X-gal. (**C**) β-gal assays were performed on the same samples. After culturing overnight, subcultures were set up in LB supplemented with 0.5% glucose and appropriate antibiotics. All subcultures were grown aerobically (i.e. with shaking), but additionally cultures of cells possessing pUNI-RH or pUNI-PROM were also set up in H_2 saturated media (bubbled in a sterile manner), which were then sealed and incubated without shaking to help induce anaerobiosis. Incubation of all subcultures was maintained at 37 ^{o}C for six hours, after which the β-gal assay was performed. Error bars represent SEM (n=3). Vectors used: **RH**: pUNI-RH; **HoxAJ***: pUNI-hoxAJ*; **HoxA**: pUNI-hoxA; **-ve**: pUNI-PROM. Colonies were grown for 24 hours at 37^{o}C in aerobic, or 100% H_2 conditions.

3.3.4 Constructing an RH-dependent live/die screen

Next, it was considered that a better reporter system may be one that encodes antibiotic resistance and one that could be present in multi-copy. It was envisaged that this would allow for easier screening as only cells with sufficient H_2-mediated transcription should survive. Such a live/die screen would also be beneficial for the utilisation of directed evolution; with ever-increasing quantities of antibiotic being used to drive ever greater endogenous H_2 production.

The reporter gene chosen, *aac(3)-IV*, is native to *Klebsiella pneumoniae*, and confers an apramycin-resistant phenotype. This was inserted into the CmI^R vector pSB1C13, and put under the control of either the *C. necator* SH or MBH promoters; which was achieved by cloning the 500 bp upstream region of the SH/MBH operons. The resultant plasmid constructs were named pSB-SHp-Apra and pSB-MBHp-Apra, respectively (Plasmid Table 7.6).

The *in vivo* activity of the RH system was then investigated. To do this, the strains MC4100 and its derivative, FTD147 (Δ*hyaB,* Δ*hybC,* Δ*hycE*) were transformed with pUNI-RH and pSU-A1-X, along with either pSB-SHp-Apra or pSB-MBHp-Apra. Furthermore, because it was thought a triple transformant growing on a fourth antibiotic may be highly stressed, a third strain was engineered. Called FTD147-hyp, this strain is in a FTD147 background but has the *hypA1-X* operon inserted onto the chromosome at the *tatD* locus by pMAK705 integration. FTD147-hyp was transformed pUNI-RH and either of pSB-SHp-Apra and pSB-MBHp-Apra.

Cultures were grown in LB supplemented with appropriate antibiotics, after which centrifugation was performed. Pellets were washed twice with 50 mM Tris.HCl pH 7.5 buffer before being normalised to an OD_{600} = 1. Serial dilutions were then carried out from 10^0 to 10^{-6} with 4 µL of each dilution spotted onto LB agar plates supplemented with 0.8 % (w/v) glucose, appropriate antibiotics, 0.5 mM methyl viologen (used to help with enzyme activity) and one of three concentrations of apramycin: 0, 50 or 100 µg mL^{-1}. The plates were then incubated at 37 ^oC for 17 hours either under an anaerobic atmosphere to induce fermentation with the

intention being that endogenous H_2 production would drive the expression of *aac(3)-IV*, or under 100% H_2, which would give the maximum possible signal. The resultant colonies are shown in Figure 3.9.

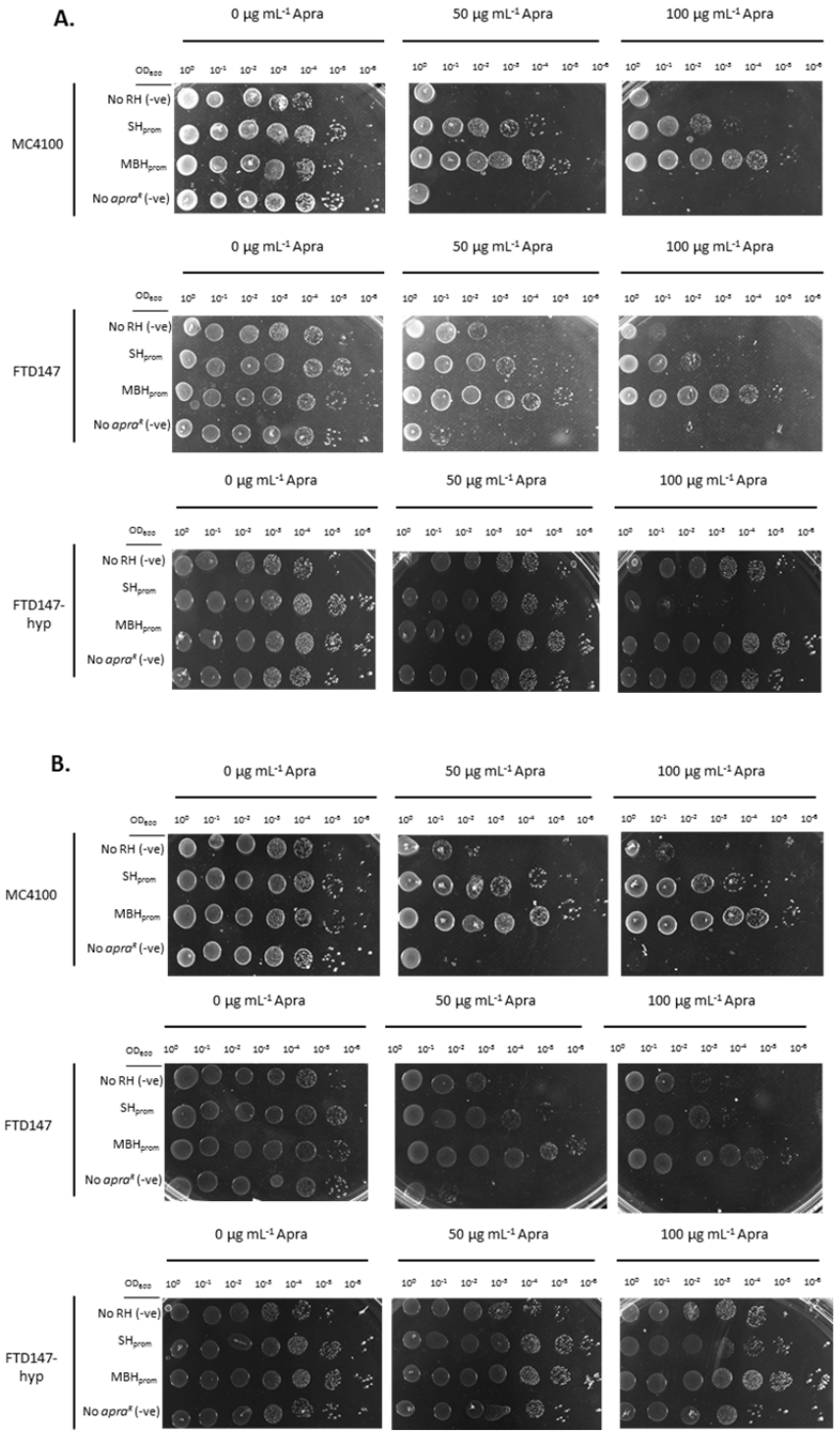

Figure 3.9 Live/die screen to examine RH biosensor functionality. The strains MC4100, FTD147 and FTD147-hyp were transformed the appropriate vectors were normalised to OD_{600} = 1, before 10x serial dilutions were performed from 10^0 to 10^{-6}. 4 µL samples of each dilution were plated on LB agar supplemented with 0.8 % (w/v) glucose, appropriate antibiotics, 0.5 mM methyl viologen and one of three concentrations of apramycin: 0, 50 or 100 µg mL^{-1}. Plates were then incubated for 17 hours at 37 ^oC in either (**A**) anaerobic conditions or (**B**) 100 % H_2 atmosphere. Vectors used in transformations were as follows: **No RH (-ve)**: pUNI-PROM, pSB-MBHp-Apra, pSU-A1-X; **SH_{prom}**: pUNI-RH, pSB-SH_p-Apra, pSU-A1-X; **MBH_{prom}**: pUNI-RH, pSB-MBHp-Apra, pSU-A1-X; **No *apra*^{R} (-ve)**: pUNI-RH, pSB1C3, pSU-A1-X. FTD147-hyp strains were transformed in the same manner *sans* pSU-A1-X, and so grown on agar without kanamycin added.

A number of things may be interpreted from these data. First, it may tentatively be concluded that the RH system could be functional; with both FTD147 and MC4100 showing markedly more antibiotic resistance at 100 µg mL^{-1} Apra than the controls in the H_2 atmosphere (Figure 3.9B). MC4100 also exhibited enhanced growth in the anaerobic conditions, although, surprisingly, so did FTD147 (Figure 3.9A). A strain with abolished Hyd-1, Hyd-2 and especially Hyd-3 will exhibit no endogenous H_2 production during fermentation, and so these findings may suggest that the expression through the SH/MBH promoters is not solely H_2 dependent. The FTD147-hyp strain also grew well in both anaerobic and 100 % H_2 conditions, however the controls also exhibited apramycin resistance so little can be drawn from these data.

It appeared that the MBH promoter construct gave increased antibiotic resistance compared to the SH counterpart, is perhaps contrary to the literature where it has previously been suggested that the SH promoter was 'stronger' (Schwartz *et al*., 1998).

It was hypothesised that 100 % H_2 might induce higher apramycin resistance than anaerobiosis in MC4100 due to the greater partial pressure of H_2. However the data in Figure 3.9 suggest no real difference was observed. This can either be explained by there being non-H_2 mediated transcription occurring as previously suggested, or that the RH system signal is saturated by low levels of H_2, such that maximum gene expression occurs at physiological concentrations. This latter supposition is a possibility as the K_m for RH *in vitro* has been measured to be only 5 µM H_2. (Pierik *et al*., 1998). As such, greater signal fidelity would be required in order to be able to discriminate between differences in H_2 levels that may be produced by mutants during fermentation, which is the long term purpose of this work. To help achieve this, it was decided to employ an amplification step to boost the signal (see Section 3.3.5).

3.3.5 Amplification of the biosensor signal

One conclusion drawn from the data presented in Section 3.3.4 was that the output signal from the biosensor constructs was saturated at a low concentration of H_2. In an attempt to rectify this, an amplification step was used, employing the tetrathionate two-component system native to *S. enterica* (Figure 3.10). This involved inserting the genes *ttrS* and *ttrR*, which encode a tetrathionate-sensing histidine-kinase and an associated response regulator respectively, into the reporter system. In addition to the TtrRS two-component system, the expression of *ttrB* also requires the presence of the anaerobiosis-associated global transcription factor FNR (Hensel *et al*., 1999) and probably ModE (Guymer *et al*., 2009). However, these should be present in the *E. coli* cells if grown in the same anoxic conditions as done previously in the live/die screens.

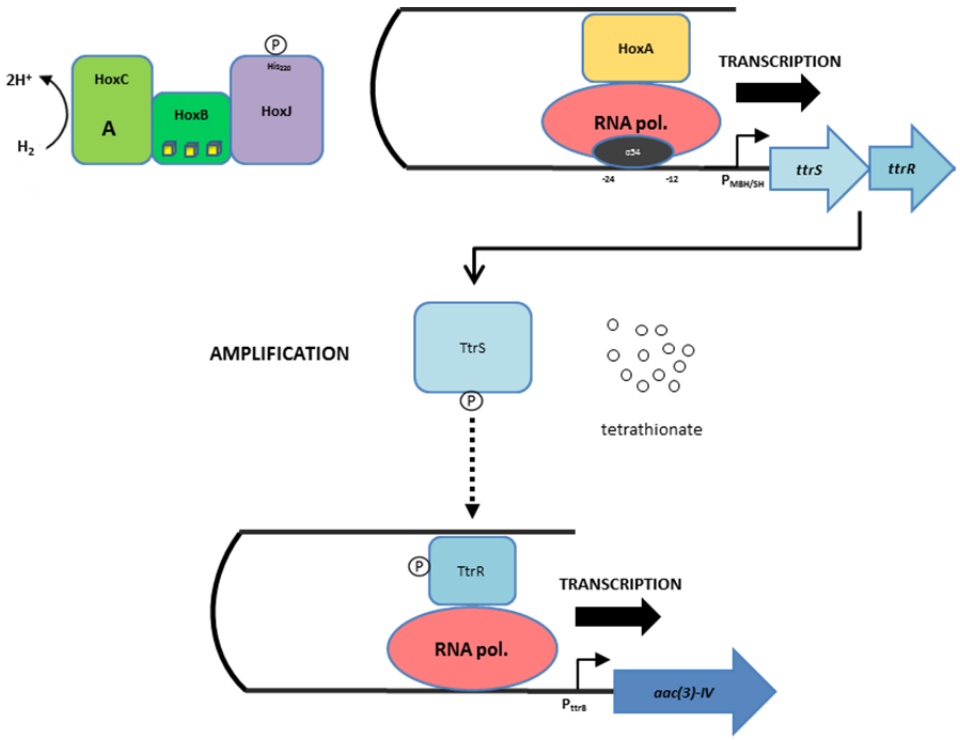

Figure 3.10 Amplification of the RH signal using the tetrathionate two-component system from *S. enterica*. The original RH system was modified to control expression of the tetrathionate sensing two-component system native to *Salmonella*. Genes encoding the histidine kinase, TTrS, and its associated response regulator, TtrR, were placed under the control of the SH promoter. Then, on a separate vector, the Apra^R gene, *aac(3)-IV*, was placed under the control of the TtrSR-operated promoter of *ttrB*. In the presence of tetrathionate, TtrSR induces transcription. It was envisaged that adding this amplification step may help magnify small changes in H_2 levels with a larger discrepancy in the output signal of reporter gene expression, to help with result interpretation.

The *ttrSR* operon was thus put under the control of the SH promoter in the medium copy-number, kanamycin-resistant vector pSU40; yielding the construct pSU40-SHp-ttrSR. The apramycin resistance gene, *aac(3)-IV*, was then placed in the vector pSB1C3 under the control of the *ttrB* promoter; the resultant construct was named pSB-ttrBp-Apra.

Strains to test both the RH and Hyd-2 biosensor constructs were transformed and cultured in the same manner as before. Agar plates were also made as before, but with the addition of 1 mM final concentration of potassium tetrathionate, required to induce the TtrRS amplification step (James *et al*., 2013). Furthermore, the maximum concentration of apramycin used was increased to 200 μg mL^{-1} as opposed to the previous 100 μg mL^{-1}, in order to select for higher stringency of reporter gene expression.

For testing the amplifier in conjunction with the RH version of the biosensor, the strain FTD147-hyp was used. This was done as it was thought that the extra vector required for introduction of the *hypA1-X* operon, in addition to pUNI-RH, pSU40-SHp-ttrSR, pSB-ttrBp-Apra and the apramycin, may be a high stress on cell growth. The results are shown in Figure 3.11.

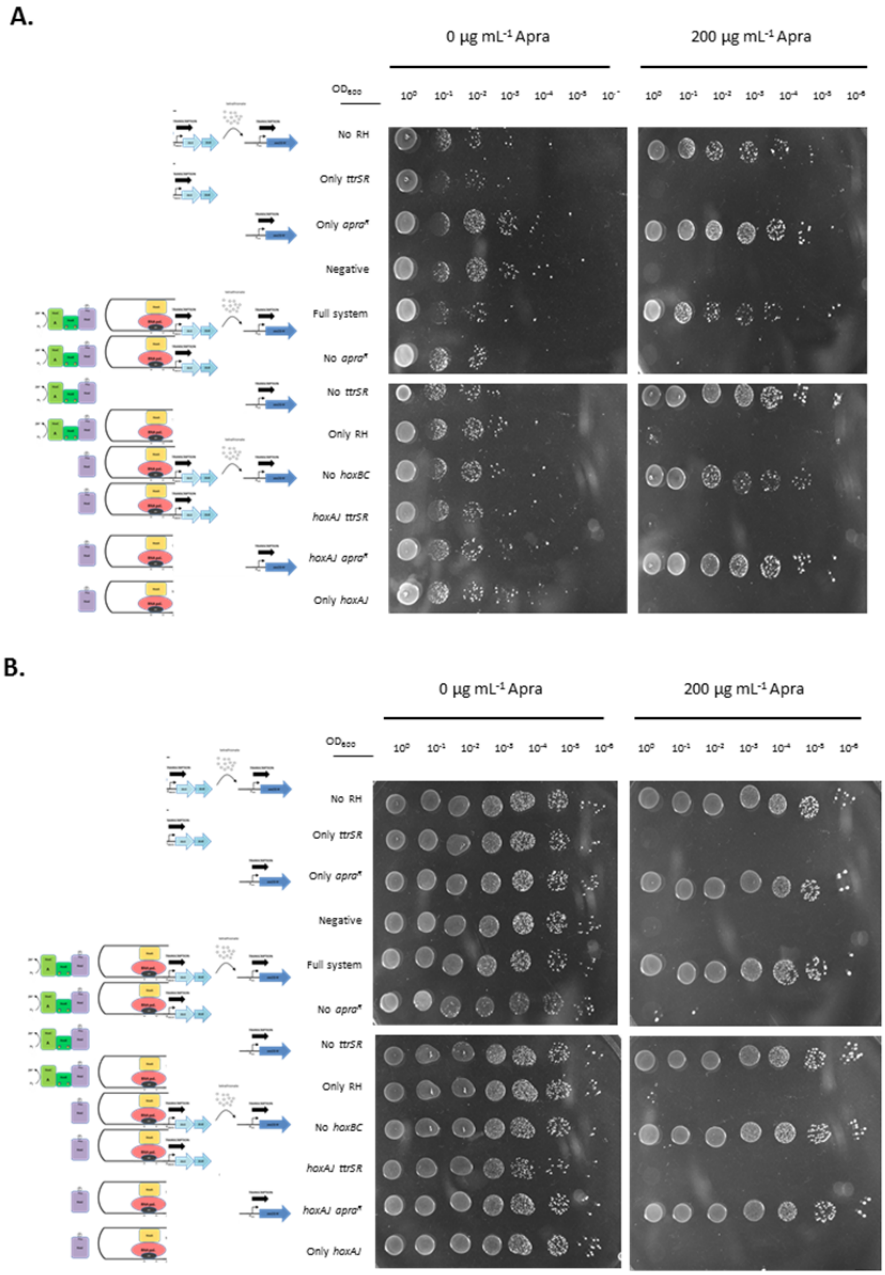

Figure 3.11 Live/die screen to assess amplification of the RH signal. The strain FTD147-hyp was used to examine whether utilisation of the *ttrRS* two-component system could improve the signal output of the RH H_2 biosensor. The transformed strains were prepared and grown as before, before being plated on LB agar containing 0.8 % (w/v) glucose, appropriate antibiotics, 1 mM tetrathionate, 0.5 mM MV and either 0 or 200 µg mL^{-1} apramycin. As before, plates were incubated in either (**A**) anaerobic or (**B**) H_2 atmospheres at 37 ^{o}C for 17 hours. The various components of the RH and Amplifier systems expressed in each colony are represented pictorially on the left. Vectors used for transformations were as follows: **No RH**: pUNI-PROM, pSU40-SHp-ttrSR, pSB-ttrBp-Apra; **Only *ttrSR***: pUNI-PROM, pSU40-SHp-ttrSR, pSB1C3; **Only *apra*^{R}**: pUNI-PROM, pSU40, pSB-ttrBp-Apra; **Negative**: pUNI-PROM, pSU40, pSB1C3; **Full system**: pUNI-RH, pSU40-SHp-ttrSR, pSB-ttrBp-Apra; **No *apra*^{R}**: pUNI-RH, pSU40-SHp-ttrSR, pSB1C3; **No *ttrSR***: pUNI-RH, pSU40, pSB-ttrBp-Apra; **Only RH**: pUNI-RH, pSU40, pSB1C3; **No *hoxBC***: pUNI-hoxAJ, pSU40-SHp-ttrSR, pSB-ttrBp-Apra; ***hoxAJ ttrSR***: pUNI-hoxAJ, pSU40-SHp-ttrSR, pSB1C3; ***hoxAJ apra*^{R}**: pUNI-hoxAJ, pSU40, pSB-ttrBp-Apra; ***Only hoxAJ***: pUNI-hoxAJ, pSU40, pSB1C3.

The data here suggest that, with the amplifier, there is some H_2-correlated gene expression. This is because there was increased apramycin resistance when a cell possessing the complete RH and amplifier systems was grown in the presence of H_2 compared to anoxic growth, with colonies observed at the 10^{-6} dilution compared to only 10^{-4} under anoxic conditions. Whilst this is encouraging, there are caveats. It appears that the controls which contain *aac(3)-IV* also showed antibiotic resistance, suggesting that the *ttrB* promoter is 'leaky', and transcription is not solely reliant upon the *ttrRS* system. It is interesting to note that the expression of the full apparatus seems to confer a lower antibiotic resistance in anaerobic conditions than the controls (Figure 3.11A).

3.3.6 Attempts to adapt Hyd-2 as a biosensor

Instead of trying to move the whole RH system into *E. coli*, it was considered that HoxBC could be substituted with other [NiFe]-hydrogenases known to be active in *E. coli* and so give rise to a functional regulatory hydrogenase.

The strategy was devised to attempt to recruit *E. coli* Hyd-2 to work in tandem with the HoxJ*-HoxA system (Figure 3.12A). Two modifications would be required for this to be possible. First, a soluble version of Hyd-2 would need to be present in the cytosol, as native Hyd-2 is membrane-bound and located in the periplasm. Second, a method to adhere HoxJ* to the Hyd-2 small subunit HybO would need to be devised. Thus, when cloning genes to encode for this putative Hyd-2 biosensor, *hybO* was modified to remove sequence encoding the Tat-signal peptide between residues Asp2 and Ala37 (preventing translocation to the periplasm) and the C-terminal transmembrane helix, which was taken to begin at residue Gly333. Furthermore, HybO was engineered to contain a fusion to the C-terminal region of HoxB, which is hypothesised to act as a docking site for the HoxJ* kinase (Figure 3.12B). Two lengths of this HoxB 'tail' were grafted onto HybO: a 'short' version equating to the red portion as seen in

Figure 3.12B (from residue Asp305 to the end), or a 'long' version (from Pro280 to the end) corresponding to the orange and red regions in Figure 3.12B. This was done using Fusion PCR (Chapter 7, Section 7.5.12). Therefore, in total two operons encoding this Hyd-2 biosensor were constructed; with either the 'long' or 'short' *hybO* genes placed upstream of the optimised *hoxAJ** genes (Figure 3.12C). These operons were then inserted into pUNI-PROM to generate pUNI-hybO^{long}AJ* and pUNI-hybO^{short}AJ* respectively (Plasmid Table 7.6). In order to construct the whole Hyd-2 biosensor system, these vectors would be used to transform an *E. coli* strain with a Δ*hybO* genotype, leaving the natively produced Hyd-2 large subunit, HybC, to associate with the modified HybO, and hopefully HoxJ* also.

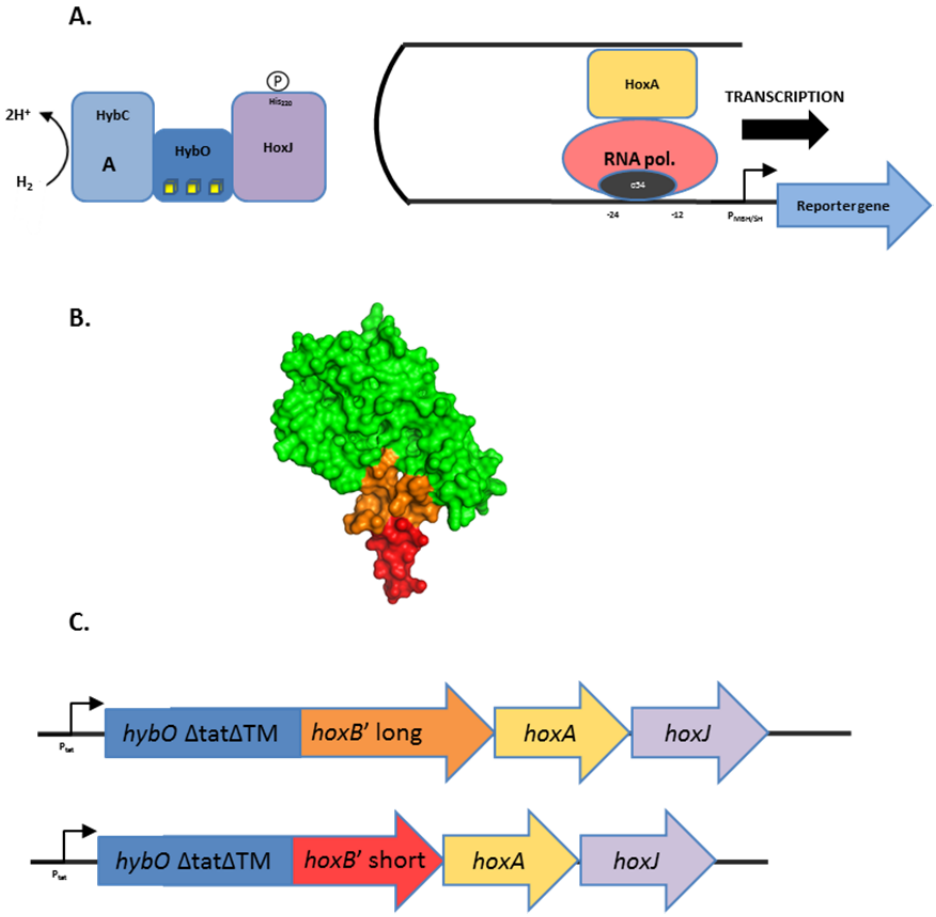

Figure 3.12 Hyd-2 as a biosensor (**A**) Illustration of how it was hoped to replace the HoxBC subunits of RH with a soluble Hyd-2 from *E. coli* to for the H_2 Biosensor (**B**) Predicted structure of HoxB given by Phyre[2] (Kelley *et al.*, 2015) and visualised using PyMOL (v1.3)(DeLano, 2002). The C-terminal tail that is hypothesised to permit interaction with HoxJ is coloured orange and red, with red at the end of the peptide from the proline residue Asp305 to the end, and the orange region from Pro280 to Asp305. (**C**) Two operons were constructed to encode the 'Hyd-2 Biosensor'. In either case, *hoxA* and *hoxJ* were inserted downstream of the *hybO* gene which, along with being engineered to encode for a protein without a tat signal sequence or transmembrane helix, also encoded for a C-terminal fusion of the HoxB tail. This was either a 'long version'; corresponding to the orange and red regions shown in (**B**), or a 'short' version which encoded for only the red region shown in (**B**). When inserted into pUNI-PROM, the resultant vectors were called pUNI-hybO^{long}AJ* and pUNI-hybO^{short}AJ* respectively.

After the assembly of these operons was verified, ^{35}S-methionine radiolabelling was again performed to ensure the proteins were properly synthesised (Figure 3.13). By comparison of the protein bands produced by the whole operons (*hybO^{long}AJ** and *hybO^{short}AJ**) with those of the partial operons (*hybO^{long}, hybO^{short} and hoxAJ**) it can be seen that both complete constructs gave rise to the full suite of required proteins.

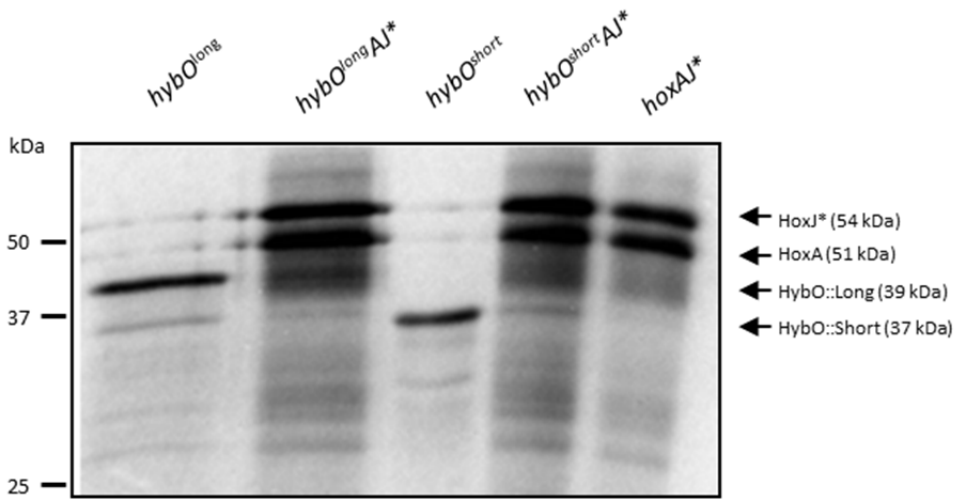

Figure 3.13 Both operons encoding the Hyd-2 biosensor are fully expressed. Radiolabelling was used to examine protein synthesis of the two operons constructed to encode for the Hyd-2 Biosensor apparatus, containing either the 'short' or 'long' HybO::HoxB fusion proteins. K38 [pGP1-2] cells were transformed with vectors encoding the partial operons, pUNI-hybO^{long}, pUNI-hybO^{short} and pUNI-hoxAJ*, or the complete operons pUNI-hybO^{long}AJ* and pUNI-hybO^{short}AJ*. Labelling of the plasmid-encoded proteins was carried out in whole cells before samples were then separated by SDS–PAGE (12% w/v polyacrylamide), fixed, and visualised by autoradiography.

Now it was confirmed the two Hyd-2 biosensor constructs were properly expressed in *E. coli*, functionality was then assessed. First, *in vitro* hydrogenase assays were performed using the redox-dye BV, in an attempt to ensure the Hyd-2 components of this new system were still functional. The strain HJ001 (MC4100, Δ*hyaB*, Δ*hybOA*, Δ*hycE*, Δ*iscR*) has abolished hydrogenase activity, and as such was chosen as the strain to examine the functionality of these modified Hyd-2 constructs. HJ001 cells were transformed with either pUNI-hybO^{long}AJ*, pUNI-hybO^{short}AJ* or pUNI-PROM. Single colonies were then used to inoculate 100 mL of LB supplemented with 0.4 % (w/v) fumarate, 0.5 % (w/v) glycerol and appropriate antibiotics. This media supplementation, in conjunction with subsequent anaerobic growth at 37 ^{o}C for 17 hours, stimulated the production of HybC from the chromosome.

Cells were then harvested by centrifugation, lysed *via* sonication, and the resultant crude extract used in the BV assay. As can be seen in Figure 3.14, both the 'long' and 'short' versions of the HybO-HoxB chimeras exhibited hydrogenase activity, with the long version having

approximately 2.5 times as much activity, suggesting that both versions of the modified HybO small subunit can still form a complex with the HybC large subunit.

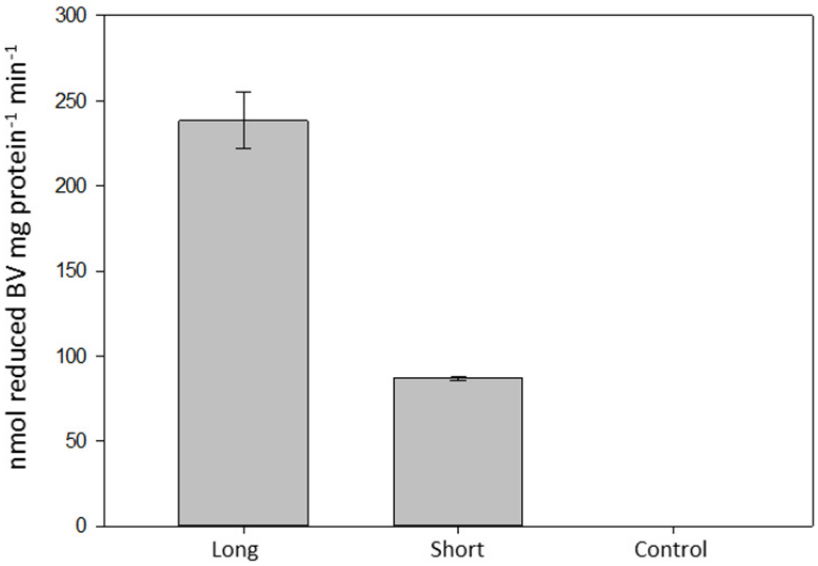

Figure 3.14 The two HybO-HoxB constructs exhibit *in vitro* hydrogenase activity. HJ001 cells possessing either UNI-hybO^{long}AJ* (**Long**), pUNI-hybO^{short}AJ* (**Short**) or pUNI-PROM (**Control**), were grown anaerobically in LB containing 0.4 % fumarate and 0.5 % glycerol to induce HybC expression from the chromosome. Crude extracts were then used in an *in vitro* hydrogenase assay using the redox dye benzyl viologen (BV). BV reduction (H_2 oxidation) was monitored at 578 nm in a UV-vis spectrometer. 1 mL quartz cuvettes were filled with H_2-saturated buffer (50 mM Tris.HCl pH 7.5) and 13 mM BV. This was titrated with sodium dithionite to an absorbance of 0.4 - 0.7, before the reaction was started by the addition of 50 µL of crude extract. Protein concentration was measured by Bradford assay. **Long**: pUNI-hybO^{long}AJ*; **Short**: pUNI-hybO^{short}AJ*; **Control**: pUNI-PROM. Error bars represent SEM (n=3).

Next, it was endeavoured to examine *in vivo* activity of the whole Hyd-2 biosensor. Initially, *lacZ*, was used as the reporter gene, again *via* the use of IC011 λMBH$_p$-lacZ. This strain was transformed with a vector to constitutively express one of the two Hyd-2 biosensor operons (pUNI-hybO^{long}AJ* or pUNI-hybO^{short}AJ*) or a negative control (pUNI-PROM). Transformants were cultured anaerobically overnight at 37 ^{o}C in LB supplemented with 0.5 % (v/v) glycerol, 0.4 % (w/v) fumarate and appropriate antibiotics to induce *hybC* expression on the chromosome. Subcultures were then set up in LB containing 0.5 % (w/v) glucose and

antibiotics, and incubated in the following three different manners to expose the cells to aerobic, anaerobic, or 100 % H_2 conditions. For aerobic growth, a universal filled with 5 mL media was used and incubated at 37 ^{o}C with shaking. For the anaerobic condition, a universal filled with 20 mL media was inoculated and incubated without shaking. For the H_2 condition, media was bubbled in a sterile fashion with H_2, before 20 mL was inoculated and incubated without shaking. After 6 hours incubation, the cells were harvested and used in the β-gal assay, which yielded the data seen in Figure 3.15. As can be seen from the results, H_2 did not give an increase in β-gal activity relative to the negative control for cells possessing either pUNI-hybO^{long}AJ* or pUNI-hybO^{short}AJ*, suggesting there was no H_2-mediated transcription occurring. Therefore it was concluded that the Hyd-2 Biosensor construct may not be functional. However, given the very low LacZ activity recorded as with the RH biosensor constructs, it was decided this reporter strain was not the ideal way to test the constructs, so the new Live/Die reporter screen was used.

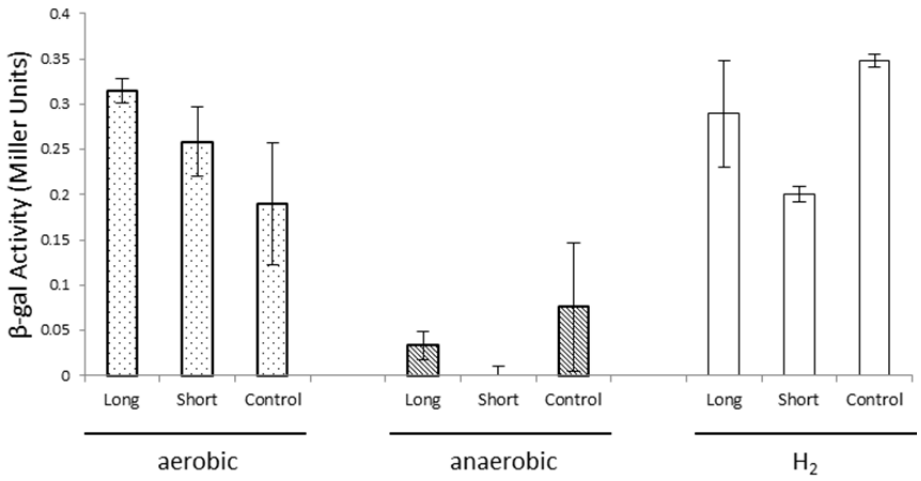

Figure 3.15 β-gal assays suggest Hyd-2 biosensor may not be functional. Assays were performed with both 'long' and 'short' constructs in the strain IC011 λMBH$_p$-lacZ. Cells were grown anaerobically at 37^{o}C overnight in 0.5% glycerol 0.4% fumarate and appropriate antibiotics, before being used to inoculate LB supplemented with 0.5% glucose and appropriate antibiotics. All subcultures were grown aerobically with shaking (**aerobic** conditions)**,** without shaking (**anaerobic** conditions) or without shaking but in H_2 saturated media (**H_2** conditions) Incubation of these subcultures was maintained at 37 ^{o}C for six hours, after which cells were normalised for OD_{600} and then used in the β-gal assay. Vectors used: **Long**: pUNI-hybO^{long}AJ*; **Short**: pUNI-hybO^{short}AJ*; **Control**: pUNI-PROM. Error bars represent SEM (n=3).

Next, the apramycin-based live/die screen was performed on the Hyd-2 biosensor constructs. The strains RJ608 (MC4100 Δ*hybO*) and IC011 (MC4100 Δ*hyaB,* Δ*hycE,* Δ*hybOA*) were transformed with pSB-MBHp-Apra and either pUNI-hybO^{long}AJ* or pUNI-hybO^{short}AJ*. The pSB-MBHp-Apra plasmid was initially chosen over pSB-SHp-Apra due to the previous data using the RH constructs (Figure 3.9) suggesting the MBH promoter was 'stronger'.

Cultures were grown anaerobically in LB supplemented with 0.5% (v/v) glycerol, 0.4% (w/v) fumarate and appropriate antibiotics, after which centrifugation was performed. Pellets were washed twice with 50 mM Tris.HCl pH 7 buffer before being normalised to an OD_{600} = 1. Serial dilutions were then carried out from 10^0 to 10^{-6} before 4 µL of each dilution was then spotted onto LB agar plates supplemented with 0.8 % (w/v) glucose, appropriate antibiotics, 0.5 mM methyl viologen and one of three concentrations of apramycin: 0, 50 or 100 µg mL^{-1}. The plates were then incubated at 37 ^{o}C for 17 hours, under either an anaerobic atmosphere to induce fermentation with the intention being that endogenous H_2 production would drive the expression of *aac(3)-IV*, or 100% H_2, which would give the maximum possible signal. The data yielded are shown in Figure 3.16.

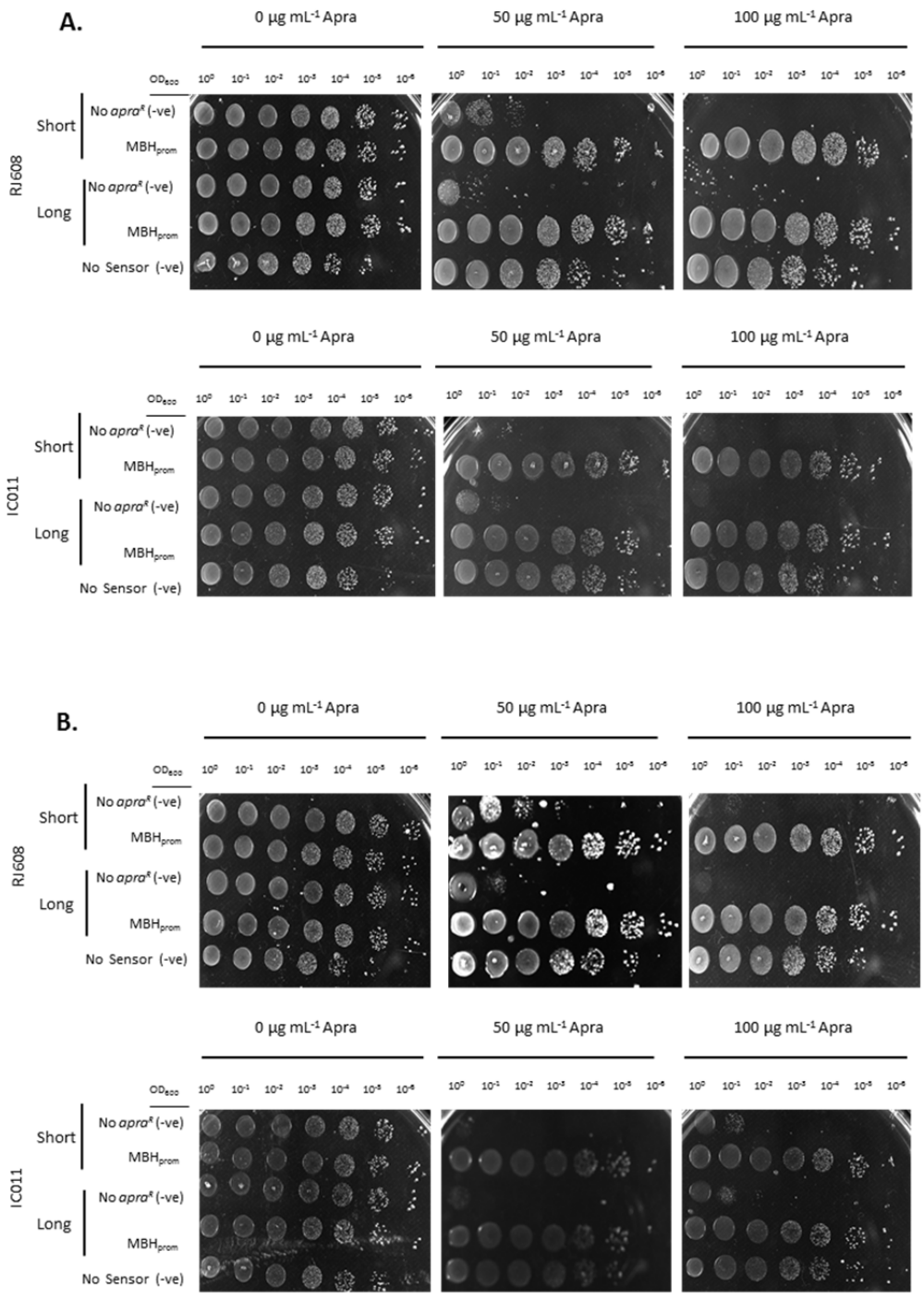

Figure 3.16 Live/die screen to examine Hyd-2 biosensor functionality using MBHp. The strains RJ608 (MC4100 Δ*hybO*) and IC011 (MC4100 Δ*hyaB,* Δ*hycE,* Δ*hybOA*) were transformed with appropriate vectors as listed below to examine the functionality of the Hyd-2 biosensor constructs, in terms of H_2-mediated expression of the apramycin-resistance gene, *aac(3)-IV*. Transformants were cultured anaerobically overnight in LB supplemented with 0.5 % glycerol, 0.4% fumarate and appropriate antibiotics. Cultures were then plated as previously described on LB agar supplemented with 0.8 % (w/v) glucose, appropriate antibiotics, 0.5 mM methyl viologen and one of three concentrations of apramycin: 0, 50 or 100 µg mL $^{-1}$. Plates were then incubated for 17 hours at 37 ^{o}C in either (**A**) anaerobic conditions or (**B**) 100 % H_2 atmosphere. Vectors used for transformations were as follows: **No *apra*^{R} (-ve)**: pUNI-hybO^{short}AJ*/ pUNI-hybO^{long}AJ*, pSB1C3; **MBH$_{prom}$**: pUNI-hybO^{short}AJ*/ pUNI-hybO^{long}AJ*, pSB-MBHp-Apra, **No Sensor (-ve)**: pUNI-PROM, pSB-MBHp-Apra.

The full Hyd-2 Biosensor constructs seemed to only confer slightly greater apramycin resistance than the negative control ('No *apra*^{R} (-ve)'), with only a few more colonies present in the 10^{-6} dilutions, suggesting the system was weakly functional at best. Furthermore, the presence of H_2, either present artificially in the atmosphere, or endogenously produced by the RJ608 strain, does not appear to induce more resistance.

The procedure was then repeated with pSB-SHp-Apra to see if this elicited a better response. The data is shown in Figure 3.17.

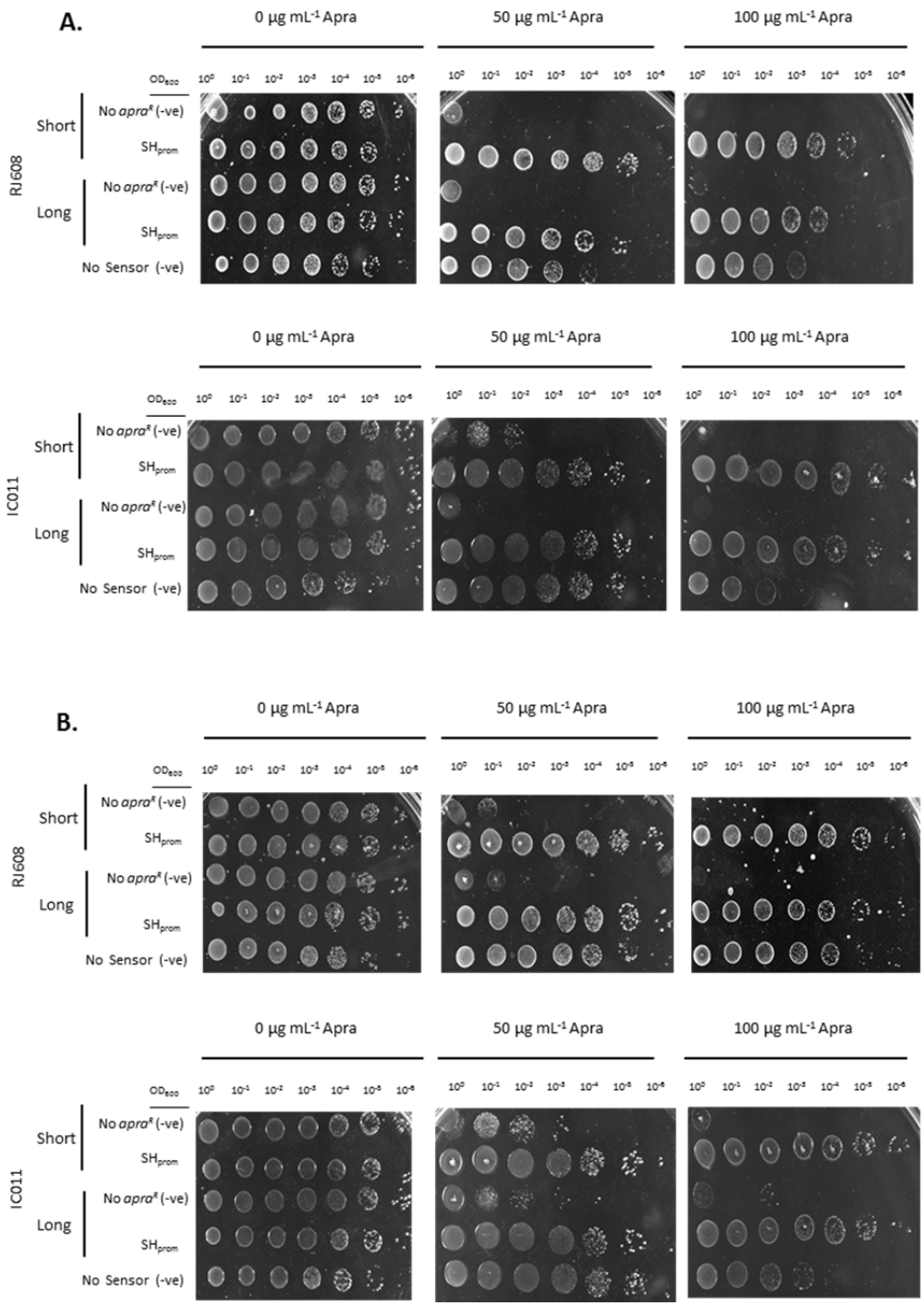

Figure 3.17 Live/die screen to examine Hyd-2 biosensor functionality using SHp. The live/die screen was repeated for the Hyd-2 biosensor constructs using the SH promoter instead of the previous MBH promoter. IC011 or RJ608 cells were transformed with the vectors as described below. Transformants were cultured anaerobically overnight in LB supplemented with 0.5 % glycerol, 0.4% fumarate and appropriate antibiotics. Cultures were then plated as previously described on before being incubated in either (**A**) an anoxic atmosphere or (**B**) a 100 % H_2 atmosphere on LB agar LB agar supplemented with 0.8 % (w/v) glucose, appropriate antibiotics, 0.5 mM methyl viologen and one of three concentrations of apramycin: 0, 50 or 100 µg mL^{-1}. Plates were then incubated for 17 hours at 37 ^{o}C in either (**A**) anaerobic conditions or (**B**) 100 % H_2 atmosphere. Vectors used for transformations were as follows: **No *apra*^{R} (-ve)**: pUNI-hybO^{short}AJ*/ pUNI-hybO^{long}AJ*, pSB1C3; **SH$_{prom}$**: pUNI-hybO^{short}AJ*/ pUNI-hybO^{long}AJ*, pSB-SHp-Apra, **No Sensor (-ve)**: pUNI-PROM, pSB-SHp-Apra.

It is noteworthy that the SH promoter::*aac(3)-IV* constructs resulted in a bigger discrepancy between the full Hyd-2 biosensor constructs (both the Long and Short versions) and the negative controls, with colony growth exhibited at 10^{-6} dilutions as opposed to 10^{-3} dilutions respectively. This is a greater difference than that seen with the MBH promoter constructs in Figure 3.16. This is interesting as it is contrary to the findings of using the RH system (Figure 3.9), and corroborates the literature that the SH promoter allows for greater transcription (Schwartz *et al*., 1998). However, perhaps the key conclusion from these data related to the fact the apramycin resistance did not correlate with H_2 levels, as this result was also observed in IC011 cells in an anaerobic atmosphere (Figure 3.17A). This suggests that, in their current states at least, the Hyd-2 biosensor constructs are not fully functional.

Next, the tetrathionate-based amplifier construct was used in tandem with the Hyd-2 biosensor construct. Because previous data had suggested there was no difference between the long and short versions of the HybO::HoxB fusions (Figures 3.16 and 3.17), it was decided to only test the long version here. Additionally, as the SH promoter was previously seen to elicit a greater response than the MBH promoter (Figures 3.16 and 3.17), the SH promoter was solely used here. The strains RJ608 and IC011 were again used, to help examine the effects of endogenous and exogenous H_2 on stimulation of the biosensor system. The results are shown in Figure 3.18.

IC011 shows a marginally greater apramycin resistance when the full Hyd-2 biosensor and amplifier constructs are expressed in 100 % H_2 compared to anoxic conditions, with colony growth exhibited at the 10^{-3} concentration compared to the best growing control which only grew to 10^{-2}. However the same result is not seen in RJ608, as would be expected if the complete system was functional. Again, it can be seen that the controls that possess the *aac(3)-IV* gene still show a degree of apramycin resistance, and so imply a certain level of H_2-independent transcription from the SH promoter. Thus, from the data presented here it is inconclusive whether the Hyd-2 biosensor is exhibiting H_2-mediated transcription.

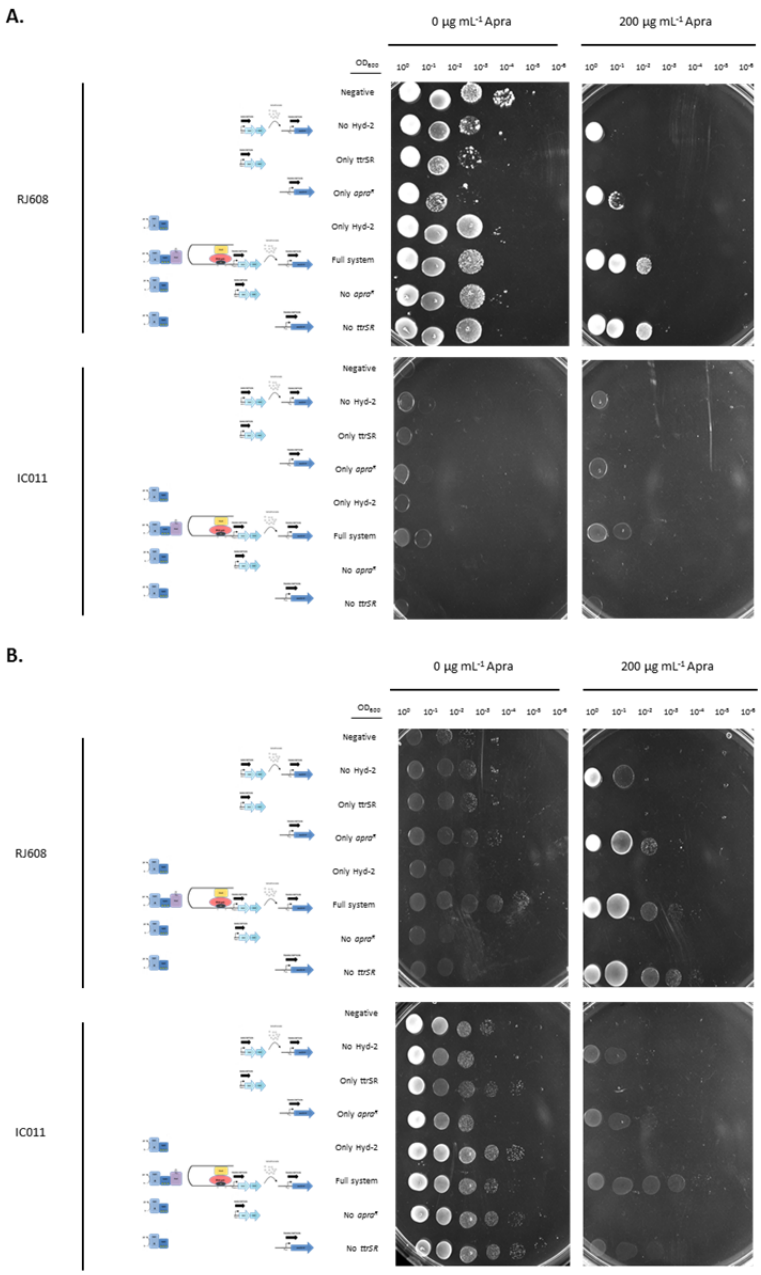

Figure 3.18 Live/die screen to assess amplification of the Hyd-2 biosensor signal. The strains RJ608 (MC4100 Δ*hybO*) and IC011 (MC4100 Δ*hyaB,* Δ*hycE,* Δ*hybOA*) were transformed with vectors to allow for the amplification of the Hyd-2 biosensor, using the Long version of the HybO::HoxB fusion and the SH promoter. Transformants were cultured anaerobically overnight in LB containing appropriate antibiotics, 0.5 % glycerol and 0.4% fumarate. Cells were then plated on LB agar containing with 0.8 % (w/v) glucose, appropriate antibiotics, 1 mM tetrathionate, 0.5 mM MV and either 0 or 200 µg mL $^{-1}$ apramycin. These plates were then incubated in either an (**A**) anoxic or (**B**) H_2 atmosphere. The various components of the RH and Amplifier systems expressed in each colony are represented pictorially on the left. Vectors used for transformations were as follows: **Negative**: pUNI-PROM, pSU40, pSB1C3; **No Hyd-2**: pUNI-PROM, pSU40-SHp-ttrSR, pSB-ttrBp-Apra; **Only *ttrSR***: pUNI-PROM, pSU40-SHp-ttrSR, pSB1C3; **Only *apra*^{R}**: pUNI-PROM, pSU40, pSB-ttrBp-Apra; **Only Hyd-2**: pUNI-hybO^{long}AJ*, pSU40, pSB1C3; **Full system**: pUNI-hybO^{long}AJ*, pSU40-SHp-ttrSR, pSB-ttrBp-Apra; **No *apra*^{R}**: pUNI-hybO^{long}AJ*, pSU40-SHp-ttrSR, pSB1C3; **No *ttrSR***: pUNI-hybO^{long}AJ*, pSU40, pSB-ttrBp-Apra.

3.4 **Discussion**

It is apparent from the data presented in this Chapter that, despite the numerous modifications made, both the RH H_2 biosensor and the derivative Hyd-2 biosensor are not yet functioning as well as hoped. Indeed, given the time again, the statistical analysis performed for the β-gal assay data in Figure 3.8C would have been done earlier, and work done to try and optimise the biosensor then, as opposed to constructing further vectors and strains for additional testing. The bulk of this discussion will therefore consist of troubleshooting. Hypotheses for the lack of functionality will be proposed, discounted where possible, and so leaving those that remain as areas for future work to address.

3.4.1 Possible problems with the upstream promoter regions

One possible problem with the system was hypothesised to be that the entire requisite HoxA binding site may in fact not be present in the 500 bp upstream regions of the SH/MBH promoters as originally suspected. Normally, 500 bp upstream would be considered sufficient to contain the whole promoter region required for σ^{54}-related transcription, with enhancer sites usually found only about 100 bp upstream of the promoter site itself (Schwartz *et al*., 1998). However, perhaps HoxA is an exception. Enhancer loci may in fact be located up to 1 Mbp upstream from the promoter itself (Blackwood and Kadonaga, 1998), with such distal DNA sequences still being in close proximity in terms of DNA secondary structure due to coiling etc. (Xu and Hoover, 2001). Thus, it may be possible that these loci could be located anywhere on the 450 kbp pHG1 megaplasmid.

The non-H_2-correlated gene transcription observed can be explained in a couple of ways. First, is possible that the MBH and SH promoter regions used may contain other transcription factor binding sites apart from the HoxA site, such that transcription through these sites is not solely related to the activity of RH. Indeed, in *C. necator*, MBH/SH transcription has been reported to

also be subject to catabolite repression, with the presence of organic acids conducive to growth such as pyruvate and succinate overriding any H_2-dependent expression (Friedrich *et al*., 1981b; Jugder *et al*., 2015). When the carbon source is glycerol or formate, however, no catabolite repression is observed, and expression through the SH and MBH is similar to during lithoautotrophic growth on H_2 and CO_2 (Jugder *et al*., 2015; Lenz *et al*., 2002). This makes sense; *C. necator* uses its hydrogenase machinery during lithoautotrophic growth, when preferable electron sources are unavailable. It is feasible, therefore that the choice of carbon sources used here, namely LB media supplemented with glucose, is affecting the biosensor apparatus, perhaps through another promoter present in the 500 bp promoter regions used in this work. Future work could instead employ glycerol and formate as the carbon sources. Indeed the benefit of the latter is that formate is the substrate for the main H_2 evolving complex in *E. coli*, FHL, and so would give best levels of endogenous H_2 production if a wild-type strain was used.

Similarly, the presence of glucose in the agar for the Hyd-2 biosensor plate assays will also pose problems for proper formation of any putative chimeric Hyd-2 biosensor. This is because CRP is known to repress the *hyb* operon, and so production of HybC cannot proceed (Richard *et al*., 1999). Again, the carbon source should be reconsidered. Glycerol is known to induce expression of the *hyb* operon, thus perhaps the same mixture of glycerol (to induce *hybC* expression) and formate (to allow for FHL H_2 evolution) could be used, as for the RH biosensor construct.

Indeed, an *in silico* analysis was performed using the promoter prediction online software, *Softberry BPROM* (www.softberry.com), in order to identify other promoter sites in the SH promoter region that may be causing the downstream gene expression to be controlled by factors other than the action of the biosensor system. This software predicted that the SH promoter region contained three transcription factor binding sites for σ^{70}-associated transcription in *E. coli*: one for FNR, and one for each of ArgR and ArgR2, which sense arginine

and function as transcription repressors of L-arginine biosynthesis (although ArgR2 has not been identified in *E. coli*) (Maas, 1994; Nicoloff *et al*., 2004). It follows that these may be interfering with the H_2-mediated transcription of the system, and further work is required to remove these extraneous promoter sites. Alternatively, the *E. coli* host could be grown in the absence of arginine to examine whether this improves expression of the transcription of the reporter genes. ArgR has not been identified in *C. necator* H16, however arginine-mediated regulation is known to be well conserved across divergent bacterial lineages (Nicoloff *et al*., 2004) suggesting it is probably present. As the RH transcription naturally operates in *C. necator* during lithoautotrophic growth, it is likely that L-arginine levels would be low, and ArgR repression would not occur.

In *C. necator*, σ^{54} synthesis is induced in the presence of glycerol or fructose carbon sources (Schwartz *et al*., 1998), it could therefore be hypothesised that the failure of the RH to work as well as hoped in this study could be due to the *E. coli* host being cultured in glucose media. Naturally, σ^{54} is involved in expression of nitrogen-related genes (Hunt and Magasanik, 1985), it may be assumed therefore that the gene encoding σ^{54}, *rpoN,* is in turn induced in such conditions. However, it is known that *fdhF*, the gene encoding for the formate dehydrogenase in FHL, is under the control of a σ^{54} RNA polymerase (Birkmann *et al*., 1987). There must therefore be σ^{54} sigma factor present in a fermentative *E. coli* cell, and so this cannot be why the transcriptional activity of the RH is apparently only weakly functional.

3.4.2 Possible problems with the synthetic RH operon

Another explanation for the problems in getting a functional biosensor may be that there is an aberration with the heterologously expressed RH machinery in *E. coli.* Whilst radiolabelling suggests the four HoxCBAJ proteins are properly synthesised, perhaps there are other factors at play inside the *E. coli* cells preventing proper function. For example, it was previously

commented that HoxA is unusual in that it is the dephosphorylated version of the response regulator that induces transcription. A native *E. coli* phosphatase may be removing the phosphate group and thus causing gene expression in absence of H_2. This could be tested for *via* the use of phospho-specific antibodies, for example.

It was shown in Figure 3.6 that *hoxJ** may contain a terminator sequence to interfere/prevent the transcription of downstream genes, and it was explained that the constructs were re-made to ensure this was the last gene in the operon. However, even with this modification, it is noticeable in the radiolabelling experiments, for both the RH (Figure 3.7) and Hyd-2 biosensor (Figure 3.9), that the downstream addition of *hoxAJ** into the operon seemed to result in the bands of proteins corresponding to the upstream genes to become less prominent. It was hypothesised that this may be due to HoxA or HoxJ* possessing a high abundance of methionine and/or cysteines, leading to a shortage of these amino acids. However, these proteins do not in fact contain significantly different levels of Met or Cys residues compared to the other proteins (Figure 3.19).

Protein	N° Met (%)	N° Cys (%)
HoxC	10 (2 %)	9 (1.8 %)
HoxB	9 (2.5%)	16 (5 %)
HoxA	7 (1.4 %)	4 (0.8 %)
HoxJ*	12 (2.6 %)	3 (0.6 %)
HybO short	6 (1.6 %)	13 (3.5%)
HybO long	6 (1.5 %)	13 (3.3 %)

Figure 3.19 Sulfur-containing residues of the RH machinery. The ^{35}S-Methionine radiolabelling performed in this work repeatedly resulted in HoxA and HoxJ* giving more prominent bands than the other proteins. The peptide sequences of the four RH components, and the two HybO::HoxB fusions used in this study were analysed for methionine and cysteine content to see if this could account for the observed phenomenon. Cysteine content was examined because it also contains sulfur, and can be produced in the cell from methionine. However, HoxA and HoxJ do not contain significantly higher amounts of Met or Cys than the other proteins.

Another possible explanation for the reduction in the strength of the protein bands seen when genes were co-expressed with *hoxAJ** downstream was hypothesised to be transcriptional interference; defined as “the suppressive influence of one transcriptional process, directly and *in cis* on a second transcriptional process” (Shearwin *et al*., 2005). The reverse complement sequences of *hoxAJ** was therefore analysed for the presence of the T7 promoter site consensus sequence 5’-ACTCACTA-3’ (Schneider and Stephens, 1990). This could interfere with transcription of the forward *hoxCBAJ** sequences during radiolabelling by convergence of RNA polymerases. Such a mechanism has previously been reported in *E. coli*, albeit *via* the viral promoters from coliphage 186 (Callen *et al*., 2004). However, no such promoter was found.

In this chapter, indeed in this Thesis, the Shine-Dalgarno *E. coli* consensus sequence and linker sequence 5’-AGGAGGAAAAAAA-3’ was used. However, other features of the mRNA may affect ribosome binding and/or movement along the transcript during translation. This so-called ‘ribosome drafting’, is related to the mRNA secondary structure, which may impede efficient ribosome recruitment (Espah Borujeni and Salis, 2016). This could account for the observed influence the addition of *hoxAJ** had on apparently reducing expression of the upstream genes; perhaps the secondary structure of the transcript from the T7 promoter to the end of *hoxCBAJ** was such that ribosome binding efficiency was reduced compared to when *hoxAJ** was absent. This is reflected in the literature where is has been demonstrated that even distal downstream sequences can effect mRNA structure and impede translation (Salis *et al*., 2009). One way to overcome this could be to split the RH/ Hyd-2 biosensor operons in two, with a terminator sequence inserted upstream of *hoxAJ**. The reason this may occur in mRNA of the optimised *hoxCBAJ** operon constructed in this thesis, but not that derived from the wildtype *hoxABCJ* operon in *C. necator* would of course be due to the different RNA sequence, due to the rearranged gene positions, and the partially different codon usage.

Another potential remedy to this problem could be to vary the RBS and/or linker sequences used. The freely available software *RBS Calculator* (Salis, 2011) allows for the efficiency of

translation initiation to be predicted from a thermodynamic model. Modifications can be made to the sequences (either by altering the Shine-Dalgarno sequence, the linker sequence, or altering the codon usage in the genes themselves) to help ensure mRNA secondary structure isn't such that it folds on itself and inhibits ribosome movement. The *hoxCBAJ** operon, as found in pUNI-RH was therefore analysed using *RBS Calculator* to examine the efficiency of translation (Figure 3.20).

Gene	Translation initiation rate (au)	ΔG_{total} (kcal/mol)	$\Delta G_{mRNA:rRNA}$ (kcal/mol)	ΔG_{mRNA} (kcal/mol)
*hox*C	907.53	2.25	-31.88	-23.2
hoxB	309.83	4.64	-698.17	-701.29
hoxA	473.54	3.7	-65.78	-70.0
*hoxJ**	2513.99	-0.01	-152.58	-147.9
*hoxJ**	593.03	3.2	-687.48	-686.4

Figure 3.20 Analysis of the translation efficiency of each gene in the optimised *CBAJ operon as found in pUNI-RH using *RBS Calculator*.** The complete DNA sequence from the transcriptional start site from the tat promoter of pUNI-RH was analysed. Translation initiation rate an indication of the efficiency an mRNA transcript derived the DNA sequence input, a higher score equates to more efficient translation. ΔG_{total} indicates the thermodynamic favourability of the formation of the pre-initiation translation complex, more negative equates to higher favourability. $\Delta G_{mRNA:rRNA}$ indicates how strongly the ribosomal RNA binds to the mRNA, again negative value indicates greater strength. ΔG_{mRNA} shows how strong the secondary structure mRNA transcript is folded, with a more negative value indicating greater strength. **Red text**: the same analysis was performed, but using a different sequence region about *hoxJ**.

Here it can be seen that in this analysis the expression of *hoxJ** is about an order of magnitude greater than the other three genes. Indeed it was seen that of the four genes, only *hoxJ** transcript translation had a thermodynamically favourable ΔG_{total}. All four genes showed a strong mRNA secondary structure, but this was particularly prevalent in *hoxB*. Perhaps this large discrepancy in translation efficiency explains the apparent differential protein synthesis seen during radiolabelling.

An important caveat with this analysis is that the RBS is limited to 2000 bp. As the *hoxCBAJ** operon is 5,444 bp long, so it had to be divided up in order to cover the whole operon. This is of course not ideal as it means the whole mRNA transcript produced from pUNI-RH is not analysed exactly how it would be present in the cell. Altering the length of upstream or downstream DNA sequences when analysing translation efficiency of a gene gives big differences in the output calculations. For example, the analysis of *hoxJ** was altered to run from 250 bp upstream of *hoxA* to as far downstream of *hoxJ** as possible, which yielded that data in red text seen above in Figure 3.20.

The same process was then carried out for the Hyd-2 biosensor constructs (Figure 3.21). Here it can be seen that the translation efficiency of both pUNI-hybO^{long}AJ*and pUNI-hybO^{short}AJ* is of comparable levels to that seen in for the RH biosensor. However, particularly for pUNI-hybO^{long}AJ*, it can be seen that HoxJ* synthesis is predicted to be far higher relative to the other proteins encoded by the operon. Translation of the *hoxJ** mRNA transcript is three two orders of magnitude higher than for *hybO* and three orders of magnitude higher than *hoxA*.

Gene	Predicted translation initiation rate (au)	ΔG_{total} (kcal/mol)	$\Delta G_{mRNA:rRNA}$ (kcal/mol)	ΔG_{mRNA} (kcal/mol)
hybO long	730.75	2.73	-40.18	-52.2
hoxA (*hybO long*)	59.43	8.31	-429.88	-436.11
*hoxJ** (*hybO* long)	24159.98	-5.04	-153.58	-147.4
hybO short	730.75	2.73	-40.18	-43.82
hoxA (*hybO* short*)*	84.04	7.54	-397.41	-1.19
*hoxJ** (*hybO* short)	3186.31	-0.54	-125.68	-121.6

Figure 3.21 Analysis of the translation efficiency of each gene in both Hyd-2 biosensor operons as found in pUNI-hybO^{long}AJ* and pUNI-hybO^{short}AJ*using *RBS Calculator*. The complete DNA sequence from the transcriptional start site from the tat promoter of pUNI-RH was analysed. Translation initiation rate an indication of the efficiency an mRNA transcript derived the DNA sequence input, a higher score equates to more efficient translation. ΔG_{total} indicates the thermodynamic favourability of the formation of the pre-initiation translation complex, more negative equates to higher favourability. $\Delta G_{mRNA:rRNA}$ indicates how strongly the ribosomal RNA binds to the mRNA, again negative value indicates greater strength. ΔG_{mRNA} shows how strong the secondary structure mRNA transcript is folded, with a more negative value indicating greater strength.

The rationale behind the optimisation of the first 20 codons of the RH genes in the *hoxCBAJ** operon was that this would help maximise the efficiency of translation initiation, after which the nascent mRNA would be long enough to ensure the continuation of the process. However, it may in fact be the case that the complete opposite approach would improve protein synthesis. Specifically, there is evidence to suggest that rare codons at the 5' end of a gene may improve translation efficiency, again hypothesised to be related mRNA secondary structure (Goodman *et al*., 2013).

An attempt was made to verify that this heterologously produced RH was functional (enzymatically active) *in vitro* using redox dye-linked assays (using BV and MV) on crude extracts; however no activity was observed. This is an important observation since an inactive

RH has little chance of activating downstream transcription. However, it is known that the RH exhibits little *in vitro* H_2-oxidising activity using artificial electron acceptors even when the system is synthesised in *C. necator* (Buhrke *et al*., 2001). As it was shown in Chapter 2, other hydrogenases from *C. necator*, specifically the SH, exhibited lower activity in *E. coli* than in its native organism, it was possible that a similar phenomenon was occurring here for the RH.

When this is taken into account along with the fact that the RH exhibits very low activity even in *C. necator* (Pierik *et al*., 1998), this may mean that any RH activity in *E. coli* is extremely low and difficult to detect *in vitro*. Alternatively, this lack of activity may indeed suggest a non-functional RH produced by *E. coli*. HoxB has been hypothesised to harbour unusual [Fe-S] clusters that deviate from the usual three in hydrogenase small subunits (two [4Fe-4S] and one [3Fe-4S](Volbeda *et al*., 1995)). HoxB has been instead predicted by some to contain two [2Fe-2S] clusters and additional cofactor, once thought to be non Fe-S in nature (Bernhard *et al*., 2001), but now hypothesised to be [4Fe-3S-3O] cluster (Buhrke *et al*., 2005b). It has been proposed that such clusters form from normal [4Fe-4S] clusters reacting with O_2 and H_2O (Rousset *et al*., 1998), and that one may occur in the RH of *C. necator* due to its natural operation under aerobic conditions (Buhrke *et al*., 2005b). If this was the case, then it would be important to ensure the RH biosensor in *E. coli* was synthesised in the presence of O_2. This would somewhat diminish the utility of the system to measure the endogenous H_2 production in *E. coli* which occurs during anaerobiosis. It should however be noted that more recent work suggests that HoxB instead contains three [4Fe-4S] clusters (Shafaat *et al.*, 2013)

3.4.3 Towards improving the Biosensor systems

The data in this Chapter suggests the RH and even Hyd-2 biosensors may be functioning at a basal level. Engineering of the proteins may thus need to be performed to improve the functionality of both systems in the *E. coli* host. One example could be a Gly468Val mutation to

HoxA, which is known to confer temperature tolerance to the protein, and allow it to properly function at temperatures above 33 ^{o}C (Zimmer *et al*., 1995).

For the Hyd-2 biosensor, work could be done to attempt to improve the cross talk between the different components of this chimeric system. The HybC, HybO and HoxJ* subunits may need further modification to allow for better interaction to improve complex stability, and/or allow for more efficient electron relay between the [Fe-S] clusters present in HybO to HoxJ*. For example, in this study the region of HoxB grafted onto HybO was merely judged by eye, going by the predicted protein structure of HoxB. This rather crude approach may have left out crucial residues required for proper association with HoxJ*. A more in-depth structural analysis of how HoxB and HoxJ interact, perhaps via crystallisation studies, may elucidate useful information to this end.

It was previously discussed that the alteration of the carbon sources in which the *E. coli* cells were grown from glucose to glycerol and formate may help activate the system, as it will better mimic the conditions in which expression through the SH/MBH promoters is naturally induced in *C. necator*. An alternative course of action would be to find out the specific DNA sequence to which HoxA binds in these promoter regions. If this was known, the promoter regions used could be reduced from the 500 bp used in this Thesis down to the discrete, HoxA specific sequence. This would be advantageous as it would remove the effects of any of the other transcriptional regulators that could possibly interfere with the reporter gene expression being solely in response to H_2 levels. A technique known as DNA footprinting (Galas and Schmitz, 1978) could be used in order to find where specifically HoxA binds in the MBH/SH promoter regions. For example DNA footprinting has been employed, in tandem with another technique known as a electrophoretic mobility shift assay (Hellman and Fried, 2007), in order to identify the recognition sequences the chitin-metabolism-associated CdsR regulator in *Pseudoalteromonas piscicida* (Miyamoto *et al*., 2007).Chromatin immunoprecipitation sequencing (ChIP-seq) is a more modern, ultra-high throughput approach that can be

performed in parallel to find multiple binding sites of a DNA –binding protein on the genome scale (Johnson *et al.*, 2007).

The possible aberrant function of the HypF1 maturase, as was discussed in more detail in Chapter 2, also has implications for the activity of the RH. It is known that HypF1 is particularly important for proper RH formation, and its absence cannot be rescued by the presence of HypF2 (Buhrke *et al*., 2001). It is not known if the *E. coli* HypF can compensate either. Further work ought to be done to fully establish whether the HypF1 product from the *hypA1-X* operon is properly formed.

3.4.4 Other potential hydrogenase candidates to use

The H_2-dependent (RH controlled) expression of MBH and SH in *C. necator* is not unique; other instances in nature show a use of hydrogenases to mediate transcription, such as in *Bradyrhizobium japonicum* (Black *et al*., 1994). More specifically, hydrogenase expression being regulated by two component systems is not unique; a similar system occurs in *Rhodobacter capsulatus* (Elsen *et al*., 1996; Richaud *et al*., 1991). Indeed, this system has been adapted to function as a biosensor for H_2 production in the algae *Chlamydomonas reinhardtii*, where intact *R. capsulatus* cells (engineered to express a reporter gene in response to H_2) were suspended over the growing algae to monitor H_2 evolution (Wecker and Ghirardi, 2014).

Even in *E. coli*, the expression of the Hyd-3-encoding *hyc* operon appears to be (albeit non-specifically) controlled by a similar regulatory mechanism involving HydH/G in response to high zinc and lead concentrations (Leonhartsberger *et al*., 2001).

In *S. enterica*, the transcriptome differs in response to H_2, specifically the expression of genes involved in carbon source utilisation and metabolism, and likely plays an important role in pathogenicity (Lamichhane-Khadka *et al*., 2011; Maier, 2005). If the specific mechanism for H_2-

dependent gene transcription could be identified, this could be used to develop a biosensor, either in *Salmonella* itself, or exported to *E. coli*, where it may be easier to employ than the RH due to the close relatedness of these two enteric species. Indeed, preliminary work has begun to elucidate this process, with constructs having already been engineered, utilising genes that showed the greatest upregulation in response to H_2: *aceB* and *fhuA* (Lamichhane-Khadka *et al*., 2011).

4. Characterisation of a chimeric metalloenzyme for H_2 production from pyruvate

4.1 **Introduction**

4.1.1 Natural modes of H_2 production in *E. coli* metabolism

By far the most predominant mode of H_2 production in *E. coli* is due to the action of the formate hydrogenlyase (FHL) complex, which operates during fermentation. In mixed acid fermentation numerous end-products are made, of which formate is but one. Thus, of all the carbon passing through glycolysis during fermentation, only a fraction — that which is converted to formate — is available for use from a H_2-production perspective. Therefore, one approach to boosting *E. coli* H_2 production would be to utilise new and different molecules present in the fermentative cell as electron donors. One particularly interesting candidate is pyruvate; a key central metabolite in glycolysis.

4.1.2 Pyruvate::ferredoxin oxidoreductase

Contrary to most aerobic organisms, where the crucial step of pyruvate decarboxylation is performed by the multi-enzyme complex pyruvate dehydrogenase, in Archaea, amitochondriate eukaryotes and obligate anaerobic bacteria, such as the *Clostridium* genus, pyruvate processing is carried out by a single enzyme called pyruvate::ferredoxin oxidoreductase (PFOR) (Chabriere *et al*., 1999; Hrdy and Muller, 1995; Ma *et al*., 1997). Specifically, PFOR catalyses the oxidation and decarboxylation of pyruvate *via* reaction with coenzyme-A to produce acetyl-CoA, CO_2 and two low potential electrons that are used to reduce a small, cytoplasmic [Fe-S] protein called ferredoxin (Fd) (Furdui and Ragsdale, 2000), although PFORs are also able to reduce flavodoxins (Yakunin and Hallenbeck, 1998). The reaction, which has a standard redox potential (E_0') of around −540 mV (Chabriere *et al*., 1999; Lupton *et al*., 1984), is summarised below:

$$\text{Pyruvate } (CH_3COCOO^-) + CoA + 2Fd^{ox} \leftrightarrow \text{acetyl-CoA} + CO_2 + 2H^+ + 2Fd^{red}$$

Intruigingly, it has been reported that in the absence of these electron acceptors in *Clostridium thermoacetium*, PFOR can exhibit direct hydrogenase activity itself, with protons reduced to H_2 (Menon and Ragsdale, 1996).

4.1.3 Linking PFOR activity to the hydrogen-evolving Hyd-3

The PFOR from *Thermotoga maritima* can be produced in an active form in *E. coli* (Kelly *et al*., 2015). Genes encoding the PFOR components (α, β, γ and δ subunits) alone, and also together with a gene encoding a ferredoxin from *T. maritima*, were incorporated into vectors pUNI-Tm-POR and pUNI-Tm-Fd-POR, respectively (Kelly *et al*., 2015). These vectors could be used to drive H_2 production in an *E. coli* strain, but only when co-expressed with an operon producing an active [FeFe]-hydrogenase from another thermophile (Kelly *et al*., 2015).

For this work it was hypothesised that the reduced ferredoxin (E_m approximately -500 mV) produced by PFOR could be engineered to pass its low potential electrons on to almost any other redox enzyme system (Kelly, 2013). One possibility was that the PFOR could be engineered to replace the formate dehydrogenase-H component of FHL in *E. coli* and so supply electrons for the hydrogen-evolving Hyd-3 isoenzyme. With this in mind, *E. coli* strains were constructed that would produce ferredoxin-Hyd-3 fusion proteins (FTF2013 and FTF2015, Strain Table 7.1). These strains were constructed by Dr. Jen McDowall, Dr. Constanze Pinske, Professor Tracy Palmer and Dr. Grant Buchanan (University of Dundee).

First, an *E. coli* K-12 MG1655 derivative carrying a *hycE*^{His} allele (MG059e1; McDowall *et al*., 2014) was modified by the addition of a Δ*fdhF* allele to give strain MGE1dZ (McDowall *et al*., 2015). Next, a Δ*nuoA-L*::Apra^R allele was prepared and used to generate an MGE1dZ Δ*nuoA-L*::Apra^R strain. Using pMAK705, an allele was prepared that encoded a ferredoxin fused to HycB *via* a HA epitope tag. Flanking this allele was sequence that would allow its direct replacement of the *hycAB* genes on the chromosome. This Δ*hycAB*::*fd-hycB* allele was

transferred to the chromosome of the MGE1dZ Δ*nuoA-L*::Apra^{R} strain to give FTF2013. Finally, the FTF2013 strain was transformed with pREP4 (encoding the LacI repressor) before an inducible promoter was placed in front of the engineered *fd-hycBCDEFGHI* operon on the *E. coli* chromosome to yield the final FTF2015 strain, which enables IPTG induction of the ferredoxin-Hyd-3 fusion protein. It was hoped that expressing pUNI-Tm-Fd-POR and/or pUNI-Tm-POR (Table 7.6) in these strains would allow the Fd-Hyd-3 fusion protein to be reduced by PFOR and so allow H_2 evolution directly from pyruvate.

4.2 **Aims**

The aim of the work presented in this Chapter was to characterise the *in vivo* activity of a ferredoxin-Hyd-3 chimera when co-expressed with PFOR. This involved an attempt to confirm fusion protein production in the cell, before H_2 yield determination using gas chromatography. HPLC was then used to observe any effects producing the chimera and non-native enzyme had on the products of mixed acid fermentation.

4.3 **Results**

4.3.1 Synthesis of the ferredoxin::Hyd-3 fusion

The first step in the characterisation of the ferredoxin::Hyd-3 fusion protein was to show the enzyme complex was synthesised in the cell. This was done *via* Western immunoblot analysis using antibodies against the HA-tag present in the linker between HycB and ferredoxin (Fd). The strains MC4100, FTF2013 and FTF2015 were used to inoculate Universal tubes filled with 20 mL LB media supplemented with 0.8 % (w/v) glucose and appropriate antibiotics, before being incubated for 17 hours at 37 ^{o}C without shaking (to induce anaerobiosis). For the FTF2015 strain, a second Universal was prepared as above, but with the addition of 1 mM IPTG in the media to allow for overexpression of the Fd-HA-HycB encoding genes on the chromosome. Fractionation was then performed and whole cell, soluble and total membrane fractions were then used in Western immunoblot analysis using αHA antibodies. The data are shown in Figure 4.2.

It can be observed that whilst no HA tag was detected in any of the FTF2013 fractions, it was detected in FTF2015 whole cell fractions (W) during both constitutive and overexpression (FTF2015 and FTF2015 + IPTG lanes), with more protein being present after overexpression of the genes (Figure 4.1). Furthermore, following overproduction the Fd-HA-HycB peptide was detected in the total membrane fraction (Figure 4.1), although at a lower level than that present in the whole cell fraction. Therefore, whilst it appears that the ferredoxin-HycB fusion is being made and the complex is forming to some degree (as in order for a HA-tag to be detected in the membrane, so the HycB-HA-Fd fusion must be anchored by at least some of the Hyd-3 complex), the whole complex seems to be unstable. The reason for this latter supposition is that the band intensity in the membrane fraction is much weaker following fractionation (indeed non-apparent in the non-overexpressed FTF2015 sample) than in the whole cells.

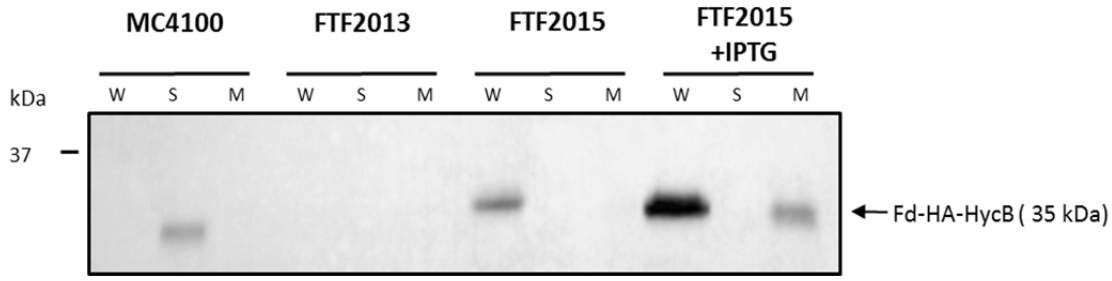

Figure 4.1 The ferredoxin-Hyd-3 fusion protein can be synthesised in the cell. Single colonies of FTF2013, FTF2015 and the negative control strain MC4100 were used to inoculate Universal tubes filled with 20 mL LB media supplemented with 0.8 % (w/v) glucose and appropriate antibiotics, before being incubated for 17 hours at 37 ^{o}C without shaking to induce anaerobiosis. A second culture of FTF2015 was prepared with the same media but with an addition of 1mM IPTG. Cells were harvested by centrifugation to yield whole cell (W) samples and fractionation performed to give soluble (S) and total membrane (M) samples of each culture. These were then subjected to Western immunoblot analysis using αHA-tag antibody.

4.3.2 Assessing the functionality of the Fd-Hyd-3 fusion enzyme

Now that is was established that the fusion protein and chimeric complex was forming in the cell, the next step was to examine its activity *in vivo*, which was done using gas chromatography. FTF2013 and FTF2015 were transformed with pUNI-PROM (control), pUNI-Tm-POR or pUNI-Tm-Fd-POR before being used to inoculate sealed Hungate tubes containing 5 mL of anaerobic M9 buffer supplemented with 0.8 % (w/v) glucose, 0.2 % (w/v) casacids and appropriate antibiotics. In the case of FTF2015 an additional set of cultures was prepared with media containing 1 mM IPTG to allow for overproduction of the Fd-HA-HycB fusion. Cultures were left to grow at 37 ^{o}C without shaking to induce anaerobiosis for 24 hours, after which the H_2 content of the headspace was measured by gas chromatography. The results are shown in Figure 4.3. It can be seen that, whilst no more H_2 is seen in the FTF2013 tests strains when compared to the negative control (pUNI-PROM), the system does appear functional in FTF2015. It is apparent that providing additional Fd in tandem with PFOR, *via* the pUNI-Tm-Fd-POR vector, results in more H_2 production than merely expressing PFOR by itself (pUNI-Tm-POR) (Figure 4.2).

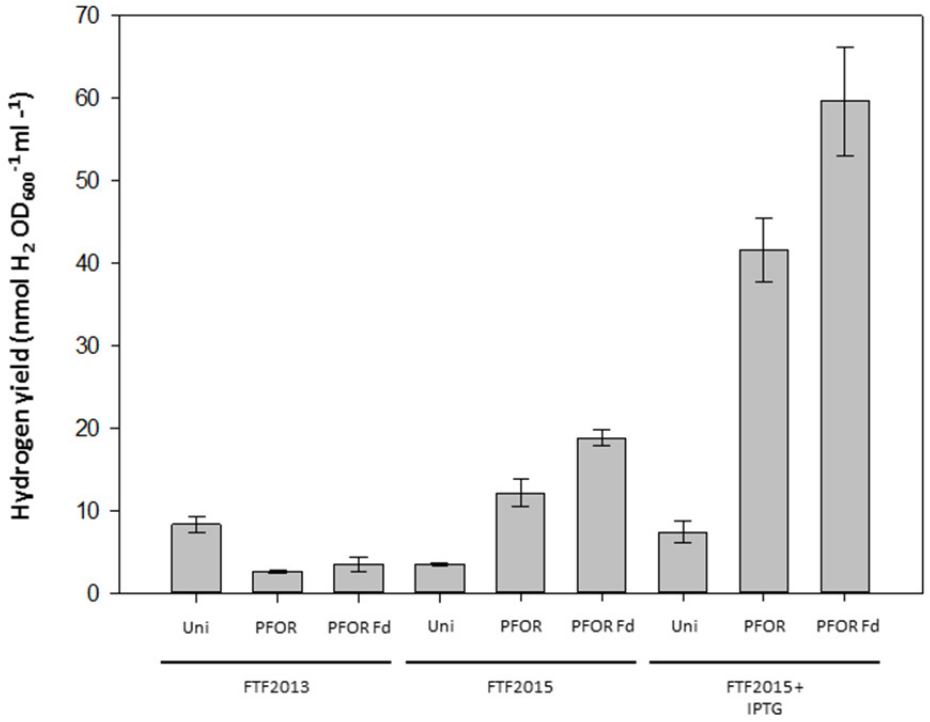

Figure 4.2 The Fd-Hyd-3 chimera exhibits H_2 evolution in the presence of PFOR. The strains FTF2013 and FTF2015 were transformed with pUNI-PROM, pUNI-Tm-POR or pUNI-Tm-Fd-POR. Resultant colonies were grown anaerobically overnight in LB with appropriate antibiotics at 37 ^{o}C. Cells were then washed with anaerobic M9 media supplemented with 0.8 % (w/v) glucose, 0.2 % (w/v) casacids and appropriate antibiotics, after which the OD_{600} was normalised to 0.01 in 100 µL. This resultant sample was then used to inoculate sealed Hungate tubes (purged of O_2 with N_2) containing 5 mL of this same anaerobic M9 media. An additional set of Hungate tubes was set up for the FTF2015 cells containing 1 mM IPTG to allow for overexpression of the *hycB-HA-fd* gene fusion. Cultures were left to grow for 48 hrs at 37 ^{o}C without shaking, after which the OD_{600} was measured and the H_2 content in the headspace measured *via* GC. Error bars represent SEM (n=3).

4.3.3 Effect of Fd-Hyd-3 fusion and PFOR on the cell metabolome

Now that it was shown that the Fd-Hyd-3 fusion was functional, it was endeavoured to explore what effect this might have on the metabolic state of the cell. It could be imagined that the consumption of such a central compound as pyruvate would have a knock-on effect on the metabolome, so this was examined by HPLC. Specifically, the influence the chimera had on some of the main end products of mixed-acid fermentation: lactate, formate and acetate, as well as succinate and pyruvate, was measured.

FTF2013 and FTF2015 were transformed with pUNI-PROM, pUNI-Tm-POR or pUNI-Tm-Fd-POR as before. Transformants were used to inoculate 16 mL LB media supplemented with 0.8 % (w/v) glucose and appropriate antibiotics. Another set of cultures were set up for the FTF2015 strains that also contained 1 mM IPTG for overexpression. Cultures were grown for 24 hours, after which cells were harvested by centrifugation. The supernatant was passed through a 0.2 µm filter to remove residual cells and debris and the resultant spent fermentation media was analysed with an Aminex HPX-87H organic-acid column at 0.5 mL min^{-1} and 55 °C. Organic acids were detected by UV absorption at 210 nm. A standard curve of organic acid standards was prepared and used to quantify the concentrations of lactate, formate, acetate, succinate and pyruvate. Sample concentrations were normalised by $OD_{600.}$The concentrations of compounds in virgin media (LB + 0.8% (w/v) glucose – with and without IPTG) were also analysed. Representative elution profiles are shown in Figure 4.3.

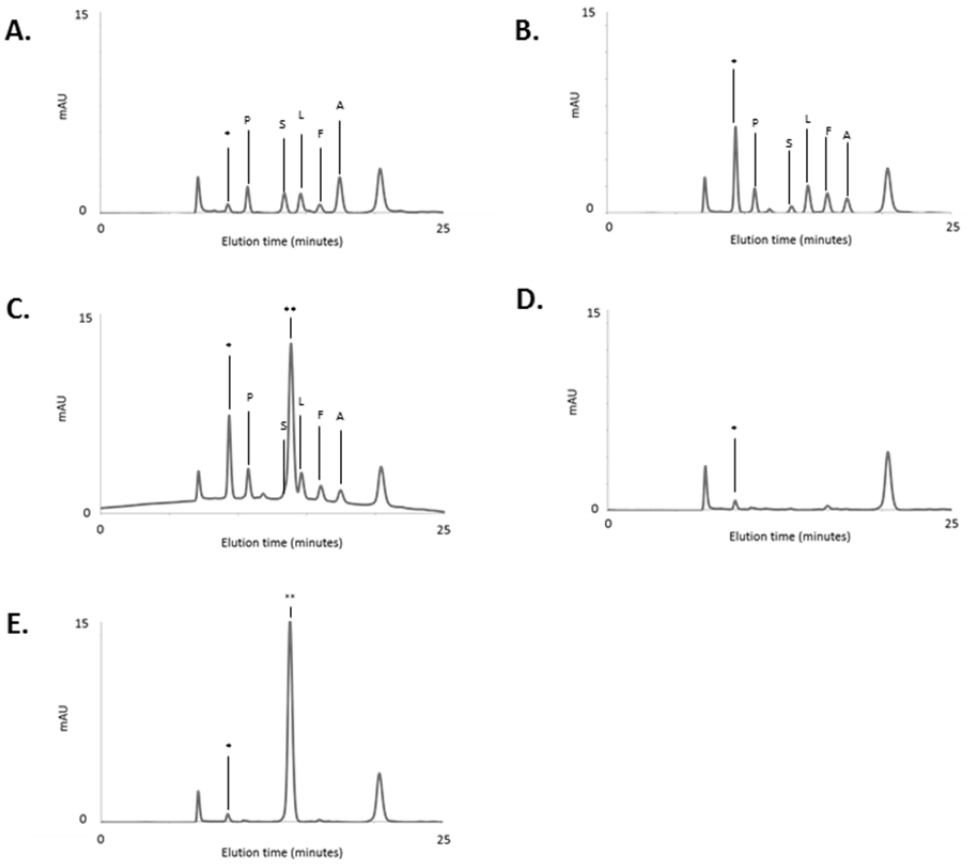

Figure 4.3 Representative HPLC elution profiles to show organic acid content in spent fermentation broth. FTF21013 and FTF2015 were each transformed with pUNI-PROM, pUNI-Tm-POR or pUNI-Tm-Fd-POR, before being used to inoculate Universals filled with 16 mL LB + 0.8 % (w/v) glucose were inoculated. Additional cultures were set up for the FTF2015 samples as before but also containing 1 mM IPTG. After the cultures were subject to anaerobic growth at 37 ^{o}C for 24 hours, OD_{600} was measured before cells were pelleted by centrifugation at 4000 rpm. The supernatant was passed through a 0.2 µm syringe filter and analysed by HPLC. For HPLC analysis, 5 µL of fermentation broth was separated at 0.5 mL min^{-1} and 55 °C using a Dionex UltiMate 3000 HPLC system, fitted with an Aminex HPX-87H organic acid column, with absorbance monitored at 210 nm. Organic acid standards were used all with R^2 values greater than 99.90%. Peaks with elution times corresponding to these elution times have been identified P: pyruvate; S: succinate; L: lactate; F: formate; A: acetate. Traces are numbered as follows: **A**: MC4100 + pUNI-PROM; **B**: FTF2015 + pUNI-Tm-Fd-POR; **C**: FTF2015 + pUNI-Tm-Fd-POR + IPTG; **D**: virgin LB media; **E**: virgin LB media + IPTG. Two unidentified peaks of interest are marked by '*' and '**'.

After the HPLC was performed, the area of each peak corresponding to pyruvate, acetate, formate, lactate and succinate was integrated. These were then normalised by reference to the calibration standards, and also OD_{600} of the original cultures, in order to calculate the

respective relative extracellular concentrations present in the fermentation broth. The results of this are illustrated in Figure 4.4.

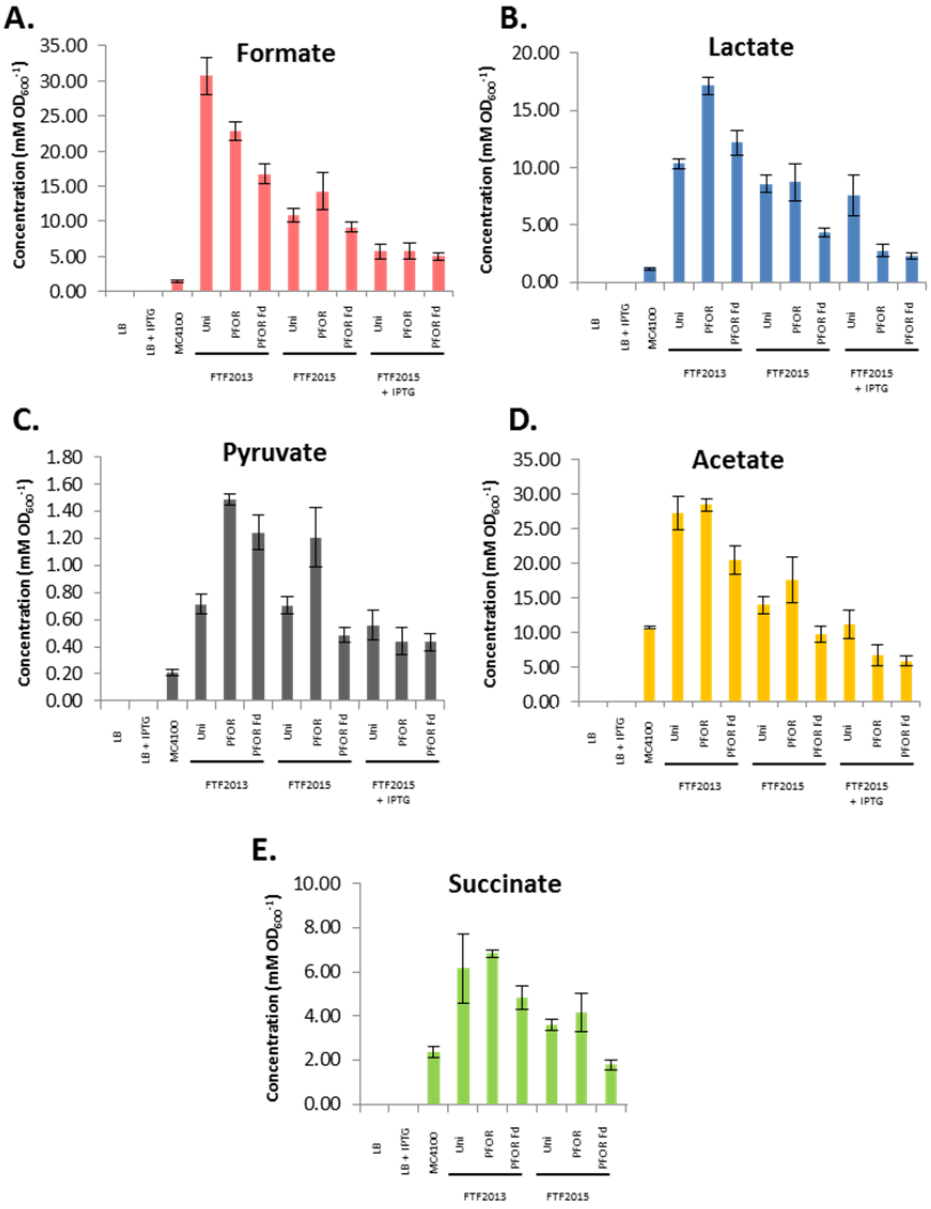

Figure 4.4 The influence of the Fd-Hyd-3 fusion and PFOR on the *E. coli* metabolome. FTF21013 and FTF2015 were each transformed with pUNI-PROM, pUNI-Tm-POR or pUNI-Tm-Fd-POR, before being used to inoculate Universals filled with 16 mL LB + 0.8 % (w/v) glucose. Additional cultures were prepared for the FTF2015 samples containing 1 mM IPTG. After the cultures were subject to anaerobic growth at 37 ^{o}C for 24 hours, OD_{600} was measured before cells were pelleted by centrifugation at 4000 rpm. The supernatant was passed through a 0.2 µm syringe filter and analysed by HPLC. For HPLC analysis, 5 µL of fermentation broth was separated at 0.5 mL min^{-1} and 55 °C using a Dionex UltiMate 3000 HPLC system, fitted with an Aminex HPX-87H organic acid column, with absorbance monitored at 210 nm. Organic acid standard curves were used all with R^2 values greater than 99.90%. Data were normalised by OD_{600}. Error bars represent SEM (n=3). **Uni**: pUNI-PROM; **PFOR**: pUNI-Tm-POR; **PFOR Fd**: pUNI-Tm-Fd-POR; **MC4100**: MC4100 transformed with pUNI-PROM.

In these experiments the starting concentration of glucose added to the rich media was 0.8% (w/v), which is the equivalent to 44 mM D-glucose. Under these conditions the MC4100 positive control strain produced 1.5 mM OD_{600}^{-1} of formate after 24 hours (Figure 4.4A). This can be compared with the FTF2013/pUNI-PROM strain (carrying Δ*fdhF* and *fd::hycB* modifications that would inactivate FHL), which accumulates formate to 30.6 mM OD_{600}^{-1} in the growth medium. Importantly, when the PFOR, Fd and Fd-Hyd-3 system is produced at its maximum level (FTF2015/pUNI-Tm-Fd-POR + IPTG) the extracellular formate level drops to 5.7 mM OD_{600}^{-1}, which is indicative of pyruvate being directed away from the endogenous PFL enzyme towards the heterologous PFOR system.

Lactate is an alternative product of pyruvate that often appears in stationary phase as the expression of the gene encoding the NADH-dependent lactate dehydrogenase is at its highest. Like formate, lactate levels are also higher in the FTF2013 strain (for example reaching 17.2 mM OD_{600}^{-1} in the FTF2013/pUNI-Tm-PFOR samples) compared to the MC4100 control strain, which produces 1.2 mM OD_{600}^{-1} (Figure 4.4B). This may mean high formate levels are inhibiting PFL (which is readily reversible) leading to an accumulation of pyruvate and thus extra substrate for lactate dehydrogenase. Indeed, low levels of pyruvate itself can be detected in the growth medium even though it is itself not considered to be an end-point acid of mixed acid fermentation (Figure 4.4). The relative levels of pyruvate do largely follow those of formate and lactate in the FTF2013 mutant strains (Figure 4.4). And in all cases, when the PFOR, Fd and Fd-Hyd-3 system (FTF2015/pUNI-Tm-Fd-POR + IPTG) is maximally produced the balance of pyruvate/lactate/formate is returned to low levels seen in the control strain (Figure 4.4).

Succinate and acetate levels can also be monitored using this technique (Figures 6.4D and 6.4E). Although there is some increase in the extracellular levels of these compounds when the MC4100 strain is compared to FTF2013 (Figure 4.4), in both cases this is around a two times increase. Note that a large peak was detected in the HPLC traces in all samples containing IPTG

that had a retention time very similar to succinate. As such it was not possible to determine relative succinate production for any samples containing IPTG.

4.4 **Discussion**

4.4.1 A novel enzyme system is functional in *E. coli*

The work presented in this Chapter has demonstrated that a new hydrogenase fusion construct is functional, and allows for the utilisation of new substrates in *E. coli* for H_2 production: specifically pyruvate indirectly, and reduced ferredoxin directly. This latter finding is particularly salient as, whilst it is known that [FeFe] hydrogenases can associate with ferredoxins, such as in the alga *Chlamydomonas reinhardtii* (Chang *et al*., 2007), and the thermophilic bacteria, *Thermotoga maritima*, the species where the genes used in this study originated (Blamey and Adams, 1994), [NiFe]-hydrogenase::ferredoxin complexes are more unusual. A notable exception to this is found in the cyanobacterium *Synechocystis* sp. PCC 6803 (Gutekunst *et al*., 2014), which also involves the action of PFOR. The proposed mechanism for the PFOR and Fd::Hyd-3 operation is shown in Figure 4.4.

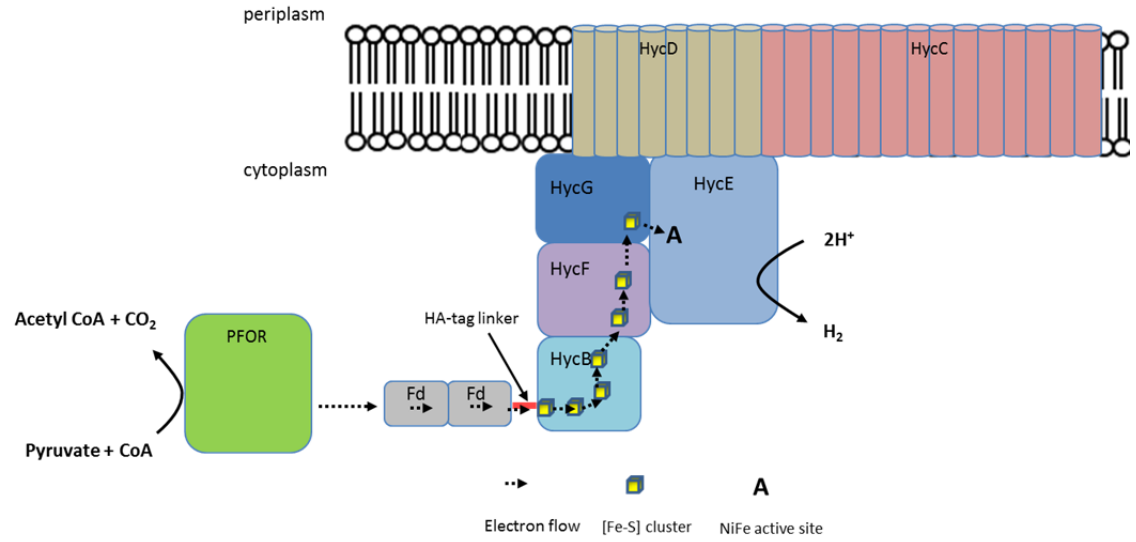

Figure 4.5 Proposed mechanism by which the PFOR Hyd-3::Fd chimera generates H_2 production from pyruvate. The formate dehydrogenase H subunit of the *E. coli* FHL complex has been replaced by a ferredoxin (Fd) covalently bound to the N-terminus of HycB *via* a HA-tag. As ferredoxins often exist as functional dimers, and because Fd is not a stably-attached subunit of PFOR, so the additional Fd encoded by pUNI-Tm-Fd-POR is hypothesised to help shuttle electrons between PFOR and HA-tagged Fd as well as allowing dimerization of Fd. The heterologously expressed PFOR from *T. maritima*, also encoded by pUNI-Tm-Fd-POR, is then thought to reduce ferredoxin *via* the oxidation of pyruvate. The electrons can then relay through the [Fe-S] clusters of Hyd-3 to allow for the evolution of H_2 from protons by HycE.

That a [NiFe]-hydrogenase is able to obtain electrons from ferredoxin has implications for the long term goal of producing H_2 at industrial scale. This is because despite [FeFe]-hydrogenases being typically more biased to H_2 evolution that their [NiFe]-hydrogenase counterparts (Mulder *et al*., 2011), they are also more susceptible to O_2 attack to the extent that they can be permanently inactivated (Ghirardi *et al*., 2007). This may be problematic if an industrial scale batch culture that is periodically emptied and refilled, with a risk of O_2 contamination at each stage, were to be used to generate H_2. On the other hand, O_2 only transiently inhibits most [NiFe]-hydrogenases and so these may be seen as more desirable enzymes to be used for H_2-evolution.

In this work, it was observed that synthesis of additional Fd from the vector pUNI-Tm-Fd-POR resulted in an increase in H_2 production compared to the pUNI-Tm-POR experiments.

Ferredoxins often exist as functional dimers, a fact that might explain the result seen here. Similarly, overproduction of the HycB-HA-ferredoxin fusion also resulted in markedly greater H_2 production compared to the non-overexpressed case (Figure 4.2). This probably indicates the modified Hyd-3 is rather labile, and an overabundance of the fusion protein increases the likelihood of the complete formation of the complex. Indeed, even the native FHL configuration is unstable, with formate dehydrogenase subunit, FdhH, having only a loose attachment to HycB (Sawers, 1994). This use of a HA-tag linker to covalently connect ferredoxin to HycB was based on previous work to more strongly adhere FdhH using the same method (McDowall *et al*., 2015).

The characterisation data shown in Figure 4.1 align with the activity data in Figure 4.2. It was shown by Western immunoblot analysis that the Fd-HycB fusion was only clearly detected in FTF2015, and only weakly in the strain FTF2013. This is reflected in the GC data where FTF2015 shows slightly greater H_2 production than FTF2013 during constitutive expression conditions. Similarly, the Fd-HycB fusion is only detected in the membrane fraction (thus indicating FHL complex assembly) during overproduction in the FTF2015 strain. Again, this is reflected by the markedly increased H_2 production exhibited as shown in Figure 4.3. Despite no detection of the fusion at all in FTF2013, nor in the membrane in the non-overproducing FTF2015, these cultures still showed some H_2-evolving activity. It should be noted that these assays measure accumulation of H_2 over several hours, so even low levels of enzyme activity can be detected. It should also be noted that these strains retain a functional Hyd-2 in the cell. Although Hyd-2 is only poorly expressed in the presence of high amounts of glucose, especially in minimal media, it is conceivable that reverse electron transport through Hyd-2 could be occurring.

4.4.2 Reconciliation of GC and HPLC data

It was inevitable that the use of a compound with such a central role to cellular metabolism as pyruvate as a direct substrate for H_2 production would have effects on the metabolic state of the cell. Indeed, HPLC data (Figure 4.4) presented in this Chapter neatly fits the GC results describing the *in vivo* activity of the Fd-Hyd-3/PFOR system (Figure 4.2).

First, the general negative correlation between extracellular pyruvate concentration and H_2 production was found. Although pyruvate would not normally be located outside the cell, the low levels here and their relative changes contribute to an intuitive result as a greater pyruvate oxidising enzymatic activity would mean a reduction in substrate levels.

The reduction in pyruvate concentration fits with the observed lower levels of the end products of mixed acid fermentation lactate, formate and acetate, observed in instances where the chimeric PFOR enzyme is fully active. Furthermore, it appears these correlate neatly with the GC data in Figure 4.2; the higher the activity of the complex, the lower the observed concentration of these organic acids.

Unfortunately it was not possible to detect succinate concentrations by HPLC in the samples where IPTG was added to the media as these samples exhibited a large peak, presumably IPTG, that had an elution time similar to that of succinate. As such the succinate peak was masked. The ability to detect IPTG was unexpected; but whilst the 210 nm absorbance wavelength was chosen to detect carboxylic acid groups (of which IPTG contains none), it is possible that the IPTG molecule must contain another bond that exhibits a resonance frequency similar to the carboxyl group. If it becomes important to circumvent this, a couple of approaches could be tried. Firstly, the *fd-HA-hycB* fusion could be re-engineered to have overexpression induced by another molecule, although this could be laborious. A more expedient solution may be to alter the HPLC protocol, perhaps by changing the column, such that the elution times increased and the peaks on the purification trace were resultantly spread out.

Besides the IPTG peak, another unverified peak was noted in the traces, as illustrated in Figure 4.3 by '*'. It could possibly be acetyl Co-A leaking from the cells, as it appears pronounced in the samples taken from strains with the chimeric enzyme apparatus (Figure 4.3), and PFOR activity would result in acetyl-CoA generation.

With hindsight, it may have been better practice to measure intracellular metabolite concentrations as opposed to the extracellular concentrations in the fermentation broth. However, the two should correlate as the end products of mixed acid fermentation are excreted upon production (at least initially in the case of formate (Sawers, 2005)), either in the dissociated states *via* the action of H+/monocarboxylic acid symporters or by free diffusion in their undissociated states (Warnecke and Gill, 2005). The latter is more relevant in this case due to the low intracellular pH associated with mixed acid fermentation. Furthermore, *E. coli* is also known to possess a pyruvate exporter to balance metabolite levels (Kreth *et al*., 2013), and so the extracellular pyruvate level will also correlate somewhat with that inside the cell.

A schematic to illustrate how the new metabolic system fits into cell physiology is presented in Figure 4.6.

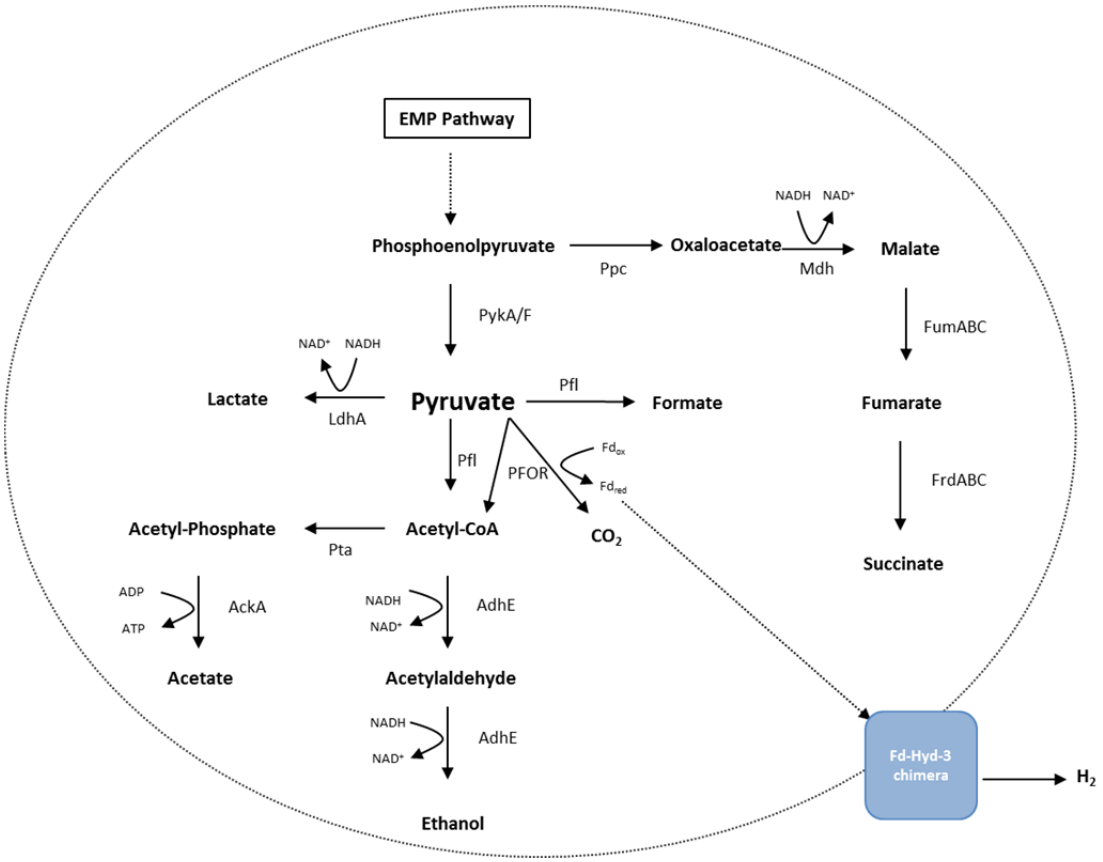

Figure 4.6 Possible influence of the Fd-Hyd-3 enzyme on mixed acid fermentation. This schematic illustrates the main carbon sinks during fermentation in FTF2013/FTF21015 cells when expressing the pUNI-Tm-Fd-POR vector, and is helpful for explaining the HPLC results of Figure 4.3. Pyruvate is oxidised by PFOR, reducing the soluble ferredoxin, which is in turn oxidised by the modified FHL complex ('FHL Fusion') to produce H_2. This action of PFOR directly reduces [pyruvate], with the knock-on effect of less substrate available for LdhA, Pta Pfl, and so lower concentrations of lactate, acetate and formate respectively. Enzyme abbreviations: Ppc: phosphoenolpyruvate carboxylase; Mdh: malate dehydrogenase; FumABC: fumarase; and FrdABC: fumarate reductase PykA/F: pyruvate kinase; LdhA: lactate dehydrogenase; Pfl: pyruvate formate lyase Pta: phosphotransacetylase; AckA: acetate kinase; AdhE: alcohol dehydrogenase. FHL: formate hydrogenlyase (containing Hyd-3). EMP Pathway: Embden–Meyerhof–Parnas Pathway.

The HPLC parameters as described were set up to detect carboxylic bonds, and as such pyruvate — in addition to the organic acid end products of mixed acid fermentation — could be detected. However, this meant that it was not possible to measure the level of the other major end product of fermentation, ethanol. In order to detect ethanol, a refractive index detector is required. Whilst refractive index detectors have a lower sensitivity than detectors set up for UV wavelength measurement as used here, they have the advantage of being universal detectors. Thus other potential metabolites of interest could be measured too, such

as glucose and acetyl-CoA; an important step for full characterisation of this new metabolomics pathway for H_2 generation.

4.4.3 Strategies to further improve enzymatic activity

An in depth characterisation of the chimeric enzyme complex is required. Specifically, protein modelling should be performed to examine how the HA-tag peptide linker could affect the distance between Fd and the first [Fe-S] cluster of HycB. With the consideration that efficient spontaneous electron transfer requires distances between cofactors of no more than ~14 Å (Page *et al*., 1999); this structural data would be of great assistance in determining how to further improve activity.

Multiple components of the new fusion enzyme are susceptible to O_2. Whilst [NiFe]-hydrogenases are not as sensitive to O_2 attack as [FeFe]-hydrogenase enzymes, the activity of Hyd-3 is nonetheless hampered by aerobiosis. PFOR exhibits similar transient inactivity upon contact with oxygen, with aeration causing its activity to fall to just 3 %, although this is recovered upon return to anaerobiosis (Pan and Imlay, 2001). Likewise, the activity of 'bacterial type' [4Fe-4S] ferredoxins as used here has been shown to be irreversibly compromised by oxygen (Harklau *et al*., 2001). Whilst efforts were taken to ensure anaerobiosis was maintained at all times during cell growth, oxygen attack may still have occurred at some level. Future work could involve performing all steps during the assessment of activity in an anaerobic chamber, as this may lead to increased H_2 yield.

It would be beneficial for characterisation purposes to generate a soluble version of this modified Fd-Hyd-3 fusion in the cell. However, it has hitherto been impossible to generate a soluble active form of Hyd-3, as mutants deficient in the membrane subunits, HycD and HycC, exhibit abolished activity (McDowall *et al*., 2015), and both membrane subunits are required for H_2 production *in vivo* (Sauter *et al*., 1992). Why this is the case is uncertain, however the

structural similarity of Hyd-3 to respiratory Complex I invites speculation that Hyd-3 activity is similarly linked to proton translocation across the membrane.

The activity of pyruvate formate lyase could also be abolished in an attempt to create a greater pyruvate pool and so increase substrate availability for the chimera, and in turn increase H_2 production. Whilst doing this would impact upon acetyl-CoA production, it would be hoped that this could be compensated for by the acetyl-CoA synthesis by the PFOR subunit. Likewise, if the hitherto unidentified locus encoding the pyruvate exporter (Kreth *et al*., 2013) was located, a knock-out mutant may help boost intracellular pyruvate concentrations.

Conversely, if the goal is to purely maximise H_2 yield, then it may be desirable to abolish Hyd-2 activity in the FTF2015 strain. Having a functional Hyd-2 in the cell runs the risk of some of the H_2 evolved by the chimeric complex being re-oxidised by Hyd-2. This may occur during anaerobic respiration using fumarate as an electron acceptor (Ballantine and Boxer, 1986). Indeed, it has even been suggested that Hyd-2 can associate with fumarate reductase in a 'membrane microdomain' to lead to fumarate reduction *via* the oxidation of H_2 (Kelly, 2013; Vignais and Billoud, 2007). The fact that most of the samples exhibited succinate production (bar the IPTG containing samples where succinate concentrations could not be determined) suggested that some level of this anaerobic respiration must be possible in the media used.

The problem is thus that the H_2 yield measured by the GC experiment (Figure 4.2) may underplay quite how much is evolved by the chimera. Alternatively, the gene phosphoenolpyruvate carboxylase (Ppc) could be knocked-put to prevent the reductive path of the TCA cycle occurring during anaerobiosis. Abolishing the activity of an enzyme so central to metabolism confers fitness disadvantages (Peng and Shimizu, 2004), so ideally a system would be devised to maintain biosynthesis of Ppc during aerobiosis, but cessate production during fermentation. Perhaps the employment of the ArcA/B two component regulatory system could be employed for such a purpose.

5. Further characterisation of a chimeric metalloenzyme for H_2 production

5.1 **Introduction**

5.1.1 Glycerol is a desirable substrate for industrial H_2 production

Glycerol can be seen as a hugely desirable, if not the ideal, carbon source from which to synthesise H_2 on a large scale. It is a major waste product during the synthesis of other biofuels; with 1 kg of glycerol being generated during the synthesis of every 10 kg of biodiesel, for example (Yazdani and Gonzalez, 2007). The expansion of the biodiesel industry has in turn increased the availability of glycerol, with the corollary that the price of glycerol has dropped substantially (Yazdani and Gonzalez, 2007). Thus, it could be envisaged that biodiesel and bioH_2 industries could operate in tandem, with very little waste. Furthermore, the highly reduced state of the carbon atoms present in glycerol molecules theoretically could mean a higher yield of fermentation end products such as H_2 compared to other carbon sources (Yazdani and Gonzalez, 2007).

5.1.2 Glycerol metabolism in *E. coli*

There had been a long-standing consensus in the literature that, within the Enterobacteriaceae, only species that could produce 1,3-propanediol, such as *Klebsiella pneumoniae*, could ferment glycerol in the purest sense (Booth, 2005). *E. coli*, amongst others, was thought to strictly require the use of respiratory electron receptors for glycerol-3-phosphate respiration (Lin, 1976; Miki and Lin, 1973). The paradigm was that glycerol is first imported across the membrane *via* the glycerol transporter GlpF (Borgnia and Agre, 2001) before action of the glycerol kinase GlpK leads to glycerol-3-phosphate (Glyc-3-P) synthesis from the phosphorylation of glycerol. Under aerobic conditions, the oxidation of this Glyc-3-P could then be coupled to quinone reduction *via* the action of the membrane-anchored Glyc-3-P dehydrogenase, GlpD (Walz *et al*., 2002), with O_2 the ultimate electron acceptor. Under anoxic conditions other terminal electron acceptors are employed, such a fumarate or nitrate,

with the quinone pool again used as an intermediary. Whilst the quinone pool is still reduced by the oxidation of Glyc-3-P, in anoxic conditions it is *via* the action of an anaerobic Glyc-3-P dehydrogenase, which is encoded by the *glpABC* operon (Schryvers and Weiner, 1982).

In both aerobic and anaerobic cases, the oxidation of Glyc-3-P produces dihydroxyacetone phosphate (DHAP), which is an intermediate in the Embden-Meyerhof-Parnas glycolytic pathway. It is a substrate of the enzyme triose-phosphate isomerase (TIM), which acts to interchange DHAP with glyceraldehyde-3-phosphate (GA3P). A schematic to summarise these glycerol metabolism pathways is shown in Figure 5.1. Anaerobically, this process generates menaquinol and it is likely that this is the source from which Hyd-2 obtains electrons for H_2 generation during glycerol metabolism that was first discovered during the course of this work (Blbulyan and Trchounian, 2015; Pinske *et al*., 2015a; Sargent, 2016). Operating in reverse, Hyd-2 can carry out a function as a "redox-release valve" (Pinske *et al*., 2015a), preventing the quinone pool from becoming over reduced by transducing the pmf to quinol oxidation and proton reduction in the absence of external electron acceptors.

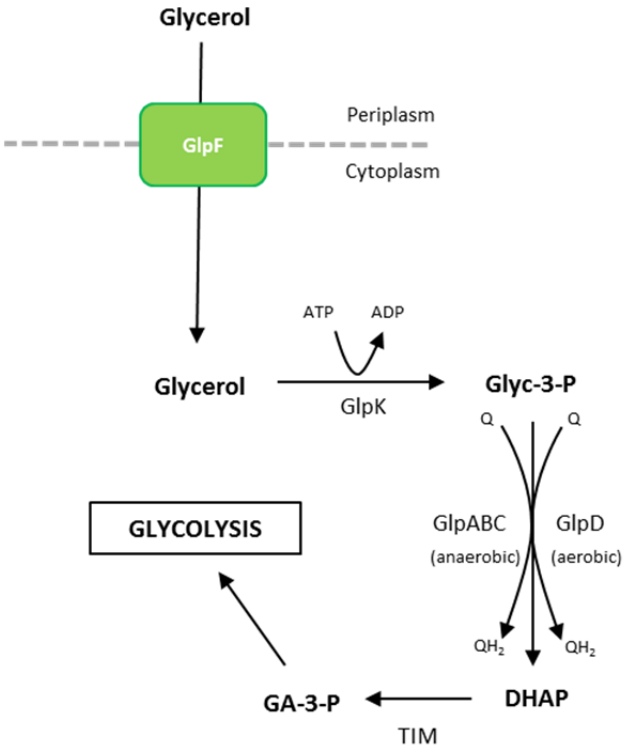

Figure 5.1 Respiratory metabolism of glycerol in *E. coli*. Non-fermentative metabolism of glycerol can occur in both anaerobic and aerobic conditions. Glycerol is first imported into the cell by the transporter GlpF, after which it is converted to glycerol-3-phosphate (Glyc-3-P) by the glycerol kinase, GlpK. The oxidation of Glyc3-P to dihydroxyacetone phosphate (DHAP) is carried out by one of two glycerol dehydrogenases: one encoded by *glpD* and used under aerobic conditions, or the second, encoded by *glpABC,* and used under anaerobic conditions. In either case, the quinone is reduced to quinol with either O_2 or another final electron receptor under aerobic or anaerobic conditions, respectively. The enzyme triose isomerase (TIM) then converts DHAP to glyceraldehyde-3-phosphate (GA-3-P), which enters the final stages of the glycolytic pathway.

It has subsequently been reported that *E. coli* is in fact able to 'ferment' glycerol under certain conditions, specifically with tryptone supplementation, a higher concentration of glycerol, lower potassium and phosphate concentrations, and a lower pH (Dharmadi *et al*., 2006; Gonzalez *et al*., 2008). Under such conditions, glycerol is fermented *via* a central pathway to dihydroxyacetone-P (DHAP), by the action of both a type-II glycerol dehydrogenase, called GldA, and a dihydroxyacetone kinase (DHAK) (Figure 5.2). This DHAP can then be fed into glycolysis where ATP and NADH synthesis occur. Therefore, in certain conditions glycerol can be catabolised *via* substrate level phosphorylation for energy derivation; i.e. fermentation. Aside from this central pathway, auxiliary reactions also produce 1,2-propanediol and ethanol,

and are required to consume NADH to maintain redox balance, or allow for ATP generation (Gonzalez *et al*., 2008). Formate is also generated during mixed acid fermentation by the action of pyruvate formate-lyase (PFL). This can in turn be used as a substrate for H_2 evolution by FHL. It is possible that Hyd-2 may also contribute to H_2 evolution to some extent. The generated formate could also be oxidised by formate dehydrogenase-O to reduce the quinone pool, which could be used to reduce protons by the action of Hyd-2 in turn (Kelly, 2013).

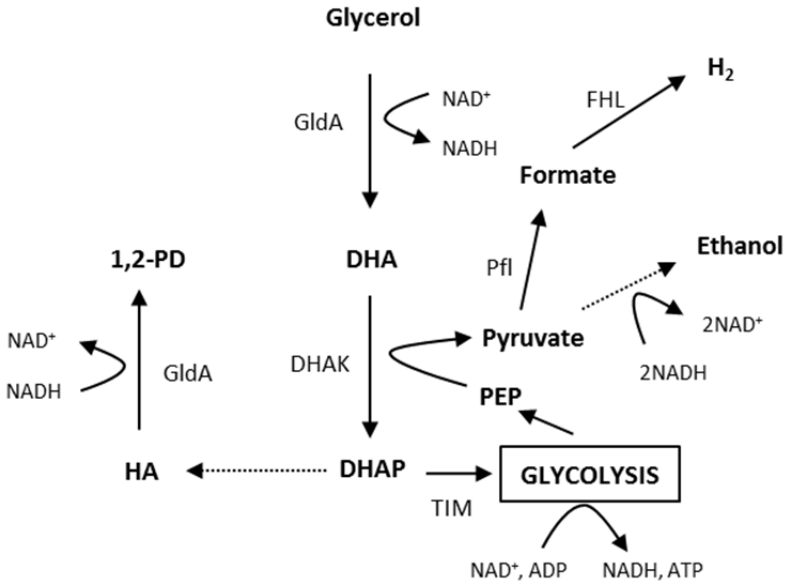

Figure 5.2 Glycerol fermentation can occur in specific conditions in *E. coli*. In the absence of external electron acceptors glycerol can still be metabolised. Glycerol is first converted to dihydroxyacetone (DHA) by the type-II glycerol dehydrogenase, GldA. This is in turn converted to dihydroxyacetone phosphate (DHAP) by the dihydroxyacetone kinase, DHAK. DHAP can then be used as a feedstock for glycolysis (by prior conversion to glyceraldehyde-3-phosphate), resulting in the generation of ATP to power the cell. Reducing equivalents are balanced by production of the standard mixed acid fermentation end products, such as ethanol, but also by production of 1,2 propanediol (1,2-PD). This reaction is also catalysed by GldA and uses hydroxyacetone (HA), a derivative of DHAP, as a substrate. Formate, also derived pyruvate during fermentation, can then be used as a substrate for FHL to generate H_2 Adapted from Gonzalez *et al*. (2008).

It has therefore been seen that *E. coli* can naturally generate H_2 from glycerol by two methods: during late stages of anaerobic respiration (and possibly fermentation) when electron acceptors become scarce, by the action of Hyd-2; and also by the activity of FHL during fermentation.

However, from a biotechnological view, there are caveats with both of these native processes that mean that *E. coli* cannot efficiently utilise glycerol for H_2 production. Specifically, both processes are likely subject to product inhibition. The bidirectional nature of Hyd-2 means that any evolved H_2 could potentially be re-oxidised. Similarly, it has been shown that glycerol fermentation is diminished in the presence of molecular hydrogen (Murarka *et al*., 2008). This is a problematic if the goal is to generate industrial-scale quantities of biohydrogen, as the high partial pressures of H_2 that would accumulate in a large-scale batch culture would presumably impede continued efficient catalysis. A solution to this problem could be to design an irreversible synthetic pathway that would not re-oxidise any of the H_2 yield.

5.1.3 Thiosulfate reductase in *Salmonella enterica*

Thiosulfate reductase (hereafter referred to using its genetic abbreviation Phs: **p**roduction of **h**ydrogen **s**ulfide) is native to *Salmonella enterica* serovar Typhimirium and its biochemical properties were recently explored as a possible route to utilising glycerol as a precursor to H_2 production (Kelly, 2013). The Phs complex is encoded by the *phsABC* operon and consists of the subunits PhsA, PhsB and PhsC (Heinzinger *et al*., 1995). PhsA is a periplasmic-orientated protein containing the bis(molybdopterin guanine dinucleotide) (MGD) cofactor at its active site (Hinsley and Berks, 2002). PhsC is a haem *b*-containing integral membrane protein that also contains the site of menaquinol oxidation (Berks *et al*., 1995). PhsB is situated between PhsC and PhsA and contains four [Fe-S] clusters allowing it to act as an electron relay between the two other subunits. A schematic of the Phs complex is shown in Figure 5.3.

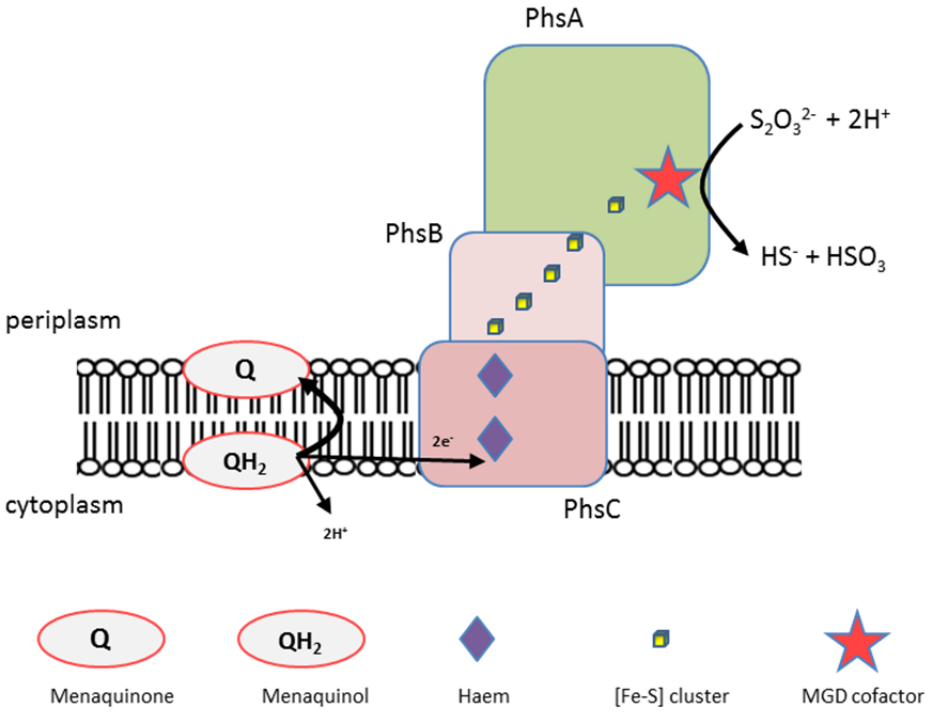

Figure 5.3 The thiosulfate reductase complex from *S. enterica*. A heterotrimeric complex consisting of PhsA, PhsB and PhsC, thiosulfate reductase permits the reduction of thiosulfate ($S_2O_3^{2-}$) to hydrogen sulfite (HS^-) and sulfide (HSO_3) *via* the oxidation of menaquinol. The cell is able to overcome the thermodynamic unfavourability of this reaction (in standard conditions) by the transduction of the pmf.

It has been demonstrated that PhsABC is able to carry out the highly endergonic reduction of thiosulfate by menaquinol with glycerol as the sole carbon source (Stoffels *et al*., 2012). The thiosulfate/HS^- + sulfate standard redox potential is around -400 mV (Thauer *et al*., 1977) with that of NAD^+/NADH being -320 mV and glycerol-3-phosphate/DHAP around -190 mV (Thauer *et al*., 1977). Thus an input of energy is required to use thiosulfate as a terminal electron acceptor and this is achieved by transduction of the proton motive force (pmf) by the PhsC protein (Sasahara *et al*., 1997).

5.1.4 A Hyd-2/thiosulfate reductase chimera exhibits activity *in vitro*

At the outset of this work the Hyd-2 core catalytic subunits (HybOC) had been shown to be reversible *in vitro* (Lukey *et al*., 2010). It was envisaged that the construction of a chimeric Hyd-2::thiosulfate reductase fusion could allow the use of menaquinol, produced by the respiratory metabolism of glycerol, and the coupling of the pmf directly to the reduction of protons to H_2 (standard redox potential of -414 mV) (Kelly, 2013). The hypothesis led to the substitution of the PhsA subunit in thiosulfate reductase with HybO and HybC, the small and large subunits of Hyd-2, respectively.

A translational fusion of HybO to PhsB was engineered, where the HybO signal peptide was retained but the protein was truncated to remove the C-terminal transmembrane helix yet maintain all of its redox centres, including the distal [Fe-S] cluster. Two versions of the *hybO*::*phsB* fusion were cloned, encoding a shorter or longer version of HybO containing less or more of the C-terminal sequence. The gene encoding the fusion protein was then cloned into the *E. coli* expression vector pUNI-PROM, along with *phsC*, to generate pUNI-OSPhs (shorter version of HybO, terminated at Ala-310) and pUNI-OLPhs (longer version of HybO, terminated at Gly330). The resultant vectors would then be introduced into the strain IC011 (MC4100 ∆*hyaB*, ∆*hycE* ∆*hybOA*), which retains an intact *hybC*, to allow for the completed Hyd-2::Phs complex to form. A schematic of the resultant fusion protein is shown in Figure 5.4.

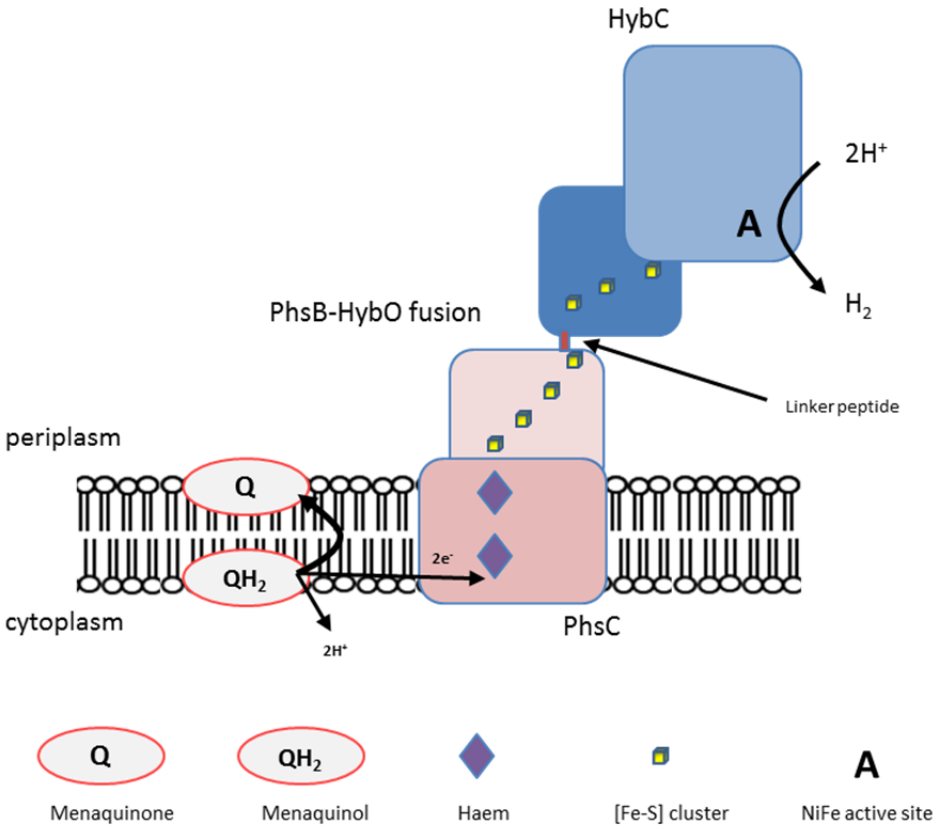

Figure 5.4 A Phs-Hyd-2 chimera to allow for H_2 production from the oxidation of glycerol in *E. coli*. Thiosulfate reductase, native to *S. enterica*, was modified and produced in *E. coli*. The large and small subunits of the complex, PhsA and PhsB respectively, were substituted for a HybO-PhsB fusion, with HybO being the small subunit of *E. coli* Hyd-2. Produced in a strain with *hybC*, the resultant chimeric complex should form in the cell. If functional this would allow for the production of H_2 from the quinone pool, which could be supplied by glycerol metabolism.

Previous characterisation of this chimeric complex has been reported (Kelly, 2013). First, it was shown that (mena)quinone and ATP synthase are essential for formate-dependent thiosulfate reduction, but H_2 metabolism is not (Kelly, 2013). Then, assays with the artificial electron accepter benzyl viologen (BV) confirmed that the HybO and HybC components of both the OSPhs and OLPhs chimeric complexes could still form a functional hydrogenase module that exhibited activity *in vitro* (Kelly, 2013). Whole-cell *in vivo* assays using a Clark-type electrode showed that both constructs were capable of H_2 evolution directly from glycerol (Kelly, 2013). A further modification was then made to the OSPhs construct. Specifically, the linker peptide between PhsB and truncated HybO was altered from the HA-tag linker used originally to a

shorter linker consisting of four glycine and one serine residues. This new vector was named pUNI-OSFlexAPhs (Kelly, 2013). It was hoped that this new arrangement would allow the [Fe-S] clusters in HybO and PhsB to better align such that electron relay between the two subunits improved. This is because the small R-groups of the residues in this linker may allow for better flexibility, as previously reviewed (Chen *et al*., 2013). The linker used in both pUNI-OSPhs and pUNI-OLPhs, and one used in this modified pUNI-OSFlexAPhs are shown in Figure 5.5.

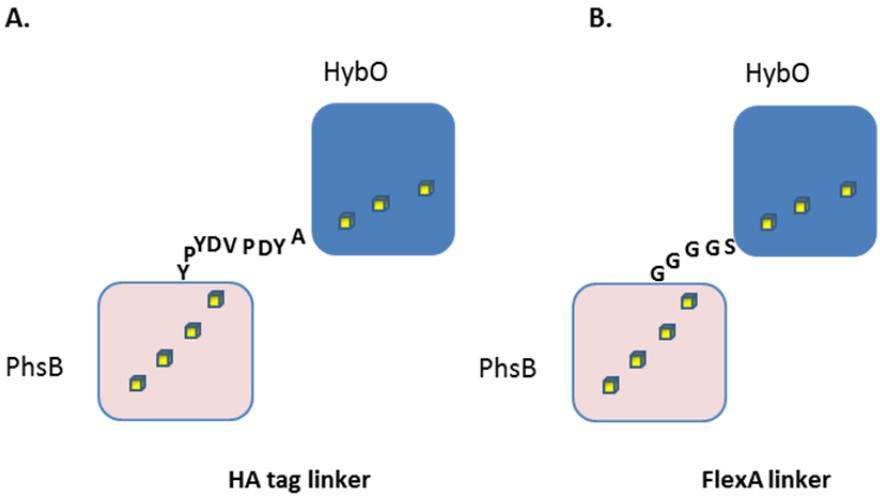

Figure 5.5 The design of various linker peptides between PhsB and HybO. (**A**) The original chimeric complexes, as illustrated in Figure 5.4 and encoded by pUNI-OSPhs and pUNI-OLPhs, had a linker peptide correlating to the *H. influenza* haemagglutinin (HA) tag. *in vitro* studies showed a low level of activity of these complexes, with OSPhs being higher (Kelly, 2013). (**B**) Therefore a new linker was designed in OSPhs, to see if activity could be augmented. This new linker, called FlexA and encoded by pUNI-OSFlexAPhs, was shorter and smaller, consisting of only four glycines and one serine residue.

5.1.5 Proteorhodopsin

An important consideration is that the $2H^+ + 2\ e^- \rightarrow H_2$ half reaction has greater negative standard potential ($E^{0'}$) of -414 mV compared to an $E^{0'}$ of -402 mV for the $S_2O_3^{2-} + e^- \rightarrow HS^- + SO_3^{2-}$ half reaction. Therefore, the putative menaquinol dependent production of H_2 ($E^{0'}$ menaquinone + 2 e^- → menaquinol = -74 mV) by the chimeric complex is even more endergonic than the natural Phs reaction. In an effort to maintain the pmf, which is the key to

driving this reaction 'uphill', proteorhodopsin could be used (Figure 5.6). Native to marine bacterioplankton (Beja *et al*., 2000), proteorhodopsin – henceforth called PR – is a light-driven proton pump, and has previously been shown to be functionally expressed in *E. coli* to augment pmf in a light dependent manner (Tipping *et al*., 2013). Previous work using whole cell assays on a Clark-type electrode has indicated that using the PR system in tandem with the Hyd-2-Phs chimera could help boost H_2 evolution through maintenance, or even boosting, of the pmf (Kelly, 2013).

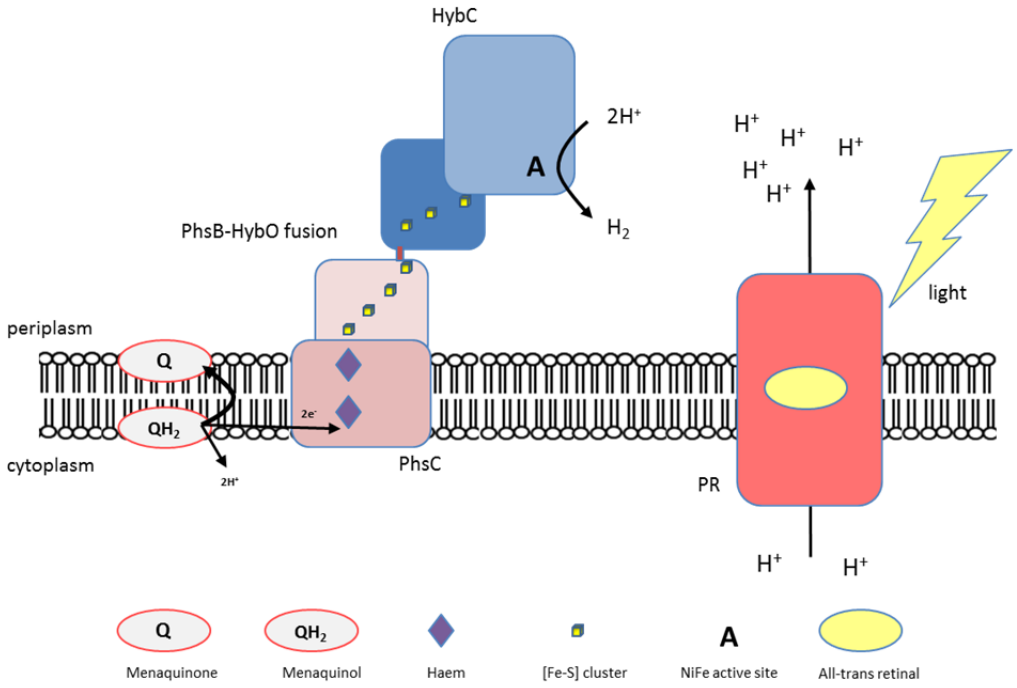

Figure 5.6 The co-production of proteorhodopsin to augment the yield of the Phs-Hyd-2 chimera in *E. coli*. Proteorhodopsin (PR) is a proton pump that exports H^+ to the periplasm in a light-dependent manner. It is known that the natural thiosulfate reductase system in *S. enterica* requires the pmf in order to perform the endergonic reduction of thiosulfate by oxidation of the quinol pool (Stoffels *et al*., 2012). Thus, it is hypothesised that this extra boost to the pmf by PR could help improve activity of the Phs-Hyd-2 fusion and so result in greater H_2 production.

5.2 **Aims**

The aim of this Chapter is to build on previous unpublished work (Kelly, 2013) and to further assess the *in vivo* functionalities of the Hyd-2::PhsBC fusions in terms of H_2 production. Furthermore, it will also be investigated whether co-production of the light-dependent H^+-pump proteorhodopsin can enhance any activity seen. In addition, the first steps of characterising further-modified Hyd-2::Phs fusions will also be begun.

5.3 **Results**

5.3.1 Predictive modelling of chimeric constructs

Previously (Kelly, 2013), three variants of the HybO-PhsB fusion were designed in an attempt to find an optimum arrangement to allow for most efficient electron relay between the [Fe-S] clusters in the two subunits. OSPhs was engineered as it was reasoned that a reduction in the C-terminal region of HybO may allow for better association with PhsB. Similarly the FlexA variant was produced as it was hoped the new linker peptide may allow for better subunit interaction compared to the HA linker sequence.

An *in silico* analysis was performed to ascertain how these modifications may affect [Fe-S] alignment in the fusions. The protein structure modelling software Phyre^2 (Kelley *et al*., 2015) uses both protein homology and *ab initio* methods to estimate the 3D structure of a protein. The translated sequences of the genes encoding OLPhs, OSPhs and OSFlexAPhs were subjected to an 'intensive' Phyre^2 prediction. Whilst Phyre^2 gives a final model output that is produced from an amalgamation of many protein homologues, certain proteins are considered by the software to be particularly close matches for sections of the predicted peptide. The output gives a breakdown of all proteins used in the modelling, with a 'confidence' score rating the probability that this protein and the protein sequence input are homologues, and a '%ID' score to indicate the degree of similarity between the two.

For OLPhs, OSPhs and OSFlexAPhs, the HybO region of the peptide sequence input was most closely matched with the small subunit of the [NiFe]-hydrogenase from *Allochromatium vinosum* (PDB 3MYRe) (Ogata *et al*., 2010), with a confidence score = 100, and a %ID = 49. Similarly, in all three cases the predicted structure of PhsB subunit of the fusion peptide was most closely aligned with NrfC protein subunit from polysulfide reductase (PDB 2VPYb) (Jormakka *et al*., 2008), with a confidence score = 100, and ID = 41%.

Using these highly matched homologues, subunit replacement was performed on the Phyre[2] predicated structures for OLPhs (Figure 5.7A), OSPhs (Figure 5.7B) and OSFlexAPhs (Figure 5.7C) in PyMOL. The in-built measurement tool in PyMOL then used to estimate the distances between the closest [Fe-S] clusters in the PhsB and HybO halves of the fusion protein (image number 6 in each case). From this modelling it can be seen that FlexA is predicted to have the shortest distance between [Fe-S] clusters at 12.8 Å, with the same distance being 19.9 Å in OSPhs and 17.3 Å in OLPhs.

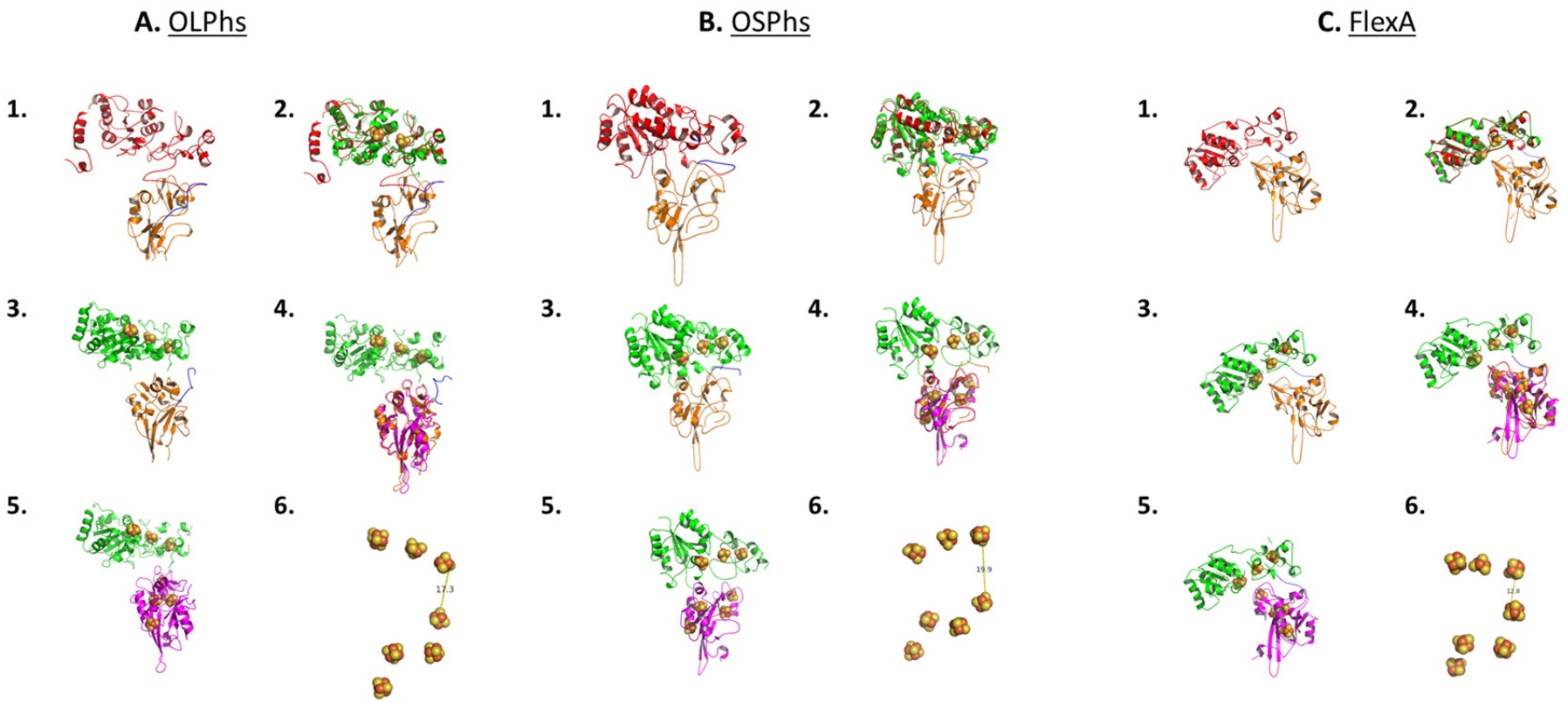

Figure 5.7 Phyre[2] predictive modelling of HybO-PhsB constructs allows for an estimate of [Fe-S] cluster distance. (**1**) Predictive model output given by Phyre[2]. Red region represent HybO, orange region represents PhsB, blue region represents linker peptide. (**2**) Superimposition of 3MYRe (green) complete with [Fe-S] clusters over predicted model. (**3**) Removal of the HybO region of the predictive model. (**4**) Superimposition of 2vpyB (purple) complete with [Fe-S] clusters over predicted model. (**5**) Removal of the PhsB region of the predictive model. (**6**) Arrangement of the [Fe-S] clusters as arranged in (**5**). Estimation of the distance between the two closest [Fe-S] clusters equating to the HybO and PhsB regions, as calculated by PyMOL, is given in Å.

5.3.2 Assessment of the Phs-Hyd-2 chimeras *in vivo* activity by gas chromatography

The strain IC011 (MC4100 Δ*hyaB*, Δ*hycE* Δ*hybOA*) was transformed with one of either pUNI-PROM (control), pUNI-OSPhs, pUNI-OLPhs or pUNI-OSFlexAPhs, along with either pSU-PROM (control) or pSU-PR, and used to inoculate 25 mL LB supplemented with 0.4 % (w/v) fumarate, 0.5 % (v/v) glycerol to induce expression of *hybC* from the chromosome. The media was also supplemented with the PR co-factor all-trans retinal, to a final concentration of 20 µM, following the protocol of (Walter *et al*., 2007). Successful production of the proteorhodopsin holoenzyme was assumed by the pink colour of transformants, as was observed in the original study when PR was produced in *E. coli* (Beja *et al*., 2000) (Figure 5.8). Cultures were then incubated overnight at 37 ^{o}C, without shaking to induce anaerobiosis, and in the dark (to prevent retinal degradation).

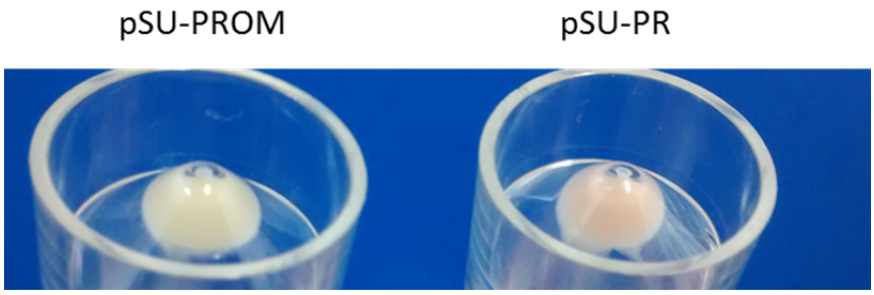

Figure 5.8 Cell colour suggests production of proteorhodopsin. IC011 cell were transformed with pUNI-OSPhs along with either pSU-PROM or pSU-PR. After anaerobic growth of transformants in LB supplemented with 0.4 % (w/v) fumarate, 0.5 % (v/v) glycerol and 20 µM all-trans retinal in the dark for 17 hours, cells were pelleted by centrifugation. After washing with 1 × PBS (that had been prior sparged of O_2), the colour of the respective pellets was then compared.

M9 minimal media supplemented with 0.5% (v/v) glycerol, 20 µM all-trans retinal and appropriate antibiotics was sparged for 1.5 hours with N_2 to remove dissolved O_2. Next, the overnight cultures were centrifuged and the resultant pellet washed twice with anaerobic PBS buffer. The cells were then resuspended in 1.5 mL of the same buffer. Next, 200 µL of this suspension was then used to inoculate 5 mL of sparged M9 media inside a Hungate tube. The

filling of the Hungate tubes with media, their sealing, and the subsequent inoculation, were all carried out in an anaerobic cabinet to ensure no O_2 was present. The tubes were then placed in a transparent waterbath, either covered in tin foil to block light or left uncovered, and the waterbath evenly lit using tungsten light bulbs (Figure 5.9).

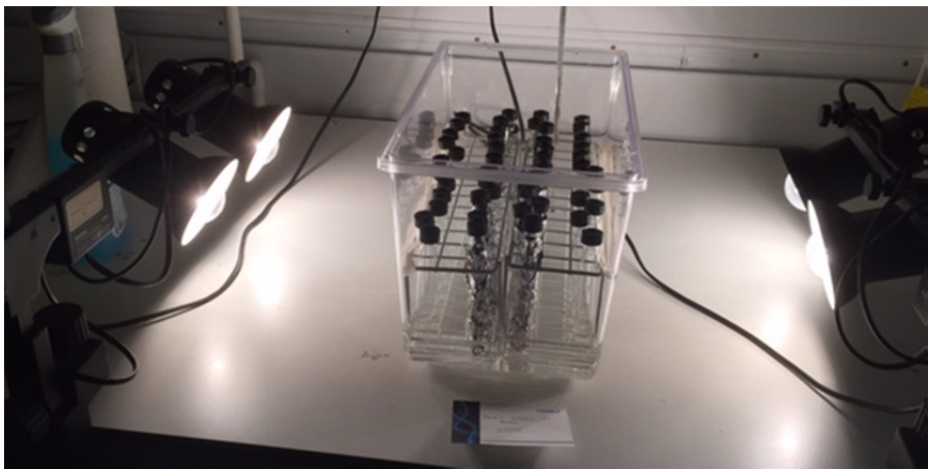

Figure 5.9 Incubation of cultures to investigate light-augmented H_2 production from glycerol. Hungate tubes were placed in a transparent waterbath, submerged in water at 37 ^{o}C to allow for heat dissipation, and evenly lit with light. Cultures exposed to light were placed at the edge of the tank to allow for best light exposure, whilst the 'dark' samples were placed in the middle and completely covered in tin-foil.

The cultures were incubated for 24 hours without shaking at 37 ^{o}C, after which the H_2 content in the headspace was measured in a single-end point assay by gas chromatography. The chromatogram (Shimadzu GC-2014) employed N_2 as the carrier gas with a flowrate of 25 mL min^{-1}, and the total amount of hydrogen in the headspace (10 mL) was calculated based on a standard curve. The resultant data are shown in Figure 5.10.

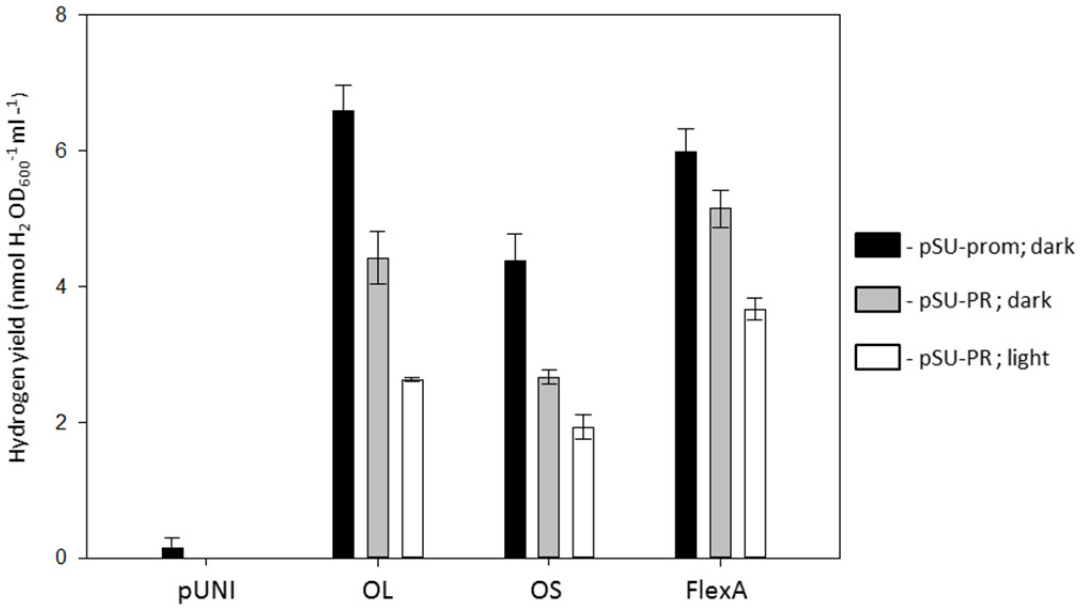

Figure 5.10 All three variants of the Phs-Hyd-2 chimeric metalloenzyme exhibit functionality *in vivo*. *E. coli* strain IC011 was transformed with pSU-PR or pSU-PROM along with pUNI-PROM, pUNI-OSPhs, pUNI-OLPhs or pUNI-OSFlexAPhs. After overnight growth in LB supplemented with 0.5 % glycerol and 0.4 % fumarate, cells were washed with anaerobic PBS buffer, and used to inoculate Hungate tubes filled with anaerobic M9 media with 0.5% glycerol and 20 µM all-trans retinal. Tubes were then either covered in tin-foil or let uncovered, before being illuminated and incubated at 37 ^{o}C for 24 hours. Gas chromatography was then performed on the headspace to examine H_2 content. Vectors used: **OL**: pUNI-OLPhs; **OS**: pUNI-OSPhs; **FlexA**: pUNI-OSFlexAPhs; **pUN**I: pUNI-PROM. Error bars represent standard error (n = 3).

It can be seen (Figure 5.10) that cells possessing any of the three variants of the Phs-Hyd-2 chimeric complex produced H_2, whilst the negative control (pUNI) did not. The modified 'FlexA' linker did not increase H_2 production of the short version of the fusion (OS) (Figure 5.10). The OL-Phs fusion gave the greatest H_2 yield. Secondly, it is apparent that the addition of proteorhodopsin (and illumination with light) did not result in greater H_2 evolution in any case.

The same experiment was previously carried out with the same protocol as above, only with the addition of 0.2% (w/v) casamino acids to the M9 media. The data are presented in Figure 5.11.

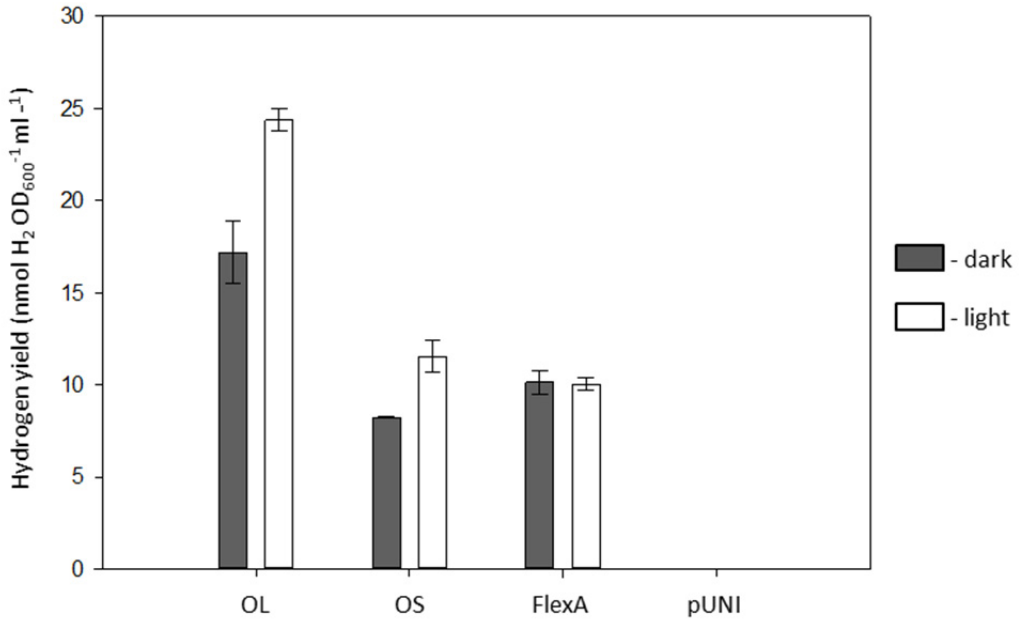

Figure 5.11 Casamino supplementation leads to greater H_2 evolution in all three fusion constructs. *E. coli* strain IC011 was transformed with pSU-PR along with pUNI-PROM, pUNI-OSPhs, pUNI-OLPhs or pUNI-OSFlexAPhs. After overnight growth in LB supplemented with 0.5 % glycerol and 0.4 % fumarate, cells were washed and used to inoculate Hungate tubes filled with anaerobic M9 media with 0.2 % casacids, 0.5% glycerol and 20 µM all-trans retinal. Tubes were then either covered in tin-foil or let uncovered, before being illuminated and incubated at 37 ^{o}C for 24 hours. Gas chromatography was then performed on the headspace to examine H_2 content. Vectors used: **OL**: pSU-PR2, pUNI-OLPhs; **OS**: pSU-PR2, pUNI-OSPhs; **FlexA**: pSU-PR2, pUNI-OSFlexAPhs; **pUN**I: pSU-PR2, pUNI-PROM. Error bars represent standard error (n = 2).

The first observation from these data (Figure 5.11) in comparison to those in Figure 5.10 is that the addition of casamino acids to the media resulted in an increase in H_2 evolution. Second, it is apparent that light exposure gave no significant difference in H_2 evolution in cultures possessing both the proteorhodopsin and any of the Phs-HybO machinery, with p values > 0.05 for (0.08, 0.20 and 0.91 for OLPhs, OSPhs and OSFlexAPhs respectively). This corroborates the conclusion from the data presented in Figure 5.10.

5.3.3 New construct design in an attempt to further improve H_2 yield

After these data were gathered, new vectors were generated by Dr Ciarán Kelly in an attempt to allow for better expression of the Phs-Hyd-2 associated genes. These are based on the pCK302 vector backbone (Plasmid Table 7.6), and allow for L-rhamnose-dependent gene expression (Kelly *et al*., 2016). The same gene construct found in OSPhs (encoding for PhsC and the more truncated version of HybO-PhsB fusion) was moved into pCK302 and associated with different RBS sequences with predicted translation initiation rates (calculated *via* the *RBS Calculator* software) of either 5000 arbitrary units or 20,000 arbitrary units. These new vectors were named pCK250 or pCK251, respectively. The same was also done for the OLPhs constructs, with these new vectors called pCK252 and pCK253, respectively.

5.3.3.1 Transcription and translation from new rhamnose-dependent constructs

To examine the protein production from the new L-rhamnose-regulated constructs, the strain IC011 was transformed with pCK250, pCK251, pCK252, pCK253, or the empty vector pCK302. Successful transformants were then used to inoculate Universal tubes filled with 25 mL LB supplemented with 0.5 % (w/v) glycerol, 0.4 % (w/v) fumarate appropriate antibiotics and 0.4 mg mL^{-1} L-rhamnose. Cultures were incubated without shaking at 37 ^{o}C overnight, before normalisation for OD_{600}, and samples used for SDS-PAGE (12% w/v polyacrylamide gel). The resultant gel obtained is shown in Figure 5.11, where it can be seen that protein bands of corresponding size to both OLPhs and OSPhs are observed, although these were not confirmed by mass spectroscopy. The protein band ostensibly identified as OSPhs seems to be stronger for pCK250 compared to pCK251. This implies that the RBS calculated to have the lower translation initiation rate nonetheless resulted in better protein yield in this instance than the RBS predicted to have a better translation rate.

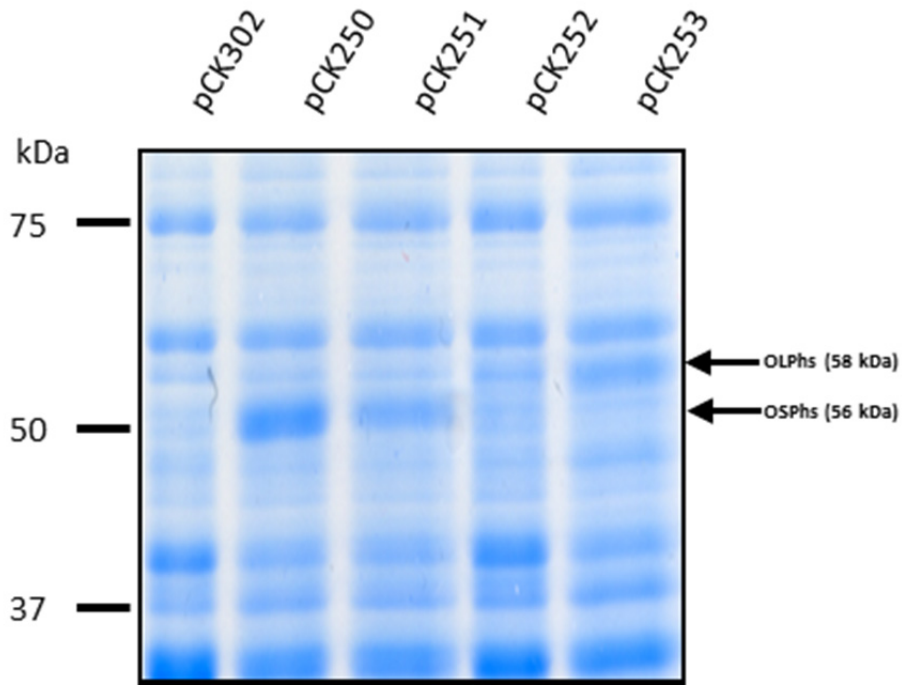

Figure 5.12 L-Rhamnose-regulated constructs allow for production of PhsB-HybO fusion peptides. *E. coli* strain IC011 was transformed with the plasmids pCK250, pCK251, pCK252, pCK253, or the empty vector pCK302. Transformants were grown overnight anaerobically at 37 ^{o}C in LB supplemented with 0.5 % (w/v) glycerol, 0.4 % (w/v) fumarate and 0.4 mg mL^{-1} L-rhamnose. After normalisation for OD_{600} appropriate volumes of whole cell samples were analysed by SDS-PAGE.

After this data was gathered, Western immunoblotting was performed in an effort to establish whether the bands seen were indeed the PhsB-HybO fusion peptides (Figure 5.12). The same whole cell samples as before were treated to both (Figure 5.12A) αHyd-2 polyclonal antibody and (Figure 5.12B) αHA monoclonal antibody. Both antibodies detected the same protein bands, giving confidence that the fusion proteins were correctly synthesised.

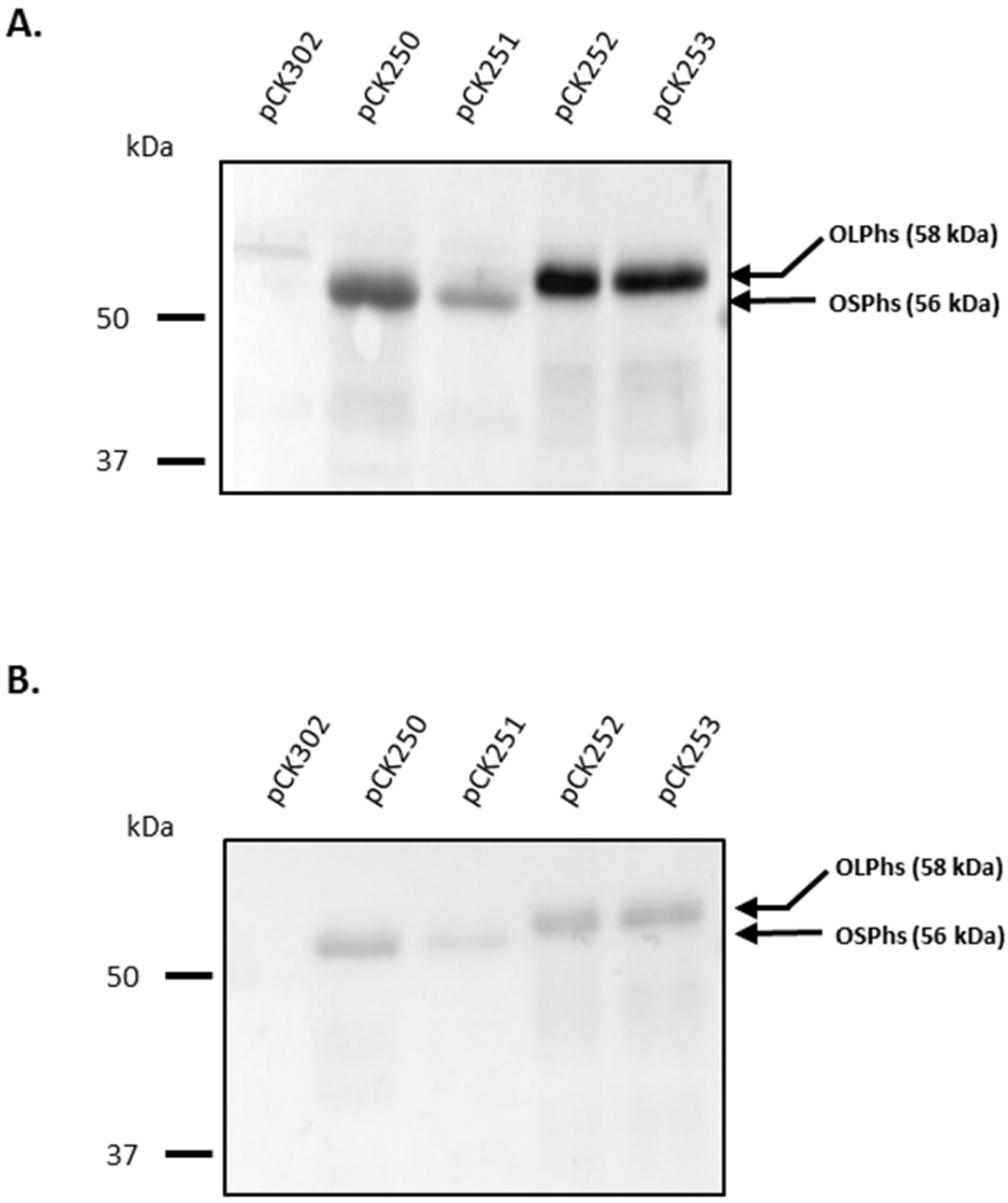

Figure 5.13 Western immunoblots establish production of the PhsB-HybO fusion proteins. *E. coli* strain IC011 was transformed with the plasmids pCK250, pCK251, pCK252, pCK253, or the empty vector pCK302. Transformants were grown overnight anaerobically at 37 ^{o}C in LB supplemented with 0.5 % (w/v) glycerol, 0.4 % (w/v) fumarate and 0.4 mg mL^{-1} L-rhamnose. After normalisation for OD_{600} appropriate volumes of whole cell samples were mixed with equal volume of Laemmli buffer, boiled and run on the gel, after which western immunoblotting was performed with either (**A**) αHyd-2 or (**B**) αHA-tag antibodies.

5.4 **Discussion**

5.4.1 Further characterisation of a novel metalloenzyme in *E. coli*

The work presented in this Chapter built upon the previous characterisation work showing the thiosulfate reductase/Hyd-2 chimeric protein complexes exhibit H_2 production using the quionol pool in the *E. coli* (Kelly, 2013). Ultimately it has been shown that *E. coli* has been engineered to utilise glycerol as a substrate for hydrogen evolution *via* a novel pathway. As such, it has built upon work previously published (Kelly, 2013).

Interestingly the *in vivo* activity presented here, where it seemed that the longer version of the PhsB-HybO fusion (OLPhs) exhibited the greatest activity, which is in contrast to the previously reported *in vitro* and *in vivo* data where OSPhs was found to evolve more H_2 (Kelly, 2013). *In vivo* data can be seen as the more powerful evidence of how the system functions because it assesses enzyme activity *in situ*, as opposed to in artificial conditions. Furthermore, in actuality it is specifically only the hydrogenase component of the enzyme complex that is assessed by *in vitro* hydrogenase assays (i.e. the HybC-mediated conversion of H_2 to protons). Not only is this reaction the reverse of the physiologically relevant direction of H_2 evolution, but it does not directly assess whether the PhsCB components are functional themselves nor in terms of linking their activity to the Hyd-2 components of the chimera.

The yield of H_2 observed here is very low, with a maximum of ~ 7 nmol OD_{600}^{-1} mL^{-1} observed when glycerol was the sole carbon source (Figure 5.10). One hypothesis to explain this is that there may be an eventual lack of ATP in the cell. The first step for respiratory glycerol metabolism is to phosphorylate glycerol to glycerol-3-phosphate by the ATP-dependent glycerol kinase (GlpK) (Figure 5.1). Therefore, if ATP is limited in the cell, this process will be halted and there will be an eventual cessation of quinone pool reduction, with a corollary of H_2 evolution by the chimeric protein complex also halting. This ATP deprivation might also explain why the cells could not grow in the media described in this Chapter.

5.4.2 Insights into HybO-PhsB fusion peptides *via* predictive modelling

Any observed H_2-production differences between the different fusion lengths may be explained by a difference in [Fe-S] cluster alignment between the PhsB and HybO halves of the fusion protein. It known that altering the distance between [Fe-S] clusters can have dramatic effects of electron transfer efficiency (Moser *et al.*, 1992). Different lengths of peptide linker will allow for different conformations between the PhsB and HybO components of the fusion and so different [Fe-S] associations. As the data in Figure 5.11 seem to show that the OLPhs gave rise to most H_2 evolution, so it is possible that this arrangement allowed for closer localisation of [Fe-S] clusters, and so more efficient electron relay. An additional explanation for the higher OLPhs construct activity is that the longer region of the remaining C-terminal transmembrane helix of HybO may mean that the distal [Fe-S] cluster present in this subunit is retained. This would again mean that electron transfer in this case is more efficient compared to OSPhs/OSFlexAPhs. The predicative modelling presented in Figure 5.7 was therefore carried out to see if these hypotheses were possibly true.

When building the predictive models of the HybO-PhsB fusion peptides using Phyre, it was thought crucial to use the 'intensive' option in the software. The ability to utilise *ab initio* modelling deemed essential for attempting to accurately model the linker peptide regions; particularly salient given that the purpose of this exercise was to determine [Fe-S] cluster distance about this region. It was seen in Figure 5.7 that the OSFlexAPhs construct— the truncated version of the HybO C-terminal tail and a shorter linker peptide (four glycines and a serine) than the HA-tag linker in OLPhs and OSPhs— gave the shortest distance between HybO and PhsB [Fe-S] clusters. At only 12.8 Å, this distance is under the threshold of 14 Å that has been proposed necessary for efficient electron relay (Page *et al.*, 1999), whilst OLPhs and OSPhs had distances greater than this, at 17.3 Å and 19.9 Å respectively (Figure 5.7).

It may therefore have been predicted that the OSPhsFlexA construct would exhibit most efficient H_2 evolution; however this was not seen in the data presented in Figures 5.11 or 5.10.

There are a number of possible explanations for this, due to caveats associated with the predictive modelling procedure used here. The first is that the Phyre[2] structure is an amalgamation of many protein homologues. However, in calculating the [Fe-S] cluster distances, only the two homologues with greatest similarity to the HybO and PhsB subunit regions were employed. As such, the [Fe-S] cluster position in each region is unlikely to be completely accurate. Another factor to consider is that it is computationally difficult to predicted unstructured regions of peptides, such as the linker peptides here. Whilst *ab initio* modelling can aid to an extent, there will always uncertainty associated with the final model in such sequences.

Furthermore, the Phyre[2] output structure is a static image; however in reality such unstructured regions may be flexible to an extent. As such it may be that the distances measured in Figure 5.7 are only accurate transiently in the protein, and that they may be shorter or longer in reality. Indeed the OSFlexAPhs was designed for its hypothesised flexibility: the small side chains of glycines (an H atom) could allow for unencumbered contortion of the linker chain. As such, the calculated distances between the [Fe-S] in HybO and PhsB may therefore be regarded only as estimates. An interesting dilemma arises when discussing linker peptides: is a short peptide better in allowing for closer association, or is a longer flexible peptide better at allowing the two subunits more freedom to arrange? Ultimately, it seems that the only way to determine this is to test the structures experimentally.

5.4.3 GC data suggests PR does not aid chimera functionality

It was speculated at the beginning of this work that the endergonic nature of the oxidation of menaquinol to the reduction of protons to H_2 would necessitate the use of the pmf to drive the reaction. It was therefore hypothesised that the heterologous co-expression of the genes

encoding the proteorhodopsin light-dependent proton pump in addition to the Phs:Hyd-2 chimera may therefore induce a boost in H_2 evolution. However the GC data presented in both Figures 5.10 and 5.11 led to the conclusion that this was not the case. This finding is at odds with experiments previously performed on these constructs. Specifically, *in vivo* work using a Clark-type electrode on IC011 cells possessing pUNI-OSPhs and pSU-PR showed that illumination lead to augmented H_2 yield (Kelly, 2013). It is therefore inconclusive whether the PR really does assist the activity of the chimeric enzyme complexes.

The first step to addressing this question in future work would be to confirm that the heterologously produced proteorhodopsin is itself truly functional. Whilst it appears that the holoenzyme is properly formed, due to the pink colour of the recombinant colonies (Figure 5.8); it has not been shown whether or not it is actually able to contribute to the pmf in our hands. Whilst more problematic than eukaryotic cells due the small size and double membrane, numerous techniques have been employed to probe the pmf in bacteria (Kashket, 1985). One example is to first treat the cell with valinomycin to permeabilise the cell membranes to K^+ ions (or its analogue $^{86}Rb^+$) which will then be distributed according to the pmf value (Kashket, 1985; Schummer and Schiefer, 1983). A more recent method to measure pmf changes in *E. coli* has been devised that coincidentally employs a proteorhodopsin itself (Zajdel *et al*., 2014). The heterologous expression of genes encoding a 'proteorhodopsin optical proton sensor' (PROPS) has been shown to be able to detect transient fluctuations in the *E. coli* pmf.

Of course it must be re-iterated that it has been demonstrated by others that it is possible for proteorhodopsin to be successfully produced by recombinant *E. coli* (Tipping *et al*., 2013; Walter *et al*., 2007). As such, an alternative, and perhaps more likely, explanation for the data observed in this Chapter is the PR holoenzyme is produced and able to properly function in *E. coli*, but the conditions used in the assays here were not conducive to optimal PR stimulation. For one, tungsten light bulbs are notoriously inefficient light sources, with a lot of energy being

converted to heat as opposed to light, and so it was possible that this would raise the culture temperature above the optimal 37 ^{o}C for *E. coli* growth. Whilst steps were taken to mitigate this; Hungate tubes were submerged in water during incubation in an attempt to dissipate this heat, perhaps this adversely affected the cells. Future experiments could instead use green LED lights which do not emit so much heat. An additional benefit of LED use would be that the wavelengths emitted could be tailored to that for maximum PR excitation, which is ~ 525 nm (Beja *et al*., 2000). Indeed, a laser with λ = 532 nm has previously been used to successfully stimulate heterologously produced PR in *E. coli* (Tipping *et al*., 2013). It may also be the case that even 37 ^{o}C is too high for optimal activity of the PR. Previously, *E. coli* cultures possessing PR were incubated at only 30 ^{o}C (Tipping, *et al*., 2013), and so future work could involve trying this lower temperature in an attempt to improve PR activity. Light attenuation through the culture/media/waterbath may also be a factor impeding PR activity. Ideally a thin flask with a large surface area would be employed to maximise cell light exposure.

5.4.4 Possible strategies to further improve enzyme activity

Another possible strategy that could potentially boost activity would be to co-localise the Phs-Hyd-2 fusion and PR together in the membrane, as was first proposed by Kelly (2013). The traditionally held view in molecular biology was that the plasma membrane merely functioned as a solvent for membrane-bound proteins, which were free to move about *via* diffusion and come into contact with each other by chance; the so-called 'fluid-mosaic model' (Singer and Nicolson, 1972). More recently however, lateral compartmentalisation of membrane components into structures called membrane microdomains (MMDs) have been discovered both in eukaryotes (reviewed in Malinsky *et al.*, 2013) and— more relevantly for the purposes of this Thesis— proposed to exist in bacteria (Bramkamp and Lopez, 2015). Disruption of membrane composition by mutation of polyisoprenoid lipid synthesis genes leads to abolishment of the sensor kinase KinC activity despite KinC still being found at the plasma

membrane, indicating that KinC activity is at least partly reliant upon a specific membrane composition; something characteristic of microdomains in other systems (Lopez and Kolter, 2010). However, it is known known how many types of MMD are present in bacteria, nor how their composition is regulated or how they are formed. Nevertheless, perhaps MMDs could be employed in this work to co-localise PR in the vicinity of the Phs-Hyd-2 fusion protein to ensure maximum H^+ concentration could be maintained about the chimeric enzyme.

The membrane bound hydrogenase (MBH) of *C. necator* is known to be functionally linked to cytochrome *b*, which is necessary for the transfer of electrons released from the oxidation of H_2 to the reduction of ubiquinone to ubiquinol during aerobic lithoautotrophic growth (Bernhard *et al*., 1997). Thus, this enzyme could perhaps be utilised instead during fermentative growth in *E. coli* to operate in reverse to utilise the (mena) quionol pool to generate H_2.

Hyd-1 is physiologically active as a dimer of dimers (Volbeda *et al*., 2012), and similar configuration is seen in the three uptake hydrogenases of *S. enterica*: Hyd-1, Hyd-2 and Hyd-5 (Bowman *et al*., 2014). Similarly, the proteins of greatest homology to the HybO-PhsB fusions as predicted by the Phyre^2 software, 3MYR (chain E) and 2VPY (chain B), are known to be from complexes that exist as functional dimers (Jormakka *et al*., 2008; Ogata *et al*., 2010). The structure of Hyd-2 itself has not yet been resolved, however the Hyd-2-type hydrogenase from *Citrobacter* sp. S-77 has recently been crystallised, so structural resolution may be possible in the near future (Muhd Noor *et al*., 2016). If Hyd-2 is indeed functional as a dimer of dimers, it may therefore be the case that the chimeric association is interfering with proper oligomerisation. Future work ought to examine whether the chimeric enzyme complex still allows for functional association of all the subunits, and if not then modifications to the constructs could be engineered to permit this, which may confer a pronounced increase in activity.

Analysis of the stoichiometry of the chimeric complex might also provide insight into ways to augment the activity of the system. Whilst the *hybO-HA-phsB* and *phsC* genes are located on the medium copy-number vector, under the control of the moderate constitutive *tat* promoter, *hybC* is located on the chromosome and under the control of the natural *hyb* operon promoter. As such, it is likely that HybC may be at a lower level than the rest of the requisite apparatus. Boosting expression of *hybC*, perhaps by placing it on the same vector as the rest of the genes, may remove this possible limiting factor and result in more efficient H_2 production. It is hypothesised that the ratio of HybO::PhsB to PhsC to HybC is 1:1:1. This is because the predicted homologues as matched by Phyre[2] for the HybO::PhsB fusion both exist as dimers (Jormakka *et al*., 2008; Ogata *et al*., 2010).

Future work will also of course entail the characterisation of the new suite of vector constructs described in Section 5.3.3. Both *in vitro* and *in vivo* assays will be required to examine whether the modifications in these new constructs will allow for more efficient H_2 evolution.

5.4.5 Further work to confirm the route to quinol pool reduction

In order to confirm that the glycerol is indeed the ultimate source of the menaquinol, other carbon sources need to be tried. Formate is one particularly salient sole carbon source to try with these constructs. This is because it may be that glycerol fermentation is actually occurring at some level. If this was the case, then glycerol could be converted to pyruvate, and then on to formate as a fermentation end product. If appropriate electron acceptors are available, formate dehydrogenase-O or N could then oxidise this formate and reduce the quinone pool in the process. Resultantly, the Hyd-2:Phs chimera could be obtaining its quinol substrates *via* this route, as opposed to *via* glycerol respiration. However, if formate was tested as the sole carbon source, and no H_2 was produced, then this glycerol fermentation pathway could be ruled out.

5.4.6 Glycerol fermentation in *E. coli*

At the beginning of this Chapter it was mentioned that it was long thought *E. coli* was incapable of fermenting glycerol, but that recently this was determined to not be wholly the case (Dharmadi *et al*., 2006; Gonzalez *et al*., 2008). Nevertheless, *E. coli* is not naturally capable of anaerobic growth when glycerol is the sole carbon source, and the work presented in this chapter was towards trying to generate a strain to be able to do so. Ultimately this was unsuccessful; preliminary attempts at the *in vivo* growth assays involved inoculating the M9 minimal media supplemented with solely glycerol, and leaving the cultures to grow. However after 72 hours no increase in OD_{600} was seen, and so the protocol was modified to add a bulk of cells to the media and measure merely glycerol-dependent H_2 production, and not biomass increase.

This lack of growth is interesting when it is considered that casacids were also added to the medium as previously it has been described that amino acid supplementation (albeit tryptone) permitted fermentative growth on glycerol (Dharmadi *et al*., 2006; Gonzalez *et al*., 2008; Murarka *et al*., 2008). This is a strange conclusion to draw, as the addition of amino acids means that glycerol would now not be the sole carbon source. The cell is able to utilise amino acids for energy, either *via* gluconeogenesis or immediately in to either branch of the anaerobic TCA cycle. The addition of casacids did seem to result in greater H_2 evolution than glycerol alone (comparing the data in Figure 5.10 and 5.11). This suggests that some of these amino acids (or some other component of the casacids supplement) is allowing for the quinol pool to be enriched, or potentially even helping boost the pmf.

In addition to the addition of tryptone, a number of other steps are also required for true glycerol fermentation (Dharmadi *et al*., 2006). The first was to increase the concentration of glycerol in the minimal media from the standard 0.5 % (v/v) (as used in this Chapter) to 1 %.

Secondly, it was necessary to lower potassium and phosphate levels, as these ions inhibited enzymes involved in the glycerol fermentation pathway such as GldA (Truniger and Boos, 1994). Furthermore, the presence of a functional FHL (not present in strain IC011) – likely to allow for the requisite high intracellular [CO_2] – was required (Dharmadi *et al*., 2006). These steps could then be taken for future work on the Phs-Hyd-2 fusion here to examine whether activity is improved.

As was mentioned in the introduction to this Chapter (Section 5.1.2), Hyd-2 contributes towards H_2 production in natural glycerol metabolism in *E. coli.* When this is taken in conjunction with the above point of FHL being required for glycerol fermentation, it is clear that the native hydrogenases of *E. coli* play a crucial role in allowing the cell to utilise this carbon source. However, in this work the strain IC011 was used, which is abolished of native hydrogenase activity. This was done to ensure any H_2 evolved by the cells must be derived from the Phs-Hyd-2 chimera; however it is likely that these mutations severely compromise any hoped-for ability to grow on glycerol solely. Now that the data presented in this chapter indicates that the chimera is operating, the system could be inserted back into a strain with intact Hyd-2 and FHL, to see if the cell is better able to survive on solely glycerol, and can produce more H_2. If this is done, it may be beneficial to also include *hybC* onto the vector construct, so that there is not competition for HybC between the native Hyd-2 and the Phs-Hyd-2 fusion.

6. Future perspectives

6.1 **Introduction**

Hydrogenases represent a lineage of proteins that has its origins at the dawn of life and, despite their complexity, they carry out one of the simplest and most fundamental reactions in the reversible conversion of molecular hydrogen to protons and electrons. Natural selection has moulded them over billions of years to efficiently carry out catalysis at the rates needed for the survival of their host cells. However, these rates are not sufficient for their direct utilisation in industrial-scale biohydrogen production by modern civilisation. Clearly, metabolic engineering is imperative in order to improve microbial H_2 yields if biohydrogen is to become an industrially viable energy source.

Myriad attempts at utilising synthetic biology to augment hydrogenase activity have been reported in the literature. The bulk of this concluding Chapter will describe some examples, and also attempt to categorise them into broad themes. These will be: the alteration of native *E. coli* metabolism; heterologous expression of foreign genes in a host cell; engineering of fusion peptides to construct artificial chimeric enzymes; and finally, compartmentalisation of metabolic pathways. This latter category will also describe preliminary work performed during the course of this project, and outline ways in which such work can be continued. This Chapter will also focus on how protein engineering has traditionally been carried out, particularly in hydrogenases, before describing how the development of a hydrogen screen could revolutionise the field. During the discussion of these topics it will therefore become evident how the work presented in this Thesis fits into the broader field of hydrogenase research.

6.2 **The alteration native *E. coli* metabolism**

One route to augmenting *E. coli* H_2 production is to modify the native hydrogenases themselves. One such example has been described where a modification to the large subunit of Hyd-1 (HyaB) in *E. coli*, specifically by an E73Q substitution, was shown to exhibit *in vitro* catalytic H_2 production at approximately twice the rate of the native enzyme (Flanagan *et al*., 2016). Interestingly, whilst the native Hyd-1 has a bias to H_2 oxidation, the modified version had an activity shifted away from this direction. Crucially, whilst the position of this residue is close to the proximal [Fe-S] cluster which is required to confer O_2 tolerance, the ability of the enzyme to tolerate aerobiosis was unaffected.

Another example of the native *E. coli* hydrogenases being engineered for improved H_2 production was performed on Hyd-3, which is the enzyme responsible for the vast majority of *E. coli* H_2 evolution *via* its involvement in the FHL complex. Here, random mutagenesis was performed by error-prone PCR (epPCR) on the Hyd-3 large subunit, HycE, to generate a suite of variants that exhibited increased activity, approximately eight times higher than the native enzyme (Maeda *et al*., 2008a). Gene shuffling was then undertaken to combine these mutants to further increase H_2 evolution to 23 times higher than the wild-type strain. Surprisingly, a truncation at residue 366 of HycE, to remove the C-terminal 204 amino acids including (predicted) active site residues, was found to increase H_2 evolution to 30 times the wild-type value. Another salient aspect of Maeda *et al*., 2008a was the development of a screening assay to analyse the mutants of the epPCR for augmented activity. This was based on a chemochromic membrane containing tungsten oxide that gave a blue colour in the presence of H_2 produced by the bacterial colonies.

Maeda and co-workers (2008b) performed targeted mutagenesis to alter the natural metabolism of *E. coli* to improve H_2 yields. This was done through modulating the expression of a number of genes in three broad categories. First was the abolition of the activity of the two uptake hydrogenases Hyd-1 and Hyd-2, *via* deletions of *hyaB* and *hybC*, respectively.

Second, formate levels were increased in the cell cytoplasm to allow for early induction of, and more substrate for, FHL. This was achieved through a combination of deleting the genes encoding the formate transporters FocA and FocB (Maeda *et al*., 2008b) and those encoding the non FHL-associated respiratory formate dehydrogenases, *fdnG* and *fdoG.* Third, the expression of genes encoding the transcriptional regulators FhlA and HycA was altered. FhlA is a transcriptional activator of the *hyc* and *hyp* operons encoding for FHL, and so *fhlA* was overexpressed in the cell. Conversely, *hycA* was deleted, as HycA acts to inhibit the function of FhlA.

Ultimately a Δ*hyaB* Δ*hybC* Δ*hycA* Δ*fdoG* strain overexpressing *fhlA* was found to produce 141 times more H_2 per mole formate than the wild-type strain. This strain also gave rise to a 50 % increase in H_2 yield, equating to 0.7 mol H_2 per mole of glucose. However, despite all these modifications, it is still apparent that the H_2 yield is still far below the theoretical limit of 2 mol H_2 per mol glucose (Hallenbeck and Ghosh, 2012). It shows that relying solely on the modification of native *E. coli* metabolism will not be sufficient for industrial-scale bioH_2 production.

6.3 Heterologous expression of foreign genes in a host cell

An alternative strategy to augment H_2 evolution in *E. coli* is the heterologous production of hydrogenases from other species to complement those native to the host cell. Chapter 2 of this Thesis described the heterologous production of the SH from *C. necator* in *E. coli* in an effort to use a new substrate – the abundant NADH cofactor in a fermentative cell – for H_2 evolution.

The strategy of heterologous expression to augment *E. coli* H_2 production is well-established. Previous examples of the biosynthesis of functional non-native hydrogenases include the [FeFe]-hydrogenases HydA1 from *Chlamydomonas reinhardtii* and HydA (CpI) from *Clostridium pasteurianum* (Kuchenreuther *et al*., 2010). This is beneficial as, in general, [FeFe]-hydrogenases are more biased towards H_2 evolution that their [NiFe] counterparts (Fontecilla-Camps *et al*., 2007).

A number of [NiFe]-hydrogenases have also been heterologously produced in *E. coli*. For example, the NADP-dependent SH1 [NiFe]-hydrogenase native to *Pyrococcus furiosus* has been shown to be functional when heterologously produced by recombinant *E. coli* (Sun *et al*., 2010). What is more, the native *E. coli* Hyp machinery was able to complement the absence of their *P. furiosus* homologues to produce functional SH1. This result echoes the findings of the heterologous SH expression reported in Chapter 2 of this Thesis where the *E. coli* maturases could assemble the *C. necator* hydrogenase, and vice versa.

The oxygen-tolerant hydrogenases from the marine bacteria *Alteromonas macleodii* and *Thiocapsa roseopersicina*, produced by aerobically-grown recombinant *E. coli,* have been shown to exhibit activity *in vitro* (Weyman *et al*., 2011). Likewise, expression of the genes encoding the small and large subunits of the oxygen tolerant, Group 1 membrane-bound hydrogenase from *Hydrogenovibrio marinus* has been reported to allow recombinant *E. coli* to perform H_2 evolution in 10% O_2 (Kim *et al*., 2011). However possible caveats with this include

the unsuitability of the *E. coli* strain used. This strain, BL21 DE3, is known to have aberrant metalloprotein biosynthesis (Pinske *et al*., 2011). Also, that the mechanism by which this heterologous hydrogenase obtains electrons for H_2 evolution is not clear.

Recombinant *E. coli* expressing genes encoding the NADH-dependent [NiFe]-hydrogenase from the cyanobacterium *Synechocystis* sp. PCC 6803 have shown augmented rates of H_2 evolution (Maeda *et al*., 2007; Zheng *et al*., 2012). This occurred through a combination of factors: by first suppressing the transcription of genes encoding the native uptake hydrogenases Hyd-1 and Hyd-2; production of H_2 by the heterologous hydrogenase itself; and an increase in formate (re)assimilation to boost FHL activity. Similarly, in *Enterobacter aerogenes*, another species that can be used in dark fermentation for bioH_2 production, the heterologous expression of these same genes resulted in a 152% increase in H_2 production compared to the wild-type strain (Song *et al*., 2016).

6.4 **Engineering of fusion peptides to construct artificial chimeric enzymes**

As the field of synthetic biology grows, so the scope for re-modelling a host cell's metabolism increases further. Instead of merely altering the native machinery through overexpression and/or deletion of genes, or by heterologous expression of foreign enzymes, the generation of chimeric, or even entirely artificial, enzymes becomes a greater possibility. Chapters 4 and 5 of this Thesis described the characterisation of fusion proteins that combined elements of native *E. coli* hydrogenase machinery with apparatus from other species and exhibited new modes of H_2 evolution.

The [FeFe]-hydrogenase native to *Caldanaerobacter subterranus* has been shown to allow for H_2 production from the NADH pool in a fermentative *E. coli* cell when co-produced with the PFOR and ferredoxin from *T. maritima* (Kelly *et al*., 2015). This work can be seen as an advance from the examples of simple heterologous expression previously discussed, as in this case machinery from multiple species was successfully combined to produce a functional synthetic enzyme, integrated in *E. coli* metabolism. It echoes work that described the construction of a synthetic pathway in *E. coli* to generate bioH_2 (Agapakis *et al*., 2010). In this study, codon optimised genes encoding the [FeFe]-hydrogenase and ferredoxin from *Clostridium acetobutylicum*, the [FeFe]-hydrogenase associated maturases from *Chlamydomonas reinhardtii* and the PFOR from *Desulfovibrio africanus* allowed for construction of an artificial pathway using pyruvate as a substrate for H_2, similar to that discussed in Chapter 4 of this Thesis (Agapakis *et al*., 2010).

6.5 **Compartmentalisation of metabolic pathways**

Compartmentalisation, i.e. the co-localisation of functionally-associated cellular machinery with required metabolites, is a common feature found in nature that helps increase the rate and efficiency of biochemical processes and in some cases protects the wider cell from toxic reaction intermediates. It was long accepted that, whilst numerous membrane-bound organelles exist in eukaryotic cells for this purpose, prokaryotes did not possess such structures in the cytosol for compartmentalisation; although Gram-negative bacteria do house myriad specialised biochemical processes in the periplasm. However, it has recently been discovered that proteinaceous structures analogous to organelles do occur in some prokaryotic species. These are known as bacterial microcompartments, or BMCs (Yeates *et al*., 2008).

BMCs consist of 'shell protein' subunits arranged as circular multimers, which are in turn arranged into a 3-dimensional polyhedral structure (Crowley *et al*., 2010; Kerfeld *et al*., 2005). Hexameric multimers form the faces of the polyhedron, whereas hexameric forms are present at the vertices (Kerfeld *et al*., 2005; Wheatley *et al*., 2013). Pores exist in some of the shell protein hexamers to permit the movement of small metabolites between the lumen of the BMC and the cytosol, with a diameter of approx. 70 Å (Sagermann *et al*., 2009; Yeates *et al*., 2011).

Salmonella enterica possesses a BMC used to house the suite of enzymes responsible for the catabolism of 1,2-propanediol (1,2-PD) (Bobik *et al*., 1999). The so called 'Propanediol utilisation (Pdu) BMC' is approximately 100 nm in diameter, and whilst it still has a polyhedral shape it is more irregular than other BMCs such as the carboxysome (Bobik *et al*., 1999; Havemann *et al*., 2002) (Figure 6.1A). The *pdu* operon is comprised of 23 genes (Bobik *et al*., 1999), encoding eight shell proteins subunits, in addition to the enzymes for 1,2-PD metabolism (Figure 6.1B). Of the eight shell proteins, seven (PduABB'JKUT) associate to form hexameric tiles that form the faces of the BMC. The vertices of the shell are formed by homo

pentamers of PduN (Havemann and Bobik, 2003; Lawrence *et al*., 2014). There is evidence that PduJ, which comprises approximately 20% of the BMC, forms the edges of the BMC hexameric faces (Cheng *et al*., 2011). PduB and PduB' are both encoded by *pduB*, which consists of two overlapping genes in-frame, resulting in identical protein sequences with the exception of PduB being 27 residues longer than PduB' due different transcriptional start sites (Parsons *et al*., 2008). It has been shown that at least two of the associated enzymes, PduP aldehyde dehydrogenase and the PduCDE diol dehydratase, are targeted to the inside of the BMC by way of short N-terminal sequences on the PduP and PduD subunits, respectively, which bind to short C-terminal helices of the shell proteins (Fan and Bobik, 2011; Fan *et al*., 2010).

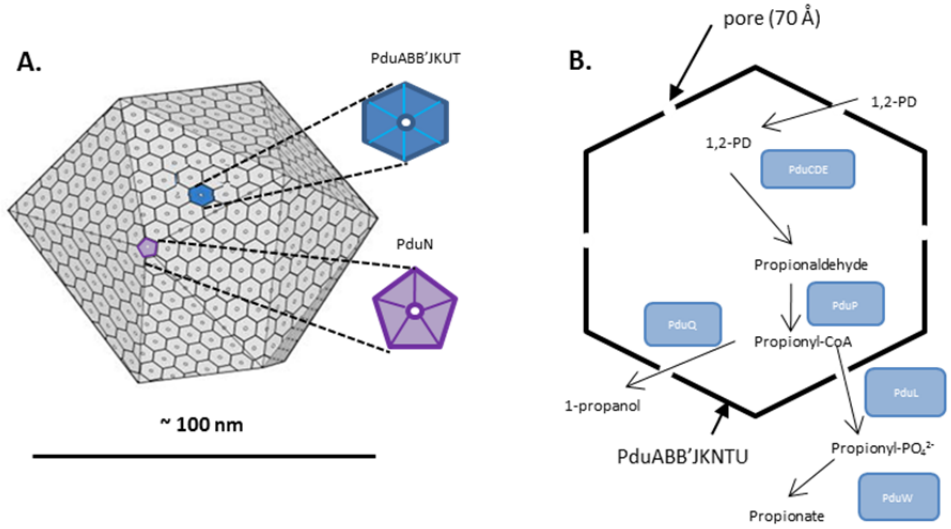

Figure 6.1 The Pdu BMC from *S. enterica*. (**A**) The proteinaceous BMC structure is composed of seven shell protein subunits, PduABB'JKUT, arranged into hexamers to make up the faces of the polyhedral shell, while the vertices are composed of homopentamers of PduN. Each hexamer and pentamer facet contains a pore to allow for translocation of metabolites through the shell. Adapted from (Yeates *et al*., 2011). (**B**) Various enzymes inside the BMC are involved in the metabolism of 1,2-propanediol, in addition to vitamin B_{12} (not represented in schematic for simplicity). Adapted from Fan *et al*. (2012).

BMCs are thought to be the largest proteinaceous compartments found in any bacterial cell, with the shell alone consisting of approximately 4000 subunits encapsulating another 10-15,000 proteins, and a total mass of between 100 and 600 MDa (Cheng *et al*., 2008). This large size of BMCs mean most full reaction pathways could be contained entirely within in the BMC,

and so they have been recognised to have great potential for biotechnological applications. Previous attempts have been made to utilise them as intracellular 'bioreactors' carrying out novel reactions in a host cell, for example the utilisation of the Pdu BMC from *Citrobacter freundii* in *E. coli* to efficiently carry out the conversion of pyruvate to ethanol (Lawrence *et al*., 2014). Furthermore, it has been demonstrated that heterologously produced proteins can be targeted to the lumen of BMCs *via* adherence of the N-terminal targeting sequences of PduP (Fan *et al*., 2010).

A bank of synthetic operons has been constructed to allow for the production of BMC shell proteins in *E. coli* (Sargent *et al*., 2013). One of these operons, cloned into the 'pUNI-BMC' plasmid, possesses genes encoding for all of the *S. enterica* Pdu shell proteins, complete with His-tags to allow for purification by affinity chromatography, under the control of the constitutive *tat* promoter (Plasmid Table 7.6) (Sargent *et al*., 2013). It is possible that such an apparatus can be used to augment hydrogenase activity to increase efficiency of the enzymes and ultimately improve H_2 yield.

6.5.1 Co-encapsulation of SH and GAPDH within a BMC

Preliminary work was begun during this project to employ a synthetic biology approach to utilise a synthetic *pdu* operon based on the genes encoding the *S. enterica* Pdu BMC in *E. coli*. It was envisaged that by co-encapsulating the heterologously produced NADH-consuming SH from *C. necator* alongside the NADH-evolving glyceraldehyde 3-phosphate dehydrogenase (GAPDH), so relative substrate concentrations in the vicinity of the SH could be boosted, H_2 yield could potentially be increased from current levels outlined in Chapter 2 of this Thesis (Figure 6.2).

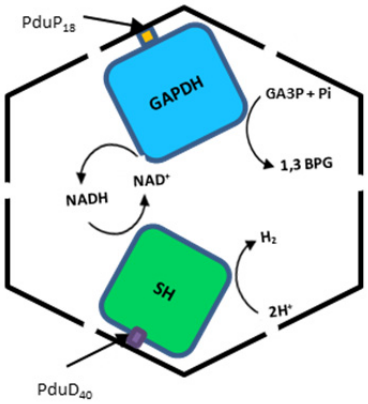

Figure 6.2. Proposed co-localisation of SH and GAPDH in a BMC. The NADH-evolving enzyme GAPDH could be co-encapsulated inside a BMC with the NADH-consuming SH to boost hydrogenase activity *via* a local increase in substrate concentration. To do this both the GAPDH and SH would be targeted to the BMC by translational fusions to N-terminal peptide sequences of PduP and PduD respectively. Selected molecule abbreviations: GA3P: glyceraldehyde-3-phosphate; 1,3BPG: 1,3-bisphosphoglycerate.

In order to target both the SH complex and GAPDH inside the BMC each enzyme was fused to a different signal peptide. The SH complex was targeted to the BMC *via* a translational fusion of the first 40 amino acid residues of *S. enterica* PduD to the N-terminus of the SH hydrogenase small subunit, HoxY. This 40 residue sequence has previously been shown to be sufficient for successful targeting of peptides to the inside of the Pdu BMC (Fan and Bobik, 2011; Sargent *et al*., 2013). Furthermore, to aid in complex detection, a HA-tag was placed at the C-terminus of HoxY. The gene encoding this modified HoxY, along with the rest of the codon optimised SH operon, was placed under the control of the constitutive *tat* promoter in the vector pSU-SH-$PduD_{40}HoxY^{HA}$.

In order to allow for the targeting of GAPDH to the BMC, a DNA sequence coding for the first 18 residues of the PduP protein from *S. enterica* was engineered onto the beginning of the gene *gapA* on the chromosome of *E. coli* HJ002 (MC4100, Δ*hyaB*, Δ*hybOA*, Δ*hycE*, Δ*iscR*, Δ*adhE)*, resulting in a new strain called HJ003. This 18 residue peptide sequence has previously been shown to be sufficient for encapsulation of PduP into the Pdu BMC, and is thought to adhere to the C-terminal helix of the PduA shell protein (Fan *et al*., 2012; Lawrence *et al*.,

2014). This chromosomal modification was done by pMAK705-based homologous recombination.

Preliminary attempts were made to assess the *in vivo* activity of the $PduD_{40}$-SH fusion when co-expressed with the $PduP_{18}$-GAPDH and the BMC-encoding plasmid. The HJ003 (encoding $PduP_{18}$-GAPDH) and HJ002 (containing native GAPDH) strains were transformed with pUNI-BMC and pSU-SH-$PduD_{40}HoxY^{HA}$ or pSU-SH (or the appropriate empty control plasmids pUNI-PROM and pSU-PROM). The strains were grown under anaerobic conditions at 37 ^{o}C for 48 hours in Hungate tubes containing M9 minimal supplemented with 0.8% glucose, 0.2% casamino acids and appropriate antibiotics. The H_2 in the headspace was then determined by gas chromatography in a single end-point assay (Figure 6.3).

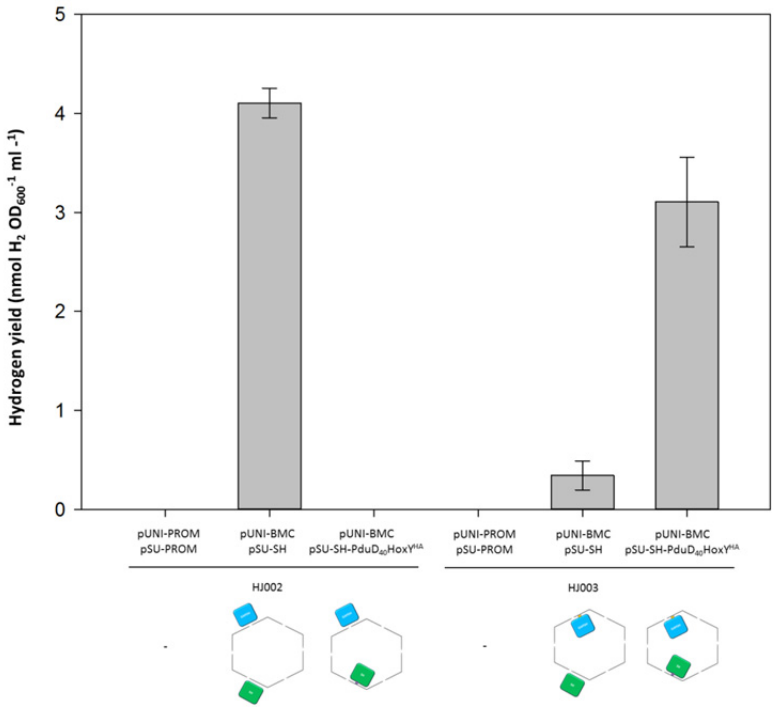

Figure 6.3 Co-production of PduD-SH and PduP-GAPDH with a BMC does not boost H_2 yield. Various arrangements of the BMC shell protein, SH and GAPDH were produced in the cytosol by transforming HJ002 and HJ003 with various combinations the vectors pUNI-PROM + PSU-PROM, pUNI-BMC + pSU-SH or pUNI-BMC + pSU-SH-$PduD_{40}HoxY^{HS}$. The schematics below the graph illustrate whether GAPDH or SH are predicted to be inside or outside the BMC.

The data suggest that, as also shown in Chapter 2, the recombinant SH is functional in the *adhE* mutant (Figure 6.3). The low, but detectible, levels of H_2 can be attributed to the low copy number vector and non-inducible promoter that is driving SH production in this system. Interestingly, when the SH is modified by the addition of a PduD targeting tag – and is co-expressed with genes encoding a BMC – the H_2 production activity drops to undetectable levels (Figure 6.3). Remarkably, hydrogenase activity can be restored by production of the PduP-GAPDH protein (Figure 6.3), suggesting that co-localization of PduD-SH and PduP-GAPDH either within a BMC itself, or shacked close together on shell proteins, is important for providing substrate for the hydrogenase. This may imply that the BMC shell impedes metabolite translocation, despite the 70 Å diameter of the pores being undoubtedly large enough to accommodate the movement of NADH (~20 Å), glycerate-3-phosphate (~8 Å) and 1,3-Bisphosphoglycerate (~10 Å) between the BMC lumen and the cytosol. Certainly, some modelling could be done in an attempt to describe the (in)efficiency of molecule flux into and out of the BMC.

Nevertheless, the data in Figure 6.3 show no signs of the hoped-for boost in hydrogen yield. Various approaches could be taken to improve this system. The data presented in Chapter 2 suggested that the *E. coli* Hyp machinery can partially substitute for the dedicated HypA2-X apparatus as found in *C. necator* to make functional SH. Therefore it was decided, due to time constraints, when designing the BMC experiments that the *hypA2-X* operon was extraneous. Because of this, it was not cloned into an additional vector, which would be required due to the ampicillin resistant pUNI-BMC and kanamycin resistant pSU-SH-$PduD_{40}HoxY^{HA}$ having the same resistance as the two previously made *hypA2-X* operons. Nonetheless, it would be better practice to include this operon, preferably by incorporation into the chromosome as an unmarked insertion - as was done for *hypA1-X* (Chapter 3).

Clearly, [NiFe]-hydrogenases are multi-subunit, multi-cofactor redox enzymes. Assembly of such an enzyme requires the concerted action of numerous accessory proteins. Thus, targeting

a [NiFe]-hydrogenase to a BMC poses several challenges, especially as encapsulation of immature or inactive precursor proteins may be highly likely. Further work is required to ascertain whether the SH and GAPDH are truly inserted inside the BMC in their complete forms.

6.5.2 Heterologous production of the Pdu BMC in *E. coli*

It is perhaps salient to note that the gene encoding the shell protein PduM is absent from the vector pUNI-BMC used in this study. PduM has previously been reported to be an essential part of the BMC architecture for proper assembly and function, the absence of which causes malformed a BMC (Sinha *et al*., 2012), therefore perhaps its absence is resulting in incomplete BMC formation. This could account for the lack of an increase in SH activity when co-localised with GAPDH; the two enzymes may not be completely encapsulated and so NADH may be able to diffuse away from the enzyme.

Interestingly, it has been reported that one of the shell proteins forming pores in the Pdu BMC, PduT, provides an adherence point for a [4Fe-4S] cluster (Parsons *et al*., 2008). It has been hypothesised that this [Fe-S] cluster permits electron flow between the interior of the BMC and the cytosol, or that it facilitates a mechanism to transport whole [Fe-S] clusters into the BMC to replace damaged present in enzymes within. Either way, this may have a role to play in the results seen in this study, perhaps interfering with the redox state of the BMC and SH. It may also provide an opportunity for further engineering to help recruit more electrons into the BMC, and help augment activity of an encapsulated hydrogenase. This could be used in tandem with a system that involves adhering enzymes to the outer surface of the BMC, through the use of the PduV N-terminal signal peptide (Parsons *et al*., 2010).

Further engineering that could be performed on the BMC system may involve reducing the number of shell proteins involved. The Pdu BMC from *Citrobacter freundii* is able to form from

a minimum of PduA-B-B'-J-K-N subunits, with PduU and PduT extraneous, however the *S. enterica* version has been shown to still form in the absence of PduA and PduK (Cheng *et al*., 2011).

Another route to compartmentalisation of hydrogenases enzymes was achieved through the use of RNA scaffolds (Delebecque *et al*., 2011). Here, [FeFe]-hydrogenases and ferredoxins were anchored onto 1-dimensional or 2-dimensional RNA fibres with a resultant increase in H_2 evolution compared to the specially organised control. The authors describe the superiority of RNA scaffolds over protein adherence being that the former can allow for precise orientation of components on a nanometre scale.

Yet another example of compartmentalisation augmenting H_2 yield comes from a paper that was discussed in Section 6.4. The work by Agapakis *et. al* 2010 in developing a synthetic pathway in *E. coli* to generate $BioH_2$ involved co-localisation of the ferredoxin with the hydrogenase to improve electron transfer. Various methods to doing this were attempted: through altering subunit conformations to improve association; direct protein-protein fusion using a linker peptide; or tethering both to a common scaffold. Whilst the latter strategy has been shown to improve the flux through an artificial pathway by 77 times (Dueber *et al*., 2009), in this instance the use of a fusion peptide to link to two subunits was most efficacious; resulting in four times more H_2 evolution (Agapakis *et al*., 2010). Clearly, co-localisation is an effective strategy in synthetic biology, and the utility of peptide linkers to anchor two otherwise foreign proteins was shown to allow for functional chimeras in this Thesis in Chapters 4 and 5.

6.6 **Protein engineering**

The methods employed for engineering modifications in proteins fall into two broad categories; directed or 'rational' protein design, and random mutagenesis. Rational design involves prior knowledge of the protein in question, with specific changes made in specific locations in an attempt to alter functionality in a desired way. This 'genotype first' is called *reverse genetics*, deviating from the traditional genetic approach of firstly examining phenotype and then trying to discern the genetic basis behind it. One such technique used in this approach is site-directed mutagenesis, where PCR can be used to specifically alter certain gene sequences, resulting in a desired change in the encoded protein.

The major advances in bioinformatics over the past few decades have vastly improved the scope of protein engineering in this manner. The use of sequence-based evolutionary approaches has led to the identification of conserved, and thus likely functionally-important, domains of proteins where engineering can be focused upon (Chen and Zeng, 2013). Likewise the development of crystallography techniques has allowed for identification of structural pockets of functional importance (Lutz, 2010).

Whilst rational design helps to quickly identify the regions of a protein that could be altered for improved functionality, it does have drawbacks. First, it is time-intensive; the reliance on prior knowledge requires much research before engineering can even begin. Furthermore, even simple bacterial systems have complex regulation, such that engineering single proteins or even pathways may not lead to significant improvement (Marcheschi *et al*., 2013). For a similar reason, rational design may not give the desired phenotype. Variant proteins may still not function as predicted, with a plethora of unexpected results possible (Marcheschi *et al*., 2013).

The alternative approach, random mutagenesis, escapes many of these problems. A *forward genetics* approach, random mutagenesis involves first creating a multitude of mutants and then screening for those with the desired phenotype, and the genotypic change responsible

subsequently identified (Cobb *et al*., 2012). It is a particularly useful technique when the relevant metabolic pathway or protein is poorly defined or unknown. Random mutagenesis is performed by altering the genome at random points, either by UV irradiation, treatment with chemicals such as the alkylating agent *N*-methyl-*N''*-nitro-*N*nitrosoguanidine (NTG) or transposon mutagenesis (the latter being used to knock-out genes) (Marcheschi *et al*., 2013). Unlike rational design, random mutagenesis does not require much prior knowledge, the mutagenesis itself is relatively easy to perform, and it can serendipitously lead to the discovery of unexpected beneficial mutations.

The work presented in Chapter 3 detailed work towards the construction of a screening method for H_2 production in *E. coli*. Ultimately this was unsuccessful at this juncture, but the discussion of that Chapter detailed possible avenues to explore in order to get the system functional. The main caveat with random mutagenesis is the requirement for a high-throughput screen to efficiently examine the many mutants generated for improved functionality. In many cases, such as for *E. coli* hydrogenases there is not a currently such a method, although a hydrogenase screen has been developed in the alga *Chlamydomonas reinhardtii* (Wecker and Ghirardi, 2014). One method to screen a mutant library in an effective high-throughput manner is to set up some kind of directed evolution, where there is a selection pressure for mutants to evolve the desired trait. Indeed, it has been suggested that directed evolution has become the primary strategy for the tailoring of protein (Lutz, 2010).

The future strategy of protein engineering is likely to be a hybrid approach between rational design and random mutagenesis. So-called 'semi-rational' engineering still involves random mutagenesis, but on a more targeted area of a protein that prior bioinformatics research on sequence, structure or function, or even computational prediction algorithms have identified as being salient (Lutz, 2010). Doing so results in drastically reduced mutant library size, so makes screening less of an issue, and also allows for directed evolution to yield the desired results over fewer generations.

Such tailored random-mutagenesis involves generating mutations in a specific sequence, and can be done by or error-prone PCR (epPCR) if the target protein/ protein domain is known. Site saturation mutagenesis is a related technique which employs a codon in the primers of the form NNN, NNB, NNS or NNK (where N = A/T/G/C, B = C/G/T, S = C/G, K = G/T) and so insert any of the 20 proteinogenic amino acids at the corresponding position (Nov, 2012).

Another exciting technique is gene-shuffling, in which a set of genes is digested by DNase, before primerless PCR is performed to anneal fragments with overlapping ends (Meyer *et al*., 2014). Despite their being complex metalloenzymes, gene shuffling has been shown to be feasible in variant-generation in heterologously expressed [FeFe]-hydrogenases in *E. coli* (Nagy *et al*., 2007). The potential of gene-shuffling has been shown in [NiFe]-hydrogenases too; the employment of the technique (along with epPCR and saturation mutagenesis) in the aforementioned study (Maeda *et al*., 2008a) allowed for the surprising discovery that a 204 residue truncation in HycE dramatically increased the H_2 evolution of FHL. Such a serendipitous finding illustrates the power of gene-shuffling, and augers well for future hydrogenase research.

6.7 The future of industrial biohydrogen production

In truth, it may be that a single modified cell, containing all requisite apparatus for industrial-scale H_2 production, is unfeasible. Instead perhaps 'dual systems' of various organisms acting in synergy is more realistic. In particular, the yields associated with the dark fermentation of organic waste by enteric bacteria may be forever limited as ever greater yields make it increasingly thermodynamically unfavourable to produce more product (Benemann, 1996). It has been proposed that dark fermentation could first take place using Enterobacteriaceae in tandem with Clostridia to generate H_2 *via* formate and NADH *via* reduced ferredoxin, respectively (or indeed modified Enterobacteriaceae in similar ways as described in this Thesis to produce H_2 by these latter pathways). The accumulated organic acids as a result of this dark fermentation could then be fed to organisms such as purple non-sulfur photosynthetic bacteria that can perform photofermentation. Light could be used to power the conversion of these organic acids to H_2 *via* the action of nitrogenase enzymes (Hallenbeck and Ghosh, 2009).

An alternative strategy is to combine organic components with inorganic components to generate hybrid fuel cells and/or electrolysis devices for H_2 consumption/evolution. The original approach was to adsorb purified hydrogenases to electrodes, to act as biocatalysts in place of the more expensive precious metals. An example of this was the anchoring of purified hydrogenase from *Clostridium pasteurianum* and *Desulfovibrio desulfuricans* to TiO_2 nanoparticles to allow for light-dependent H_2 evolution (Cuendet *et al*., 1986). Similarly, *E. coli* hydrogenases have been successfully used to catalyse H_2 oxidation in a fuel cell electrode *via* association with palladium nanoparticles (Orozco *et al*., 2010). Whilst *in vitro* applications of enzymes directly may seem advantageous - adsorbing only enzymes onto an electrode will allow for greater density than if whole cells are used – in many ways whole cell applications are more desirable. The benefits of utilising whole cells include the automatic assembly of hydrogenases by the cellular machinery; protection from inhibitors; the ability to self-repair; and there being no need for protein purification. Thus, it may be that a hybrid biotic/abiotic

device, combining living cells with inorganic substances, is the future of such modified fuel cell technology. A recent example of such work the heterologous expression of genes encoding the [FeFe]-hydrogenases, PFORs and ferredoxins from a number of species can allow *E. coli* cells to perform photocatalytic H_2 production acting as a biocatalyst in conjunction with an inorganic TiO_2 semiconductor (Honda *et al*., 2016).

6.8 **Concluding remarks**

The broad aim of the work presented in this Thesis was to employ elements of synthetic biology in order to help augment *E. coli* H_2 production. First, heterologous expression of genes encoding otherwise foreign machinery in *E. coli* was undertaken. Specifically, this was by the biosynthesis of the SH from *C. necator*, in an effort to utilise the abundant NADH found in a fermentative cell (Chapter 2). Furthermore, the beginnings to integrate multiple exogenous proteins in *E. coli* was begun by the attempt to insert the SH inside the *S. enterica* Pdu bacterial microcompartment, in an attempt to boost the hydrogenase activity by co-localisation with a native *E. coli* protein, GAPDH, as was discussed in this Chapter.

Second, protein engineering to create chimeric enzyme complexes to perform novel functions in the host cell was reported. This was by both the characterisation of a novel system to produce H_2 *via* heterologous expression of PFOR and a Hyd-3: ferredoxin chimera to allow for H_2 evolution from pyruvate (Chapter 4), and also by the further characterisation of a thiosulfate reductase:Hyd-2 hybrid to utilise the quinol pool, and ultimately glycerol, as a substrate for H_2 evolution (Chapter 5).

Work was also carried out towards the development of an intracellular hydrogen sensor to allow for the construction of a screening method for augmented hydrogen production in *E. coli* (Chapter 3). This was done not only by heterologous expression of genes encoding the foreign RH apparatus from *C. necator*, but also by integrating these with the native Hyd-2 hydrogenase in an attempt to make a functional chimera.

Through biotechnology, hydrogenase enzymes show great promise in helping address our future energy needs. As the field of synthetic biology continues to flourish, our knowledge of the workings of metabolic systems deepens, and our expertise in re-engineering biochemistry for our needs broadens ever-further, so the potential key role these remarkable enzymes hold

towards helping solve some of the biggest issues posed to society becomes closer to being a reality.

7. Materials and methods

7.1 **Bacterial strains**

The bacterial strains used in this study, listed in Table 7.1, were all derived from *Escherichia coli* K-12. The common cloning and stocking strain was DH5α, although in cases where restriction enzymes sensitive to dam methylation were used, such as *Xba*I, the DNA was first passed through JM110. The strain K38, carrying the plasmid pGP1-2, was used for ^{35}S-Methionine radiolabelling.

Strain	Relevant Genotype	Antibiotic Resistance	Reference
MC4100	F$^-$, *araD139*, Δ(*argF-lac*)U169, *ptsF25*, *deoC1*, *relA1*, *flbB5301*, *rspL150*	None	(Casadaban, 1976)
FTD147	As MC4100 but Δ*hyaB, hybC, hycE*	None	(Redwood *et al*., 2008)
FTD147-hyp	As FTD147, Δ*tatD*::*hypA1-X*	None	This work
DH5α	F-, ϕ80d*lacZ*ΔM15, Δ(*lacZYA-argF*)U169, *deoR*, *recA1*, *endA1*, hsdR17(r_K-, m_K+), *phoA*, *supE44*, λ-, *thi*-1, *gyr*A96, *rel*A1	None	(Grant *et al*., 1990)
JM110	*rpsL* (Str^r) *thr leu thi-1 lacY galK galT ara tonA tsx dam dcm supE44* Δ*(lac-proAB)* [F' *traΔ36 proAB lacI^q* Δ*M15*]	None	Agilent Technologies
RJ608	As MC4100, Δ*hybO*	None	(Jack *et al*., 2004)
IC010	as MC4100, Δ*hyaB*, Δ*hycE*	None	(Deplanche *et al*., 2010)
IC011	as MC4100, Δ*hyaB*, Δ*hybOA*, Δ*hycE*	None	(Kelly, 2013)
HJ001	as MC4100, Δ*hyaB*, Δ*hybOA*, Δ*hycE*, Δ*iscR*	None	This work
HJ002	as HJ001, Δ*adhE*	None	This work
HJ003	As HJ002, ϕPduP$_{18}$::*gapA* (produces the PduP signal peptide on mature GAPDH protein)	None	This work
HJ004	As HJ002, Δ*ldhA*	None	This work
BEF314	as MC4100, Δ*hypB-E*::*cam*	Cml	(Jacobi *et al*., 1992)
BW25113	F$^-$, Δ(*araB–D*)567, Δ(*rhaD–B*)568, Δ*lacZ4787*(::*rrnB-3*), *hsdR514*, *rph-1*	None	(Baba *et al*., 2006)
JW2696	as BW25113, Δ*hypA* ::*kan*	Kan	(Baba *et al*., 2006)
JW2697	as BW25113, Δ*hypB*::*kan*	Kan	(Baba *et al*., 2006)
JW2698	as BW25113, Δ*hypC*::*kan*	Kan	(Baba *et al*., 2006)
JW2699	as BW25113, Δ*hypD*::*kan*	Kan	(Baba *et al*., 2006)
JW2700	as BW25113, Δ*hypE*::*kan*	Kan	(Baba *et al*., 2006)
JW5433	as BW25113, Δ*hypF*::*kan*	Kan	(Baba *et al*., 2006)
K38 [pGP1-2]	HfrC, *phoA4*, *pit*-10, *tonA22*, *ompF627*, *relA1*, λ$^+$, pGP1-2 encodes T7 RNA polymerase	Kan	(Lyons and Zinder, 1972; Tabor and Richardson, 1985)
IC011 λMBH$_p$-lacZ	introduction of *Cupriavidus necator* MBH promoter region (500 bp upstream) controlling the reporter gene *lacZ* into λ attachment site *via* λRS45	Kan	C. Pinske, unpublished

FTF2013	MG1655 His-HycE, Δ*fdhF*, Δ*nuoA-L*::*Apra,* ∆*hycAB*::*ferredoxin-hycB fusion*	Apra	T. Palmer, unpublished
FTF2015 [pREP4]	As FTF2013 but T5 promoter controlled expression of *fdx*-HA-*hycB*. pREP4 allows encodes for IPTG inducible expression of T5 polymerase	Apra, Kan	T. Palmer, unpublished

Table 7.1 Table of bacterial strains used in this study.

7.2 **Cell culturing**

Aerobic growth of cells was achieved by culturing in Luria Bertani (LB) medium at 37 ^{o}C with vigorous shaking at 200 rpm, with an air to liquid ratio of 4:1. Anaerobiosis was achieved by completely filling the sealed growth vessels with LB medium and incubating without agitation at 37 ^{o}C. Alternatively, the medium was bubbled with N_2 in a sterile manner prior to inoculation to remove dissolved O_2, and after inoculation the vessel was sealed and the headspace purged of O_2 by additional of more N_2.

Growth on solid media was achieved using LB media containing 1.5 % agar, with incubation at 37 ^{o}C. Plates were stored at 4 ^{o}C for a maximum of fourteen days. Long term, strains were cryogenically stored at -80 ^{o}C after flash freezing with liquid N_2. Plasmids were stocked in the cloning strain DH5α at -80 ^{o}C.

7.3 Media and additives

Medium	Components	Sterilised	Quantity (L^{-1})
Luria Bertani medium (LB) (Sambrook, 2001)	NaCl		10 g
	Tryptone	autoclave	10 g
	Yeast Extract		5 g
LB-agar	NaCl		10 g
	Tryptone	autoclave	10 g
	Yeast Extract		5 g
	Agar		15 g
M9 medium	100 mM $CaCl_2$ *	filtered	1 mL
	10x M9 salts *	autoclave	100 mL
	1 M $MgSO_4$ *	filtered	2 mL
	1% Thiamine *	filtered	1 mL
	Trace element SLA (Hormann and Andreesen, 1989) *	filtered	

Table 7.2 Growth media used in this study. Media constituents sterilised by autoclaving unless indicated by a '*' in which case it was sterilised individually before addition to the media

Media Supplement	Stock concentration	Working concentration
Glucose	20%	0.5%, 0.8 %
Glycerol	50%	0.5%
IPTG	1 M	2 mM
Sodium fumarate	16%	0.4%
$NiS0_4$	100 mM	1 µM
$FeCl_3$	100 mM	10 µM
Casacids	20%	0.2%
Tetrathionate	250 mM	1 mM
All-trans retinal	354 mM in ethanol	20 µM
X-gal	20 mg mL^{-1} in Dimethylformamide	20 µg mL^{-1}
Trace elements (g L^{-1}) 0.48 g $FeCl_3.6H_2O$ 0.33 g $MnCl_2.4H_2O$ 0.36 g $CaCl_2.2H_20$ 2 g $ZnCl_2$ 0.2 g H_3BO_3 0.1 g $CoSO_4$	1000x	1x
M9 salts (g L^{-1}) 10 g NH_4Cl 5 g NaCl 30 g KH_2PO_4 64 g $NaH_2PO_4.7H_2O$	10x	1x

Table 7.3 Media supplements and their concentrations. Each stock was prepared in distilled water unless otherwise stated and filter sterilised prior to use.

Antibiotic	Stock concentration (mg mL^{-1})	Solvent	Final concentration (µg mL^{-1})
Ampicillin	125	Water	100
Kanamycin	50	Water	50
Chloramphenicol	25	80% (v/v) ethanol	25
Apramycin	50	Water	50
Rifampicin	20	100% (v/v) methanol	400

Table 7.4 Antibiotics used in this study. Each stock was filter sterilised prior to use.

7.4 Buffers and solutions

Buffer/Solution	Component
APS	10% ammonium persulphate
Sodium dithionite	1% (w/v) dithionite Dissolved in 1mM NaOH
DNA loading buffer	0.25% (w/v) bromophenol blue 0.25% (w/v) xylene cyanol blue 40% (w/v) sucrose
Laemmli sample buffer (2x)	62.5 mM Tris HCl pH 6.8 2% (w/v) SDS 5% (v/v) β-mercaptoethanol 25% (v/v) glycerol 0.01% (w/v) bromophenol blue
Lysozyme (60 mg mL^{-1})	6% lysozyme (from chicken egg white) Dissolved in 1 mL Tris (HCl) pH 7.5
Mg buffer (10x)	100 mM Tris HCl pH 7.5 12 mM $MgCl_2$
Phosphate buffer pH 7.0	Na_2HPO_4 to desired molarity (pH in NaH_2PO_4)
SDS-running buffer (5x)	25 mM Tris HCl pH 8.3 192 mM glycine 0.5% (w/v) SDS
Carbonate transfer buffer	10 mM $NaCHO_3$ pH 9.9 3 mM Na_2CO_3 20% (v/v) methanol
TAE buffer	40 mM Tris HCl pH 8.0 1.142% (v/v) acetic acid 1 mM EDTA
Transformation buffer (TSB)	20 mL LB 1 mL 1 M $MgSO_4$ 1 mL DMSO 2 g PEG 6000
Tris buffered saline (TBS)	20 mM Tris HCl pH 7.6 137 mM NaCl
TBS Tween	As TBS but 0.1 % (v/v) Tween-20
Tris.HCl	50 mM Tris HCl Adjusted to required pH by the addition of HCl
Ni-purification buffer A (unless otherwise stated)	50 mM Tris HCl pH7.5 150 mM NaCl 50 mM imidazole
Ni-purification buffer B (unless otherwise stated)	50 mM Tris HCl pH7.5 150 mM NaCl

	1 M imidazole
Benzyl viologen (BV)	250 mM (stock)
Methyl viologen (MV)	250 mM (stock)
Z buffer pH 7.0	1 L Milli-Q 16.1 g Na_2HPO_4. $7H_2O$ 5.5 g $Na_2H_2PO_4$. H_2O 0.75 g KCl 0.246 g $MgSO_4$. $7H_2O$ 2.7 mL β-Mercaptoethanol
ONPG solution	4 mg mL^{-1} ONPG 0.1 M Phosphate buffer pH 7.0

Table 7.5 Buffers used in this study.

7.5 **Molecular biology techniques**

7.5.1 Plasmid DNA preparation

The QIAprep spin miniprep kit (Qiagen) was used to extract plasmid DNA from *E. coli* strains for use in cloning or subsequent transformations. A stationary phase culture of cells containing the plasmid of interest was grown in 5 mL LB with appropriate antibiotics. Cells were then pelleted by centrifugation at 3000 x *g* for 10 minutes, after which the manufacturer's protocol as specified in that kit was carried out. Plasmid DNA was then eluted either in the buffer supplied, or in sterile double distilled H_2O. Plasmids used in this study are listed in Table 7.6.

If the concentration of DNA was required to be known, this was quantified spectrophotometrically using the NanoDrop ND-1000 system (Thermo Scientific), by measuring peak absorbance at 260 nm.

7.5.2 Tables of plasmids

Plasmid Name	Description	Antibiotic Resistance	Reference
pUNI-PROM	as pT7.5 (Tabor and Richardson, 1985) with *tatA* promoter and RBS cloned *Eco*RI-*Bam*HI	Amp	(Jack *et al*., 2004)
pSU-PROM	as pSU40 (Bartolome *et al*., 1991) with *tatA* promoter and RBS cloned *Eco*RI-*Bam*HI	Kan	(Jack *et al*., 2004)
pUNI-SH	as pUNI-PROM with synthetic *hoxFUYHWI* operon cloned *Bam*HI-*Hind*III	Amp	This work
pSU-SH	As pSU-PROM with synthetic *hoxFUYHWI* operon cloned *Bam*HI-*Hind*III	Kan	This work
pUNI-A2-X	as pUNI-PROM with synthetic *hypA2B2F2C1D1E1X* operon cloned *Bam*HI-*Hind*III	Amp	This work
pSU-A2-X	as pSU-PROM with synthetic *hypA2B2F2C1D1E1X* cloned *Bam*HI-*Hind*III	Kan	This work
pUNI-A1-X	as pUNI-PROM with synthetic *hypA1B1F1C1D1E1X* cloned *Bam*HI-*Hind*III	Amp	This work
pSU-A1-X	as pSU-PROM with synthetic *hypA1B1F1C1D1E1X* cloned *Bam*HI-*Hind*III	Kan	This work
pQE80-SH	as pQE80 (Qiagen) with synthetic *hoxFUYHWI* operon cloned *Bam*HI-*Hind*III	Amp	This work
pQE80-SH-HoxY^{HIS}	As pQE80-SH, but hexahistidine tag encoding sequence inserted at 5' region of *hoxY*.	Amp	This work
pUNI-BMC	Produces PduA, PduB^{His}, PduT, PduU^{His}, PduN^{His}, PduJ and PduK^{His}	Amp	(Sargent *et al*., 2013)

pSU-SH-PduD_{40}HoxY^{HA}	As pSU-PROM, but with *hoxFUYHWI* cloned *Bam*H1-*Hind*III. Encodes for SH with HoxY modified with PduD_{40} at N-terminus and a HA-tag at the C-terminus	Kan	This work
pUniR1-hoxAJ*	Wild type sequences of *hoxAJ* from *C. necator* inserted into pUNI-PROM *Bam*HI-*Xba*I. QuickChange used to engineer the mutation S422G in HoxJ required for function	Amp	This work
phypA1-X/hoxBC	Wild type sequences of *hoxBC and A1-X* from *C. necator* inserted in pACY-Duet1™ (Novagen). *hypA1-X* inserted in MCS1 EcoRI/HindIII with *hoxBC* (not sub cloned) in MCS2 as *Bgl*II/*Avr*II	Cml	This work
pUNI-hoxA	As pUNI-PROM but optimised *hoxA* inserted *Bam*HI/*Bgl*II – XbaI *via* suicide ligations.	Amp	This work
pUNI-hoxAJ*	As but pUNI-hoxA optimised *hoxJ* (with S422G mutation) inserted *Bam*HI/*Bgl*II – *Xba*I *via* suicide ligations.	Amp	This work
plitmus-hoxC	As pT.75 (Tabor and Richardson, 1985) but with the plitmus MCS (New England Biolabs). Optimised *hoxC* inserted *Bam*HI/*Bgl*II-*Xba*I by suicide ligations.	Amp	This work
plitmus-hoxB	As pT.75 (Tabor and Richardson, 1985) but with the plitmus MCS (New England Biolabs). Optimised *hoxB* inserted *Bam*HI/*Bgl*II-*Xba*I by suicide ligations.	Amp	This work
plitmus-hoxCB	As plitmus-hoxC but optimised *hoxB* inserted *Bam*HI/*Bgl*II-*Xba*I by suicide ligations.	Amp	This work
plitmus-hoxCBAJ*	As plitmus-hoxCB but optimised *hoxAJ** inserted *Bam*HI/*Bgl*II-*Xba*I by suicide ligations.	Amp	This work

pUNI-RH	As pUNI-PROM, but optimised complete RH operon (*hoxCBAJ**) inserted *Bam*HI – *Hind*III, cut out from previously made plitmus-hoxCBAJ*	Amp	This work
pSU18-hyp	AS pSU18 (Bartolome *et al*., 1991), but *hypA1-X* operon cloned *Bam*HI-*Hind*III	Cml	This work
pUNI-hybO^{long}	As pUNI-PROM, but *hybO* Δtat signal sequence, ΔC-terminal transmembrane domain::sequence encoding last 69 aa of HoxB from *C. necator*. Cloned *Bam*HI/*Bgl*II-*Xba*I suicide ligations.	Amp	This work
pUNI-hybO^{short}	As pUNI-PROM, but *hybO* Δtat signal sequence, ΔC-terminal transmembrane domain::sequence encoding last 44 aa of HoxB from *C. necator*. Cloned *Bam*HI/*Bgl*II-*Xba*I suicide ligations.	Amp	This work
pUNI-hybO^{long}AJ*	As pUNI-hybO^{long}, but *hoxAJ** cloned *via Bam*HI/*Bgl*II-*Xba*I suicide ligations.	Amp	This work
pUNI-hybO^{short}AJ*	pUNI-hybO^{short}, but *hoxAJ** cloned *via Bam*HI/*Bgl*II-*Xba*I suicide ligations.	Amp	This work
pSB1C3	High copy BioBrick assembly plasmid.	Cml	http://partsregistry.org/wiki/index.php/Part:pSB1C3
pSB-SHp-Apra	As pSB1C3, but SH promoter region (500 bp) from *C. necator* cloned *Eco*RI-*Hind*III and the apramycin resistance gene *aac(3)-IV* from *K. pneumoniae* cloned *Hind*III-*Xba*I.	Cml	This work
pSB-MBHp-Apra	As pSB1C3, but MBH promoter region (500 bp) from *C. necator* cloned *Eco*RI-*Hind*III and the apramycin resistance gene *aac(3)-IV* from *K. pneumoniae* cloned *Hind*III-*Xba*I.	Cml	This work
pSU40		Kan	(Bartolome *et al*., 1991)

pSU40-SHp-ttrSR	As pSU40, but SH promoter cloned *Eco*RI-*Xba*I, and the *ttrSR* operon native to *S. enterica* cloned *Xba*I-*Xho*I.	Kan	This work
pSB-ttrBp-Apra	As pSB1C3, but the promoter region (200 bp) upstream of *ttrB* as found in *S. enterica* cloned *Eco*RI-*Xba*I, and *aac(3)-IV* cloned *Xba*I-*Pst*I.	Cml	This work
pUNI-Tm-POR	*Th. maritima* PFOR operon (*TM0015-0018*) cloned *Xba*I – *Hind*III into pUNI-PROM	Amp	(Kelly, 2013)
pUNI-Tm-Fd-POR	*Th. maritima* Fd gene (*TM0927*; *Xba*I - *Hind*III) and PFOR operon (*TM0015-0018*; *Bam*HI - *Xba*I) cloned into pUNI-PROM	Amp	(Kelly, 2013)
pMAK705	Low copy temperature sensitive plasmid	Cml	(Hamilton *et al*., 1989)
pSU-PR	Proteorhodopsin gene cloned *Sal*I - *Hind*III into pSU-PROM	Kan	(Kelly, 2013)
pUNI-OSPhs	Fusion gene of highly-truncated *hybO* and *phsB* with HA-tag linker peptide and *phsC* cloned *Bam*HI - *Hind*III into pUNI-PROM	Amp	(Kelly, 2013)
pUNI-OLPhs	Fusion gene of a less-truncated *hybO* and *phsB* with HA-tag linker peptide and *phsC* cloned into pUNI-PROM	Amp	(Kelly, 2013)
pUNI-OSFlexAPhs	As pUNI-OSPhs but HA-tag linker replaced with a flexible peptide linker	Amp	(Kelly, 2013)
pCK302	Expression vector to allow for L-rhammose gene expression	Amp	(Kelly *et al*., 2016)
pCK250	As pCK302, with gene encoding OSPhs (highly-truncated *hybO* and *phsB* with HA-tag linker peptide and *phsC*) cloned behind synthetic RBS with a predicted translation	Amp	C. Kelly, unpublished

	rate = 5k au		
pCK251	As pCK302, with gene encoding OSPhs (highly-truncated *hybO* and *phsB* with HA-tag linker peptide and *phsC*) cloned behind synthetic RBS with a predicted translation rate = 20k au	Amp	C. Kelly, unpublished
pCK252	As pCK302, with gene encoding OLPhs (less-truncated *hybO* and *phsB* with HA-tag linker peptide and *phsC*) cloned behind synthetic RBS with a predicted translation rate = 5k au	Amp	C. Kelly, unpublished
pCK253	As pCK302, with gene encoding OLPhs (less-truncated *hybO* and *phsB* with HA-tag linker peptide and *phsC*) cloned behind synthetic RBS with a predicted translation rate = 20k au	Amp	C. Kelly, unpublished

Table 7.6 Plasmids used in this study.

7.5.3 Preparation of competent cells and transformation with plasmid DNA

In this work, cells were generally transformed *via* the chemical-competency method using TSB (DMSO) (Chung and Miller, 1988). To prepare competent cells in this manner, 5 mL LB with appropriate antibiotics was inoculated with 50 µL of cell culture that had been grown to stationary phase. This new culture was then incubated at 37 ^{o}C with shaking at 200 rpm to induce aerobiosis for approximately 2 hours, until the cell density had reached OD_{600} = 0.3-0.4. The culture was then submerged in ice for 10 minutes to cessate further growth, after which cells were pelleted by centrifugation at 2773 x *g* for 10 minutes. The resultant pellet was resuspended in 500 µL ice-cold TSB medium and either kept on ice until transformation, or immediately frozen in liquid N_2 and stored at – 80 ^{o}C for later use.

Transformation was carried out by incubation of 100 µL competent cells with 0.1-1 µg DNA on ice for 30 minutes. Cells were subjected to heat shock by placing this transformation mix in 42 ^{o}C for 90 seconds before being returned to ice for 3 minutes. To allow for expression of the resistance gene on the plasmid, 1 mL LB was added to the transformation mix and the Eppendorf incubated at 37 ^{o}C with shaking at 200 rpm for 1 hour. The cells were pelleted by centrifugation at 16,000 x *g* for 1 minute, resuspended in 100 µL LB before being plated on LB-agar medium containing appropriate antibiotics.

In certain instances, particularly with large vectors, chemical transformation had a poor efficiency. At these times, electroporation was used to transform cells (Sambrook, 2001). In this case, 200 mL of LB media was inoculated 1 in 100 dilution of the previously prepared culture at stationary phase. This new subculture was grown aerobically with agitation at 37 ˚C to an OD_{600} = 0.3-0.4 whereupon the culture immediately placed in ice for 10 minutes. As before, cells were pelleted by centrifugation at 2773 x *g* for 10 minutes. The pellet was twice washed with ice-cold, sterile Milli-Q water before a final wash with 75 mL 10% ice-cold glycerol was performed. The pellet was resuspended by vortexing in 400 µL 10% ice-cold glycerol. Aliquots of 50 µL were used in transformations, to which approximately 200 ng of plasmid DNA

was added. After 30 minutes incubation, the cells were transferred to an ice-cold 2 mm electroporation cuvette (Molecular BioProducts) and an electrical pulse applied (2.5 kV voltage, 25 μF capacitance, 200 Ω resistance, 2 mm cuvette length) using a GenePulser Xcell electroporator (BioRad). 1 mL of LB medium was added to the cuvette and the cells mixed by gentle pipetting. The suspension was then transferred to an Eppendorf tube and incubated for one hour at 37 ^{o}C, and plated as before.

7.5.4 Polymerase chain reaction (PCR)

The polymerase chain reaction (PCR) is a technique to amplify DNA fragments by many orders of magnitude, and is useful for a variety of purposes. For 'diagnostic' PCR purposes, i.e. to check genotype of plasmid or genomic DNA for successful gene deletion/insertion, GoTaq DNA polymerase (BioRad) was typically used, as per the manufacturer's instructions. When genomic DNA was to be amplified, a so-called 'Colony PCR' was performed. Here a single bacterial colony was suspended in 50 μL Milli-Q water, from which 3 μL was then taken as the DNA template for the reaction mix. For DNA amplification for use in cloning, the high-fidelity Herculase II polymerase (Agilent Technologies) was used instead. In this case, approximately 200 ng of plasmid or genomic DNA was used as the template. Table 7.7 outlines the standard reaction mixes used for both GoTaq and Herculase II PCR, whilst Table 7.8 shows the standard cycling procedure, which was carried out in a thermocycler (Bio-Rad S1000). Table 7.9 lists the primers used in this study.

Component	Volume
10 x buffer (Herc)/5 x buffer (GoTaq)	5 µL (HercII)/10 µL (GoTaq)
Forward primer (10 µM)	1.5 µL
Reverse primer (10 µM)	1.5 µL
dNTPs (20 µM)	1.0 µL
Polymerase	1.0 µL (HercII)/0.5 µL (GoTaq)
DNA template	1.0 µL
Milli-Q water	39.0 µL (HercII)/34.5 µL (GoTaq)
Total	**50 µL**

Table 7.7 PCR reaction mix used for GoTaq or Herculase II polymerase.

Step	Temperature	Time	Number of Cycles
Initial denaturation	95 °C	5 m	1
Denaturation	95 °C	30 s	
Annealing	50 – 60 °C	30 s	29
Elongation	72 °C	1 m/kb	
Final elongation	72 °C	5 m	1

Table 7.8 Cyclic conditions for PCR reactions performed in this study.

7.5.5 Table of primers

Name	Sequence 5' to 3'	Details
HoxF_C'HIS_Fd	CGCCTCGAGAGATCTGCATGCAGGAGGAAAAAAAAAATGTCTATCCAGATCACC	Allows for generation of C terminal His-tag of SH subunit HoxF within the SH operon in a vector. Cut linear PCR product with *Xho*I and ligate together to form circularised plasmid.
HoxF_C'HIS_Rv	CGCCTCGAGTTATTAGTGATGGTGATGGTGATGGCCGCTGCTACCCTGGAAGTACAGGTTTTCACG GGTAACTTCTTCCAGG	Allows for generation of C terminal His-tag of SH subunit HoxF within the SH operon in a vector. Cut linear PCR product with *Xho*I and ligate together to form circularised plasmid.
Pdu_{40}_HoxY_1	CCGCGCTAGCAGGAGGAAAAAAAAAATGGAAATTAATGAAAAATTGCTGCGCC	Allows for the modification of the SH operon in a vector, by attachment of Pdu_{40} peptide sequence onto the N-terminal region and HA tag onto the C-terminal region of the SH hydrogenase small subunit HoxY. PCR product cut with *NheI* and then re-ligated to get vector containing modified operon. Used in conjunction with Pdu_{40}_HoxY_2/3/4.
Pdu_{40}_HoxY_2	ATTTCGTCTTTGTGCGGCGCACGAGCGGTCTGTGGTGCTGTGGATGC	Allows for the modification of the SH operon in a vector, by attachment of Pdu_{40} peptide sequence onto the N-terminal region and HA tag onto the C-terminal region of the SH hydrogenase small subunit HoxY. PCR product cut with *NheI* and then re-ligated to get vector containing modified operon. Used in conjunction with Pdu_{40}_HoxY_1/3/4.
Pdu_{40}_HoxY_3	GCATCCACAGCACCACAGACCGCTCGTGCGCCGCACAAAGACGAAAT	Allows for the modification of the SH operon in a vector, by attachment of Pdu_{40} peptide sequence onto the N-terminal region and HA tag onto the C-terminal region of the SH hydrogenase small subunit HoxY. PCR product cut with *NheI* and

		then re-ligated to get vector containing modified operon. Used in conjunction with Pdu_{40}_HoxY_1/2/4.
Pdu_{40}_HoxY_4	GCGCGCTAGCTTATTAAGCGTAATCTGGAACATCGTATGGGTAGTCGTAACGGTTGATAGAAGACG	Allows for the modification of the SH operon in a vector, by attachment of Pdu_{40} peptide sequence onto the N-terminal region and HA tag onto the C-terminal region of the SH hydrogenase small subunit HoxY. PCR product cut with *NheI* and then re-ligated to get vector containing modified operon. Used in conjunction with Pdu_{40}_HoxY_1/2/3.
PduP_gapA_insert_chk_Fd	GAATGGATTCTTCACTTACC	Used to check successful integration of $PduP_{18}$::*gapA* into chromosome.
PduP_gapA_insert_chk_Rv	TTGTGAGACGGGCCATCAACGG	Used to check successful integration of $PduP_{18}$::*gapA* into chromosome.
HoxY_N'His_Fd	GCGCTCGAGATGCATCACCATCACCATCACAGCAGCGGCGAAAACCTGTACTTCCAGGGTCGTGCGCCGCACAAAGACG	Allows for generation of N-terminal His-tag on SH small subunit HoxY. *Xho*I used to ligate together ends of PCR product.
HoxY_N'His_Rv	GCGCTCGAGTTCCTCCTGCTAGCGCATGCTTATTATTTGTCTTCACC	Allows for generation of N-terminal His-tag on SH small subunit HoxY. *Xho*I used to ligate together ends of PCR product.
HoxY_C'His_Fd	GCGCTCGAGGCTAGCATCGATAGGAGGAAAAAAAAAATGTCTCGTAAACTGGTTATCG	Allows for generation of N-terminal His-tag on SH small subunit HoxY. *Xho*I used to ligate together ends of PCR product.
HoxY_C'His_Rv	GGCCTCGAGTTATTAGTGATGGTGATGGTGATGGCCGCTGCTACCCTGGAAGTACAGGTTTTCGTCGTAACGGTTGATAGAAGACGG	Allows for generation of N-terminal His-tag on SH small subunit HoxY. *Xho*I used to ligate together ends of PCR product.
HoxF_C'His_Fd	CGCCTCGAGAGATCTGCATGCAGGAGGAAAAAAAAAATGTCTATCCAGATCACC	Allows for generation of C-terminal His-tag of HoxF.
HoxF_C'His_Rv	CGCCTCGAGTTATTAGTGATGGTGATGGTGATGGCCGCTGCTACCCTGGAAGTACAGGTTTTCACGGGTAACTTCTTCCAGG	Allows for generation of C-terminal His-tag of HoxF.

HoxA_Fd	GCGCAGATCTAGGAGGAAAAAAAAATGTCTGACAAACAGGCGACCGTTCTGGTTGTTGACGACGA AACCCGTTCTCAGGACGCG	Used to optimise the first 20 codons of *hoxA* for expression in *E. coli*. Enables construction of *hoxCBAJ** operon by suicide ligations.
HoxA_Rv	GCGCTCTAGAGGATCCTCATTTCTCCTCCAAGCCAAAGCGCAACAGCTTCTGACGTAATCCGACGCG CGATAGACC	Used to optimise the first 20 codons of *hoxA* for expression in *E. coli*. Enables construction of *hoxCBAJ** operon by suicide ligations.
HoxB_Fd	GCGCAGATCTAGGAGGAAAAAAAAAATGAACGCGCCGGTTTGCACCGGTCTGGCGTCTGCGAAACC GGGTGTTCTGAACGTTCTG	Used to optimise the first 20 codons of *hoxB* for expression in *E. coli*. Enables construction of *hoxCBAJ** operon by suicide ligations.
HoxB_Rv	GCGCTCTAGAGGATCCCTATTTCAGCCGCGTCTTGCGAATGGCTGGCGCGATCAGCGGATGATCTG CCGTGGCATT	Used to optimise the first 20 codons of *hoxB* for expression in *E. coli*. Enables construction of *hoxCBAJ** operon by suicide ligations.
HoxC_Fd	GCGCAGATCTAGGAGGAAAAAAAAAATGGAACGTCTGGTTGTTGGTCCGTTCAACCGTGTTGAAGG TGACCTGGAAGTTAACCTG	Used to optimise the first 20 codons of *hoxC* for expression in *E. coli*. Enables construction of *hoxCBAJ**operon by suicide ligations.
HoxC_Rv	GCGCAGATCTAGGAGGAAAAAAAAAATGGAACGTCTGGTTGTTGGTCCGTTCAACCGTGTTGAAGG TGACCTGGAAGTTAACCTGGAGGTCG	Used to optimise the first 20 codons of *hoxC* for expression in *E. coli*. Enables construction of *hoxCBAJ** operon by suicide ligations.
HoxJ_Fd	GCGCAGATCTAGGAGGAAAAAAAAAATGTCTTCTAAACGTACCACCACCTCTTCTGGTTCTCACGGTG TTGACCTGGACGCGATG	Used to optimise the first 20 codons of *hoxJ* for expression in *E. coli*. Enables construction of *hoxCBAJ**operon by suicide ligations.
HoxJ_Rv	GCGCTCTAGAGGATCCTCAACGCCGGTCTGCGGACGACCCCTTGTCGTGAGCAGCTGGCAGTTCGA CCGTGAACTC	Used to optimise the first 20 codons of *hoxJ* for expression in *E. coli*. Enables construction of *hoxCBAJ** operon by suicide ligations.

HoxB_N'His_Fd	GCGACTAGTATGCATCACCATCACCATCACAGCAGCGGCGAAAACCTGTACTTCCAGGGTAACGCG CCGGTTTGCACCGG	Allows for generation of N-terminal His-tag on RH small subunit HoxB. *Spe*I used to ligate together ends of PCR product.
HoxB_N'His_Rv	GCGGACTAGTTTCCTCCTAGATCCTCAATGCACGGTGCACACCATGCAGGGATC	Allows for generation of N-terminal His-tag on RH small subunit HoxB. *Spe*I used to ligate together ends of PCR product.
HoxB_C'His_Fd	CGCACTAGTAGGAGGAAAAAAAAAATGTCTGACAAGCAGGCCAC	Allows for generation of N-terminal His-tag on RH small subunit HoxB. *Nhe*I used to ligate together ends of PCR product.
HoxB_C'His_Rv	CGCACTAGTCTAGTGATGGTGATGGTGATGGCCGCTGCTACCCTGGAAGTACAGGTTTTCTTTCAGC CGCGTCTTGCGAATGGC	Allows for generation of N-terminal His-tag on RH small subunit HoxB. *Nhe*I used to ligate together ends of PCR product.
QC_Sph_Fd	CGGCGTAATAAGCTTGCGCTAGCAGG	Used to alter *Sph*I site after *hypC1* in *hypA1-X*, so can cut out *hypA1B1F1* and replace with *hypA2B2F2* to create *hypA2-X*.
QC_Sph_Rv	CCTGCTAGCGCAAGCTTATTACGCCG	Used to alter *Sph*I site after *hypC1* in *hypA1-X*, so can cut out *hypA1B1F1* and replace with *hypA2B2F2* to create *hypA2-X*.
tatD_UP_Fd	GCGCTCTAGAGGCATTTATCGCCCCAGCGCT	Amplify 500 bp upstream region from *tatD* in *E. coli*. Used for hypA1-X integration by pMAK.
tatD_UP_Rv	GCGCGAATTCCCTCCATATGACAACCGCCCTGACG	Amplify 500 bp upstream region from *tatD* in *E. coli.* Used for hypA1-X integration by pMAK.
tatD_DWN_Fd	GCGGTCGACGCGTTTTAGAGTTTGCGGAACTCG	Amplify 500 bp downstream region from *tatD* in *E. coli*. Used for hypA1-X integration by pMAK.
tatD_DWN_Rv	GCGCGGTACCCTATCCTTGCGCCCCGATTAAACGG	Amplify 500 bp downstream region from *tatD* in *E. coli*. Used for hypA1-X integration by pMAK.
ApraR_Fd	GCGCTCTAGAATGTCATCAGCGGTGG	To clone the apramycin^{R} gene, *aac(3)IV*, into pSB1C3.
ApraR_Rv	GCGCCTGCAGTCAGCCAATCGACTGG	To clone the apramycin^{R} gene, *aac(3)IV*, into pSB1C3.
SH_{prom}_ApraR_Fd	CGCGGAATTCCTGCCTCCGGTCACCCGGTGC	To clone SH_{prom} sequence before *apra*^{R} pSB1C3.
SH_{prom}_ApraR_Rv	GCGCTCTAGATCCTCCTTACTAATGTTCG	To clone SH_{prom} sequence before *apra*^{R} pSB1C3.

MBH_{prom}_ApraR_Fd	GCGCGAATTCAGTGAGCATCTGGCGTCG	To clone MBH_{prom} sequence before *apra*^{R} pSB1C3.
MBH_{prom}_ApraR_Rv	GCGCTCTAGATCTCCTAATTTCTGTATTGG	To clone MBH_{prom} sequence before *apra*^{R} pSB1C3.
SHp_Eco_Fd	CGCGGAATTCCTGCCTCCGGTCACCCGGTGC	Clone SH_{prom} into pSU40 to construct pSU40-SH_{p}-*ttrSR*.
SHp_Eco_Rv	GCGCTCTAGATCCTCCTTACTAATGTTCG	Clone SH_{prom} into pSU40 to construct pSU40-SH_{p}-*ttrSR*.
MBHp_Eco_Fd	GCGCGAATTCAGTGAGCATCTGGCGTCG	Clone MBH_{prom} into pSU40 to construct pSU40-MBH_{p}-*ttrSR.*
MBHp_Eco_Rv	GCGCTCTAGATCTCCTAATTTCTGTATTGG	Clone MBH_{prom} into pSU40 to construct pSU40-MBH_{p}-*ttrSR.*
ttrSR_Xba_Fd	GCGCTCTAGAATGAGAGGTAAAACCGTAAGG	Clone *ttrSR* into pSU40 to construct pSU40-SH_{p}-*ttrSR*. / pSU40-MBH_{p}-*ttrSR.*
ttrSR_Xba_Rv	GCGCCTCGAGTCATGGCTCATACGTTGTTCG	Clone *ttrSR* into pSU40 to construct pSU40-SH_{p}-*ttrSR*. / pSU40-MBH_{p}-*ttrSR.*
ttrBp_Eco_Fd	GCGCGAATTCGCGCCTTACGGTTTTACC	To insert $ttrB_{prom}$ into pSB1C3 in front of *apra*^{R}.
ttrBp_XbaI_Rv	GCGCTCTAGATCCCGTCCACATTGCC	To insert $ttrB_{prom}$ into pSB1C3 in front of *apra*^{R}.
HybO_Fd	GCGCAGATCTATGGAGATGGCCGAATCGG	Forward primer to allow for PCR ligation of Hyd-2 small subunit, HybO, to C-terminal peptide sequence of RH small subunit, HoxB (long or short version).
HybO_RV_ORANGE	TTCGAAGCCGGGGCCGCCCTCTTTAGC	Reverse primer to allow for PCR ligation of Hyd-2 small subunit, HybO, to C-terminal peptide sequence of RH small subunit, HoxB (long version).
HybO_Rv_RED	TTTGGGCATATCGCCGCCCTCTTTAGC	Reverse primer to allow for PCR ligation of Hyd-2 small subunit, HybO, to C-terminal peptide sequence of RH small subunit, HoxB (short version).
C'_HoxB_FD_ORANGE	GCTAAAGAGGGCGGCCCCGGCTTCGAAGAGCC	Forward primer to allow for PCR ligation of long version of HoxB C-terminal sequence onto end of HybO.
C'_HoxB_FD_RED	GCTAAAGAGGGCGGCGATATGCCCAAAGCC	Forward primer to allow for PCR ligation of short version of HoxB C-terminal sequence onto end of HybO.

C'_HoxB_RV	GCGCTCTAGAGGATCCTTATTATTTCAGCCGCGTCTTGCG	Reverse primer to allow for PCR ligation of Hyd-2 small subunit, HybO, to C-terminal peptide sequence of RH small subunit, HoxB (long or short version).

Table 7.9 Table of primers used in this study.

7.5.6 QuickChange site directed mutagenesis

QuickChange site-directed mutagenesis was undertaken during the replacement of *hypA1B1F1* with *hypA2B2F2* in the *hypA1-X* operon to construct the *hypA2-X* operon. This was required to remove the *Sph*I site at the 3' end of *hypC1* so that *Sph*I could be used as a restriction site to cut out *hypA1B1F1.* This was done using the primers QC_Sph_Fd and QC_Sph_Rv (Table 7.9).

The method employs two oligonucleotide primers about 25 bp in length. Each primer is contains the desired mutation in the middle of their sequences, but are otherwise complementary to both strands of gene sequence about the site where the mutation is to be inserted. The PCR was performed using the *PfuTurbo* (Agilent technologies) as per the manufacturer's instructions. The process yielded a nicked circular plasmid DNA product with the desired mutation thus inserted. After this, digestion with the restriction enzyme *Dpn*I was performed to digest the *dam* methylated DNA template, but not the PCR product. The PCR product was then used to transform DH5α cells, where the nicked plasmid DNA was repaired to provide intact plasmids complete with the new mutation. Plasmid DNA sequencing was then used to confirm successful insertion of the desired mutation.

7.5.7 Agarose gel electrophoresis

1% (w/v) agarose gels were prepared in 1 x TAE buffer containing 1 x GelRed (Biotium). Gels were run in 1 x TAE buffer for approximately 20 minutes at 100 V. DNA loading dye was added to the DNA in a 1:4 ratio and this loaded onto the wells of the gel. A DNA standard (1 kb ladder, Roche) was run in an adjacent lane to allow for estimate of DNA fragment size. DNA bands were visualised by UV trans-illumination using a Bio-Rad Gel Doc XR+ system.

7.5.8 DNA gel extraction and purification

DNA molecules used in cloning could be purified after digestion/PCR by performing gel electrophoresis before excising the required DNA band using the QIAquick Gel Extraction Kit (Qiagen) following the manufacturer's instructions. Alternatively, DNA could be purified directly from a reaction mixture using the QIAquick PCR Purification kit (Qiagen).

7.5.9 DNA digestion by restriction endonucleases for cloning

2 µg of DNA was digested using the appropriate restriction enzymes in buffer provided by the manufacturer (Roche) in a final volume of 50 µL. If two different restriction enzymes were required, a buffer was utilised that allowed for efficient simultaneous digestion of DNA where possible. If this was not possible, a digestion was performed using one restriction enzyme with its optimal buffer, after which DNA purification was performed and the procedure repeated for the other enzyme. Digests were incubated for at least three hours at 37°C. Digested vectors were dephosphorylated using alkaline phosphatase (Roche) by adding 1 x alkaline phosphatase buffer and 1 unit enzyme per 10 µL of volume. This was incubated for 30 minutes at 37 °C. Digests were then analysed by agarose gel electrophoresis, visualised using UV trans-illumination and bands excised.

7.5.10 DNA ligation

Digested DNA fragments were annealed to each other, or inserted into a linearised vector using T4 DNA ligase (Roche). In general, a molar ratio of insert: vector of 3:1 was used. Equation 7.1 allowed for the calculation of the appropriate amounts of DNA to use.

$$\text{Mass}_{\text{vector}}\,(\text{ng}) = \frac{\text{Length}_{\text{vector}}\,(\text{kb}) \times \text{Mass}_{\text{insert}}\,(\text{ng})}{\text{Length}_{\text{insert}}\,(\text{kb})} \times 3$$

Equation 7.1 Determination of molar ratios for DNA ligation.

DNA ligations were carried out in a final volume of 10 µL containing ligation buffer and 1 µL ligase enzyme. Ligations were incubated at 17 ^{o}C overnight, before the entire reaction mixture volume was used in the transformation of DH5α cells.

7.5.11 Suicide ligations

Suicide ligations were performed in order to sequentially insert the genes encoding the RH apparatus in *E. coli*. This technique is based upon the principle that the restriction enzymes *BamH*I and *Bgl*II, whist cutting at different sites (5'-GGATCC-3' and 5'-AGATCT-3'respectively), leave the same 'sticky end' of GATC, and therefore DNA cut with these enzymes can be ligated together. If this is done, a 'scar' sequence of 5'-GGATCT-3' is left that cannot be cut by either enzyme. Thus, by careful design of DNA inserts with a *Bgl*II site at upstream, and a *BamH*I and *Xba*I downstream of the genes to be inserted, a whole operon can be sequentially constructed, as illustrated in Figure 7.1.

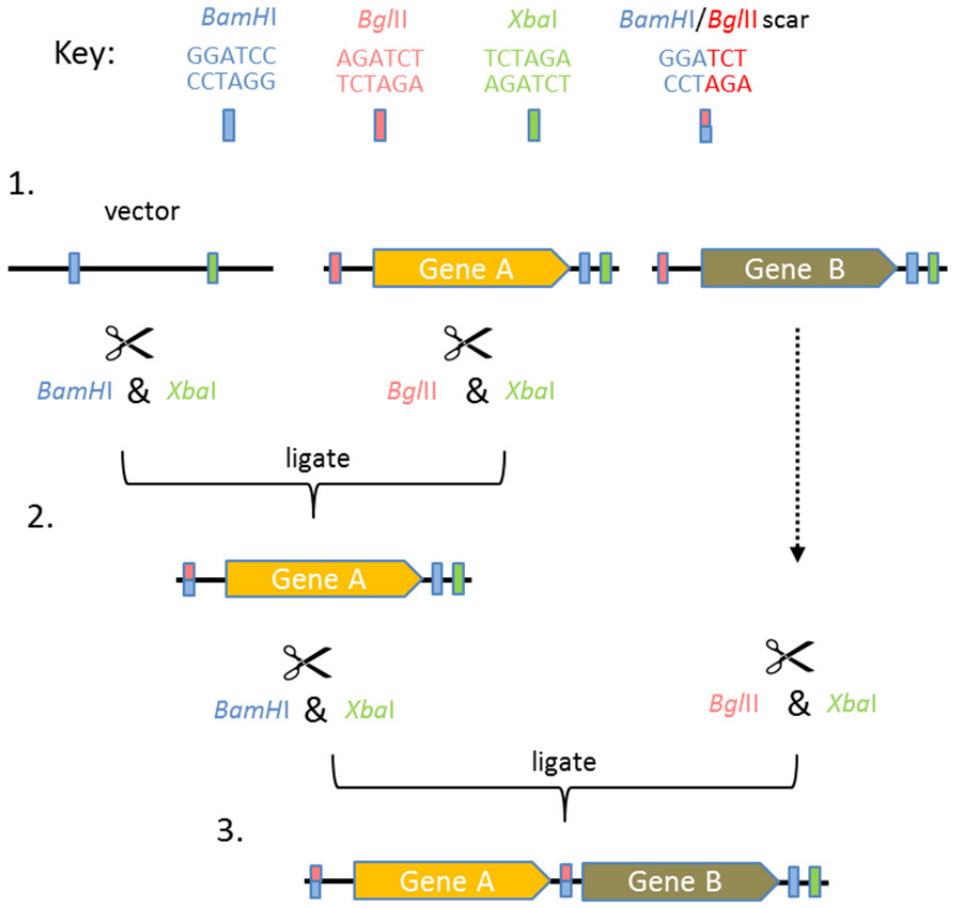

Figure 7.1 Suicide Ligations. Suicide ligations make use of the fact that *Bgl*II *and BamH*I digestion leaves the same sticky end, making it possible to anneal DNA digested with either by these enzymes together. Multiple genes can be inserted sequentially into a vector to construct an operon. **1.** Primers were designed to amplify each of the genes desired to be inserted individually, such that each PCR product contained a *Bgl*II site upstream of the gene, and a *BamH*I followed by an *Xba*I site downstream. The vector in which the genes were to be inserted had a multi cloning site containing a *BamH*I site upstream of an *Xba*I site. Digestion of the vector and first insert was performed followed by ligation. **2.** The product was therefore a vector containing the gene insert with a *BamH*I/*Bgl*II scar upstream, and *BamH*I and *Xba*I sites downstream. As the scar cannot be digested by *BamH*I or *Xba*I (or indeed *Bgl*II), so the DNA digestion can be performed as before in order to insert the next gene of interest. **3.** Thus, two genes are now inserted into the vector, and the process repeated until the entire operon is constructed.

7.5.12 Fusion PCR

When designing the Hyd-2 biosensor constructs (Chapter 2), specifically the gene encoding the HybO-HoxB tail fusion protein, the traditional approach of DNA digestion with restriction enzymes followed by ligation was not employed. Instead, fusion PCR was used. Here, the DNA inserts desired to be annealed are amplified by PCR using primers that have overhangs

complementary to the sequences of the other gene of interest (12 base pairs). The strategy to clone the hybO^{long} fusion, (i.e. the long version of the C-terminal tail of HoxB onto the end of HybO) will be described here to illustrate the technique (Figure 7.2).

First, using the primers HybO_Fd and HybO_RV_ORANGE, the modified *hybO* gene portion (producing HybO with no Tat signal sequence (which ends at Ala37), and no C-terminal transmembrane tail (which was taken to run from Asn330 to the end of the peptide)) was amplified. In another PCR reaction, the gene portion encoding the long version of the C-terminal tail of HoxB (Pro280 to the end), was amplified using the primers C'_HoxB_FD_ORANGE and C'_HoxB_RV. Next, some of the PCR products from both of these initial PCRs were used as templates in a subsequent single 'fusion' PCR. Because each of these PCR products contained a 12 bp sequence of DNA corresponding to that found in the other, and thus a 24 bp region of complementarity in total, so the two PCR products could anneal. The polymerase could then complete the rest of the complementation by overhang extension. Addition of the two extreme flanking primers into the reaction mix as well, in this case HybO_Fd and C'_HoxB_RV would ensure that this complete complementation product could also be amplified. Thus, the final PCR product formed was a fusion of the two DNA templates. This final product was then inserted into a vector using the restriction enzymes also designed into flanks of this final product. Ligations were used to transform DH5α cells, after which plasmids were purified from single colonies and subjected to DNA sequencing to confirm the sequence of the insert was correct.

The same process was performed for construction of hybO^{short} using the primers HybO_Fd, HybO_RV_RED C'_HoxB_FD_RED and C'_HoxB_RV.

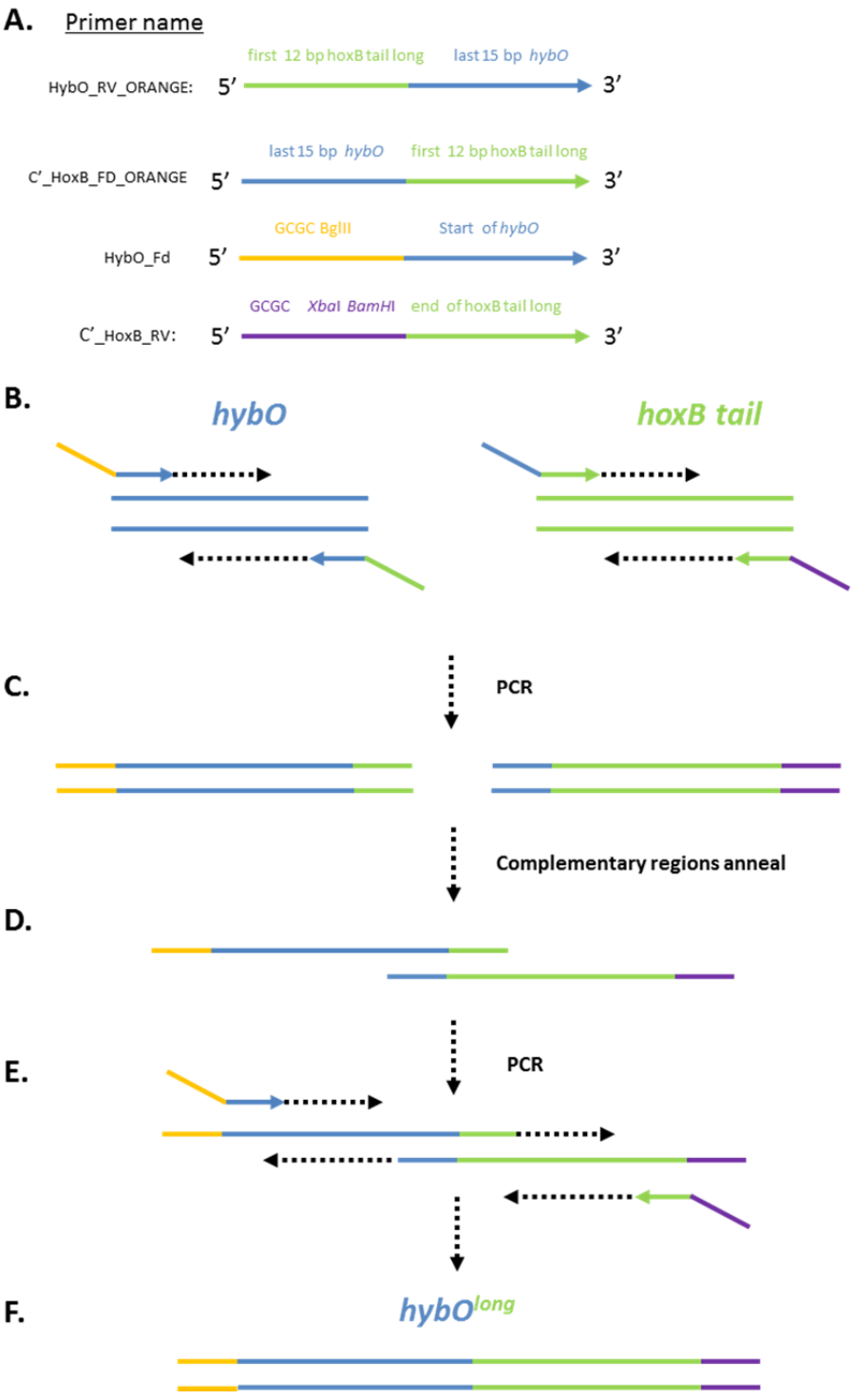

Figure 7.2 Fusion PCR. (**A**) primers used in the fusion PCR to create hybo^{long}. (**B**) Amplification of the hybO half of the final product with HybO_Fd and HybO_RV_ORANGE, and amplification of the hoxB tail (long version) with C′_HoxB_FD_ORANGE and C′_HoxB_RV. (**C**) Resultant products containing 24 bp complementarity. (**D**) When added to a new PCR reaction mixture and denatured, annealing can occur between the complementary sequences. (**E**) The polymerase uses the complementary region for extension. Addition of the two extreme primers (HybO_Fd and C′_HoxB_RV) also allows for amplification of this completely complemented DNA product. (**F**) The final product is a fusion between the two original DNA constructs. This can now be cloned into a vector using the restriction enzymes included in the original flanking primers, HybO_Fd and C′_HoxB_RV. Subsequent colony PCR can then be used to confirm correct sequence of this fusion.

7.5.13 Insertion of His-tags

His-tags were inserted onto the desired proteins, even if the gene was in the middle of an operon, by designing primers such that the entire plasmid was amplified into a linear product. Each primer, possessed the same restriction site at the immediate 5' end (bar a 4 bp overhang); the exact enzyme was chosen such that it cut nowhere else in the vector. These sites could then be used to re-circularise the PCR product by digestion and subsequent ligation. All His-tags were inserted adjacent to a TEV protease site to allow for excision of the affinity tag after purification. The high fidelity polymerase Herculase II was used for the PCR, to eliminate the chance of errors. After ligation of the PCR product, it was used to transform DH5α. Plasmids were purified from single colonies and sequenced to determine correct insertion of the His-tag. A schematic to illustrate this technique is shown in Figure 7.3.

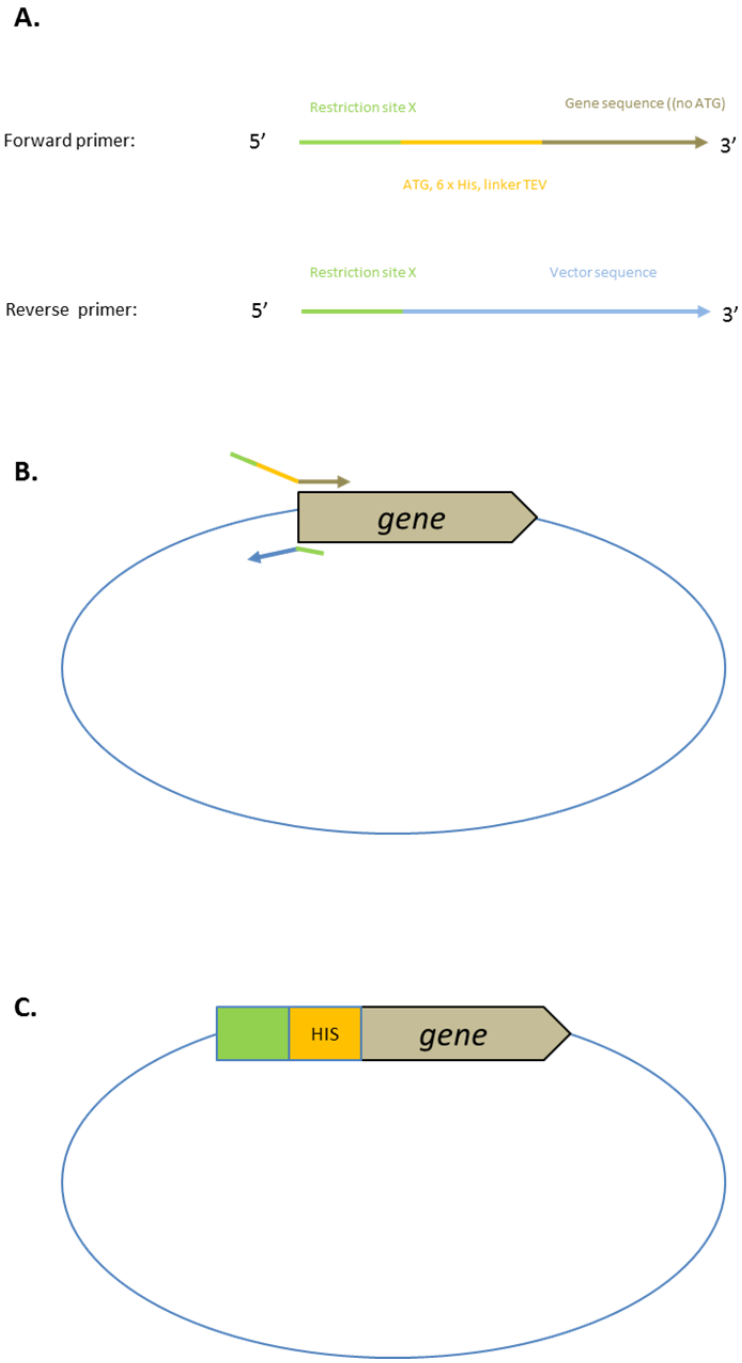

Figure 7.3 His-tag insertion schematic. Here is described the procedure to insert an N-terminal His-tag onto a protein *via* modification to the gene encoding it. The principle is the same, albeit in reverse to encode for a C-terminal His-tag. (**A**) Primers are designed with overhangs to allow for insertion of DNA sequence encoding the His-tag, along with a TEV protease site and linker region to allow for excision of the His-tag from the protein if desired. The overhangs of each primer also contain the same restriction enzyme site (X) , which is chosen such that it does not cut anywhere in the DNA template vector. (**B**) PCR is performed using the high fidelity Herculase II polymerase, forming a linear PCR product of the whole vector (not shown). (**C**) Digestion with restriction enzyme X and subsequent re-ligation allows for re-circularisation of the plasmid DNA, which now contains the gene encoding the desired His-tagged protein. Colony PCR confirms the presence of the correct vector.

7.5.14 pMAK705 homologous recombination for chromosomal gene deletion and insertion

The pmAK705 allelic exchange protocol was used to generate gene substitutions, insertions and deletions on the chromosome (Hamilton *et al*., 1989). Once the locus for the gene insertion/deletion was identified, DNA sequence corresponding to the flanking 500 bp regions upstream and downstream from said locus were cloned into the temperature sensitive suicide vector pMAK705, bookending the desired mutation in the middle. The resultant pMAK705 plasmid was then used to transform the target strain. An overnight culture was grown in LB supplemented with chloramphenicol (Cml) at 30 ^{o}C overnight. Serial dilutions were then performed (10^{-3}, 10^{-4}, 10^{-5} concentrations), and 200 µL of these plated onto LB agar supplemented with Cml. The plates were incubated at 44 ^{o}C overnight, along with a control plate of 10^{-7} dilution which was incubated at 30 ^{o}C. The temperature sensitive nature of pMAK705 means that replication cannot occur at the higher temperature, and so colonies exhibiting Cml resistance are the result of co-integration of the vector into the chromosome.

Next, 5 universals containing LB + Cml were each inoculated with five colonies and then incubated for 24 hours at 30 ^{o}C. The growth was then continued for another two cycles by transferring a loop-full of the culture into fresh LB + Cml each day. After the third day of culturing, a loop-full of each culture was streaked for single colonies onto a separate plate LB agar supplemented with Cml, which was then incubated overnight at 30 ^{o}C. During this time, the pMAK705 vector will re-circularise out of the chromosome, and either reform as it did before, still possessing the desired mutation, or recombination will occur, where the mutation will be substituted at the desired locus on the chromosome with the target gene to be replaced.

The final step was to cure the pMAK705 plasmid from the strains. To do this, twelve cultures of LB, with no antibiotic, were each inoculated with a single colony and incubated at 44 ^{o}C for 24 hours. The process was continued the next day by using a loop full of each culture to inoculate a further 12 cultures of LB media, which were incubated in the same manner. A loop of each

culture was then streaked for single colonies on LB agar with no Cml, and these plates were incubated overnight at 44 ^{o}C. Single colonies were then patched onto both LB agar with Cml, and LB agar without Cml and incubated for 30 ^{o}C overnight. Colonies exhibiting sensitivity to Cml were tested for successful integration of the desired mutation onto the chromosome by diagnostic Colony PCR.

7.5.15 DNA sequencing

DNA sequencing was performed by the DNA Sequencing Service at the School of Life Sciences, University of Dundee.

7.5.16 Synthetic operon synthesis

The optimised *hypA1-X* operon, *hypA2B2F2* and the gene encoding the $PduP_{18}$::*gapA* translation fusion were synthesised as a service by Biomatik Corporation, Ontario, Canada, and cloned into the specified vectors as listed in Table 7.6.

7.6 **Protein methods**

7.6.1 SDS-PAGE

SDS-polyacrylamide gel electrophoresis (SDS-PAGE) was used to separate denatured proteins according to their molecular mass (Laemmli, 1970). Tris-glycine SDS-PAGE gels were prepared for use with the Mini-PROTEAN II system (Bio-Rad). These consisted of both a 'resolving' region, with a typical polyacrylamide concentration between 10-12.5%, where protein bands were separated, and a 'stacking' region, where samples were loaded. The resolving gel was prepared as detailed in Table 7.10 and poured between two glass plates, leaving enough space at the top for cone insertion. A layer of isopropanol was then added on top, and the resolving gel left to polymerise. After this had occurred, the isopropanol was removed, and the stacking gel, made up as listed in Table 7.10, was quickly added. A comb was immediately inserted to allow the formation of sample wells, before the stacking gel was left to polymerise.

Resolving Gel constituents	Concentration (%)	Stacking Gel constituents	Concentration (%)
Acrylamide/bisacrylamide (37:5:1)	12-14%	Acrylamide/bisacrylamide (37:5:1)	6%
Tris.HCl pH 8.8	0.375 M	Tris.HCl pH 6.8	0.125 M
SDS	0.1% (w/v)	SDS	0.1% (w/v)
APS	0.1% (w/v)	APS	0.1% (w/v)
TEMED	0.1% (v/v)	TEMED	0.1% (v/v)

Table 7.10 Composition of the resolving and stacking gels for SDS-PAGE.

The resultant gel was submerged in a gel electrophoresis tank, which was filled with SDS running buffer. Protein samples were prepared by mixing 1:1 volume ratio with 2x Laemmli sample buffer, before heating at 100 ^{o}C for 3 minutes to allow protein denaturation to occur. A Precision Plus Protein All Blue Standards (Bio-Rad) protein marker was added in an adjacent well to the those containing the samples to allow for estimation of protein masses. The gel was run at 100 V until the dye had passed beyond the stacking/resolving gel interface, after which

the voltage was increased to 200 V until the appropriate marker had reached the bottom of the gel. To visualise protein bands, gels were then either used in semi-dry Western immunoblotting or directly visualised using Instant Blue (Expedion) stain.

7.6.2 Semi-dry Western immunoblotting

Protein samples to be analysed were first separated by SDS-PAGE as previously described. The gel was then transferred to carbonate transfer buffer (Table 7.5) for five minutes. Simultaneously, four pieces of Whatman filter paper and a piece of nitrocellulose membrane were also soaked in the same buffer. After this, two pieces of the soaked Whatman paper were placed one on top of the other on the semi-dry transfer apparatus (Bio-Rad). The nitrocellulose membrane, followed by the gel, was then placed on top of these, before the stack was completed by addition of the final two pieces of soaked filter paper. The protein bands were then transferred onto the nitrocellulose membrane by running the transfer apparatus at 175 mA for 45 minutes.

Following this, the membrane was then blocked overnight at 4 ^{o}C using TBS buffer containing 5 % milk. The blocked membrane was washed with 100 mL TBS to remove the milk solution. The membrane was then incubated with an appropriate dilution of the primary antibody serum in either TBS-Tween or TBS buffer containing 1 % milk/ 0.5% BSA for 1 hour at room temperature with shaking.

After this time the membrane was washed three times with 100 mL TBS-Tween to remove excess unbound antibody. If a secondary antibody was required, the process was repeated for this. The immunoreactive protein bands were visualised using Clarity Western ECL substrate kit (Bio-Rad) and either exposure to medical film (Konica Minolta), which was then developed in a medical film processor (SRX-101A, Konica Minolta), or by detected by a CCD camera (GeneGNOME XRQ, Syngene).

7.6.3 Determining protein concentrations

The DC Protein Assay kit (Bio-Rad) was used to determine sample protein concentration, following a modified method for a Lowry Assay (Lowry *et al*., 1951). A standard curve using bovine serum albumin (BSA) was generated for each performance of the assay, and this was used to calculate protein concentration in the samples.

7.6.4 ^{35}S-Methionine radiolabelling

The *E. coli* strain K38 (containing plasmid pGP1-2 encoding T7 RNA polymerase) (Tabor and Richardson, 1985) was transformed with the genes of interest in plasmids containing a T7 promoter upstream of the Multi Cloning Site(s). Transformants were grown overnight in LB media at 30°C, subcultured into minimal M9 media (200 mL dH_2O, 2 mM $MgSO_4$, 0.1 mM $CaCl_2$, 0.01% (w/v) thiamine, 0.4% (w/v) glucose and 20 mL M9 salts) with all amino acids added, except methionine and cysteine, to a final concentration of 0.01%. The cultures were incubated for one hour at 30°C and then at 42°C to initiate T7 RNA polymerase transcription. Rifampicin is then added to the culture to inhibit native RNA polymerase transcription and 0.01 µCi of ^{35}S-Met was added to a 1 mL aliquot of cells. Following a 30 minute incubation, samples were run on an SDS-PAGE gel and visualised by autoradiography using an SRX-101A medical film processor (Konica Minolta).

7.6.5 Purification of His-tagged proteins by nickel affinity chromatography

After cultures were grown for protein purification as specified, cells were harvested by centrifugation at 5009 x g for 20 minutes. Resuspension was performed in 50 mL Ni-purification buffer A (Table 7.5) supplemented with DNase I (Sigma-Aldrich), lysozyme (Sigma-Aldrich) and a tablet of c0mpleteEDTA-free protease inhibitor (Sigma-Aldrich). This mixture

was mixed at room temperature for 20 minutes, after which cells were further lysed by passing through an Emulsiflex C-3 cell disruptor (Avestin) three times. The lysis mixture was then centrifuged at 17,387 x g for 15 minutes to pellet the cell debris.

The supernatant was then used in nickel-affinity chromatography to isolate the His-tagged proteins, which was performed using an ÄKTA FPLC system (Amersham Biosciences). Crude extracts were applied to 5 mL HisTrap HP affinity columns (GE Healthcare) at a flow rate of 1 mL min^{-1}, which had been previously equilibrated with Ni-purification buffer A. Ten column volumes of Ni-purification buffer A were used to wash any unbound protein from the column. A linear gradient of 0-100% Ni-purification buffer B was then applied to the column to elute bound proteins over a time period of 30 minutes, with a flow rate of 1.5 mL min^{-1}. Eluted protein was collected in 1 mL fraction tubes, where subsequent analysis could take place. Protein fractions were then concentrated using a Vivaspin 10 kDa cut off spin concentrator (Sartorius).

7.7 **Hydrogenase *in vitro* activity assays**

7.7.1 Redox dye-linked hydrogenase assay

The hydrogenase assay allows for assessment of the *in vitro* hydrogen oxidation activity of enzymes, *via* coupling to the reduction of an artificial electron acceptor, which in this Thesis were the redox dyes benzyl viologen (BV) or methyl viologen (MV). Whereas the oxidised forms of these dyes are colourless, the reduced forms are purple, and so this colour change can be quantified by measuring the absorbance at 600 nm (A_{600}) in a spectrophotometer. The protocol was performed as described in (Palmer *et al*., 2010). Specifically, 3 glass balls were inserted into a quartz cuvette, before being filled 1.8 mL H_2-saturated Tris.HCl pH7.5 buffer with a final concentration of 14 mM BV/MV. This was titrated with a 1 % (w/v) sodium dithionite solution until A_{600} was stead between 0.3-0.7. The biological sample was then added to the cuvette and the resultant reduction of the redox dye measured at A_{600} at room temperature.

Purified protein or cell crude extract was used as the sample in the assay. Crude extracts were prepared by first washing cells twice with N_2-bubbled 50 mM Tris.HCl pH 7.5. They were then resuspended in 2 mL of 50 mM Tris.HCl pH 7.5, lysozyme and DNase added, followed by agitation and bubbling with N_2 at 0 ^{o}C for 30 mins. Cell lysis by French Press (8000 psi) was then carried out and crude extracts prepared by centrifugation. The protein concentration in such samples was determined by the Lowry method (Section 7.6.3). This, taken with the volume of sample added to the cuvette, allowed the mg protein added to be calculated. This could then be used in conjunction with the other variables listed in Equation 7.2 to determine the specific hydrogenase activity of the sample.

$$\mu M \text{ reduced MV/BV } mg^{-1} min^{-1} = \frac{\Delta A_{600}\ min^{-1} \times \text{cuvette volume (L)} \times 1000}{2 \times \varepsilon_{600}\ (mM^{-1}\ cm^{-1}) \times \text{protein (mg)/cells (g)} \times \text{path length (cm)}}$$

Equation 7.2 Determination of hydrogenase activity. ε_{600}BV = 7.4 mM^{-1} cm^{-1}; ε_{600}MV = 13.7 mM^{-1} cm^{-1}; cuvette volume = 0.0018 L; path length = 1 cm

7.8 **Gas chromatography (GC)**

The *in vivo* H_2 evolution of whole cells was measured *via* gas chromatography. Hungate tubes containing 5 mL of specified media was inoculated with 50 µL of pre-culture, unless otherwise stated. Incubation was then carried out in all cases at 37 ^{o}C, with tubes inverted to prevent any escape of H_2. Headspace hydrogen was quantified using a gas chromatograph (Shimadzu GC-2014). Nitrogen was used as the carrier gas with a flowrate of 25 mL min^{-1}, and the total amount of hydrogen in the headspace (10 mL) was calculated based on a standard curve. Although the data analysis software (LabSolutions lite) had an automatic peak integration tool, often the amount of H_2 in the headspace was too small to be detected in this manner. When this occurred, the H_2 peak was manually integrated. Values were normalised by considering the relative optical density (OD_{600}) of the cultures and the culture volume.

7.9 ***In vivo* biosensor activity assays**

7.9.1 Blue plate test

A blue plate assay was performed to analyse the expression of *lacZ* in response to H_2 levels in an attempt to assess the functionality of the biosensor system. LB agar plates supplemented with 0.5 % (w/v) glucose, 20 μg mL^{-1} X-gal and appropriate antibiotics were used. Successful transformants were grown overnight mL LB and appropriate antibiotics, after which a loop of culture was taken an streaked onto the plates described above. These were then incubated for 24 hours at 37 ^{o}C in either aerobic atmospheric conditions or in a 100% H_2 atmosphere.

For aerobic conditions, the plates were merely placed in a warm room set to 37 ^{o}C for the duration of the incubation. For generation of H_2 atmosphere, the plates were placed in an airtight Anaerobic Jar (Equitron) along with a 2.5 L anaerobic atmosphere generation sachet (Anaerogen). Furthermore, an Anaerobic Indicator Strip (Oxoid) was used to confirm anoxia. The jar lid was sealed, before the air inside the jar was replaced with H_2 by flushing three times with 100% hydrogen gas. A slight overpressure (1.5 atmospheres) of H_2 was maintained to prevent entry of O_2. The sealed jar was then incubated at 37 ^{o}C for 24 hours. After growth, plates were placed at 4^{o}C for 6 hours to assist in development of the blue colour, after which the plates were analysed.

7.9.2 β-gal assay

The β-galactosidase assay used was based on the protocol previously described (Reynolds *et al*., 1997). After growth of cultures, the cells were harvested by centrifugation at 2773 x *g* for 1 minute, washed with Z buffer, then resuspended in 5 mL Z buffer. The OD_{600} of the cultures was then measured, and the cultures placed on ice. 0.8 mL of culture was then placed in an Eppendorf, and 1 drop of 0.1 % SDS along with 2 drops of chloroform added using a Pasteur

pipette to lyse the cells. This was assisted *via* vortexing for 10 seconds. After this samples were equilibrated for 15 minutes in a waterbath set to 30 ^{o}C.

To start the assay, 0.2 mL of ONPG solution was added, followed by a 5 second vortex, followed by returning to the 30 ^{o}C waterbath. At this time a timer was started. When a noticeable yellow colour had developed, the reaction was stopped by addition of 0.5 mL of 1M Na_2CO_3. The time elapsed at this point was noted. The cell debris was pelleted by centrifugation at 2773 x *g* for 1 minute, before the OD_{420} and OD_{550} of the resultant supernatant was measured. The β-gal activity in Miller Units was then calculated using Equation 7.3.

$$\text{β-gal activity (Miller Units)} = \frac{1000 \times (OD_{420} - 1.75 \times OD_{550})}{\text{Time (seconds)} \times \text{Volume (mL)} \times OD_{600}}$$

Equation 7.3 Calculation of β-gal activity. Volume used in assay: 0.8 mL, Time: time of reaction, OD_{600}: cell density at start of reaction, OD_{420}: combination of absorbance by O-nitrophenol and light scattered by cell debris. OD_{550}: light scattering by cell debris.

For each sample, each OD reading was measured three times and the average taken as the sample value. Samples were assessed in triplicate.

7.9.3 Live/die screen plate assay

The Live/Die assay was performed as described in Chapter 3. When plates were to be grown in anaerobic conditions, they were placed in an airtight Anaerobic Jar (Equitron) along with an 2.5 L anaerobic atmosphere generation sachet (Anaerogen). Furthermore, an Anaerobic Indicator Strip (Oxoid) was used to confirm anoxia. When plates were to be incubated in 100 % H_2, the same process was undertaken as described in Section 7.9.1.

After growth, the plates were placed face-up on a black cloth, with the lid taken off and evenly illuminated. Photos were taken from above using a mounted Nikon D3200 digital camera. In order to better resolve colonies, all photos were altered to the same specifications in Adobe Photoshop. These were firstly converting the image to grayscale, then altering the three input levels in the ‘Layers’ setting to 3, 0.43 and 161 respectively.

7.10 High-performance liquid chromatography (HPLC) analysis of organic acids

After cell culturing in the specified media, cells were pelleted by centrifugation and discarded, before the culture supernatant was passed through a 0.2 µm filter to remove any remaining cells or debris. This resultant 'fermentation broth' was analysed with using a Dionex Ultimate 3000 HPLC system and an Aminex HPX-87H organic-acid column. The HPLC was carried out at 0.7 mL min^{-1} and 55 °C. Extracellular organic acid levels were detected by UV absorption at 210 nm. A standard curve of organic acid standards was prepared (R^2: 99.90%) and used to identify and quantify concentrations of lactate, formate, acetate, succinate and pyruvate. Sample concentrations were normalised by cell pellet wet weight. The concentrations of compounds in uninoculated media were subtracted to reveal changes in each metabolite after culture growth.

7.11 **Cell fractionation**

Cells were fractioned into crude total membrane and soluble cytoplasmic fractions to determine whether proteins were membrane-associated. Fractionation was performed on cells grown anaerobically in 500 mL LB containing specified supplements and antibiotics at 37 ^{o}C. Cells were harvested by centrifugation at 2773 x *g* for 10 minutes and washed in 50 mM Tris.HCl pH 7.5. The wet weight of the pellet was then measured, before the pellet was resuspended in 10 mL 50 mM Tris.HCl pH 7.5 per 1 g wet weight, and gently homogenised. 100 µL of this was taken as the 'Whole Cell' fraction. The suspension was then treated 5 mM EDTA, 6 mg mL^{-1} lysozyme and 60 mg mL^{-1} DNase I. Cells were then lysed by three passages through a French pressure cell (piston diameter 2/8'', Thermo Scientific) at 8000 psi, after which the cell debris and remnant un-lysed cells were spun down at 27,000 x *g* for 20 minutes. The top 1 mL of the supernatant was then centrifuged at 278,000 x *g* for 30 minutes at 4 ^{o}C in an Optima MAX-E bench-top ultracentrifuge with a TLA-100.2 rotor (Beckman) to separate the soluble and membrane fractions. 100 µL of supernatant was kept as the 'Soluble' fraction, and the remaining supernatant discarded. The insoluble pellet was resuspended in 1 mL 50 mM Tris.HCl pH 7.5, and 100 µL of this kept as the 'Membrane' fraction. All cellular fractions were mixed with 100 µL Laemmli buffer for subsequent analysis by SDS-PAGE and Western blotting.

8. Bibliography

Agapakis, C.M., Ducat, D.C., Boyle, P.M., Wintermute, E.H., Way, J.C., and Silver, P.A. (2010). Insulation of a synthetic hydrogen metabolism circuit in bacteria. Journal of biological engineering *4*, 1-15.

Aki, H., Murata, A., Yamamoto, S., Kondoh, J., Maeda, T., Yamaguchi, H., and Ishii, I. (2005). Penetration of residential fuel cells and CO_2 mitigation – case studies in Japan by multi-objective models. International journal of hydrogen energy *30*, 943-952.

Albracht, S.P., and Hedderich, R. (2000). Learning from hydrogenases: location of a proton pump and of a second FMN in bovine NADH--ubiquinone oxidoreductase (Complex I). FEBS letters *485*, 1-6.

Andrews, S.C., Berks, B.C., McClay, J., Ambler, A., Quail, M.A., Golby, P., and Guest, J.R. (1997). A 12-cistron *Escherichia coli* operon (*hyf*) encoding a putative proton-translocating formate hydrogenlyase system. Microbiology *143*, 3633-3647.

Antolini, E. (2009). Palladium in fuel cell catalysis. Energy and environmental science *2*, 915-931.

Atlung, T., Knudsen, K., Heerfordt, L., and Brøndsted, L. (1997). Effects of sigmaS and the transcriptional activator AppY on induction of the *Escherichia coli hya* and *cbdAB-appA* operons in response to carbon and phosphate starvation. Journal of bacteriology *179*, 2141-2146.

Baba, T., Ara, T., Hasegawa, M., Takai, Y., Okumura, Y., Baba, M., Datsenko, K.A., Tomita, M., Wanner, B.L., and Mori, H. (2006). Construction of *Escherichia coli* K-12 in-frame, single-gene knockout mutants: the Keio collection. Molecular systems biology *2*, 2006 0008.

Badura, A., Esper, B., Ataka, K., Grunwald, C., Woll, C., Kuhlmann, J., Heberle, J., and Rogner, M. (2006). Light-driven water splitting for (bio-)hydrogen production: photosystem 2 as the central part of a bioelectrochemical device. Photochemistry and photobiology *82*, 1385-1390.

Ball, M., and Wietschel, M. (2009). The Hydrogen economy. In Opportunities and Challenges (Cambridge: Cambridge University Press).

Ballantine, S.P., and Boxer, D.H. (1985). Nickel-containing hydrogenase isoenzymes from anaerobically grown *Escherichia coli* K-12. Journal of bacteriology *163*, 454-459.

Ballantine, S.P., and Boxer, D.H. (1986). Isolation and characterisation of a soluble active fragment of hydrogenase isoenzyme 2 from the membranes of anaerobically grown *Escherichia coli*. European journal of biochemistry *156*, 277-284.

Baradaran, R., Berrisford, J.M., Minhas, G.S., and Sazanov, L.A. (2013). Crystal structure of the entire respiratory complex I. Nature *494*, 443-448.

Barilone, J.L., Ogata, H., Lubitz, W., and van Gastel, M. (2015). Structural differences between the active sites of the Ni-A and Ni-B states of the [NiFe] hydrogenase: an approach by quantum chemistry and single crystal ENDOR spectroscopy. Physical chemistry chemical physics *17*, 16204-16212.

Barreto, L., Makihira, A., and Riahi, K. (2003). The hydrogen economy in the 21st century: a sustainable development scenario. International journal of hydrogen energy *28*, 267-284.

Barstow, B., Agapakis, C.M., Boyle, P.M., Grandl, G., Silver, P.A., and Wintermute, E.H. (2011). A synthetic system links FeFe-hydrogenases to essential *E. coli* sulfur metabolism. Journal of biological engineering *5*, 7-7.

Bartelings, H., van Beukering, P., Kuik, O., Linderhof, V., Oosterhuis, F., Brander, L., and Wagtendonk, A. (2005). Effectiveness of landfill taxation (Amsterdam: Institute for Environmental Studies, Vrije Universiteit,).

Bartolome, B., Jubete, Y., Martinez, E., and de la Cruz, F. (1991). Construction and properties of a family of pACYC184-derived cloning vectors compatible with pBR322 and its derivatives. Gene *102*, 75-78.

Beja, O., Aravind, L., Koonin, E.V., Suzuki, M.T., Hadd, A., Nguyen, L.P., Jovanovich, S.B., Gates, C.M., Feldman, R.A., Spudich, J.L.*, et al.* (2000). Bacterial rhodopsin: evidence for a new type of phototrophy in the sea. Science *289*, 1902-1906.

Benemann, J. (1996). Hydrogen biotechnology: progress and prospects. Nature biotechnology *14*, 1101-1103.

Benner, S.A., and Sismour, A.M. (2005). Synthetic biology. Nature reviews genetics *6*, 533-543.

Berks, B.C., Page, M.D., Richardson, D.J., Reilly, A., Cavill, A., Outen, F., and Ferguson, S.J. (1995). Sequence analysis of subunits of the membrane-bound nitrate reductase from a

denitrifying bacterium: the integral membrane subunit provides a prototype for the dihaem electron-carrying arm of a redox loop. Molecular microbiology *15*, 319-331.

Berney, M., and Cook, G.M. (2010). Unique flexibility in energy metabolism allows mycobacteria to combat starvation and hypoxia. PLoS One *5*, e8614.

Bernhard, M., Benelli, B., Hochkoeppler, A., Zannoni, D., and Friedrich, B. (1997). Functional and structural role of the cytochrome *b* subunit of the membrane-bound hydrogenase complex of *Alcaligenes eutrophus* H16. European journal of biochemistry *248*, 179-186.

Bernhard, M., Buhrke, T., Bleijlevens, B., De Lacey, A.L., Fernandez, V.M., Albracht, S.P., and Friedrich, B. (2001). The H_2 sensor of *Ralstonia eutropha*. Biochemical characteristics, spectroscopic properties, and its interaction with a histidine protein kinase. Journal of biological chemistry *276*, 15592-15597.

Birkmann, A., Zinoni, F., Sawers, G., and Bock, A. (1987). Factors affecting transcriptional regulation of the formate-hydrogen-lyase pathway of *Escherichia coli*. Archives of microbiology *148*, 44-51.

Black, L.K., Fu, C., and Maier, R.J. (1994). Sequences and characterization of *hupU* and *hupV* genes of *Bradyrhizobium japonicum* encoding a possible nickel-sensing complex involved in hydrogenase expression. Journal of bacteriology *176*, 7102-7106.

Blackwood, E.M., and Kadonaga, J.T. (1998). Going the distance: a current view of enhancer action. Science *281*, 60-63.

Blamey, J.M., and Adams, M.W. (1994). Characterization of an ancestral type of pyruvate ferredoxin oxidoreductase from the hyperthermophilic bacterium, *Thermotoga maritima*. Biochemistry *33*, 1000-1007.

Blbulyan, S., and Trchounian, A. (2015). Impact of membrane-associated hydrogenases on the F_0F_1-ATPase in *Escherichia coli* during glycerol and mixed carbon fermentation: ATPase activity and its inhibition by N,N'-dicyclohexylcarbodiimide in the mutants lacking hydrogenases. Archives of biochemistry and biophysics *579*, 67-72.

Bleijlevens, B., Buhrke, T., van der Linden, E., Friedrich, B., and Albracht, S.P. (2004). The auxiliary protein HypX provides oxygen tolerance to the soluble [NiFe]-hydrogenase of *Ralstonia eutropha* H16 by way of a cyanide ligand to nickel. Journal of biological chemistry *279*, 46686-46691.

Blokesch, M., Magalon, A., and Bock, A. (2001). Interplay between the specific chaperone-like proteins HybG and HypC in maturation of hydrogenases 1, 2, and 3 from *Escherichia coli*. Journal of bacteriology *183*, 2817-2822.

Blokesch, M., Paschos, A., Theodoratou, E., Bauer, A., Hube, M., Huth, S., and Bock, A. (2002). Metal insertion into NiFe-hydrogenases. Biochemical society transactions *30*, 674-680.

Blokesch, M., Rohrmoser, M., Rode, S., and Bock, A. (2004). HybF, a zinc-containing protein involved in NiFe hydrogenase maturation. Journal of bacteriology *186*, 2603-2611.

Bobik, T.A., Havemann, G.D., Busch, R.J., Williams, D.S., and Aldrich, H.C. (1999). The propanediol utilization (pdu) operon of *Salmonella enterica* serovar Typhimurium LT2 includes genes necessary for formation of polyhedral organelles involved in coenzyme B_{12}-dependent 1, 2-propanediol degradation. Journal of bacteriology *181*, 5967-5975.

Bock, A., King, P.W., Blokesch, M., and Posewitz, M.C. (2006). Maturation of hydrogenases. Advances in microbial physiology *51*, 1-71.

Bohm, R., Sauter, M., and Bock, A. (1990). Nucleotide sequence and expression of an operon in *Escherichia coli* coding for formate hydrogenlyase components. Molecular microbiology *4*, 231-243.

Bonocora, R.P., Smith, C., Lapierre, P., and Wade, J.T. (2015). Genome-scale mapping of *Escherichia coli* σ^{54} reveals widespread, conserved intragenic binding. PLoS genetics *11*, e1005552.

Booth, I.R. (2005). Glycerol and methylglyoxal metabolism. EcoSal Plus *1*.

Borgnia, M.J., and Agre, P. (2001). Reconstitution and functional comparison of purified GlpF and AqpZ, the glycerol and water channels from *Escherichia coli*. Proceedings of the national academy of science USA *98*, 2888-2893.

Bothe, H., Schmitz, O., Yates, M.G., and Newton, W.E. (2010). Nitrogen fixation and hydrogen metabolism in cyanobacteria. Microbiology and molecular biology reviews *74*, 529-551.

Bowman, L., Flanagan, L., Fyfe, P.K., Parkin, A., Hunter, W.N., and Sargent, F. (2014). How the structure of the large subunit controls function in an oxygen-tolerant [NiFe]-hydrogenase. Biochemical journal *458*, 449-458.

Bramkamp, M., and Lopez, D. (2015). Exploring the existence of lipid rafts in bacteria. Microbiology and molecular biology reviews *79*, 81-100.

Braunegg, G., Lefebvre, G., and Genser, K.F. (1998). Polyhydroxyalkanoates, biopolyesters from renewable resources: physiological and engineering aspects. Journal of biotechnology *65*, 127-161.

Brugna-Guiral, M., Tron, P., Nitschke, W., Stetter, K.O., Burlat, B., Guigliarelli, B., Bruschi, M., and Giudici-Orticoni, M.T. (2003). [NiFe] hydrogenases from the hyperthermophilic bacterium *Aquifex aeolicus*: properties, function, and phylogenetics. Extremophiles *7*, 145-157.

Buhrke, T., Bleijlevens, B., Albracht, S.P.J., and Friedrich, B. (2001). Involvement of *hyp* gene products in maturation of the H_2-Sensing [NiFe] Hydrogenase of *Ralstonia eutropha*. Journal of bacteriology *183*, 7087-7093.

Buhrke, T., and Friedrich, B. (1998). HoxX (hypX) is a functional member of the *Alcaligenes eutrophus hyp* gene cluster. Archives of microbiology *170*, 460-463.

Buhrke, T., Lenz, O., Krauss, N., and Friedrich, B. (2005a). Oxygen tolerance of the H_2-sensing [NiFe] hydrogenase from *Ralstonia eutropha* H16 is based on limited access of oxygen to the active site. Journal of biological chemistry *280*, 23791-23796.

Buhrke, T., Lenz, O., Porthun, A., and Friedrich, B. (2004). The H_2-sensing complex of *Ralstonia eutropha*: interaction between a regulatory [NiFe] hydrogenase and a histidine protein kinase. Molecular microbiology *51*, 1677-1689.

Buhrke, T., Loscher, S., Lenz, O., Schlodder, E., Zebger, I., Andersen, L.K., Hildebrandt, P., Meyer-Klaucke, W., Dau, H., Friedrich, B.*, et al.* (2005b). Reduction of unusual iron-sulfur clusters in the H_2-sensing regulatory Ni-Fe hydrogenase from *Ralstonia eutropha* H16. Journal of biological chemistry *280*, 19488-19495.

Burgdorf, T., Lenz, O., Buhrke, T., van der Linden, E., Jones, A.K., Albracht, S.P., and Friedrich, B. (2005a). [NiFe]-hydrogenases of *Ralstonia eutropha* H16: modular enzymes for oxygen-tolerant biological hydrogen oxidation. Journal of molecular microbiology and biotechnology *10*, 181-196.

Burgdorf, T., van der Linden, E., Bernhard, M., Yin, Q.Y., Back, J.W., Hartog, A.F., Muijsers, A.O., de Koster, C.G., Albracht, S.P., and Friedrich, B. (2005b). The soluble NAD^+-Reducing

[NiFe]-hydrogenase from *Ralstonia eutropha* H16 consists of six subunits and can be specifically activated by NADPH. Journal of bacteriology *187*, 3122-3132.

Burstel, I., Hummel, P., Siebert, E., Wisitruangsakul, N., Zebger, I., Friedrich, B., and Lenz, O. (2011). Probing the origin of the metabolic precursor of the CO ligand in the catalytic center of [NiFe] hydrogenase. Journal of biological chemistry *286*, 44937-44944.

Burstel, I., Siebert, E., Winter, G., Hummel, P., Zebger, I., Friedrich, B., and Lenz, O. (2012). A universal scaffold for synthesis of the $Fe(CN)_2(CO)$ moiety of [NiFe] hydrogenase. Journal of biological chemistry *287*, 38845-38853.

Casadaban, M.J., (1976). Transposition and fusion of the lac genes to selected promoters in *Escherichia coli* using bacteriophage lambda and Mu. Journal of molecular biology *104*, 541-555

Caffrey, S.M., Park, H.-S., Voordouw, J.K., He, Z., Zhou, J., and Voordouw, G. (2007). Function of periplasmic hydrogenases in the sulfate-reducing bacterium *Desulfovibrio vulgaris* Hildenborough. Journal of bacteriology *189*, 6159-6167.

Callen, B.P., Shearwin, K.E., and Egan, J.B. (2004). Transcriptional interference between convergent promoters caused by elongation over the promoter. Molecular cell *14*, 647-656.

Cameron, D.E., Bashor, C.J., and Collins, J.J. (2014). A brief history of synthetic biology. Nature reviews microbiology *12*, 381-390.

Carlson, R. (2009). The changing economics of DNA synthesis. Nature biotechnology *27*, 1091-1094.

Cartron, M.L., Maddocks, S., Gillingham, P., Craven, C.J., and Andrews, S.C. (2006). Feo – transport of ferrous iron into bacteria. Biometals *19*, 143-157.

Ceccaldi, P., Etienne, E., Dementin, S., Guigliarelli, B., Léger, C., and Burlat, B. (2016). Mechanism of inhibition of NiFe hydrogenase by nitric oxide. Biochimica et biophysica acta bioenergetics *1857*, 454-461.

Chabriere, E., Charon, M.H., Volbeda, A., Pieulle, L., Hatchikian, E.C., and Fontecilla-Camps, J.C. (1999). Crystal structures of the key anaerobic enzyme pyruvate:ferredoxin oxidoreductase, free and in complex with pyruvate. Nature structural and molecular biology *6*, 182-190.

Chakrabarti, P., and Pal, D. (2001). The interrelationships of side-chain and main-chain conformations in proteins. Progress in biophysics and molecular biology *76*, 1-102.

Chang, C.H., King, P.W., Ghirardi, M.L., and Kim, K. (2007). Atomic resolution modeling of the ferredoxin:[FeFe] hydrogenase complex from *Chlamydomonas reinhardtii*. Biophysical journal *93*, 3034-3045.

Chen, H.C. (2014). Biotechnology of lignocellulose. Theory and Practice (Springer Netherlands).

Chen, X., Schreiber, K., Appel, J., Makowka, A., Fahnrich, B., Roettger, M., Hajirezaei, M.R., Sonnichsen, F.D., Schonheit, P., Martin, W.F.*, et al.* (2016). The Entner-Doudoroff pathway is an overlooked glycolytic route in cyanobacteria and plants. Proceedings of the national academy of science USA *113*, 5441-5446.

Chen, X., Zaro, J.L., and Shen, W.C. (2013). Fusion protein linkers: property, design and functionality. Advanced drug delivery reviews *65*, 1357-1369.

Chen, Z., and Zeng, A.P. (2013). Protein design in systems metabolic engineering for industrial strain development. Biotechnology journal *8*, 523-533.

Cheng, S., Liu, Y., Crowley, C.S., Yeates, T.O., and Bobik, T.A. (2008). Bacterial microcompartments: their properties and paradoxes. Bioessays *30*, 1084-1095.

Cheng, S., Sinha, S., Fan, C., Liu, Y., and Bobik, T.A. (2011). Genetic analysis of the protein shell of the microcompartments involved in coenzyme B_{12}-dependent 1,2-propanediol degradation by *Salmonella*. Journal of bacteriology *193*, 1385-1392.

Chung, C.T., and Miller, R.H. (1988). A rapid and convenient method for the preparation and storage of competent bacterial cells. Nucleic acids research *16*, 3580.

Chung, K.C., and Zamble, D.B. (2011). The *Escherichia coli* metal-binding chaperone SlyD interacts with the large subunit of [NiFe]-hydrogenase 3. FEBS letters *585*, 291-294.

Cobb, R.E., Si, T., and Zhao, H. (2012). Directed evolution: an evolving and enabling synthetic biology tool. Current opinion in chemical biology *16*, 285-291.

Constant, P., Chowdhury, S.P., Hesse, L., Pratscher, J., and Conrad, R. (2011). Genome data mining and soil survey for the novel group 5 [NiFe]-hydrogenase to explore the diversity and ecological importance of presumptive high-affinity H_2-oxidizing bacteria. Applied and environmental microbiology *77*, 6027-6035.

Constant, P., Chowdhury, S.P., Pratscher, J., and Conrad, R. (2010). Streptomycetes contributing to atmospheric molecular hydrogen soil uptake are widespread and encode a putative high-affinity [NiFe]-hydrogenase. Environmental microbiology *12*, 821-829.

Constant, P., Poissant, L., and Villemur, R. (2009). Tropospheric H_2 budget and the response of its soil uptake under the changing environment. Science of the total environment *407*, 1809-1823.

Cracknell, J.A., Vincent, K.A., and Armstrong, F.A. (2008). Enzymes as working or inspirational electrocatalysts for fuel cells and electrolysis. Chemical reviews *108*, 2439-2461.

Crowley, C.S., Cascio, D., Sawaya, M.R., Kopstein, J.S., Bobik, T.A., and Yeates, T.O. (2010). Structural insight into the mechanisms of transport across the *Salmonella enterica* Pdu microcompartment shell. Journal of biological chemistry *285*, 37838-37846.

Cuendet, P., Rao, K.K., Gratzel, M., and Hall, D.O. (1986). Light induced H_2 evolution in a hydrogenase-TiO_2 particle system by direct electron transfer or *via* rhodium complexes. Biochimie *68*, 217-221.

Davies, J., and Davies, D. (2010). Origins and evolution of antibiotic resistance. Microbiology and molecular biology reviews *74*, 417-433.

Davila-Vazquez, G., Arriaga, S., Alatriste-Mondragón, F., de León-Rodríguez, A., Rosales-Colunga, L.M., and Razo-Flores, E. (2008). Fermentative biohydrogen production: trends and perspectives. Reviews in environmental science and biotechnology *7*, 27-45.

DeLano, W.L. (2002). The PyMOL molecular graphics system, version 1.8 Schrödinger, LLC. (San Carlos, CA: CA: DeLano Scientific;).

Delebecque, C.J., Lindner, A.B., Silver, P.A., and Aldaye, F.A. (2011). Organization of intracellular reactions with rationally designed RNA assemblies. Science *333*, 470-474.

Deplanche, K., Caldelari, I., Mikheenko, I.P., Sargent, F., and Macaskie, L.E. (2010). Involvement of hydrogenases in the formation of highly catalytic Pd(0) nanoparticles by bioreduction of Pd(II) using *Escherichia coli* mutant strains. Microbiology *156*, 2630-2640.

Dharmadi, Y., Murarka, A., and Gonzalez, R. (2006). Anaerobic fermentation of glycerol by *Escherichia coli*: a new platform for metabolic engineering. Biotechnology and bioengineering *94*, 821-829.

Dias, A.V., Mulvihill, C.M., Leach, M.R., Pickering, I.J., George, G.N., and Zamble, D.B. (2008). Structural and biological analysis of the metal sites of *Escherichia coli* hydrogenase accessory protein HypB. Biochemistry *47*, 11981-11991.

Doberenz, C., Zorn, M., Falke, D., Nannemann, D., Hunger, D., Beyer, L., Ihling, C.H., Meiler, J., Sinz, A., and Sawers, R.G. (2014). Pyruvate formate-lyase interacts directly with the formate channel FocA to regulate formate translocation. Journal of molecular biology *426*, 2827-2839.

Drapal, N., and Bock, A. (1998). Interaction of the hydrogenase accessory protein HypC with HycE, the large subunit of *Escherichia coli* hydrogenase 3 during enzyme maturation. Biochemistry *37*, 2941-2948.

Dubini, A., Pye, R.L., Jack, R., L., Palmer, T., and Sargent, F. (2002). How bacteria get energy from hydrogen: a genetic analysis of periplasmic hydrogen oxidation in *Escherichia coli*. Internation journal of hydrogen energy, 1413-1420.

Dubini, A., and Sargent, F. (2003). Assembly of Tat-dependent [NiFe] hydrogenases: identification of precursor-binding accessory proteins. FEBS letters *549*, 141-146.

Duche, O., Elsen, S., Cournac, L., and Colbeau, A. (2005). Enlarging the gas access channel to the active site renders the regulatory hydrogenase HupUV of *Rhodobacter capsulatus* O_2 sensitive without affecting its transductory activity. FEBS journal *272*, 3899-3908.

Dueber, J.E., Wu, G.C., Malmirchegini, G.R., Moon, T.S., Petzold, C.J., Ullal, A.V., Prather, K.L., and Keasling, J.D. (2009). Synthetic protein scaffolds provide modular control over metabolic flux. Nature biotechnology *27*, 753-759.

Eberz, G., Eitinger, T., and Friedrich, B. (1989). Genetic determinants of a nickel-specific transport system are part of the plasmid-encoded hydrogenase gene cluster in *Alcaligenes eutrophus*. Journal of bacteriology *171*, 1340-1345.

Eberz, G., and Friedrich, B. (1991). Three trans-acting regulatory functions control hydrogenase synthesis in Alcaligenes eutrophus. Journal of bacteriology *173*, 1845-1854.

Efremov, R.G., and Sazanov, L.A. (2012). The coupling mechanism of respiratory complex I — A structural and evolutionary perspective. Biochimica et biophysica acta - bioenergetics *1817*, 1785-1795.

Energy Information Administration. (2016). Interantional energy outlook 2016 (US energy information administration).

Elsen, S., Colbeau, A., Chabert, J., and Vignais, P.M. (1996). The hupTUV operon is involved in negative control of hydrogenase synthesis in *Rhodobacter capsulatus*. Journal of bacteriology *178*, 5174-5181.

Eroglu, E., and Melis, A. (2011). Photobiological hydrogen production: Recent advances and state of the art. Bioresource technology *102*, 8403-8413.

Espah Borujeni, A., and Salis, H.M. (2016). Translation Initiation is controlled by RNA folding kinetics *via* a ribosome drafting mechanism. Journal of the American chemical society *138*, 7016-7023.

Fan, C., and Bobik, T.A. (2011). The N-terminal region of the medium subunit (PduD) packages adenosylcobalamin-dependent diol dehydratase (PduCDE) into the Pdu microcompartment. Journal of bacteriology *193*, 5623-5628.

Fan, C., Cheng, S., Liu, Y., Escobar, C.M., Crowley, C.S., Jefferson, R.E., Yeates, T.O., and Bobik, T.A. (2010). Short N-terminal sequences package proteins into bacterial microcompartments. Proceedings of the national academy of science USA *107*, 7509-7514.

Fan, C., Cheng, S., Sinha, S., and Bobik, T.A. (2012). Interactions between the termini of lumen enzymes and shell proteins mediate enzyme encapsulation into bacterial microcompartments. Proceedings of the national academy of science USA *109*, 14995-15000.

Fauque, G., Peck, H.D., Jr., Moura, J.J., Huynh, B.H., Berlier, Y., DerVartanian, D.V., Teixeira, M., Przybyla, A.E., Lespinat, P.A., Moura, I.*, et al.* (1988). The three classes of hydrogenases from sulfate-reducing bacteria of the genus Desulfovibrio. FEMS microbiology reviews *4*, 299-344.

Flamholz, A., Noor, E., Bar-Even, A., Liebermeister, W., and Milo, R. (2013). Glycolytic strategy as a tradeoff between energy yield and protein cost. Proceedings of the national academy of science USA *110*, 10039-10044.

Flanagan, L.A., Wright, J.J., Roessler, M.M., Moir, J.W., and Parkin, A. (2016). Re-engineering a NiFe hydrogenase to increase the H_2 production bias while maintaining native levels of O_2 tolerance. Chemcial communications *52*, 9133-9136.

Fontecilla-Camps, J.C., Volbeda, A., Cavazza, C., and Nicolet, Y. (2007). Structure/function relationships of [NiFe]- and [FeFe]-hydrogenases. Chemcial reviews *107*, 4273-4303.

Fox, J.D., Kerby, R.L., Roberts, G.P., and Ludden, P.W. (1996). Characterization of the CO-induced, CO-tolerant hydrogenase from *Rhodospirillum rubrum* and the gene encoding the large subunit of the enzyme. Journal of bacteriology *178*, 1515-1524.

Friedrich, B., Buhrke, T., Burgdorf, T., and Lenz, O. (2005). A hydrogen-sensing multiprotein complex controls aerobic hydrogen metabolism in *Ralstonia eutropha*. Biochemical society transactions *33*, 97-101.

Friedrich, B., Heine, E., Finck, A., and Friedrich, C.G. (1981a). Nickel requirement for active hydrogenase formation in *Alcaligenes eutrophus*. Journal of bacteriology *145*, 1144-1149.

Friedrich, C., Friedrich, B., and Bowien, B. (1981b). Formation of the enzymes of autotrophic metabolism during heterotrophic growth of *Alcaligenes eutrophus*. Journal of general microbiology *122*, 69-78.

Fritsch, J., Scheerer, P., Frielingsdorf, S., Kroschinsky, S., Friedrich, B., Lenz, O., and Spahn, C.M. (2011). The crystal structure of an oxygen-tolerant hydrogenase uncovers a novel iron-sulphur centre. Nature *479*, 249-252.

Fritsche, E., Paschos, A., Beisel, H.-G., Böck, A., and Huber, R. (1999). Crystal structure of the hydrogenase maturating endopeptidase HYBD from *Escherichia coli*. Journal of molecular biology *288*, 989-998.

Furdui, C., and Ragsdale, S.W. (2000). The role of pyruvate ferredoxin oxidoreductase in pyruvate synthesis during autotrophic growth by the Wood-Ljungdahl pathway. Journal of biological chemistry *275*, 28494-28499.

Gaffron, H., and Rubin, J. (1942). Fermentativbe and photochemcial production of hdyrogen in algae. The Journal of general physiology *26*, 219-240.

Galas, D.J., and Schmitz, A. (1978). DNAse footprinting: a simple method for the detection of protein-DNA binding specificity. Nucleic acids research *5*, 3157-3170.

Gallucci, F., Comite, A., Capannelli, G., and Basile, A. (2006). Steam reforming of methane in a membrane reactor: an industrial case study. Industrial and engineering chemistry research *45*, 2994-3000.

Garcin, E., Vernede, X., Hatchikian, E.C., Volbeda, A., Frey, M., and Fontecilla-Camps, J.C. (1999). The crystal structure of a reduced [NiFeSe] hydrogenase provides an image of the activated catalytic center. Structure *7*, 557-566.

Gest, H., and Kamen, M.D. (1949). Studies on the metabolism of photsynthetic bacteria. : photochemical production of molecular hydrogen by growing cultures of photosynthetic bacteria. Journal of bacteriology *58*, 239-245.

Ghirardi, M.L., Posewitz, M.C., Maness, P.C., Dubini, A., Yu, J., and Seibert, M. (2007). Hydrogenases and hydrogen photoproduction in oxygenic photosynthetic organisms. Annual review of plant biology *58*, 71-91.

Ghosh, D., Bisaillon, A., and Hallenbeck, P.C. (2013). Increasing the metabolic capacity of *Escherichia coli* for hydrogen production through heterologous expression of the *Ralstonia eutropha* SH operon. Biotechnology for biofuels *6*, 122.

Giel, J.L., Rodionov, D., Liu, M., Blattner, F.R., and Kiley, P.J. (2006). IscR-dependent gene expression links iron-sulphur cluster assembly to the control of O_2-regulated genes in *Escherichia coli*. Molecular microbiology *60*, 1058-1075.

Goldet, G., Wait, A.F., Cracknell, J.A., Vincent, K.A., Ludwig, M., Lenz, O., Friedrich, B., and Armstrong, F.A. (2008). Hydrogen production under aerobic conditions by membrane-bound hydrogenases from *Ralstonia* species. Journal of the American chemical society *130*, 11106-11113.

Gong, M., Zhou, W., Tsai, M.-C., Zhou, J., Guan, M., Lin, M.-C., Zhang, B., Hu, Y., Wang, D.-Y., Yang, J.*, et al.* (2014). Nanoscale nickel oxide/nickel heterostructures for active hydrogen evolution electrocatalysis. Nature communications *5*, 4695.

Gonzalez, R., Murarka, A., Dharmadi, Y., and Yazdani, S.S. (2008). A new model for the anaerobic fermentation of glycerol in enteric bacteria: trunk and auxiliary pathways in *Escherichia coli*. Metabolic engineering *10*, 234-245.

Goodman, D.B., Church, G.M., and Kosuri, S. (2013). Causes and effects of N-terminal codon bias in bacterial genes. Science *342*, 475-479.

Goulhen, F., Gloter, A., Guyot, F., and Bruschi, M. (2006). Cr(VI) detoxification by *Desulfovibrio vulgaris* strain Hildenborough: microbe-metal interactions studies. Applied microbiology and biotechnology *71*, 892-897.

Grant, S.G., Jessee, J., Bloom, F.R., and Hanahan, D. (1990). Differential plasmid rescue from transgenic mouse DNAs into *Escherichia coli* methylation-restriction mutants. Proceedings of the national academy of science USA *87*, 4645-4649.

Greening, C., Biswas, A., Carere, C.R., Jackson, C.J., Taylor, M.C., Stott, M.B., Cook, G.M., and Morales, S.E. (2016). Genomic and metagenomic surveys of hydrogenase distribution indicate H_2 is a widely utilised energy source for microbial growth and survival. Journal of the international society for microbial ecology *10*, 761-777.

Gutekunst, K., Chen, X., Schreiber, K., Kaspar, U., Makam, S., and Appel, J. (2014). The bidirectional NiFe-hydrogenase in *Synechocystis* sp. PCC 6803 is reduced by flavodoxin and ferredoxin and is essential under mixotrophic, nitrate-limiting conditions. Journal of biological chemistry *289*, 1930-1937.

Guymer, D., Maillard, J., and Sargent, F. (2009). A genetic analysis of *in vivo* selenate reduction by *Salmonella enterica* serovar Typhimurium LT2 and *Escherichia coli* K12. Archives of microbiology *191*, 519-528.

Hakobyan, M., Sargsyan, H., and Bagramyan, K. (2005). Proton translocation coupled to formate oxidation in anaerobically grown fermenting *Escherichia coli*. Biophysical chemistry *115*, 55-61.

Hallenbeck, P.C., and Benemann, J.R. (2010). Biohydrogen - The microbiological production of hydrogen fuel. In Biohydrogen - The microbiological production of hydrogen fuel, H.R. Doelle, S., ed.

Hallenbeck, P.C., and Ghosh, D. (2009). Advances in fermentative biohydrogen production: the way forward? Trends in biotechnology *27*, 287-297.

Hallenbeck, P.C., and Ghosh, D. (2012). Improvements in fermentative biological hydrogen production through metabolic engineering. Journal of environmental management *95 Suppl*, S360-364.

Hamilton, C.M., Aldea, M., Washburn, B.K., Babitzke, P., and Kushner, S.R. (1989). New method for generating deletions and gene replacements in *Escherichia coli*. Journal of bacteriology *171*, 4617-4622.

Happe, R.P., Roseboom, W., Egert, G., Friedrich, C.G., Massanz, C., Friedrich, B., and Albracht, S.P. (2000). Unusual FTIR and EPR properties of the H_2-activating site of the cytoplasmic NAD-reducing hydrogenase from *Ralstonia eutropha*. FEBS letters *466*, 259-263.

Harklau, H., Ljones, T., and Skjeldal, L. (2001). Oxygen disruption of the 2[4Fe-4S] clusters in *Clostridium pasteurianum* ferredoxin shown by 1H-NMR. Journal of inorganic biochemistry *85*, 117-122.

Hartwig, S., Thomas, C., Krumova, N., Quitzke, V., Turkowsky, D., Jehmlich, N., Adrian, L., and Sawers, R.G. (2015). Heterologous complementation studies in *Escherichia coli* with the Hyp accessory protein machinery from *Chloroflexi* provide insight into [NiFe]-hydrogenase large subunit recognition by the HypC protein family. Microbiology *161*, 2204-2219

Häussinger, P., Lohmüller, R., and Watson, A., eds. (2011). Ullmann's encyclopedia of industrial chemistry (Weinheim: Viley-VCH).

Havemann, G.D., and Bobik, T.A. (2003). Protein content of polyhedral organelles involved in coenzyme B_{12}-dependent degradation of 1,2-propanediol in *Salmonella enterica* serovar Typhimurium LT2. Journal of bacteriology *185*, 5086-5095.

Havemann, G.D., Sampson, E.M., and Bobik, T.A. (2002). PduA is a shell protein of polyhedral organelles involved in coenzyme B_{12}-dependent degradation of 1,2-propanediol in *Salmonella enterica* serovar typhimurium LT2. Journal of bacteriology *184*, 1253-1261.

Heinzinger, N.K., Fujimoto, S.Y., Clark, M.A., Moreno, M.S., and Barrett, E.L. (1995). Sequence analysis of the *phs* operon in *Salmonella* typhimurium and the contribution of thiosulfate reduction to anaerobic energy metabolism. Journal of bacteriology *177*, 2813-2820.

Hellman, L.M., and Fried, M.G. (2007). Electrophoretic mobility shift assay (EMSA) for detecting protein-nucleic acid interactions. Nature protocols *2*, 1849-1861.

Hemberger, S., Pedrolli, D.B., Stolz, J., Vogl, C., Lehmann, M., and Mack, M. (2011). RibM from *Streptomyces davawensis* is a riboflavin/roseoflavin transporter and may be useful for the optimization of riboflavin production strains. BMC Biotechnology *11*, 119.

Hensel, M., Hinsley, A.P., Nikolaus, T., Sawers, G., and Berks, B.C. (1999). The genetic basis of tetrathionate respiration in *Salmonella* typhimurium. Molecular microbiology *32*, 275-287.

Higuchi, Y., Yagi, T., and Yasuoka, N. (1997). Unusual ligand structure in Ni-Fe active center and an additional Mg site in hydrogenase revealed by high resolution X-ray structure analysis. Structure *5*, 1671-1680.

Hinsley, A.P., and Berks, B.C. (2002). Specificity of respiratory pathways involved in the reduction of sulfur compounds by *Salmonella enterica*. Microbiology *148*, 3631-3638.

Holliger, C., Wohlfarth, G., and Diekert, G. (1998). Reductive dechlorination in the energy metabolism of anaerobic bacteria. FEMS microbiology reviews *22*, 383-398.

Honda, Y., Hagiwara, H., Ida, S., and Ishihara, T. (2016). Application to photocatalytic H_2 production of a whole-cell reaction by recombinant *Escherichia coli* cells expressing [FeFe]-hydrogenase and maturases genes. Angewandte chemie international edition English *55*, 8045-8048.

Horch, M., Lauterbach, L., Saggu, M., Hildebrandt, P., Lendzian, F., Bittl, R., Lenz, O., and Zebger, I. (2010). Probing the active site of an O_2-tolerant NAD+-reducing [NiFe]-hydrogenase from *Ralstonia eutropha* H16 by in situ EPR and FTIR spectroscopy. Angewandte chemie international edition English *49*, 8026-8029.

Hormann, K., and Andreesen, J.R. (1989). Reductive cleavage of sarcosine and betaine by *Eubacterium acidaminophilum via* enzyme systems different from glycine reductase. Archives of microbiology *153*, 50-59.

Hrdy, I., and Muller, M. (1995). Primary structure and eubacterial relationships of the pyruvate:ferredoxin oxidoreductase of the amitochondriate eukaryote *Trichomonas vaginalis*. Journal of molecular evolution *41*, 388-396.

Hunt, T.P., and Magasanik, B. (1985). Transcription of glnA by purified *Escherichia coli* components: core RNA polymerase and the products of *glnF*, *glnG*, and *glnL*. Proceedings of the national academy of science USA *82*, 8453-8457.

Hurley, J.M., and Dunlap, J.C. (2013). Cell biology: A fable of too much too fast. Nature *495*, 57-58.

Hutchison, C.A., 3rd, Chuang, R.Y., Noskov, V.N., Assad-Garcia, N., Deerinck, T.J., Ellisman, M.H., Gill, J., Kannan, K., Karas, B.J., Ma, L.*, et al.* (2016). Design and synthesis of a minimal bacterial genome. Science *351*, aad6253.

Jack, R.L., Buchanan, G., Dubini, A., Hatzixanthis, K., Palmer, T., and Sargent, F. (2004). Coordinating assembly and export of complex bacterial proteins. EMBO Journal *23*, 3962-3972.

Jack, R.L., Sargent, F., Berks, B.C., Sawers, G., and Palmer, T. (2001). Constitutive expression of *Escherichia coli* tat genes indicates an important role for the twin-arginine translocase during aerobic and anaerobic growth. Journal of bacteriology *183*, 1801-1804.

Jacobi, A., Rossmann, R., and Bock, A. (1992). The hyp operon gene products are required for the maturation of catalytically active hydrogenase isoenzymes in *Escherichia coli*. Archives of microbiology *158*, 444-451.

James, M.J., Coulthurst, S.J., Palmer, T., and Sargent, F. (2013). Signal peptide etiquette during assembly of a complex respiratory enzyme. Molecular microbiology *90*, 400-414.

Johnson, D. S., Mortazavi, A., Myers, R. M., Wold, B. (2007). Genome-wide mapping of *in vivo* protein-DNA interactions. Science *316*, 1497-1502

Jones, A.K., Sillery, E., Albracht, S.P., and Armstrong, F.A. (2002). Direct comparison of the electrocatalytic oxidation of hydrogen by an enzyme and a platinum catalyst. Chemical communications, 866-867.

Jormakka, M., Yokoyama, K., Yano, T., Tamakoshi, M., Akimoto, S., Shimamura, T., Curmi, P., and Iwata, S. (2008). Molecular mechanism of energy conservation in polysulfide respiration. Nature structural and molecular biology *15*, 730-737.

Jugder, B.-E., Chen, Z., Ping, D.T.T., Lebhar, H., Welch, J., and Marquis, C.P. (2015). An analysis of the changes in soluble hydrogenase and global gene expression in *Cupriavidus necator* (*Ralstonia eutropha*) H16 grown in heterotrophic diauxic batch culture. Microbial cell factories *14*, 42.

Jugder, B.-E., Lebhar, H., Aguey-Zinsou, K.-F., and Marquis, C.P. (2016). Production and purification of a soluble hydrogenase from *Ralstonia eutropha* H16 for potential hydrogen fuel cell applications. MethodsX *3*, 242-250.

Karp, A., and Richter, G.M. (2011). Meeting the challenge of food and energy security. Journal of experimental botany *62*, 3263-3271.

Kashket, E.R. (1985). The proton motive force in bacteria: a critical assessment of methods. Annual review of microbiology *39*, 219-242.

Kelley, L.A., Mezulis, S., Yates, C.M., Wass, M.N., and Sternberg, M.J.E. (2015). The Phyre^2 web portal for protein modeling, prediction and analysis. Nature protocols *10*, 845-858.

Kelly, C.L. (2013). Biohydrogen production in *Escherichia coli* – A synthetic biology approach. In Molecular Microbiology (Dundee: University of Dundee).

Kelly, C.L., Liu, Z., Yoshihara, A., Jenkinson, S.F., Wormald, M.R., Otero, J., Estevez, A., Kato, A., Marqvorsen, M.H., Fleet, G.W.*, et al.* (2016). Synthetic chemical inducers and genetic decoupling enable orthogonal control of the rhaBAD promoter. ACS synthetic biology.

Kelly, C.L., Pinske, C., Murphy, B.J., Parkin, A., Armstrong, F., Palmer, T., and Sargent, F. (2015). Integration of an [FeFe]-hydrogenase into the anaerobic metabolism of *Escherichia coli*. Biotechnology reports *8*, 94-104.

Kerfeld, C.A., Sawaya, M.R., Tanaka, S., Nguyen, C.V., Phillips, M., Beeby, M., and Yeates, T.O. (2005). Protein structures forming the shell of primitive bacterial organelles. Science *309*, 936-938.

Khoroshilova, N., Popescu, C., Munck, E., Beinert, H., and Kiley, P.J. (1997). Iron-sulfur cluster disassembly in the FNR protein of *Escherichia coli* by O2: [4Fe-4S] to [2Fe-2S] conversion with loss of biological activity. Proceedings of the national academy of science USA *94*, 6087-6092.

Kim, J.Y., Jo, B.H., and Cha, H.J. (2011). Production of biohydrogen by heterologous expression of oxygen-tolerant *Hydrogenovibrio marinus* [NiFe]-hydrogenase in *Escherichia coli*. Journal of biotechnology *155*, 312-319.

Kim, K.J., Kim, H.E., Lee, K.H., Han, W., Yi, M.J., Jeong, J., and Oh, B.H. (2004). Two-promoter vector is highly efficient for overproduction of protein complexes. Protein science *13*, 1698-1703.

Kreth, J., Lengeler, J.W., and Jahreis, K. (2013). Characterization of pyruvate uptake in *Escherichia coli* K-12. PLoS One *8*, e67125.

Kuchenreuther, J.M., Grady-Smith, C.S., Bingham, A.S., George, S.J., Cramer, S.P., and Swartz, J.R. (2010). High-yield expression of heterologous [FeFe] hydrogenases in *Escherichia coli*. PLoS One *5*, e15491.

Kuhns, L.G., Benoit, S.L., Bayyareddy, K., Johnson, D., Orlando, R., Evans, A.L., Waldrop, G.L., and Maier, R.J. (2016). Carbon fixation driven by molecular hydrogen results in

chemolithoautotrophically enhanced growth of *Helicobacter pylori*. Journal of bacteriology *198*, 1423-1428.

Kunkel, A., Vorholt, J.A., Thauer, R.K., and Hedderich, R. (1998). An *Escherichia coli* hydrogenase-3-type hydrogenase in methanogenic archaea. European journal of biochemistry *252*, 467-476.

Laemmli, U.K. (1970). Cleavage of structural proteins during the assembly of the head of bacteriophage T4. Nature *227*, 680-685.

Lambertz, C., Leidel, N., Havelius, K.G., Noth, J., Chernev, P., Winkler, M., Happe, T., and Haumann, M. (2011). O_2 reactions at the six-iron active site (H-cluster) in [FeFe]-hydrogenase. Journal of biological chemistry *286*, 40614-40623.

Lamichhane-Khadka, R., Frye, J.G., Porwollik, S., McClelland, M., and Maier, R.J. (2011). Hydrogen-stimulated carbon acquisition and conservation in *Salmonella enterica* serovar Typhimurium. Journal of bacteriology *193*, 5824-5832.

Laurinavichene, T.V., Zorin, N.A., and Tsygankov, A.A. (2002). Effect of redox potential on activity of hydrogenase 1 and hydrogenase 2 in *Escherichia coli*. Archives of microbiology *178*, 437-442.

Lauterbach, L., and Lenz, O. (2013). Catalytic production of hydrogen peroxide and water by oxygen-tolerant [NiFe]-hydrogenase during H_2 cycling in the presence of O_2. Journal of the American chemical society *135*, 17897-17905.

Lauterbach, L., Liu, J., Horch, M., Hummel, P., Schwarze, A., Haumann, M., Vincent, K.A., Lenz, O., and Zebger, I. (2011). The Hydrogenase subcomplex of the NAD^+-reducing [NiFe] hydrogenase from *Ralstonia eutropha* – insights into catalysis and redox interconversions. European journal of inorganic chemistry *2011*, 1067-1079.

Lawrence, A.D., Frank, S., Newnham, S., Lee, M.J., Brown, I.R., Xue, W.-F., Rowe, M.L., Mulvihill, D.P., Prentice, M.B., Howard, M.J.*, et al.* (2014). Solution structure of a bacterial microcompartment targeting peptide and its application in the construction of an ethanol bioreactor. ACS synthetic biology *3*, 454-465.

Lazarus, O., Woolerton, T.W., Parkin, A., Lukey, M.J., Reisner, E., Seravalli, J., Pierce, E., Ragsdale, S.W., Sargent, F., and Armstrong, F.A. (2009). Water-gas shift reaction catalyzed by

redox enzymes on conducting graphite platelets. Journal of the American chemical society *131*, 14154-14155.

Lenz, O., Bernhard, M., Buhrke, T., Schwartz, E., and Friedrich, B. (2002). The hydrogen-sensing apparatus in *Ralstonia eutropha*. Journal of molecular microbiology and biotechnology *4*, 255-262.

Lenz, O., and Friedrich, B. (1998). A novel multicomponent regulatory system mediates H-2 sensing in *Alcaligenes eutrophus*. Proceedings of the national academy of science USA *95*, 12474-12479.

Lenz, O., Lauterbach, L., Frielingsdorf, S., and Friedrich, B. (2015). Oxygen-tolerant hydrogenases and their biotechnological potential. In Biohydrogen, M. Rogner, ed. (De Gruyter), pp. 61-96.

Lenz, O., Zebger, I., Hamann, J., Hildebrandt, P., and Friedrich, B. (2007). Carbamoylphosphate serves as the source of CN^-, but not of the intrinsic CO in the active site of the regulatory [NiFe]-hydrogenase from *Ralstonia eutropha*. FEBS letters *581*, 3322-3326.

Leonhartsberger, S., Huber, A., Lottspeich, F., and Böck, A. (2001). The hydH/G genes from *Escherichia coli* code for a zinc and lead responsive two-component regulatory system. Journal of molecular biology *307*, 93-105.

Levin, D.B., Zhu, H., Beland, M., Cicek, N., and Holbein, B.E. (2007). Potential for hydrogen and methane production from biomass residues in Canada. Bioresource technology *98*, 654-660.

Liebgott, P.-P., Dementin, S., Leger, C., and Rousset, M. (2011). Towards engineering O_2-tolerance in [Ni-Fe] hydrogenases. Energy and environmental science *4*, 33-41.

Lin, E.C. (1976). Glycerol dissimilation and its regulation in bacteria. Annual review of microbiology *30*, 535-578.

Liu, C.C., and Schultz, P.G. (2010). Adding new chemistries to the genetic code. Annual review of biochemistry *79*, 413-444.

Lopez, D., and Kolter, R. (2010). Functional microdomains in bacterial membranes. Genes and development *24*, 1893-1902.

Lowry, O.H., Rosebrough, N.J., Farr, A.L., and Randall, R.J. (1951). Protein measurement with the Folin phenol reagent. Journal of biological chemistry *193*, 265-275.

Lubitz, W., Ogata, H., Rudiger, O., and Reijerse, E. (2014). Hydrogenases. Chemical reviews *114*, 4081-4148.

Lubner, C.E., Knorzer, P., Silva, P.J., Vincent, K.A., Happe, T., Bryant, D.A., and Golbeck, J.H. (2010). Wiring an [FeFe]-hydrogenase with photosystem I for light-induced hydrogen production. Biochemistry *49*, 10264-10266.

Ludwig, M., Schubert, T., Zebger, I., Wisitruangsakul, N., Saggu, M., Strack, A., Lenz, O., Hildebrandt, P., and Friedrich, B. (2009). Concerted action of two novel auxiliary proteins in assembly of the active site in a membrane-bound [NiFe] hydrogenase. Journal of biological chemistry *284*, 2159-2168.

Lukey, M.J., Parkin, A., Roessler, M.M., Murphy, B.J., Harmer, J., Palmer, T., Sargent, F., and Armstrong, F.A. (2010). How *Escherichia coli* is equipped to oxidize hydrogen under different redox conditions. Journal of biological chemistry *285*, 3928-3938.

Lukey, M.J., Roessler, M.M., Parkin, A., Evans, R.M., Davies, R.A., Lenz, O., Friedrich, B., Sargent, F., and Armstrong, F.A. (2011). Oxygen-tolerant [NiFe]-hydrogenases: the individual and collective importance of supernumerary cysteines at the proximal Fe-S cluster. Journal of the American chemical society *133*, 16881-16892.

Luo, X., Wang, J., Dooner, M., and Clarke, J. (2015). Overview of current development in electrical energy storage technologies and the application potential in power system operation. Applied energy *137*, 511-536.

Lupton, F.S., Conrad, R., and Zeikus, J.G. (1984). Physiological function of hydrogen metabolism during growth of sulfidogenic bacteria on organic substrates. Journal of bacteriology *159*, 843-849.

Lutz, S. (2010). Beyond directed evolution—semi-rational protein engineering and design. Current opinion in biotechnology *21*, 734-743.

Lutz, S., Jacobi, A., Schlensog, V., Bohm, R., Sawers, G., and Bock, A. (1991). Molecular characterization of an operon (hyp) necessary for the activity of the three hydrogenase isoenzymes in *Escherichia coli*. Molecular microbiology *5*, 123-135.

Lyons, L.B., and Zinder, N.D. (1972). The genetic map of the filamentous bacteriophage f1. Virology *49*, 45-60.

Ma, K., Hutchins, A., Sung, S.J., and Adams, M.W. (1997). Pyruvate ferredoxin oxidoreductase from the hyperthermophilic archaeon, *Pyrococcus furiosus*, functions as a CoA-dependent pyruvate decarboxylase. Proceedings of the national academy of science USA *94*, 9608-9613.

Maas, W.K. (1994). The arginine repressor of *Escherichia coli*. Microbiological reviews *58*, 631-640.

Macomber, L., Elsey, S.P., and Hausinger, R.P. (2011). Fructose-1,6-bisphosphate aldolase (class II) is the primary site of nickel toxicity in *Escherichia coli*. Molecular microbiology *82*, 1291-1300.

Maeda, T., Sanchez-Torres, V., and Wood, T.K. (2008a). Protein engineering of hydrogenase 3 to enhance hydrogen production. Applied microbiology and biotechnology *79*, 77-86.

Maeda, T., Sanchez-Torres, V., and Wood, T.K. (2008b). Metabolic engineering to enhance bacterial hydrogen production. Microbial biotechnology *1*, 30-39.

Maeda, T., Vardar, G., Self, W.T., and Wood, T.K. (2007). Inhibition of hydrogen uptake in *Escherichia coli* by expressing the hydrogenase from the cyanobacterium Synechocystis sp. PCC 6803. BMC biotechnology *7*, 25.

Magnani, P., Doussiere, J., and Lissolo, T. (2000). Diphenylene iodonium as an inhibitor for the hydrogenase complex of *Rhodobacter capsulatus*. Evidence for two distinct electron donor sites. Biochimica et biophysica acta - bioenergetics *1459*, 169-178.

Maier, R.J. (2005). Use of molecular hydrogen as an energy substrate by human pathogenic bacteria. Biochemical society transactions *33*, 83-85.

Maier, R.J., Olczak, A., Maier, S., Soni, S., and Gunn, J. (2004). Respiratory hydrogen use by *Salmonella enterica* serovar Typhimurium is essential for virulence. Infection and immunity *72*, 6294-6299.

Makui, H., Roig, E., Cole, S.T., Helmann, J.D., Gros, P., and Cellier, M.F. (2000). Identification of the *Escherichia coli* K-12 Nramp orthologue (MntH) as a selective divalent metal ion transporter. Molecular microbiology *35*, 1065-1078.

Malinksy, J., Opekarova, M., Grossman, G., Tanner, W. (2013). Membrane microdomains, rafts and detergent-resistant membranes in plants and fungi. Annual review of plant biology *64*, 501-529.

Malki, S., Saimmaime, I., De Luca, G., Rousset, M., Dermoun, Z., and Belaich, J.P. (1995). Characterization of an operon encoding an NADP-reducing hydrogenase in *Desulfovibrio fructosovorans*. Journal of bacteriology *177*, 2628-2636.

Manish, S., and Banerjee, R. (2008). Comparison of biohydrogen production processes. International journal of hydrogen energy *33*, 279-286.

Manyani, H., Rey, L., Palacios, J.M., Imperial, J., and Ruiz-Argueso, T. (2005). Gene products of the hupGHIJ operon are involved in maturation of the iron-sulfur subunit of the [NiFe] hydrogenase from *Rhizobium leguminosarum* bv. viciae. Journal of bacteriology *187*, 7018-7026.

Marcheschi, R.J., Gronenberg, L.S., and Liao, J.C. (2013). Protein engineering for metabolic engineering: current and next-generation tools. Biotechnology journal *8*, 545-555.

Marreiros, B.C., Batista, A.P., Duarte, A.M., and Pereira, M.M. (2013). A missing link between complex I and group 4 membrane-bound [NiFe] hydrogenases. Biochimica et biophysica acta - bioenergetics *1827*, 198-209.

Matias, P.M., Soares, C.M., Saraiva, L.M., Coelho, R., Morais, J., Le Gall, J., and Carrondo, M.A. (2001). [NiFe] hydrogenase from *Desulfovibrio desulfuricans* ATCC 27774: gene sequencing, three-dimensional structure determination and refinement at 1.8 A and modelling studies of its interaction with the tetrahaem cytochrome c3. Journal of biological inorganic chemistry *6*, 63-81.

McDowall, J.S., Hjersing, M.C., Palmer, T., and Sargent, F. (2015). Dissection and engineering of the *Escherichia coli* formate hydrogenlyase complex. FEBS letters *589*, 3141-3147.

McDowall, J.S., Murphy, B.J., Haumann, M., Palmer, T., Armstrong, F.A., and Sargent, F. (2014). Bacterial formate hydrogenlyase complex. Proceedings of the national academy of science USA *111*, E3948-E3956.

McGlynn, S.E., Ruebush, S.S., Naumov, A., Nagy, L.E., Dubini, A., King, P.W., Broderick, J.B., Posewitz, M.C., and Peters, J.W. (2007). *In vitro* activation of [FeFe] hydrogenase: new insights into hydrogenase maturation. Journal of biological inorganic chemistry *12*, 443-447.

McKinlay, J.B., and Harwood, C.S. (2010). Photobiological production of hydrogen gas as a biofuel. Current opinion in biotechnology *21*, 244-251.

Menon, N.K., Chatelus, C.Y., Dervartanian, M., Wendt, J.C., Shanmugam, K.T., Peck, H.D., Jr., and Przybyla, A.E. (1994). Cloning, sequencing, and mutational analysis of the *hyb* operon encoding *Escherichia coli* hydrogenase 2. Journal of bacteriology *176*, 4416-4423.

Menon, N.K., Robbins, J., Wendt, J.C., Shanmugam, K.T., and Przybyla, A.E. (1991). Mutational analysis and characterization of the *Escherichia coli* hya operon, which encodes [NiFe] hydrogenase 1. Journal of bacteriology *173*, 4851-4861.

Menon, S., and Ragsdale, S.W. (1996). Unleashing hydrogenase activity in carbon monoxide dehydrogenase/acetyl-CoA synthase and pyruvate:ferredoxin oxidoreductase. Biochemistry *35*, 15814-15821.

Mergaert, J., Anderson, C., Wouters, A., Swings, J., and Kersters, K. (1992). Biodegradation of polyhydroxyalkanoates. FEMS Microbiology reviews *9*, 317-321.

Messenger, S.L., and Green, J. (2003). FNR-mediated regulation of hyp expression in *Escherichia coli*. FEMS Microbiology letters *228*, 81-86.

Meyer, A.J., Ellefson, J., and Ellington, A.D. (2014). Library generation by gene shuffling. Current protocols in molecular biology / edited by Frederick M Ausubel [*et al*] *105*, Unit-15.12.

Miki, K., and Lin, E.C. (1973). Enzyme complex which couples glycerol-3-phosphate dehydrogenation to fumarate reduction in *Escherichia coli*. Journal of bacteriology *114*, 767-771.

Miyamoto, K., Okunishi, M., Nukui, E., Tsuchiya, T., Kobayashi, T., Imada, C., and Tsujibo, H. (2007). The regulator CdsS/CdsR two-component system modulates expression of genes involved in chitin degradation of *Pseudoalteromonas piscicida* strain O-7. Archives of microbiology *188*, 619-628.

Moser, C.C., Keske, J.M., Warncke, K., Farid, R.S., and Dutton, P.L. (1992). Nature of biological electron transfer. Nature *355*, 796-802.

Muhd Noor, N.D., Nishikawa, K., Nishihara, H., Yoon, K.S., Ogo, S., and Higuchi, Y. (2016). Improved purification, crystallization and crystallographic study of Hyd-2-type [NiFe]-

hydrogenase from *Citrobacter* sp. S-77. Acta crystallographica section F structural biology communications *72*, 53-58.

Mulder, D.W., Shepard, E.M., Meuser, J.E., Joshi, N., King, P.W., Posewitz, M.C., Broderick, J.B., and Peters, J.W. (2011). Insights into [FeFe]-hydrogenase structure, mechanism, and maturation. Structure *19*, 1038-1052.

Muller, M. (1993). The hydrogenosome. Journal of general microbiology *139*, 2879-2889.

Murarka, A., Dharmadi, Y., Yazdani, S.S., and Gonzalez, R. (2008). Fermentative utilization of glycerol by *Escherichia coli* and its implications for the production of fuels and chemicals. Applied and environmental microbiology *74*, 1124-1135.

Nagy, L.E., Meuser, J.E., Plummer, S., Seibert, M., Ghirardi, M.L., King, P.W., Ahmann, D., and Posewitz, M.C. (2007). Application of gene-shuffling for the rapid generation of novel [FeFe]-hydrogenase libraries. Biotechnology letters *29*, 421-430.

Naik, S.N., Goud, V.V., Rout, P.K., and Dalai, A.K. (2010). Production of first and second generation biofuels: a comprehensive review. Renewable and sustainable energy reviews *14*, 578-597.

Navarro, C., Wu, L.F., and Mandrand-Berthelot, M.A. (1993). The nik operon of *Escherichia coli* encodes a periplasmic binding-protein-dependent transport system for nickel. Molecular microbiology *9*, 1181-1191.

Naville, M., Ghuillot-Gaudeffroy, A., Marchais, A., and Gautheret, D. (2011). ARNold: a web tool for the prediction of Rho-independent transcription terminators. RNA biology *8*, 11-13.

Neidhardt, F. C., Ingraham, J. L., Schaechter, M. (1990). Physiology of the bacterial cell. A molecular approach (Sunderland, MA.: Sinauer Associates, Inc.)

Nicoloff, H., Arsene-Ploetze, F., Malandain, C., Kleerebezem, M., and Bringel, F. (2004). Two arginine repressors regulate arginine biosynthesis in *Lactobacillus plantarum*. Journal of bacteriology *186*, 6059-6069.

Norseth, T. (1981). The carcinogenicity of chromium. Environmental health perspectives *40*, 121-130.

Nov, Y. (2012). When second best is good enough: another probabilistic look at saturation mutagenesis. Applied and environmental microbiology *78*, 258-262.

Ogata, H., Kellers, P., and Lubitz, W. (2010). The crystal structure of the [NiFe] hydrogenase from the photosynthetic bacterium *Allochromatium vinosum*: characterization of the oxidized enzyme (Ni-A State). Journal of molecular biology *402*, 428-444.

Ohki, Y., Yasumura, K., Kuge, K., Tanino, S., Ando, M., Li, Z., and Tatsumi, K. (2008). Thiolate-bridged dinuclear iron(tris-carbonyl)-nickel complexes relevant to the active site of [NiFe] hydrogenase. Proceedings of the national academy of science USA *105*, 7652-7657.

Olson, J.W., and Maier, R.J. (2002). Molecular hydrogen as an energy source for *Helicobacter pylori*. Science *298*, 1788-1790.

Orozco, R.L., Redwood, M.D., Yong, P., Caldelari, I., Sargent, F., and Macaskie, L.E. (2010). Towards an integrated system for bio-energy: hydrogen production by *Escherichia coli* and use of palladium-coated waste cells for electricity generation in a fuel cell. Biotechnology letters *32*, 1837-1845.

Page, C.C., Moser, C.C., Chen, X., and Dutton, P.L. (1999). Natural engineering principles of electron tunnelling in biological oxidation-reduction. Nature *402*, 47-52.

Palmer, T., and Berks, B.C. (2012). The twin-arginine translocation (Tat) protein export pathway. Nature reviews microbiology *10*, 483-496.

Palmer, T., Berks, B.C., and Sargent, F. (2010). Analysis of Tat targeting function and twin-arginine signal peptide activity in *Escherichia coli*. Methods in molecular biology *619*, 191-216.

Pan, N., and Imlay, J.A. (2001). How does oxygen inhibit central metabolism in the obligate anaerobe *Bacteroides thetaiotaomicron*. Molecular microbiology *39*, 1562-1571.

Pandelia, M.-E., Lubitz, W., and Nitschke, W. (2012). Evolution and diversification of Group 1 [NiFe] hydrogenases. Is there a phylogenetic marker for O_2-tolerance? Biochimica et biophysica acta - bioenergetics *1817*, 1565-1575.

Parkin, A., Goldet, G., Cavazza, C., Fontecilla-Camps, J.C., and Armstrong, F.A. (2008). The difference a Se makes? Oxygen-tolerant hydrogen production by the [NiFeSe]-hydrogenase from *Desulfomicrobium baculatum*. Journal of the American chemical society *130*, 13410-13416.

Parkin, A., and Sargent, F. (2012). The hows and whys of aerobic H_2 metabolism. Current opinion in chemical biology *16*, 26-34.

Parsons, J.B., Dinesh, S.D., Deery, E., Leech, H.K., Brindley, A.A., Heldt, D., Frank, S., Smales, C.M., Lunsdorf, H., Rambach, A.*, et al.* (2008). Biochemical and structural insights into bacterial organelle form and biogenesis. Journal of biological chemistry *283*, 14366-14375.

Parsons, J.B., Frank, S., Bhella, D., Liang, M., Prentice, M.B., Mulvihill, D.P., and Warren, M.J. (2010). Synthesis of empty bacterial microcompartments, directed organelle protein incorporation, and evidence of filament-associated organelle movement. Molecular cell *38*, 305-315.

Pedrolli, D., Langer, S., Hobl, B., Schwarz, J., Hashimoto, M., and Mack, M. (2015). The ribB FMN riboswitch from *Escherichia coli* operates at the transcriptional and translational level and regulates riboflavin biosynthesis. FEBS journal *282*, 3230-3242.

Peng, L., and Shimizu, K. (2004). Effect of ppc gene knockout on the metabolism of *Escherichia coli* in view of gene expressions, enzyme activities and intracellular metabolite concentrations. Applied microbiology and biotechnology.

Peters, J.W., Lanzilotta, W.N., Lemon, B.J., and Seefeldt, L.C. (1998). X-ray crystal structure of the Fe-only hydrogenase (CpI) from *Clostridium pasteurianum* to 1.8 angstrom resolution. Science *282*, 1853-1858.

Pierik, A.J., Schmelz, M., Lenz, O., Friedrich, B., and Albracht, S.P. (1998). Characterization of the active site of a hydrogen sensor from *Alcaligenes eutrophus*. FEBS letters *438*, 231-235.

Pilkington, S.J., Skehel, J.M., Gennis, R.B., and Walker, J.E. (1991). Relationship between mitochondrial NADH-ubiquinone reductase and a bacterial NAD-reducing hydrogenase. Biochemistry *30*, 2166-2175.

Pinske, C., Bonn, M., Kruger, S., Lindenstrauss, U., and Sawers, R.G. (2011). Metabolic deficiences revealed in the biotechnologically important model bacterium *Escherichia coli* BL21(DE3). PLoS One *6*, e22830.

Pinske, C., Jaroschinsky, M., Linek, S., Kelly, C.L., Sargent, F., and Sawers, R.G. (2015a). Physiology and bioenergetics of [NiFe]-hydrogenase 2-catalyzed H_2-consuming and H_2-producing reactions in *Escherichia coli*. Journal of bacteriology *197*, 296-306.

Pinske, C., Jaroschinsky, M., and Sawers, R.G. (2013). Levels of control exerted by the Isc iron-sulfur cluster system on biosynthesis of the formate hydrogenlyase complex. Microbiology *159*, 1179-1189.

Pinske, C., and Sargent, F. (2016). Exploring the directionality of *Escherichia coli* formate hydrogenlyase: a membrane-bound enzyme capable of fixing carbon dioxide to organic acid. Microbiologyopen.

Pinske, C., Sargent, F., and Sawers, R.G. (2015b). SlyD-dependent nickel delivery limits maturation of [NiFe]-hydrogenases in late-stationary phase *Escherichia coli* cells. Metallomics *7*, 683-690.

Pinske, C., and Sawers, R.G. (2012). Delivery of iron-sulfur clusters to the hydrogen-oxidizing [NiFe]-hydrogenases in *Escherichia coli* requires the A-type carrier proteins ErpA and IscA. PLoS One *7*, e31755.

Pohlmann, A., Fricke, W.F., Reinecke, F., Kusian, B., Liesegang, H., Cramm, R., Eitinger, T., Ewering, C., Potter, M., Schwartz, E.*, et al.* (2006). Genome sequence of the bioplastic-producing "Knallgas" bacterium *Ralstonia eutropha* H16. Nature biotechnology *24*, 1257-1262.

Puigbo, P., Guzman, E., Romeu, A., and Garcia-Vallve, S. (2007). OPTIMIZER: a web server for optimizing the codon usage of DNA sequences. Nucleic acids research *35*, W126-131.

Purec, L., Krasna, A.I., and Rittenberg, D. (1962). The inhibition of hydrogenase by carbon monoxide and the reversal of this inhibition by light. Biochemistry *1*, 270-275.

Redwood, M.D., Mikheenko, I.P., Sargent, F., and Macaskie, L.E. (2008). Dissecting the roles of *Escherichia coli* hydrogenases in biohydrogen production. FEMS microbiology letters *278*, 48-55.

Reissmann, S., Hochleitner, E., Wang, H., Paschos, A., Lottspeich, F., Glass, R.S., and Bock, A. (2003). Taming of a poison: biosynthesis of the NiFe-hydrogenase cyanide ligands. Science *299*, 1067-1070.

Renewable Fuels Association (2015). Going global - 2015 ethanol industry outlook.

Reynolds, A., Lundblad, V., Dorris, D., and Keaveney, M. (1997). Assay for B-galactosidase in liquid cultures. Current protocols in molecular biology, 55-56.

Richard, D.J., Sawers, G., Sargent, F., McWalter, L., and Boxer, D.H. (1999). Transcriptional regulation in response to oxygen and nitrate of the operons encoding the [NiFe] hydrogenases 1 and 2 of *Escherichia coli*. Microbiology *145 (Pt 10)*, 2903-2912.

Richaud, P., Colbeau, A., Toussaint, B., and Vignais, P.M. (1991). Identification and sequence analysis of the hupR1 gene, which encodes a response regulator of the NtrC family required for hydrogenase expression in *Rhodobacter capsulatus*. Journal of bacteriology *173*, 5928-5932.

Roche, B., Aussel, L., Ezraty, B., Mandin, P., Py, B., and Barras, F. (2013). Iron/sulfur proteins biogenesis in prokaryotes: Formation, regulation and diversity. Biochimica et biophysica acta - bioenergetics *1827*, 455-469.

Rodrigue, A., Chanal, A., Beck, K., Muller, M., and Wu, L.F. (1999). Co-translocation of a periplasmic enzyme complex by a hitchhiker mechanism through the bacterial tat pathway. Journal of biological chemistry *274*, 13223-13228.

Romeo, T., and Snoep, J. (2005). Glycolysis and flux control. EcoSal Plus.

Romm, J. (2004). The Hype about hydrogen (Washington DC: Island Press).

Roseboom, W., Blokesch, M., Bock, A., and Albracht, S.P. (2005). The biosynthetic routes for carbon monoxide and cyanide in the Ni-Fe active site of hydrogenases are different. FEBS letters *579*, 469-472.

Rossmann, R., Maier, T., Lottspeich, F., and Bock, A. (1995). Characterisation of a protease from *Escherichia coli* involved in hydrogenase maturation. European journal of biochemistry *227*, 545-550.

Rossmann, R., Sauter, M., Lottspeich, F., and Bock, A. (1994). Maturation of the large subunit (HycE) of *Escherichia coli* hydrogenase 3 requires nickel incorporation followed by C-terminal processing at Arg537. European journal of biochemistry *220*, 377-384.

Rousset, M., Montet, Y., Guigliarelli, B., Forget, N., Asso, M., Bertrand, P., Fontecilla-Camps, J.C., and Hatchikian, E.C. (1998). [3Fe-4S] to [4Fe-4S] cluster conversion in *Desulfovibrio fructosovorans* [NiFe] hydrogenase by site-directed mutagenesis. Proceedings of the national academy of science USA *95*, 11625-11630.

Sagermann, M., Ohtaki, A., and Nikolakakis, K. (2009). Crystal structure of the EutL shell protein of the ethanolamine ammonia lyase microcompartment. Proceedings of the national academy of science USA *106*, 8883-8887.

Salis, H.M. (2011). The ribosome binding site calculator. Methods in enzymology *498*, 19-42.

Salis, H.M., Mirsky, E.A., and Voigt, C.A. (2009). Automated design of synthetic ribosome binding sites to control protein expression. Nature biotechnology *27*, 946-950.

Sambrook, J., and Russell, D. W., ed. (2001). Molecular cloning: a laboratory manual (Cold Spring Harbor, N.Y.: Cold Spring Harbor Laboratory Press).

Sargent, F. (2016). The Model [NiFe]-Hydrogenases of *Escherichia coli*. Advances in microbial physiology *68*, 433-507.

Sargent, F., Davidson, F.A., Kelly, C.L., Binny, R., Christodoulides, N., Gibson, D., Johansson, E., Kozyrska, K., Lado, L.L., Maccallum, J.*, et al.* (2013). A synthetic system for expression of components of a bacterial microcompartment. Microbiology *159*, 2427-2436.

Sasahara, K.C., Heinzinger, N.K., and Barrett, E.L. (1997). Hydrogen sulfide production and fermentative gas production by *Salmonella* typhimurium require F_0F_1 ATP synthase activity. Journal of bacteriology *179*, 6736-6740.

Sauter, M., Bohm, R., and Bock, A. (1992). Mutational analysis of the operon (*hyc*) determining hydrogenase 3 formation in *Escherichia coli*. Molecular microbiology *6*, 1523-1532.

Sawers, G. (1994). The hydrogenases and formate dehydrogenases of *Escherichia coli*. Antonie van Leeuwenhoek *66*, 57-88.

Sawers, G., and Suppmann, B. (1992). Anaerobic induction of pyruvate formate-lyase gene expression is mediated by the ArcA and FNR proteins. Journal of bacteriology *174*, 3474-3478.

Sawers, R.G. (2005). Formate and its role in hydrogen production in *Escherichia coli*. Biochemical society transactions *33*, 42-46.

Sawers, R.G., Ballantine, S.P., and Boxer, D.H. (1985). Differential expression of hydrogenase isoenzymes in *Escherichia coli* K-12: evidence for a third isoenzyme. Journal of bacteriology *164*, 1324-1331.

Sawers, R.G., and Boxer, D.H. (1986). Purification and properties of membrane-bound hydrogenase isoenzyme 1 from anaerobically grown *Escherichia coli* K12. European journal of biochemistry *156*, 265-275.

Schafer, C., Bommer, M., Hennig, S.E., Jeoung, J.H., Dobbek, H., and Lenz, O. (2016). Structure of an actinobacterial-type [NiFe]-hydrogenase reveals insight into O_2-yolerant H_2 oxidation. Structure *24*, 285-292.

Schafer, C., Friedrich, B., and Lenz, O. (2013). Novel, oxygen-insensitive group 5 [NiFe]-hydrogenase in *Ralstonia eutropha*. Applied and environmental microbiology *79*, 5137-5145.

Schiffels, J., Pinkenburg, O., Schelden, M., Aboulnaga el, H.A., Baumann, M.E., and Selmer, T. (2013). An innovative cloning platform enables large-scale production and maturation of an oxygen-tolerant [NiFe]-hydrogenase from *Cupriavidus necator* in *Escherichia coli*. PLoS One *8*, e68812.

Schink, B., and Schlegel, H.G. (1979). The membrane-bound hydrogenase of *Alcaligenes eutrophus*. I. Solubilization, purification, and biochemical properties. Biochimica et biophysica acta *567*, 315-324.

Schneider, K., and Schlegel, H.G. (1976). Purification and properties of soluble hydrogenase from *Alcaligenes eutrophus* H 16. Biochimica et biophysica acta *452*, 66-80.

Schneider, T.D., and Stephens, R.M. (1990). Sequence logos: a new way to display consensus sequences. Nucleic acids research *18*, 6097-6100.

Schryvers, A., and Weiner, J.H. (1982). The anaerobic sn-glycerol-3-phosphate dehydrogenase: cloning and expression of the *glpA* gene of *Escherichia coli* and identification of the *glpA* products. Canadian journal of biochemistry *60*, 224-231.

Schubert, T., Lenz, O., Krause, E., Volkmer, R., and Friedrich, B. (2007). Chaperones specific for the membrane-bound [NiFe]-hydrogenase interact with the Tat signal peptide of the small subunit precursor in *Ralstonia eutropha* H16. Molecular microbiology *66*, 453-467.

Schummer, U., and Schiefer, H.G. (1983). Electrophysiology of mycoplasma membranes. The Yale journal of biology and medicine *56*, 413-418.

Schut, G.J., and Adams, M.W. (2009). The iron-hydrogenase of *Thermotoga maritima* utilizes ferredoxin and NADH synergistically: a new perspective on anaerobic hydrogen production. Journal of bacteriology *191*, 4451-4457.

Schwartz, E., Buhrke, T., Gerischer, U., and Friedrich, B. (1999). Positive transcriptional feedback controls hydrogenase expression in *Alcaligenes eutrophus* H16. Journal of bacteriology *181*, 5684-5692.

Schwartz, E., and Friedrich, B. (2001). A physical map of the megaplasmid pHG1, one of three genomic replicons in *Ralstonia eutropha* H16. FEMS microbiology letters *201*, 213-219.

Schwartz, E., Gerischer, U., and Friedrich, B. (1998). Transcriptional regulation of *Alcaligenes eutrophus* hydrogenase genes. Journal of bacteriology *180*, 3197-3204.

Schwartz, E., Henne, A., Cramm, R., Eitinger, T., Friedrich, B., and Gottschalk, G. (2003). Complete nucleotide sequence of pHG1: a *Ralstonia eutropha* H16 megaplasmid encoding key enzymes of H_2-based ithoautotrophy and anaerobiosis. Journal of molecular biology *332*, 369-383.

Self, W.T., Grunden, A.M., Hasona, A., and Shanmugam, K.T. (1999). Transcriptional regulation of molybdoenzyme synthesis in *Escherichia coli* in response to molybdenum: ModE-molybdate, a repressor of the modABCD (molybdate transport) operon is a secondary transcriptional activator for the hyc and nar operons. Microbiology *145*, 41-55.

Shearwin, K.E., Callen, B.P., and Egan, J.B. (2005). Transcriptional interference –a crash course. Trends in genetics *21*, 339-345.

Shepard, E.M., McGlynn, S.E., Bueling, A.L., Grady-Smith, C.S., George, S.J., Winslow, M.A., Cramer, S.P., Peters, J.W., and Broderick, J.B. (2010). Synthesis of the 2Fe subcluster of the [FeFe]-hydrogenase H cluster on the HydF scaffold. Proceedings of the national academy of science USA *107*, 10448-10453.

Shafaat, H.S., Rudiger, O., Ogata, H., Lubitz, W. (2013). [NiFe] hydrogenases: A common active site for hydrogen metabolism under diverse conditions. Biochimica et biophysica acta *1827*, 986-1002.

Shetty, R.P., Endy, D., and Knight, T.F. (2008). Engineering BioBrick vectors from BioBrick parts. Journal of biological engineering *2*, 5-5.

Shima, S., Pilak, O., Vogt, S., Schick, M., Stagni, M.S., Meyer-Klaucke, W., Warkentin, E., Thauer, R.K., and Ermler, U. (2008). The crystal structure of [Fe]-hydrogenase reveals the geometry of the active site. Science *321*, 572-575.

Shomura, Y., and Higuchi, Y. (2012). Structural basis for the reaction mechanism of S-carbamoylation of HypE by HypF in the maturation of [NiFe]-hydrogenases. Journal of biological chemistry *287*, 28409-28419.

Singer, S. J., and Nicolson, G. L. (1972). The fluid mosaic model of the structure of cell membranes. Science *175*, 720-731.

Sinha, S., Cheng, S., Fan, C., and Bobik, T.A. (2012). The PduM protein is a structural component of the microcompartments involved in coenzyme B_{12}-dependent 1,2-propanediol degradation by *Salmonella enterica*. Journal of bacteriology *194*, 1912-1918.

Skibinski, D.A.G., Golby, P., Chang, Y.-S., Sargent, F., Hoffman, R., Harper, R., Guest, J.R., Attwood, M.M., Berks, B.C., and Andrews, S.C. (2002). Regulation of the Hydrogenase-4 operon of *Escherichia coli* by the σ^{54}-dependent transcriptional activators FhlA and HyfR. Journal of bacteriology *184*, 6642-6653.

Soboh, B., Stripp, S.T., Bielak, C., Lindenstrauss, U., Braussemann, M., Javaid, M., Hallensleben, M., Granich, C., Herzberg, M., Heberle, J.*, et al.* (2013). The [NiFe]-hydrogenase accessory chaperones HypC and HybG of *Escherichia coli* are iron- and carbon dioxide-binding proteins. FEBS letters *587*, 2512-2516.

Sokolova, T.G., Jeanthon, C., Kostrikina, N.A., Chernyh, N.A., Lebedinsky, A.V., Stackebrandt, E., and Bonch-Osmolovskaya, E.A. (2004). The first evidence of anaerobic CO oxidation coupled with H_2 production by a hyperthermophilic archaeon isolated from a deep-sea hydrothermal vent. Extremophiles *8*, 317-323.

Song, W., Cheng, J., Zhao, J., Zhang, C., Zhou, J., and Cen, K. (2016). Enhancing hydrogen production of *Enterobacter aerogenes* by heterologous expression of hydrogenase genes originated from Synechocystis sp. Bioresource technology *216*, 976-980.

Stoffels, L., Krehenbrink, M., Berks, B.C., and Unden, G. (2012). Thiosulfate reduction in *Salmonella enterica* is driven by the proton motive force. Journal of bacteriology *194*, 475-485.

Stojanowic, A., Mander, G.J., Duin, E.C., and Hedderich, R. (2003). Physiological role of the F_{420}-non-reducing hydrogenase (Mvh) from *Methanothermobacter marburgensis*. Archives of microbiology *180*, 194-203.

Stripp, S.T., Lindenstrauss, U., Sawers, R.G., and Soboh, B. (2015). Identification of an isothiocyanate on the HypEF complex suggests a route for efficient cyanyl-group channeling during [NiFe]-hydrogenase cofactor generation. PLoS One *10*, e0133118.

Su, W., Porter, S., Kustu, S., and Echols, H. (1990). DNA-looping and enhancer activity: association between DNA-bound NtrC activator and RNA polymerase at the bacterial *glnA* promoter. Proceedings of the national academy of science USA *87*, 5504-5508.

Sun, J., Hopkins, R.C., Jenney, F.E., McTernan, P.M., and Adams, M.W. (2010). Heterologous expression and maturation of an NADP-dependent [NiFe]-hydrogenase: a key enzyme in biofuel production. PLoS One *5*, e10526.

Suppmann, B., and Sawers, G. (1994). Isolation and characterization of hypophosphite--resistant mutants of *Escherichia coli*: identification of the FocA protein, encoded by the pfl operon, as a putative formate transporter. Molecular microbiology *11*, 965-982.

Tabor, S., and Richardson, C.C. (1985). A bacteriophage T7 RNA polymerase/promoter system for controlled exclusive expression of specific genes. Proceedings of the national academy of science USA *82*, 1074-1078.

Tamagnini, P., Axelsson, R., Lindberg, P., Oxelfelt, F., Wunschiers, R., and Lindblad, P. (2002). Hydrogenases and hydrogen metabolism of cyanobacteria. Microbiology and molecular biology reviews *66*, 1-20, table of contents.

Taylor, B.L., and Zhulin, I.B. (1999). PAS domains: internal sensors of oxygen, redox potential, and light. Microbiology and molecular biology reviews *63*, 479-506.

Thauer, R.K., Jungermann, K., and Decker, K. (1977). Energy conservation in chemotrophic anaerobic bacteria. Bacteriological reviews *41*, 100-180.

Thauer, R.K., Kaster, A.K., Goenrich, M., Schick, M., Hiromoto, T., and Shima, S. (2010). Hydrogenases from methanogenic archaea, nickel, a novel cofactor, and H_2 storage. Annual review of biochemistry *79*, 507-536.

Tian, F., Toon, O.B., Pavlov, A.A., and De Sterck, H. (2005). A hydrogen-rich early Earth atmosphere. Science *308*, 1014-1017.

Tipping, M.J., Steel, B.C., Delalez, N.J., Berry, R.M., and Armitage, J.P. (2013). Quantification of flagellar motor stator dynamics through *in vivo* proton-motive force control. Molecular microbiology *87*, 338-347.

Tominaga, T., Watanabe, S., Matsumi, R., Atomi, H., Imanaka, T., and Miki, K. (2013). Crystal structures of the carbamoylated and cyanated forms of HypE for [NiFe] hydrogenase maturation. Proceedings of the national academy of science USA *110*, 20485-20490.

Truniger, V., and Boos, W. (1994). Mapping and cloning of *gldA*, the structural gene of the *Escherichia coli* glycerol dehydrogenase. Journal of bacteriology *176*, 1796-1800.

Umbach, F. (2010). Global energy security and the implications for the EU. Energy policy *38*, 1229-1240.

UN Department of Economic and Social Affairs (2015). World population propsects 2015 revision.

Unden, G., and Bongaerts, J. (1997). Alternative respiratory pathways of *Escherichia coli*: energetics and transcriptional regulation in response to electron acceptors. Biochimica et biophysica acta *1320*, 217-234.

US Environemental Protection Agency (2008). Document for hydrogen production: proposed rule for mandatory reporting of greenhouse gases (Washington DC: Government Printing Office).

Van der Linden, E., Burgdorf, T., Bernhard, M., Bleijlevens, B., Friedrich, B., and Albracht, S.P. (2004). The soluble [NiFe]-hydrogenase from *Ralstonia eutropha* contains four cyanides in its active site, one of which is responsible for the insensitivity towards oxygen. Journal of inorganic biochemistry *9*, 616-626.

van der Linden, E., Burgdorf, T., de Lacey, A.L., Buhrke, T., Scholte, M., Fernandez, V.M., Friedrich, B., and Albracht, S.P. (2006). An improved purification procedure for the soluble [NiFe]-hydrogenase of *Ralstonia eutropha*: new insights into its (in)stability and spectroscopic properties. Journal of inorganic biochemistry *11*, 247-260.

Vandamme, P., and Coenye, T. (2004). Taxonomy of the genus *Cupriavidus*: a tale of lost and found. International journal of systematic and evolutionary microbiology *54*, 2285-2289.

Vaneechoutte, M., Kampfer, P., De Baere, T., Falsen, E., and Verschraegen, G. (2004). *Wautersia* gen. nov., a novel genus accommodating the phylogenetic lineage including *Ralstonia eutropha* and related species, and proposal of *Ralstonia [Pseudomonas] syzygii* (Roberts *et al*. 1990) comb. nov. International journal of systematic and evolutionary microbiology *54*, 317-327.

Verhagen, M.F., O'Rourke, T., and Adams, M.W. (1999). The hyperthermophilic bacterium, *Thermotoga maritima*, contains an unusually complex iron-hydrogenase: amino acid sequence analyses versus biochemical characterization. Biochimica et biophysica acta *1412*, 212-229.

Verlinden, R.A., Hill, D.J., Kenward, M.A., Williams, C.D., and Radecka, I. (2007). Bacterial synthesis of biodegradable polyhydroxyalkanoates. Journal of applied microbiology *102*, 1437-1449.

Vignais, P.M., and Billoud, B. (2007). Occurrence, classification, and biological function of hydrogenases: an overview. Chemical reviews *107*, 4206-4272.

Vijayaraghavan, K., and Mohd Soom, M.A. (2006). Trends in bio-hydrogen generation – A review. Environmental sciences *3*, 255-271.

Volbeda, A., Amara, P., Darnault, C., Mouesca, J.M., Parkin, A., Roessler, M.M., Armstrong, F.A., and Fontecilla-Camps, J.C. (2012). X-ray crystallographic and computational studies of the O_2-tolerant [NiFe]-hydrogenase 1 from *Escherichia coli*. Proceedings of the national academy of science USA *109*, 5305-5310.

Volbeda, A., Charon, M.H., Piras, C., Hatchikian, E.C., Frey, M., and Fontecilla-Camps, J.C. (1995). Crystal structure of the nickel-iron hydrogenase from *Desulfovibrio gigas*. Nature *373*, 580-587.

Volbeda, A., Garcin, E., Piras, C., de Lacey, A.L., Fernandez, V.M., Hatchikian, E.C., Frey, M., and Fontecilla-Camps, J.C. (1996). Structure of the [NiFe] Hydrogenase active site: evidence for biologically uncommon Fe ligands. Journal of the American chemical society *118*, 12989-12996.

Volbeda, A., Martin, L., Cavazza, C., Matho, M., Faber, B.W., Roseboom, W., Albracht, S.P., Garcin, E., Rousset, M., and Fontecilla-Camps, J.C. (2005). Structural differences between the

ready and unready oxidized states of [NiFe] hydrogenases. Journal of biological inorganic chemistry *10*, 239-249.

Wait, A.F., Brandmayr, C., Stripp, S.T., Cavazza, C., Fontecilla-Camps, J.C., Happe, T., and Armstrong, F.A. (2011). Formaldehyde—a rapid and reversible inhibitor of hydrogen production by [FeFe]-hydrogenases. Journal of the American chemical society *133*, 1282-1285.

Walter, J.M., Greenfield, D., Bustamante, C., and Liphardt, J. (2007). Light-powering *Escherichia coli* with proteorhodopsin. Proceedings of the national academy of science USA *104*, 2408-2412.

Walz, A.C., Demel, R.A., de Kruijff, B., and Mutzel, R. (2002). Aerobic sn-glycerol-3-phosphate dehydrogenase from *Escherichia coli* binds to the cytoplasmic membrane through an amphipathic alpha-helix. Biochemical journal *365*, 471-479.

Warnecke, T., and Gill, R.T. (2005). Organic acid toxicity, tolerance, and production in *Escherichia coli* biorefining applications. Microbial cell factories *4*, 25-25.

Waugh, R., and Boxer, D.H. (1986). Pleiotropic hydrogenase mutants of *Escherichia coli* K12: growth in the presence of nickel can restore hydrogenase activity. Biochimie *68*, 157-166.

Wecker, M.S., and Ghirardi, M.L. (2014). High-throughput biosensor discriminates between different algal H_2 -photoproducing strains. Biotechnology and bioengineering *111*, 1332-1340.

Weiss, B.P., Yung, Y.L., and Nealson, K.H. (2000). Atmospheric energy for subsurface life on Mars? Proceedings of the national academy of science USA *97*, 1395-1399.

Weyman, P.D., Vargas, W.A., Chuang, R.Y., Chang, Y., Smith, H.O., and Xu, Q. (2011). Heterologous expression of *Alteromonas macleodii* and *Thiocapsa roseopersicina* [NiFe] hydrogenases in *Escherichia coli*. Microbiology *157*, 1363-1374.

Wheatley, N.M., Gidaniyan, S.D., Liu, Y., Cascio, D., and Yeates, T.O. (2013). Bacterial microcompartment shells of diverse functional types possess pentameric vertex proteins. Protein science *22*, 660-665.

Wolf, I., Buhrke, T., Dernedde, J., Pohlmann, A., and Friedrich, B. (1998). Duplication of hyp genes involved in maturation of [NiFe] hydrogenases in *Alcaligenes eutrophus* H16. Archives of microbiology *170*, 451-459.

Wolfram, L., Friedrich, B., and Eitinger, T. (1995). The *Alcaligenes eutrophus* protein HoxN mediates nickel transport in *Escherichia coli*. Journal of bacteriology *177*, 1840-1843.

Wu, L.F., Mandrand-Berthelot, M.A., Waugh, R., Edmonds, C.J., Holt, S.E., and Boxer, D.H. (1989). Nickel deficiency gives rise to the defective hydrogenase phenotype of hydC and fnr mutants in *Escherichia coli*. Molecular microbiology *3*, 1709-1718.

Wu, L.F., Navarro, C., de Pina, K., Quenard, M., and Mandrand, M.A. (1994). Antagonistic effect of nickel on the fermentative growth of *Escherichia coli* K-12 and comparison of nickel and cobalt toxicity on the aerobic and anaerobic growth. Environmental health perspectives *102 Suppl 3*, 297-300.

Xu, H., and Hoover, T.R. (2001). Transcriptional regulation at a distance in bacteria. Current opinion in microbiology *4*, 138-144.

Yakunin, A.F., and Hallenbeck, P.C. (1998). Purification and characterization of pyruvate oxidoreductase from the photosynthetic bacterium *Rhodobacter capsulatus*. Biochimica et biophysica acta *1409*, 39-49.

Yazdani, S.S., and Gonzalez, R. (2007). Anaerobic fermentation of glycerol: a path to economic viability for the biofuels industry. Current opinion in biotechnology *18*, 213-219.

Yeates, T.O., Kerfeld, C.A., Heinhorst, S., Cannon, G.C., and Shively, J.M. (2008). Protein-based organelles in bacteria: carboxysomes and related microcompartments. Nature reviews microbiology *6*, 681-691.

Yeates, T.O., Thompson, M.C., and Bobik, T.A. (2011). The protein shells of bacterial microcompartment organelles. Current opinion in structural biology *21*, 223-231.

Zajdel, T., Teravest, M., Rad, B., and Maharbiz, M. (2014). Probing the dynamics of the proton-motive force in *E. coli*. In Paper presented at the 2014 IEEE Sensors Conference (Valencia, Spain).

Zbell, A.L., and Maier, R.J. (2009). Role of the Hya hydrogenase in recycling of anaerobically produced H_2 in *Salmonella enterica* serovar Typhimurium. Applied and environmental microbiology *75*, 1456-1459.

Zheng, H., Zhang, C., Lu, Y., Jiang, P.-X., and Xing, X.-H. (2012). Alteration of anaerobic metabolism in *Escherichia coli* for enhanced hydrogen production by heterologous expression

of hydrogenase genes originating from Synechocystis sp. Biochemical engineering journal *60*, 81-86.

Zimmer, D., Schwartz, E., Tran-Betcke, A., Gewinner, P., and Friedrich, B. (1995). Temperature tolerance of hydrogenase expression in *Alcaligenes eutrophus* is conferred by a single amino acid exchange in the transcriptional activator HoxA. Journal of bacteriology *177*, 2373-2380.